MICROFACIES AND WIRELINE LOG ANALYSIS OF THE UPPER LEONARDIAN FIRST BONE SPRING CARBONATE MEMBER, DELAWARE BASIN, SOUTHEAST NEW MEXICO

A Thesis

by

HARRISON RICE HASTINGS

Submitted to the Office of Graduate and Professional Studies of
Texas A&M University
in partial fulfillment of the requirements for the degree of

MASTER OF SCIENCE

Chair of Committee,	John R. Giardino
Co-Chair of Committee,	Juan Carlos Laya
Committee Member,	Kevin R. Gamache
Head of Department,	Michael C. Pope

May 2018

Major Subject: Geology

ABSTRACT

Allochthonous carbonate deposits in the First Bone Spring Carbonate (FBSC) interval exhibit complex architectural and compositional heterogeneity. The episodic and chaotic depositional nature of these deposits results in the development of complex stratigraphic relationships with organic-rich pelagic deposits in deep-open marine settings. In the FBSC, these organic-rich deposits are informally recognized as the Avalon and Leonard shales and are significant unconventional hydrocarbon reservoirs targeted by industry today. Bone Spring detrital carbonates have been studied previously for their potential as conventional hydrocarbon reservoirs near basin margins. However, the nature of detrital carbonate strata in the FBSC changes significantly in a deep, basin-centered setting, where such deposits not only lack potential as hydrocarbon reservoirs, but also represent geologic inhibitors to drilling and completion of horizontal wells targeting the aforementioned interbedded Avalon and Leonard shales. Considering the economic significance of emerging unconventional hydrocarbon exploration targeting FBSC member strata in deep marine, basin centered settings, further investigation of these deposits is highly relevant and of interest. In addition to the compositional, stratigraphic, and depositional heterogeneity associated with deep slope and basin FBSC deposits, diagenetic processes further increase the difficulty in accurately characterizing and predicting detrital carbonate strata within the interval. Because encountering these deposits in the lateral negatively impacts well performance and economics, understanding their compositional variation and distribution throughout the FBSC is

crucial, and will facilitate new development strategies for unconventional exploration of the FBSC, not only focused on more efficient exploitation of hydrocarbons through improved drilling and completion, but also more accurate quantification of risk achieved through better understanding and increased resolution of complex FBSC strata in a deep basinal setting.

Heterogeneity of the FBSC was constrained through the identification and definition of representative microfacies utilizing detailed core description, petrographic studies, and XRD data analysis. Coordination of the identified microfacies into 'correlation associations' facilitated the establishment of characteristic petrophysical properties and signature log responses, which in turn enables the identification and prediction of defined facies and their associated physical properties in the subsurface using commonly available, limited data sets away from core data. It was determined that heavily silicified carbonate strata are the greatest degraders to reservoir quality of a given interval and are inhibitors to drilling efficiency. The non-standard incorporation of diagenetic elements for the definition and differentiation of microfacies and correlation associations was useful for improving core-to-log correlation quality in this study. The abundant presence of originally siliceous sponge spicules and radiolarians, and greater ability for diagenetic pore fluids to permeate a deposit were identified as factors which increase silicification susceptibility of a given FBSC deposit. Empirical data gained through this research provides the framework for future studies to further improve our understanding of diagenetic processes, physical properties, and related implications associated with FBSC deposits in deep, slope and basin settings.

DEDICATION

I dedicate this thesis to my family, I owe everything to their constant love and support. I love you Mom, Dad, Andrew, and Kellie.

ACKNOWLEDGEMENTS

First, I would like to thank my committee chair Dr. Rick Giardino, co-chair Dr. Juan Carlos Laya, and committee member Kevin Gamanche for their guidance and support throughout the completion of this research. A special thanks to Dr. Laya, for coming on as my co-chair in the later stages of my project to provide crucial guidance and direction I needed; and my gratitude to Dr. Giardino who remained my advisor throughout a momentously difficult time in his, and his family's lives.

This research would not have been possible without the generous contributions and funding from Cimarex Energy Co., Concho Resources, and Core Laboratories, Inc., and the support of Dave Witter at Cimarex Energy, Pat Welch at Concho Resources, and Steve Alexander at Core Lab. My sincere thanks to Steve Alexander for the many arrangements he made for me to observe core data, and to have data prepared and sent to me. Steve went out of his way to ensure I received the data I needed, and I am truly grateful for his efforts. My thanks also to Pat Welch, who orchestrated my receiving permission to access the core, and associated petrophysical and mineralogical data, without which this research would not have been possible. My most sincere thanks to Mr. Witter, for not only facilitating access to the software, data, and funding which enabled me to complete my research, and Master's Degree at Texas A&M, but also for presenting me with the opportunity to be a part of the Cimarex team in Midland, where I have had the privilege to learn and gain experience working alongside some of the most intelligent and knowledgeable people in the oil and gas industry today. I would also like

to thank Mr. Witter for his patience and support throughout the tumultuous process of completing this thesis.

I want to extend my thanks to Jerry Venzuela, for the work he contributed to organizing and coordinating core and thin-section data, and generating figures. He was extremely helpful in the completion of this study. My thanks to Jason Asmus, who readily provided guidance, advice, and helpful feedback throughout the process of completing this thesis. I would also like to thank Dr. Mike Pope and Dr. Juan Carlos Laya for the time, interest, and suggestions they contributed to my interpretations. My thanks to Dr. Youjun Deng for facilitating my collection of XRD data and analysis, and to Dr. Deng's student Chun-Chun Hsu for data preparation guidance in the laboratory.

I would like to thank my friends and colleagues, in addition to the faculty and staff in the Geology and Geosciences Department for their companionship, advice, and support, and for making my time as a graduate student at Texas A&M a great experience. I would specifically like to acknowledge professors Dr. Bobby Reece, Dr. Mike Pope, and Dr. Chris Houser whose courses I especially enjoyed taking and benefitted from; and Jacob Bayer, Mike Deluca, Mary Bales, Drew Davis, Kaytan Kelker, John Reed, Patrick Wagner, Akhil Amara, and my officemates Nehe, Renjei, and Kyle Cunningham for making my graduate school experience all the more enjoyable.

I would like to thank my mom and dad for their unwavering support, guidance, trust, love, and sacrifice. They are not only the two greatest role models a son could ask for, but have also devoted every part of their lives to ensuring my brother Andrew and I

are able to achieve anything in life that we put our minds to. I owe all of my past and future successes to the foundation they established for me, and could not feel more fortunate or honored to be their son.

Finally, I would like to thank my loving wife Kellie. In addition to directly contributing to the completion of this thesis, she provided me with unwavering support, love, patience, and encouragement, without which I could not have succeeded in completing this thesis. I cannot imagine a better partner to have in life, I love you Kellie.

CONTRIBUTORS AND FUNDING SOURCES

This work was supervised by a thesis committee consisting of Professors John R. Giardino (advisor) and Juan Carlos Laya (co-advisor) of the Department of Geology and Geophysics, and Professor Kevin R. Gamache of the Department of Water Management and Hydrological Sciences.

All work for this thesis was completed independently by the student.

Graduate study and this thesis research was supported by funding and contributions from Cimarex Energy Co., and contributions from Concho Resources, and Core Laboratories, Inc.

NOMENCLATURE

DPHZ	Density-Porosity Log
CA	Correlation Association
FBSC	First Bone Spring Carbonate
FS	Floatstone
GR	Gamma-Ray Log
MF	Microfacies
MS	Mudstone
ND	Neutron- and Density-Porosity
NPHI	Neutron-Porosity Log
Pe	Photoelectric Log
PS	Packstone
RHOB	Bulk-Density Log
RS	Rudstone
Rt	Uninvaded Zone ‘Deep’ Resistivity Log
SMS	Silty Mudstone
WS	Wackestone
XRD	X-Ray Diffraction

TABLE OF CONTENTS

Page

LIST OF FIGURES

Page

LIST OF TABLES

Page

1. INTRODUCTION

The size and density of resources within the Delaware Basin make it one of the premier hydrocarbon producing basins in the world today. The extensive coverage and general high quality of well data throughout the basin provides the potential to research the sedimentology and petrophysical characteristics of basin strata at a resolution not possible in many other areas of the world.

Bone Spring detrital carbonates shed from surrounding carbonate platforms were deposited along shelf and basin slopes by various mass-transport processes, and extend 10's of kilometers into deep, open-marine settings of the Delaware Basin. These, and correlative deposits have been studied extensively in Delaware Basin outcrops (King, 1948; Boyd, 1958; Rigby, 1958; King, 1962, 1965; Playton and Kerans; Janson et al., 2007; Scholle et al., 2007; Amerman et al., 2011) and in the subsurface, particularly near platform margins (Wiggins and Harris, 1985; Gawloski, 1987; Mazzullo and Reid, 1987; Saller et al., 1989b, a) where many of the thick carbonate detrital zones in the 2nd and 3rd Bone Spring Carbonate members underwent dolomitization and were the focus of industry research and exploration for years, as they represented significant conventional hydrocarbon reservoirs (figure 2). The nature of these deposits changes significantly in a deep, basin-centered setting, where allochthonous carbonates are often characterized by low porosity and permeability (Piper et al., 1997; Shipp et al., 2004; Moscardelli et al., 2006; Weimer et al., 2006; Moscardelli, 2007). In fact, in a basinal setting of the First Bone Spring Carbonate (FBSC) member, it is likely that these allochthonous carbonate

strata not only lack potential as hydrocarbon reservoirs, but also represent geologic inhibitors to drilling and completion of horizontal wells targeting the interbedded pelagic unconventional reservoir facies referred to in industry as the Avalon and Leonard shales of the FBSC. Unfortunately, outcrop based research regarding deeper slope and basin deposits in the Bone Spring Fm. are derived from severely limited outcrop exposures, few to none of which are directly correlative to the First Bone Spring Carbonate (FBSC) member in a deep-open marine setting (Gardner, 2014; Li et al., 2015). Similarly, few subsurface investigations have studied distal basin strata of the FBSC member in detail, and fewer still with regard to the allochthonous carbonate deposits of the interval. Considering the economic significance of emerging unconventional hydrocarbon exploration targeting FBSC member strata in deep marine, basin centered settings**,** further investigation of these deposits is highly relevant and of interest.

Allochthonous carbonate deposits in the FBSC exhibit complex architectural and compositional heterogeneity (Silver and Todd, 1969; Gawloski, 1987; Nester et al., 2014); further, the episodic and general chaotic depositional nature of such deposits results in the development of complex stratigraphic relationships with pelagic deposits previously deposited in the basin (Shanmugam et al., 1995; Moscardelli et al., 2006). In addition to the complex compositional, stratigraphic, and depositional heterogeneity associated with deep slope and basin FBSC strata, diagenetic processes influence reservoir quality and further increase the difficulty in accurately characterizing and predicting associated deposits.

Distal, basin centered strata of the FBSC member were studied by Asmus and Grammer (2013), who thoroughly investigated and classified reservoir scale architectural attributes of carbonate turbidites and mass-transport deposits. Although with lesser focus on the carbonate strata, (Stolz, 2014) investigated log based stratigraphy and reservoir characteristics of the Avalon shale, an informal member of the Bone Spring Fm. representing most of the pelagic and hemipelagic facies in the FBSC member. Yet, work to characterize the detailed sedimentology of FBSC deposits, particularly allochthonous carbonate strata remains to address the question: what are the sedimentological and mineralogical characteristics of these deposits?

The main objectives of this thesis are to identify the sedimentological characteristics & mineralogical composition of FBSC strata in a deep, basin centered setting, determine which deposits are most susceptible to silicification, and to correlate log data with core identified facies to calibrate signature log responses for those facies. Detailed core description, petrographic thin-section analysis, and XRD data were incorporated with a full conventional log suite to define microscale facies on the basis of sedimentological characteristics and mineralogical composition, and to identify the petrophysical and wireline log characteristics associated with those facies. This will facilitate interpretation of depositional and post depositional processes not previously achievable with conventional datasets alone, provide the framework for improved understanding of diagenetic processes and associated physical (reservoir vs. non-reservoir) properties of FBSC strata through future studies, and enable identification and

prediction of sedimentologically, mineralogically, stratigraphically, and diagenetically heterogeneous FBSC deposits in the subsurface.

These outcomes associated with realizing the objectives for this study will facilitate new development strategies for unconventional exploration of the FBSC, focused on more efficient exploitation of hydrocarbons through improved drilling and completion, and more accurate quantification of risk achieved through better understanding and increased resolution of complex FBSC strata in a deep basinal setting.

2. GEOLOGIC BACKGROUND

2.1 Regional Setting

The Delaware Basin is the major western sub-basin of the Permian Basin (figure 1). Located in West Texas and southeastern New Mexico, the basin covers a total area of approximately 33,000 km^2 (12,740 mi2), and contains up to 7,315 m (24,000') of Phanerozoic sediments, which range from 1.3 b.y. Pre-Cambrian basement rocks, to Quaternary sands and gravels (Hills, 1984; Hill, 1996). Many of the stratigraphic units in the Delaware Basin are prolific hydrocarbon source or reservoir rocks; recovery of oil and gas beginning as early as the 1920's and continuing through today has helped to establish the Delaware Basin as one of the major hydrocarbon producing basins in the world (Hill, 1996). In recent years, the emergence of unconventional drilling and well completion techniques targeting source rock intervals of the Delaware and Midland Basins has resulted in the Permian Basin rising again to the forefront of oil and gas exploration and production in the world today.

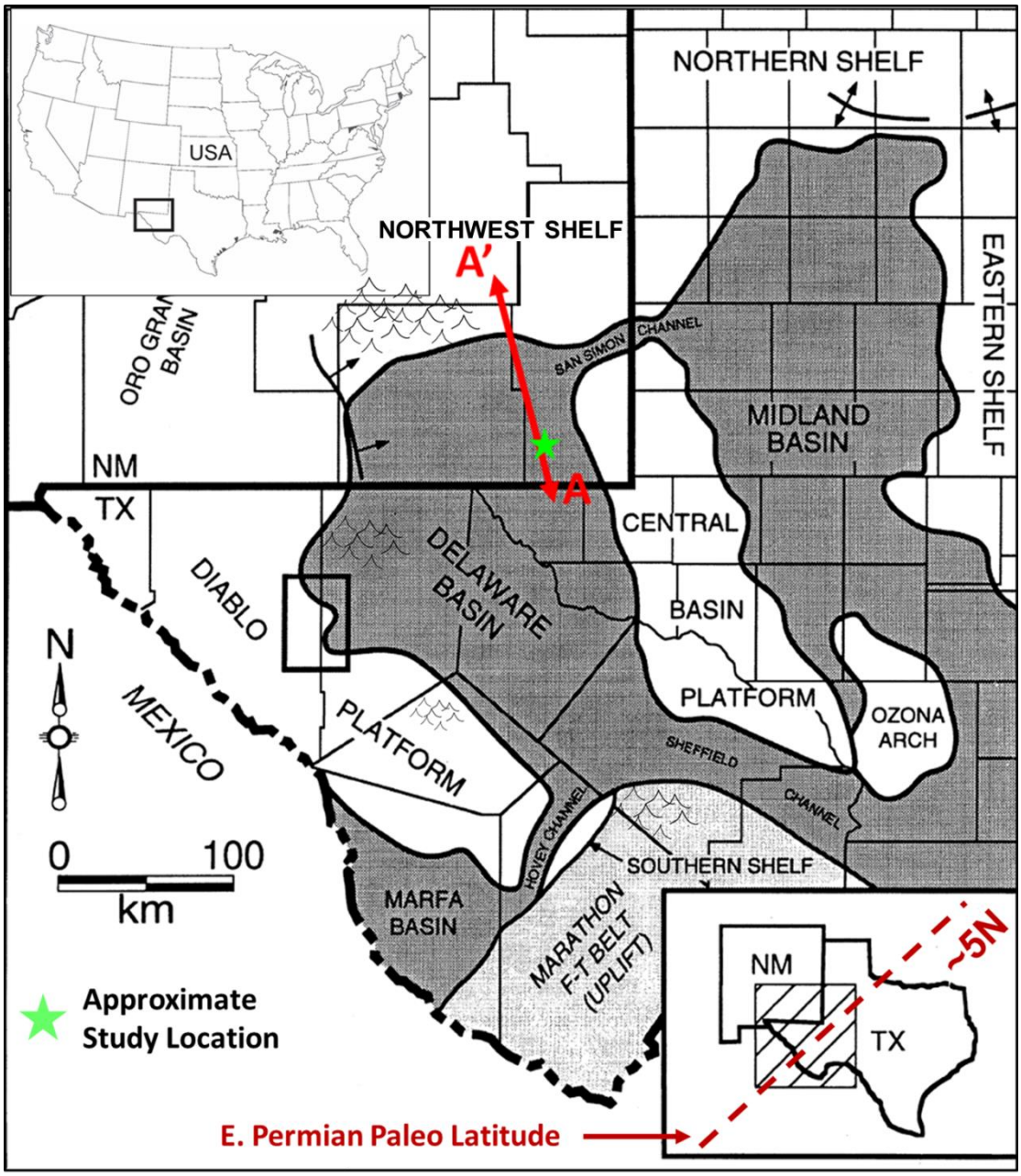

Figure 1. Regional Structural and Geographic Map of the Permian Basin. The two major sub-basins of the Permian Basin are the Delaware Basin (West) and Midland Basin (East) separated by the Central Basin Platform. The location of regional shelf to basin cross-section A-A' (figure 2) and approximate research study area are also noted. (Modified from Fitchen et al. (1995) and Li et al. (2015))

2.2 Bone Spring Formation Stratigraphy

The Bone Spring Formation of southeastern New Mexico and West Texas is a complex sequence of carbonates, sandstones, and shales deposited extensively across the Delaware Basin during early Permian, Leonardian time (280 to 270.7 Ma). The formation has an approximate maximum thickness of 1067 m (3,500'), and consists of three carbonate units subdivided by three siliciclastic units. These units are informally referred to as the 1st, 2nd, and 3rd Bone Spring Carbonate, and 1st, 2nd, and 3rd Bone Spring Sandstone intervals, respectively (figure 2, 3) (Gawloski, 1987; Hart et al., 2000). Rimmed carbonate platforms which surrounded this portion of the subsiding Delaware Basin during Leonardian time are the sources for regionally extensive, detrital, slope and basin deposits of the Bone Spring formation; these deposits are temporal equivalents to shelf deposits of the Leonardian Yeso, Abo, Clear Fork, and Wichita Formations of the surrounding Central Basin Platform (east) and the Northwest Shelf (north) (Gawloski, 1987; Mazzullo and Reid, 1987; Saller et al., 1989b; Hart et al., 2000) (figure 1, 3). Bone Spring sediments are thought to have been deposited as a result of reciprocal sedimentation caused by relative sea-level change; with carbonates deposited during transgression and highstand sequences, and clastics deposited during relative lowstands (Silver and Todd, 1969; Gawloski, 1987; Saller et al., 1989b; Hart et al., 2000).

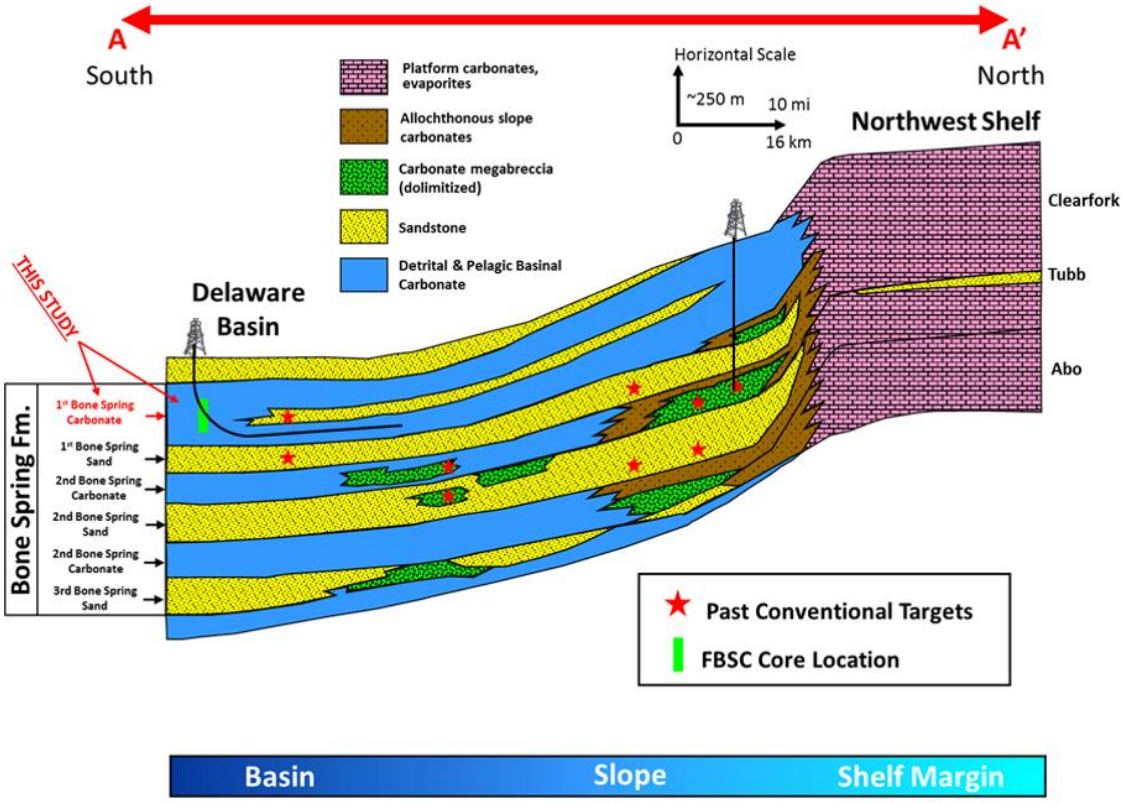

Figure 2. Regional schematic cross section illustrating general Bone Spring Fm. stratigraphy and shelf-to-basin relationships. Also displays productive Bone Spring zones for various fields; most of which have been the subject of previous studies (e.g., Gawloski (1987); Mazzullo and Reid (1987); Saller et al. (1989b)) (Modified from Montgomery (1997a); Asmus (2012))

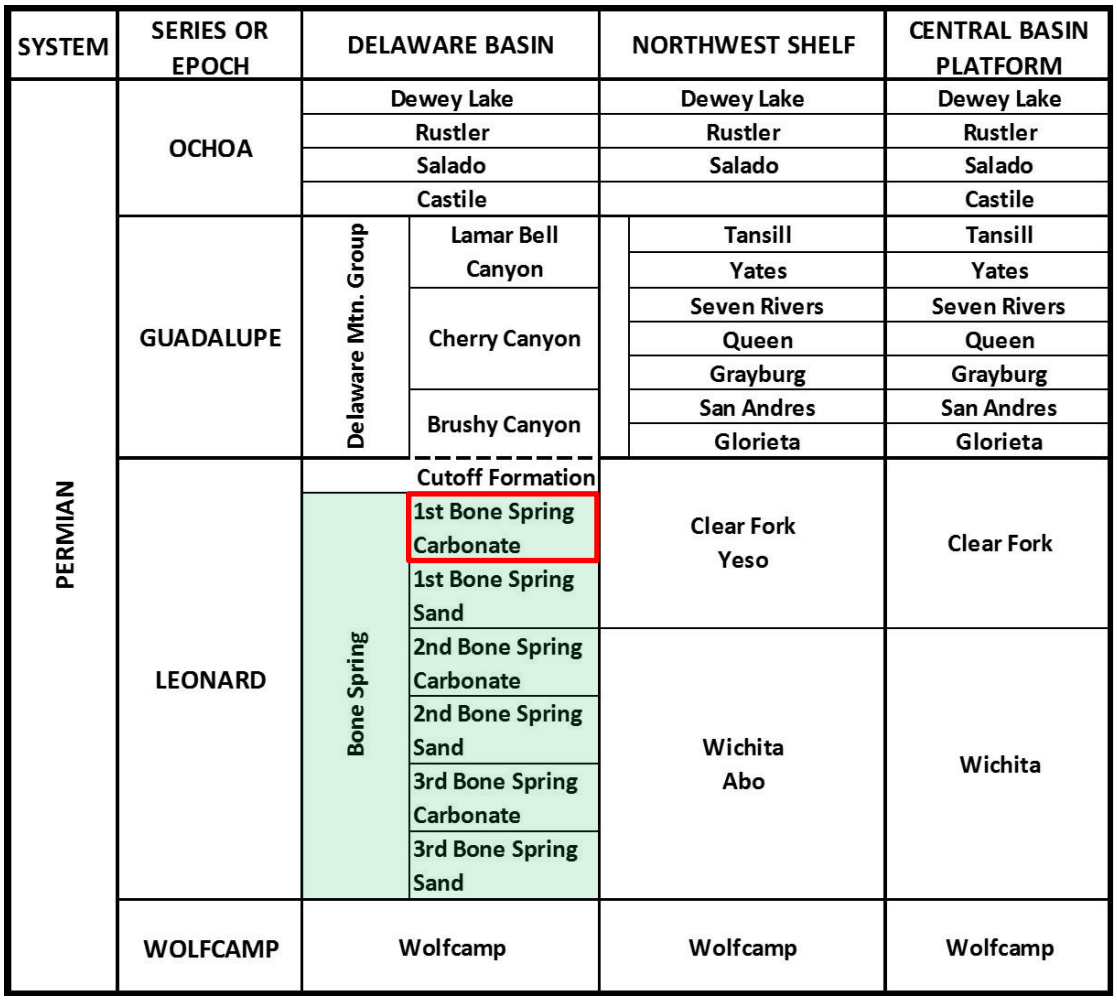

Figure 3. Generalized Stratigraphic Correlation Chart for the Permian Basin; (modified from Gawloski (1987)).

2.3 First Bone Spring Carbonate Member Stratigraphy

This study focuses on the strata in the Upper Leonardian (Lower Permian) First Bone Spring Carbonate (FBSC) member of the Bone Spring Formation in a deep basin centered setting of the Delaware Basin. The FBSC member generally consists of pelagic and hemi-pelagic mudstones and silty mudstones interbedded irregularly with regionally

extensive, slope and basin carbonate mass-transport deposits and turbidites. Organic, self-sourced, quartz-rich, pelagic and hemi-pelagic siltstones and mudstones of the FBSC represent the informal Avalon Shale member of the Bone Spring Formation, an unconventional oil and gas exploration play in the Delaware Basin since 2008 (Nester et al., 2014; Schwartz et al., 2014). Allochthonous carbonates of the Bone Spring Fm., which account for as much as 50% of the FBSC interval in the optimal Avalon play production fairway (Nester et al., 2014; Hastings, 2016), have been studied previously; particularly near basin margins where carbonate detrital deposits were historically targeted for their major conventional hydrocarbon reservoirs (Wiggins and Harris, 1985; Gawloski, 1987; Mazzullo and Reid, 1987; Saller et al., 1989b, a). In addition, these deposits have been studied and described in outcrops of the Guadalupe, Apache, and Glass Mountains by (King, 1948, 1962, 1965); Amerman (2007); (Janson et al., 2007) and several others. King (1948) as cited by Hill (1996) described exposed Bone Spring MTDs as showing ‘a great irregularity of stratification’. While these deposits have been exploited as hydrocarbon reservoirs near basin margins, their character changes significantly in a deep-basinal setting, where allochthonous carbonates are often characterized by low porosity and permeability (Piper et al., 1997; Shipp et al., 2004; Moscardelli et al., 2006; Moscardelli, 2007). Thus, it is likely that in a deep, basinal setting of the FBSC member, allochthonous carbonate strata not only lack potential as hydrocarbon reservoirs, but also represent geologic inhibitors to drilling and completion in horizontally drilled unconventional wells.

The FBSC interval ranges from ~275 to 335 m (900 to 1,100') in thickness (Figure 4). The top of the FBSC is defined on wireline logs by the top of the first clean carbonate interval beneath the Delaware Mountain Group (Figure 5), and the base of the interval is defined by the top of the First Bone Spring Sandstone member (Hart et al., 2000).

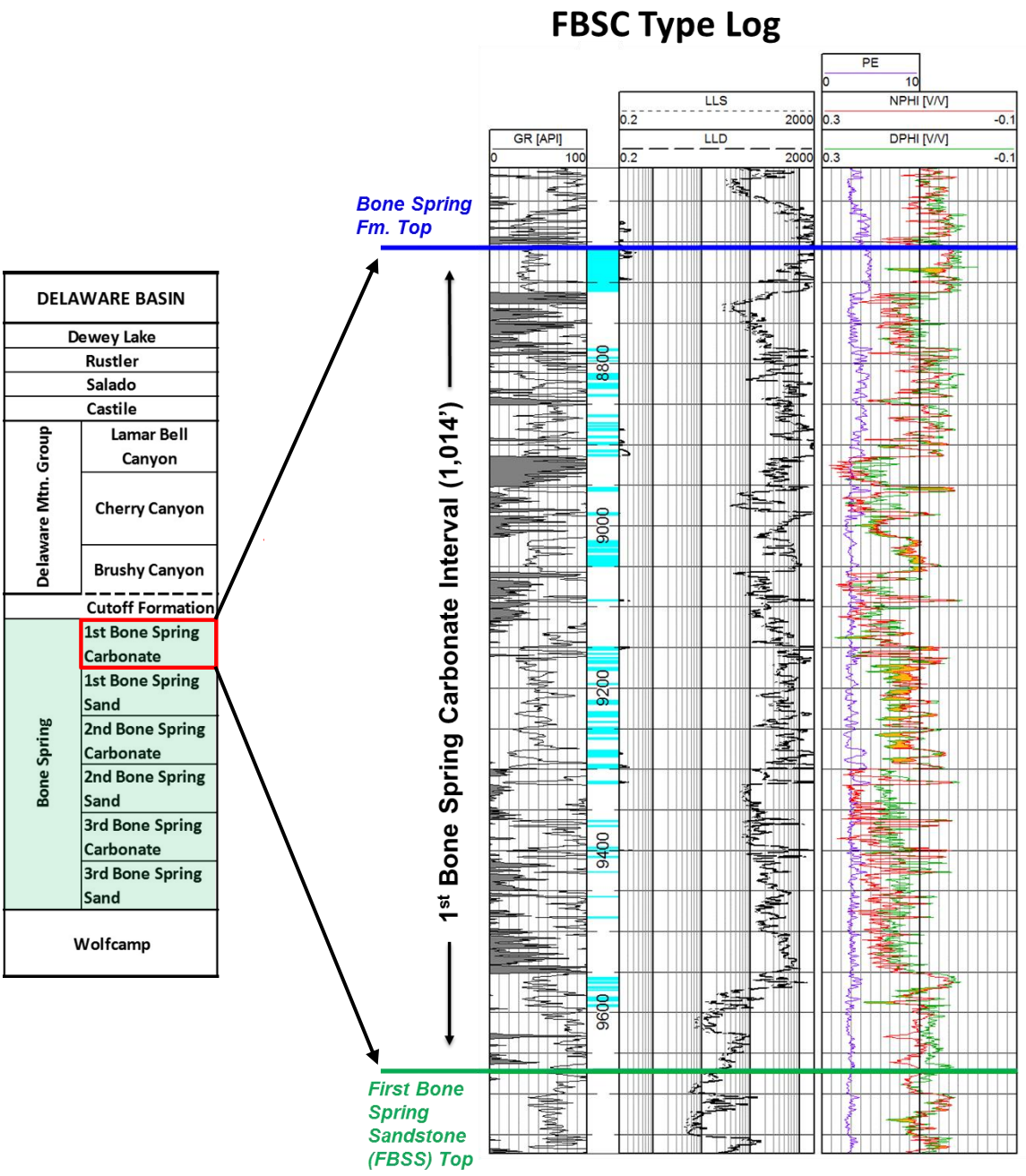

Figure 4. Type Log for the First Bone Spring Carbonate, which ranges in thickness from ~275-335 m (900-1,100 ft). On wireline logs, the top of the interval is defined by the top of the First Bone Spring Limestone (blue marker), and the base of the interval is defined by the top of the First Bone Spring Sandstone (green marker). Pelagic facies within the interval are typically recognized by 'hot' off-scale (grey fill) gamma ray values, while carbonate facies can be identified by low gamma ray values (generally < 50 api), higher resistivity, Pe values equal or close to 5, and nearly or overlapping neutron-density (NPHI) and density-porosity (DPHI) curves.

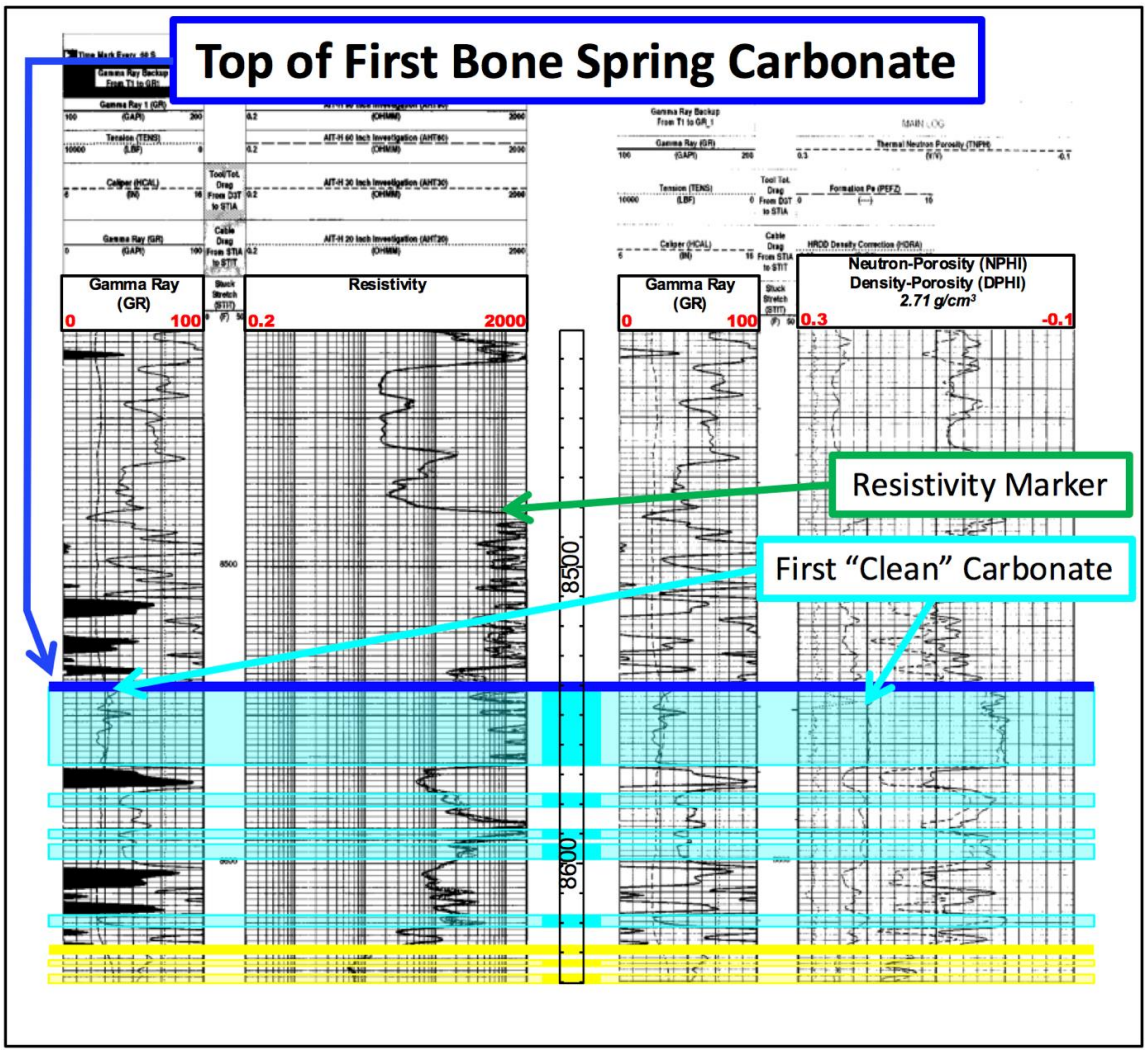

Figure 5. The top of the First Bone Spring Carbonate member is identified on wireline logs by the first "clean" carbonate interval beneath the Delaware Mountain Group. A sharp increase in resistivity ("resistivity marker") near the base of the Brushy Canyon Formation marks the lowest extent of the Delaware Mountain Group. The first "clean" carbonate can then be most easily identified by: low gamma ray values (< 50 api), high resistivity, P.E. values approximately equal to 5, and generally lower and overlapping neutron-porosity (NPHI) and density-porosity (DPHI) curves.

3. METHODOLOGY

The first objective of this investigation was to determine the extent and type of facies in the FBSC member of the Bone Spring Fm., with emphasis on lessor studied allochthonous carbonate deposits. Facies were investigated on the basis of sedimentological characteristics (e.g., sedimentary structures, texture, fabric, skeletal grains, matrix composition, bedding) and mineralogical composition.

The methodology for completing this objective involved detailed core description to identify facies on a macro-scale (macrofacies), followed by analysis of thin-sections and XRD data to determine microfacies and gain insight into diagenetic features present.

3.1 Core Acquisition and Preparation

3.1.1 Core Selection Criteria

The criteria for selecting core data for use in this study was based on the following five conditions:

1. Cored interval includes a representative portion of the First Bone Spring Carbonate member.
2. Core is located within a deep marine/basin centered location of the Delaware Basin; Lea County, NM.

3. Sufficient presence of mass-transport deposits throughout the cored interval (~ > 50% probable resedimented carbonate deposits)
4. Corresponding full log suite (gamma-ray, shallow, medium, deep resistivity, neutron-density and porosity logs) must be available.
5. Industry operator willing to share proprietary data.

3.1.2 Core Selection

Approximately 200 linear feet of conventional core data spanning a 252-foot interval of the First Bone Spring Carbonate member of the Bone Spring Fm. in southwestern Lea County, New Mexico (figure 6) was utilized for this study. The core was provided by Concho Resources, and is housed in the Core Laboratories facility located in northwest Houston. Core plugs sampled throughout the cored interval were used for XRD analysis, and to create thin sections. General core dataset information is summarized in Table 1, and core interval depths are summarized in Table 2. A full log suite corresponding to the cored well was provided by Cimarex Energy Co.

Table 1. General information associated with the cored well utilized for this study.

Core Dataset Information							
Well Name	**State/County**	**Formation**	**Total Footage**	**Total Interval**	**Top Depth**	**Base Depth**	**# of Sub Samples**
'Well A'	NM/Lea	Bone Spring	200.83'	252.12'	9,545'	9,797.12'	33

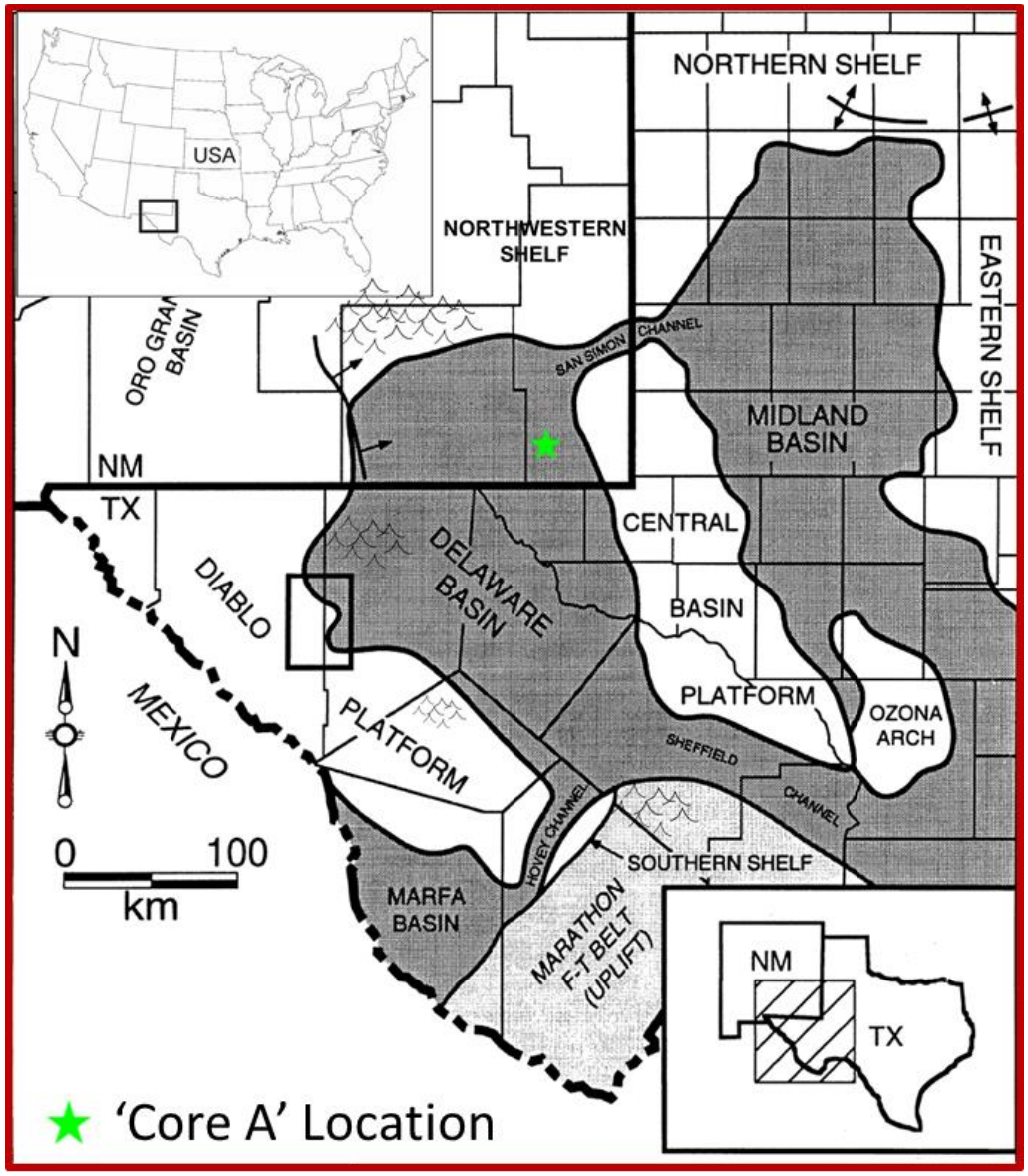

Figure 6. Map depicting the general location of the cored well in Lea County, NM. Also depicted is the general location of the cored well with respect to Delaware Basin boundaries and other regional Permian Basin structural features. See figure 2 for the approximate stratigraphic location of the cored interval (Modified from Fitchen et al. (1995) and Li et al. (2015)).

Table 2. Core depth intervals recovered throughout the 252-foot cored interval of Well A.

Core Interval Depths			
Top	**Base**	**Interval Thickness (ft)**	**# of Sub-Samples**
9,545.00	9,555.70	10.7	1
9,599.00	9,631.45	32.45	8
9,633.00	9,712.28	79.28	12
9,716.00	9,747.23	31.23	5
9,749.00	9,761.05	12.05	2
9,762.00	9,797.12	35.12	6
Total Linear Core (ft.)		200.83	
Total Interval		252.12	
Total Sub-Samples		34	

3.1.3 Core-to-log Tie

Within the Bone Spring Fm., the gamma-ray curve serves as a reliable indicator for differentiating carbonate lithology from surrounding pelagic mud-rock deposits, as carbonate-rich facies can be recognized by their lower gamma-ray values relative to the shale-baseline (Nester et al., 2014; Schwartz et al., 2014; Stolz, 2014). Using this information, a core-to-well log tie was conducted, with necessary depth shifts determined based on expected gamma ray responses to major carbonate and mud-rock contacts identified throughout the core.

3.1.4 Acquisition Obstacles

Industry focus has largely shifted to exploration of unconventional reservoirs deposited in deep marine, basin centered settings. Accordingly, academic and industry research focus in the Delaware Basin lies predominantly on hydrocarbon bearing mud-

rocks or ‘shales’, and reservoir quality sandstones; while intra-formational carbonate units (with comparably poor reservoir quality) remain of secondary interest, despite the insight gained through their study. As a result, when core data is available, it is unlikely to include a significant portion of the allochthonous carbonate deposits which are the focus of this study. Further, conventional core data acquisition is a highly expensive procedure. Consequently, existing data is rare compared to readily available log data, and is generally highly proprietary. For these reasons, acquiring adequate conventional core data for this study proved very difficult, and resulted in access to only one conventional core which satisfied the criteria outlined above.

3.2 Facies Analysis

The classification of macro- and microfacies within this cored interval of the FBSC member was conducted similarly to the work done by Laya and Tucker (2012) on Permian carbonates of the Palmarito Fm. in the Venezuelan Andes; and with regard to the methods, schemes, and classifications outlined in Flügel (2004) and Dunham (1962).

3.2.1 Core Description

Core description for this study took place from late December, 2016 through early January, 2017 in the Southwest Houston Core Laboratories facility where the core used for this study is housed. Detailed core logging was conducted at both the 1:12 and 1:120 scale in order to record observations on the bed to bed scale, and to provide a

broad overview of the cored interval. Care was taken to identify probable sedimentary structures, textures, fabrics, skeletal grains, and bedding. Degrees of apparent cementation, bioturbation, and reaction to diluted HCl were also specifically noted.

Core Descriptions and initial classifications were conducted in congruence with the methodologies outlined in Bebout and Loucks (1984) and Swanson (1981).

3.2.2 Petrographic Analysis

35 thin-sections were prepared from core-plugs which were strategically sampled from the macro-facies initially identified throughout the 252-foot cored interval of the First Bone Spring Carbonate Member. Thin-sections were then analyzed to identify compositional, mineralogical, and additional petrographic features present to 1) confirm the identification of the macrofacies defined during initial core description, and 2) determine associated microfacies and shed light diagenetic cements present.

Thin-Sections were prepared by Core Laboratories, Inc. in Northwest Houston, TX as standard 27 x 46 mm samples impregnated by blue dyed epoxy which permits visible porosity of the sample to be estimated. During analysis, each thin-section was studied and photographed at multiple scales under plane- and cross-polarized light. The stratigraphic location of each thin-section throughout the cored interval can be referenced in Appendix A. Descriptions and examples in both Flügel (2004) and Scholle and Ulmer-Scholle (2003) were utilized during analysis of the thin-sections for this study.

3.2.3 XRD Analysis

Six core plugs with corresponding thin-sections sampled from the major macrofacies identified and confirmed during core and thin-section description and analysis, were sent to the Department of Soil and Crop Sciences at Texas A&M for X-Ray Diffraction (XRD) analysis. In preparation for analysis, each sample had to be ground, and entirely sifted through a 140 mesh (0.105 mm) sieve. Bulk mineralogy for each sample was determined using semi-quantitative analysis, which allowed for improved descriptions and lithological classifications of previously identified macro- and micro-facies, and provided insight as to the composition of diagenetic cements (when present).

3.3 Silicification of Carbonate Rocks

The second objective of this investigation was to identify silicified microfacies in order to 1) determine which deposits are most susceptible to silicification, and 2) improve core-to-log correlation.

The methodology for completing this objective involved determining the criteria for recognizing silicification, to enable the identification and differentiation of silicified microfacies from non-silicified microfacies. Followed by comparing the sedimentology, petrography, and mineralogy of silicified microfacies and non-silicified microfacies in order to provide evidence for interpreting the differentiating factors which may have increased susceptibility for a deposit to become silicified.

Silicification is a diagenetic phenomenon affecting a wide variety of originally non-siliceous sediments (Knoll, 1985; Hesse, 1989). In carbonate rocks, silicification takes place in both deep- and shallow-marine environments, and involves the replacement of carbonate material by silica and/or the precipitation of pore-filling silica cement (Hesse, 1989; Flügel, 2004). Both processes may occur before, as well as after original carbonate cementation of pre-lithified host sediments. The change-over from carbonate cementation to silicification (and visa-versa) of a sediment may occur multiple times throughout the diagenetic history of a deposit (Hesse, 1989). During early diagenesis, the factors influencing which of the two processes occurs first are strongly dependent on environmental conditions; intrinsic factors (e.g., sediment composition, permeability) become more significant during later diagenetic stages (Hesse, 1989).

3.3.1 Identification

Macro-scale evidence for silicification exists (e.g. mineralized fractures, smooth surface texture), but can be easily misinterpreted. Thus, the presence of silicification is generally identified through petrographic and mineralogical analysis (e.g., thin-sections, XRD, SEM).

In thin-sections, silicification of a deposit is identified by the presence of authigenic quartz , or chert; appearing as a colorless microcrystalline aggregate similar in appearance to micrite or microspar, but with lower birefringence (Flügel, 2004). A petrographic technique for observing silicified material in thin-section was outlined by Scholle and Ulmer-Scholle (2003) who recommended inserting the first-order red

(gypsum) plate while viewing the sample under crossed nicols. Under these conditions, carbonate cement can be expected to change from first-order white through purple as the stage is rotated, while quartz will generally alternate between first-order red, green, and blue (Daley, 1987).

3.3.2 Silicification Controls and Biases

Controlling factors on silicification include depositional/geochemical environment, sediment composition, sedimentological characteristics, and other intrinsic and extrinsic factors which affect the dissolution/precipitation process (e.g., burial depth, temperature, time). The propensity for silicification based on variations of these factors, in addition to the timing of silicification relative to the well-defined diagenetic reaction sequences for carbonates, are not comprehensively defined or understood. However, many of the both intrinsic and extrinsic factors influencing silicification have been studied on a more singular basis (Newell et al., 1953; Lancelot, 1973; Kastner et al., 1977; Hesse, 1989; Hinman, 1998; Erwin and Kidder, 2000) among others. (Butts, 2014) identified and discussed *depositional environment*, *sediment composition*, and *permeability and porosity* as being three factors which are critical to influencing a deposits propensity for silicification.

Depositional Environment

Depositional setting, sedimentological controls, and particularly, changes in ocean geochemistry affect the availability and solubility of siliceous and carbonate

material, and therefore influence the propensity for the silicification or carbonate cementation of a deposit (Butts and Briggs, 2011; Butts, 2014). Silicification can occur in both deep- and shallow-water settings, though deposits in certain settings are more prone than others. Butts (2014), Erwin and Kidder (2000), and Newell et al. (1953) each made the case for silicification being enhanced and more common in open-marine (basinal), siliciclastic-poor, carbonate settings. Erwin and Kidder (2000) also specified that silicification was relatively more common in the open-marine environments of the Permian basins of West Texas and Southeast New Mexico; which was attributed to relative high silica availability and rapid burial.

Sediment Composition

Sediment composition, particularly carbonate versus siliciclastic, affects susceptibility for silicification by influencing grain solubility and interaction with clays, amongst other factors (Butts, 2014). The solubility and precipitation of silica are generally: (1) reduced in the presence of fine grained siliciclastics (Newell et al., 1953; Butts, 2014), (2) enhanced in siliciclastic poor, open-marine sediments (Erwin and Kidder, 2000; Butts, 2007), and (3) more common in carbonates than siliciclastics (Newell et al., 1953; Butts, 2004, 2007, 2014). As cited in Butts (2014), an example of the positive correlation between lithology and silicification was identified by Butts (2004) while studying an interbedded carbonate and fine grained siliciclastic outcrop with uniform faunas throughout. It was determined that silicification was significantly more common in the carbonate compared to siliciclastic lithologies. Lancelot (1973) and

(Hinman, 1998) both discussed that certain ions derived from carbonate versus clay minerals influence the rate of silica phase changes. (Kastner et al., 1977) went on to support that diagenetic silica conversion is optimal in carbonates, and retarded by clay sediments (Butts, 2014).

Permeability and Porosity

The ability for silica to infiltrate a deposit is primary for defining that deposit's susceptibility to become silicified. Although largely controlled by other intrinsic and extrinsic factors (including depositional environment and sediment composition); permeability and porosity are here considered one of the 3 major factors for determining proneness for silicification.

As discussed, silicification in carbonate rocks involves the replacement of carbonate material by silica and/or the precipitation of pore-filling silica cement (Hesse, 1989; Flügel, 2004), facilitated by infiltration and circulation of silica saturated fluids. Low-permeability deposits are therefore less likely to become silicificied because silica-saturated fluids are naturally occluded from infiltrating those deposit's pore spaces. The presence of heavy carbonate cement is a common feature which may preclude silicification by decreasing permeability (Butts, 2014), preventing the circulation of fluids which may have otherwise resulted in precipitation of, or replacement by silica. In summary, when conditions are conducive for precipitation of silica and/or dissolution of carbonate cement, lower permeability and porosity levels decrease the susceptibility for a given deposit to become silicified.

3.3.3 Silica Source

The source(s) of silica for silicification of originally non-siliceous sediments in various environments is another element which has been investigated, but not comprehensively defined. Flügel (2004) discussed the three major sources of silica in silicified sediments as being: (1) siliceous tests and skeletal elements of organisms, (2) river input of siliceous solutions from the weathering of continents in semi-arid climates (Laschet, 1984), and (3) silica supplied in solution by hydrothermal volcanic systems. However, in most instances the source of silica is thought to be biogenic (Hesse, 1989; Scholle and Ulmer-Scholle, 2003; Butts, 2014). Moreover, the dissolution of sponge spicules, diatoms, and radiolarians, which are diagenetically unstable compared to siliciclastic grains, is a commonly identified source of silica for the silicification of fine-grained, deep-marine carbonates (Hesse, 1989; Scholle and Ulmer-Scholle, 2003; Flügel, 2004).

3.3.4 Criteria for Silicification

Thin-section and XRD data analysis were used to identify the presence or absence of silicification in identified microfacies. Microfacies were identified as being silicified based on the apparent presence, and relative abundance of authigenic silica present in representative samples. Thin-section samples were analyzed to identify (when present) both authigenic silica and siliciclastic grains (generally in the form of detrital silt). It was important to determine whether siliciclastic grains were present in a sample, because XRD data did not differentiate between those grains and authigenic silica. Once

identified, the relative proportion of authigenic silica compared to the entire sample, and the relative proportion of authigenic silica compared to detrital silica grains were estimated. When applicable, the proportion of authigenic silica in a sample was confirmed and constrained in more detail utilizing XRD data. XRD analysis provided the bulk mineralogy, and hence the volumetric percentage of quartz making up a sample. Considering the previously estimated ratio of authigenic to detrital silica, relatively accurate estimations for the percentage of authigenic silica comprising a sample could be made.

For the purposes of this study, microfacies were defined as 'silicified' if they were estimated to consist of 15-20 percent or more authigenic silica. Samples were defined as chert or as being 'chertified' if 50 percent or more of the sample consisted of authigenic silica.

3.3.5 Identification of Susceptibility Factors

Once microfacies were identified and differentiated by the presence or absence of silicification. A list of the sedimentological characteristics (e.g., lithology, texture, grains, matrix, bedding, presence of burrowing/bioturbation, other sedimentary structures) and mineralogic compositions estimated during petrographic analysis, and from XRD data was compiled for silicified and non-silicified facies. The differentiating factors and substantial variation of significant factors (e.g., abundant bioturbation in silicified microfacies, compared to light bioturbation in non-silicified facies) were then identified by comparing the compiled lists. This methodology enabled identification and

consideration of the factors which likely increased susceptibility for deposits in the FBSC member to become silicified, and thus the interpretation of which deposits in the FBSC member are most prone to silicification.

The determination of microfacies being silicified or not was incorporated into the definition and discrimination of microfacies and correlation associations for this study. Correlation between standard microfacies types and petrophysical properties is difficult and often misrepresentative because the microfacies are not generally defined with consideration to diagenetic overprint (Kostic and Aigner, 2004) as cited in Flügel (2004). Thus, the incorporation of silicification to the defining characteristics of microfacies in this study will improve core-to-log correlation quality, identification of characteristic petrophysical properties, and establishment of signature log responses.

3.4 Core-to-Log Correlation

The third objective of this investigation was to correlate wireline log data with core data to generate calibrated log responses (electrofacies) for identified FBSC member facies.

The methodology for completing this objective involved organizing defined microfacies into ‘correlation associations’; followed by using crossplotting and additional log analysis techniques to identify and coordinate the petrophysical data associated with those correlation associations, and establish representative log signatures

as a means to enable the prediction of their occurrence in areas where core and additional subsurface data are not available.

3.4.1 Correlation Associations

Analysis of conventional core and accompanying data allowed for the identification of microfacies based on sedimentological characteristics and mineralogical composition. To facilitate core-to-log correlation (i.e., relation of petrophysical properties to microfacies) those microfacies were grouped into 'correlation associations' similarly the methodology used by Prélat et al. (2015), although in this study, on the basis of having similar: (1) major constituents (grain and matrix type and composition), (2) mineralogy, texture, and depositional fabric, (3) visible pore space, and (4) diagenetic features (here silicification or cementation); which are the factors outlined by Flügel (2004) as essential to consider when establishing relationships between microfacies and physical properties. Using this methodology, five correlation associations were identified which incorporate the eleven previously defined microfacies.

3.4.2 Wireline Log Analysis

Wireline log responses from the cored well of this study were cross-plotted to establish the combination of petrophysical characteristics defining each correlation association.

Asquith and Krygowski (2004) identified six crossplots applied by Pickett (1977), Asquith (1979), and Watney (1979, 1980), amongst others to establish the relationship between log data and carbonate lithology (Table 3). These cross-plots were a graphical way to interpret the interplay between the log measurements (e.g. gamma-ray, resistivity, porosity/density) used to evaluate and correlate formation lithology (Asquith and Krygowski, 2004).

Table 3. Carbonate lithology correlation crossplots applied by Pickett (1977), Asquith (1979), and Watney (1979, 1980), as cited in Asquith and Krygowski (2004).

Δt (*interval transit time*)	vs.	φ_N (*neutron porosity*)
ρ_b (*bulk density*)	vs.	φ_N (*neutron porosity*)
ρ_b (*bulk density*)	vs.	Δt (*interval transit time*)
R_t (*deep resistivity)*	vs.	φ_N (*neutron porosity*)
GR *(gamma ray)*	vs.	φ_N (*neutron porosity*)
R_t (*deep resistivity)*	vs.	φ_S (*sonic porosity*)

The log suite corresponding to the cored well for this investigation included gamma-ray (GR), bulk-density (RHOB), neutron-porosity (NPHI) and density-porosity (DPHI) (2.71 g/cm3 matrix density), invaded zone (Ri) and uninvaded zone ‘deep’ (Rt) resistivity, and photoelectric (Pe) curves. There was no sonic log available for the cored interval, so the three cross-plots which incorporate sonic log data were not used in this investigation.

The three remaining crossplots (*ρ_b (bulk density) vs. φ_N (neutron porosity)*, *R_t (deep resistivity) vs. φ_N (neutron porosity)*, and *GR (gamma ray) vs. φ_N (neutron porosity)*) were used to plot the log responses from the conventionally cored interval. Areas which delineate correlation association clusters were outlined on each crossplot, which enabled a visual-graphical representation for the range of petrophysical properties characterizing each correlation association. Average porosity (%), bulk density (g/cm^3), resistivity (ohmm), gamma-ray (gAPI), photoelectric factor, neutron- and density-porosity crossover (barns/electron), and apparent matrix density (g/cm^3) values were calculated for each correlation association. Finally, histograms displaying the distribution of petrophysical properties for each correlation association were generated, creating a third aid for comparing the log responses representative of each correlation association. Analysis of log properties, core-to-log correlation, and the range of petrophysical characteristics defining each correlation association were constrained according to methodology outlined by Doveton (1994), Prélat et al. (2015) and Asquith and Krygowski (2004), among others.

Electrofacies Analysis

In continuation of the methodology outlined by Prélat et al. (2015), the constrained petrophysical characteristics for each correlation association were used to generate calibrated log responses (electrofacies); which can be applied to extrapolate the distribution of those correlation associations away from the cored interval.

The definition of electrofacies was coined by Serra and Abbott (1982), who extended the definition of lithofacies to incorporate well log data, establishing electrofacies as, 'geologic facies characterized by all available logging data at any given depth interval'. To generate electrofacies, the petrophysical parameters for a given set of facies, (or in this study 'correlation associations') must be defined. That data is then input to a program which uses those defined parameters to calibrate a petrophysical signature and generate representative electrofacies for each correlation association.

For this investigation, porosity (%), density (g/cm3), resistivity (ohmm), neutron- and density-porosity, and gamma-ray (gAPI) data from the cored interval were input to the 'Facimage' module of Paradigm's Geolog software, which used a Multi-Resolution Graph-based Clustering (MRGC) method to calibrate representative petrophysical signatures and generate electrofacies for the 5 defined correlation associations.

With electrofacies established, the 'neural network log prediction' function of the Facimage module can be used to predict the likelihood that a defined electrofacies, and hence correlation association is present at a given depth interval based on measured log data. The program identifies a correlation association as being present if more than a user defined percentage of log parameters match with a defined electrofacies.

This methodology enabled the estimation of sedimentary facies, and thus interpretation of depositional framework and associated reservoir and non-reservoir characteristics using readily available conventional log suites. Considering the high cost and difficulty in acquiring subsurface rock data, this process is valuable because it eliminates the need for that data to make interpretations which are normally not

achievable at the scale provided by seismic and conventional log data alone. It should be noted that an initial core dataset is necessary for establishing electrofacies representative of the facies present in a given interval.

4. RESULTS

During this study, detailed description of 204 feet (62.2 m) of core, petrographic analysis of 35 representative thin-sections, and consideration of XRD data for 6 associated samples resulted in the identification of seven macrofacies, and eleven microfacies. To facilitate the correlation of microscale facies and associated petrophysical properties (core-to-log correlation), microfacies were grouped into five 'correlation associations' on the basis of having similar: matrix and grain type and composition, mineralogy and depositional texture/fabric, visible pore space, and diagenetic features. The correlation associations defined for this investigation are 1. Limestone, 2. Mudstone 3. Silicified, to heavily cemented limestone and calcareous chert, 4. Mixed argillaceous, muddy chert and siliceous—calcareous mudstone, and 5. Intraclastic floatstone and rudstone. Figure 7 and figure 8 provide images and descriptions of the macrofacies identified throughout the cored interval, and figures 9-24 provide an overview of the macroscale, petrographic, and mineralogic features associated with each identified and defined microfacies. Table 6 provides a comparison of characteristics for silicified and non-silicified facies to support interpretation of the factors which increased a given deposits susceptibility to become silicified. Table 12 lists the characteristic petrophysical values derived from log data defining each correlation association, and Figure 35 provides a visual summary of the distribution and range of the same log-derived petrophysical values characterizing each correlation association.

Appendix A provides the complete digitized version of the detailed core description conducted over the interval utilized in this study, in addition to a detailed, section by section written description of the core interval. Appendix B contains photographs of all the thin-sections utilized for this study. Appendix C contains the core-to-log correlation cross-plots generated from the eight measured and calculated log measurements utilized to characterize petrophysical properties of the five correlation associations identified in this study. Histogram plots summarized in (Figure 34) which display the range and distribution of the same measured and calculated log measurements are located in Appendix D. Lastly, Appendix E contains the raw data, and associated semi-quantitated results for the six XRD samples analyzed for this study.

4.1 Facies Analysis

Seven macrofacies and eleven microfacies from the First Carbonate Member of the Bone Spring Fm. were identified and defined based on detailed core description, petrographic studies, and XRD data analysis.

4.1.1 Macroscopic Facies

The seven identified macro-facies are briefly described in Table 4, and illustrated in figure 7 and figure 8. Depicted are the general, macro-scale characteristics of the First Bone Spring Carbonate Member facies which were identified during the initial core description, and used as a foundation for identifying the eleven associated microfacies.

Table 4. Characteristics of the First Bone Spring Carbonate Member macrofacies.

Facies	Brief Description
Massive Limestone	Massive limestone beds consisting of light gray to gray, and faintly brownish-gray wackestone and packstone. Sectionally cemented and/or silicified, occasionally vaguely laminated and silty (Figure 7a, b).
Laminated Limestone	Laminated, dark gray, gray, to greyish-brown calcareous mudstone and wackestone to packstone. Planar to irregular stratification (Figure 7c, d).
Bioturbated Limestone	Slightly to highly bioturbated, gray to faintly bluish-gray silty wackestone and packstone. Sectionally silicified and cemented, irregular stratification (Figure 7g, h).
Pelagic and Hemipelagic Mudstone	Massive to faintly laminated greyish black to dark grey mudstone to silty and/or calcareous mudstone (Figure 7e, f).
Floatstone & Rudstone	Heavily cemented, intraclastic, skeletal rudstone (Figure 8c, d) and dark gray to gray heavily deformed, intraclastic floatstone (Figure 8a, b). Contorted to chaotic, highly irregular stratification.
Chert	Heavily bioturbated to 'cloudy', dark gray to grayish-blue calcareous chert (Figure 8e), and dark gray to dark brownish-gray muddy (argillaceous) chert (Figure 8f). Irregular stratification.
Mixed Limestone-Mudstone-Chert	Interlaminated to mixed, often heavily bioturbated and cemented limestone, chert, and mudstone. Dark grey and dark grayish-blue to gray and greyish-blue 'cherty-limestone' to 'limey-chert', and dark greyish-brown to dark gray 'muddy chert' to 'cherty-mudstone'. Planar to irregular stratification (Figure 8g, h).

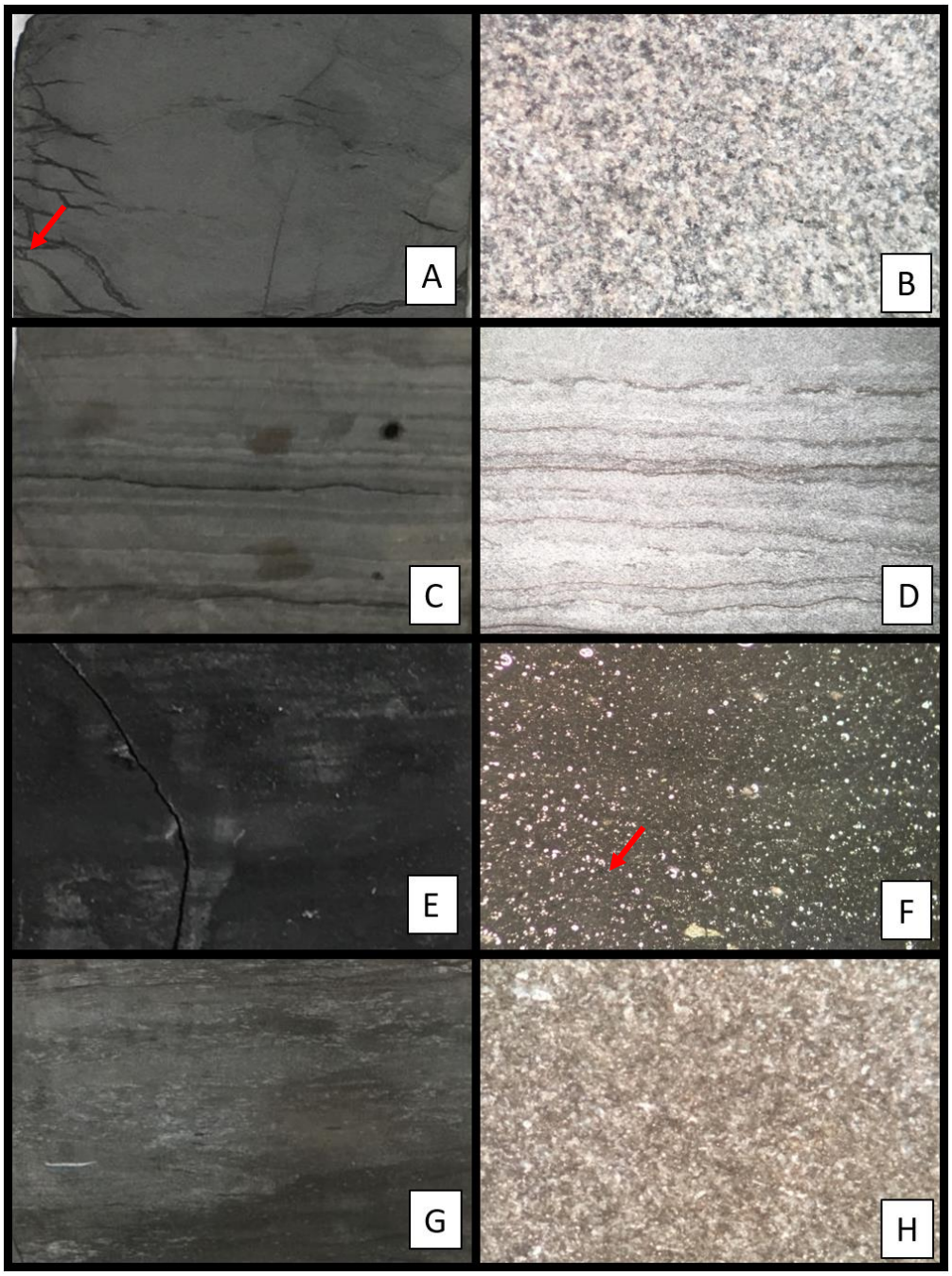

Figure 7. a) Massive limestone, note mineralized fractures (arrow). b) Massive limestone core surface at 50x magification, note wackestone to packstone texutre. c, d) Laminated limestone with planar to irregular stratification, color changes reflect changes in concentration of detrital silt, skeletal grains, clay material, and carbonate mud. e) Massive to faintly laminated pelagic, organic mudstone. f) pelagic, organic mudstone core surface at 10x magnification, grains consist of silt and sponge spicules (arrow). g) bioturbated limestone, bioturbation recognized by irregular stratification and lighter color due to higher concentration of skeletal grains relative to surrounding material. h) bioturbated limestone core surface at 10x magnification, not irregular stratification.

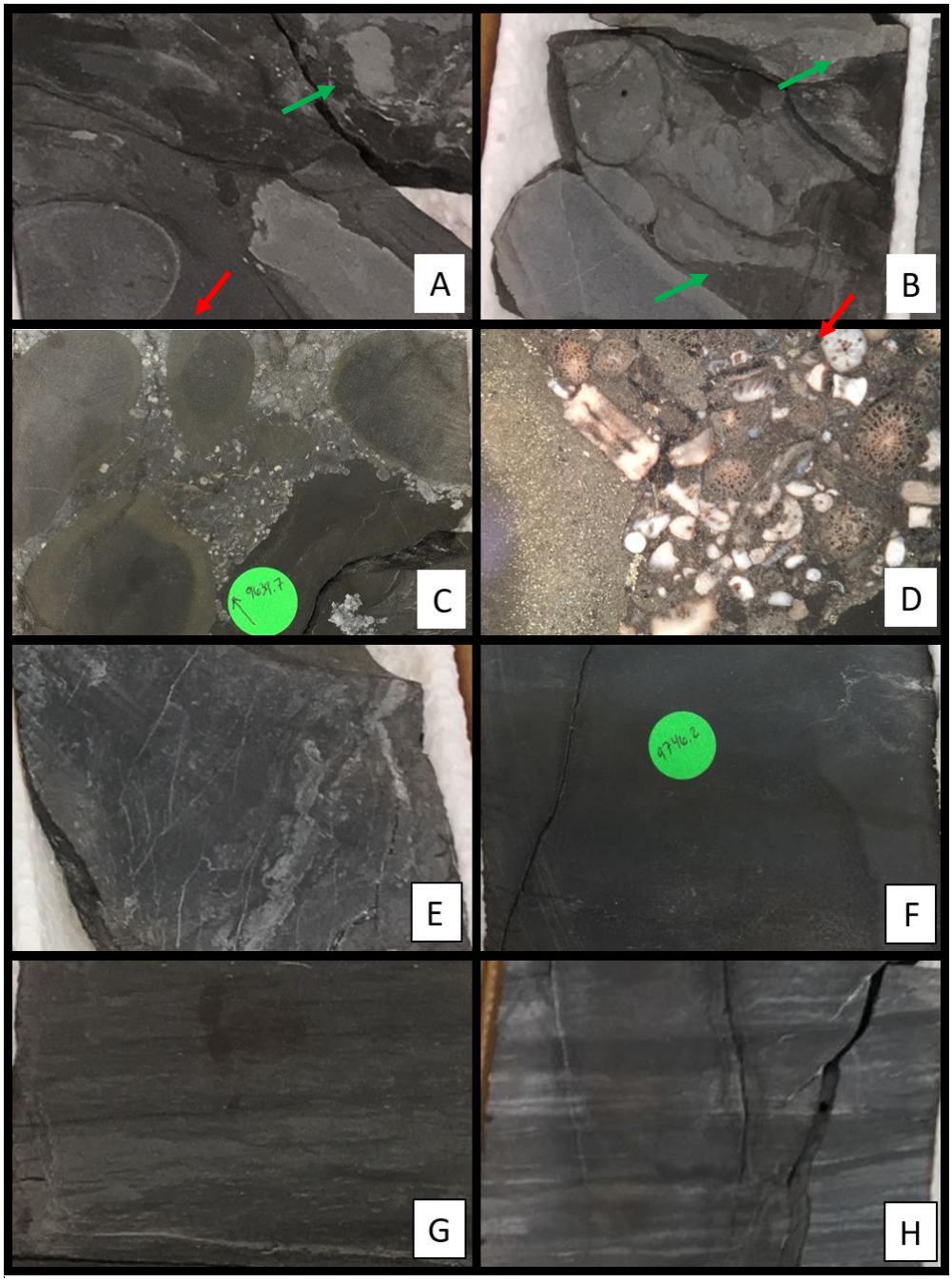

Figure 8. a, b) heavily deformed, intraclastic floatstone debrite deposit, note mudstone matrix (red arrows), contorted grains (green arrows), and chaotic, irregular stratification. c, d) Intraclastic skeletal rudstone debrite deposit, note grain supported texture and abundant, irregularly stratified skeletal grains. e) heavily bioturbated calcareous chert, note abundant fractures, irregular stratification, and 'cloudy texture'. f) dark brownish grey-blue muddy, argillaceous chert. g) interlaminated to mixed 'silicified mudstone' to 'muddy chert'. h) interlaminated dark greyish-blue to gray and greyish-blue 'cherty-limestone' to 'limey-chert'.

4.1.2 Detailed Core Description

Detailed core description (appendix A) was split into fourteen core depth intervals, based on significant changes in lithology and/or depositional texture, or gaps represented by intervals where core was not recovered. Observations were made on the bed to bed scale, and care was taken to identify probable sedimentary structures, textures, fabrics, skeletal grains, and bedding. Degrees of apparent cementation, bioturbation, and reaction to diluted HCl were also specifically noted.

Core descriptions were digitized using *DigitCore Core Logging and Data Integration Software*©, which allowed for the simultaneous, side by side visualization of wireline log data, core images, correlation association intervals, and detailed core descriptions.

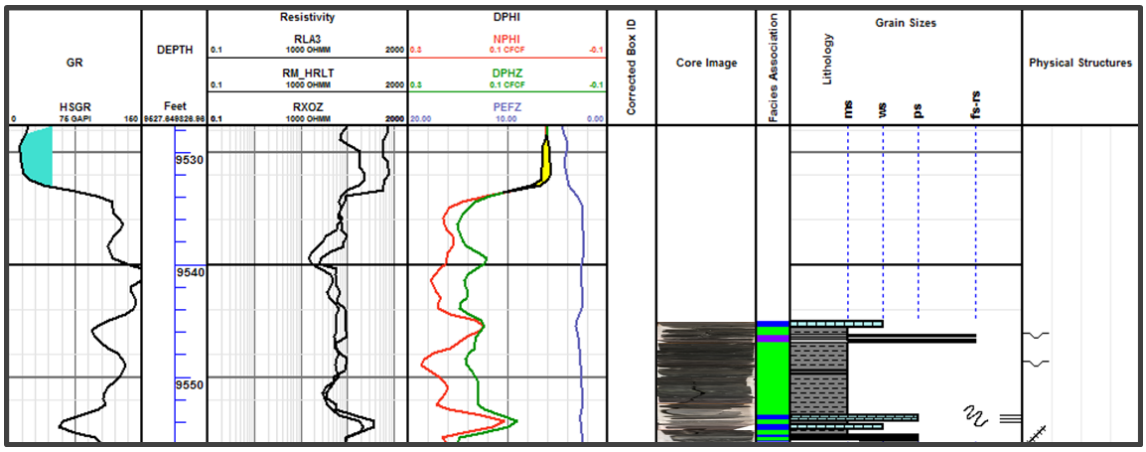

Figure 9. Digitized core description example segment at the 1:120 scale. Core descriptions were digitized using *DigitCore Core Logging and Data Integration Software*©, which allowed for the simultaneous side by side visualization of wireline log data, core images, correlation association intervals, and detailed core descriptions.

4.1.3 Microfacies

Below is a description of the identified microfacies which make up the Upper Leonardian FBSC member of the Bone Spring Fm. Microfacies were defined on the basis of sedimentological characteristics and mineralogical composition. The identified microfacies were later grouped into five correlation associations. Microfacies within these associations display similar: major constituents; mineralogy, texture, and depositional fabric; visible pore space; and diagenetic features.

Microfacies 1A. Spiculitic Mudstone to Sparse Wackestone

This microfacies is a mud-supported, highly micritic wackestone. Matrix material consists of carbonate mud, and minor clay and organic material, supporting silt-sized calcareous skeletal grains/fragments and sponge spicules (figure 9c). Micritization of grains and matrix material, and occasional microspar replacement occurs throughout.

Associated deposits consist of well sorted, mud/clay to very fine (<0.02 – <0.125 mm) grains, with very minute to no visible porosity (only seen in microfractures, possibly core induced). Beds appear grey in color, and are massive to vaguely laminated with some preferential orientation of elongate grains and minor plastic deformation, both of which are indicative of mechanical compaction. Upper contacts are sharp-irregular and occasionally gradational, lower contacts are predominantly gradational-interbedded.

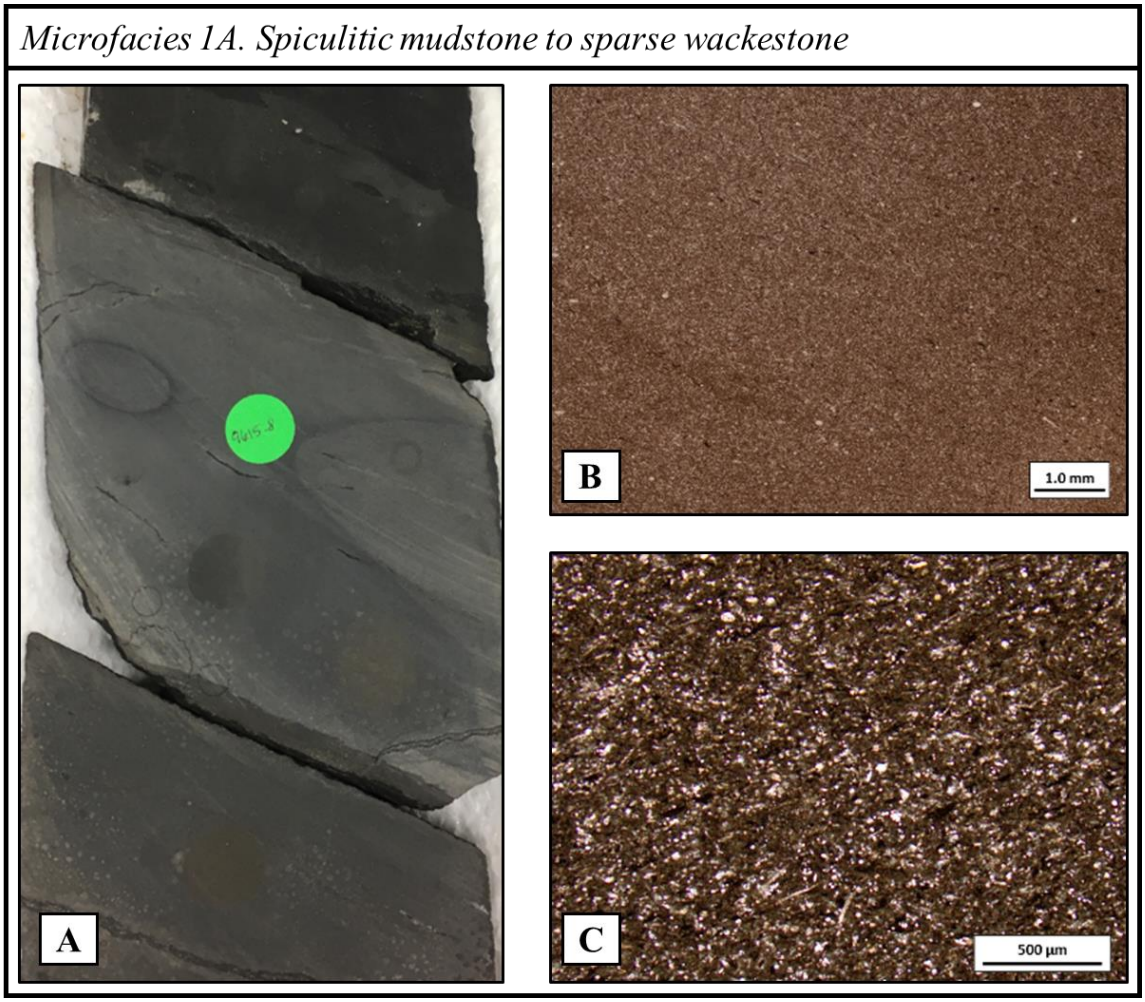

Figure 10. Macroscale and petrographic characteristics of microfacies 1A, spiculitic mudstone to sparse wackestone.

Microfacies 1B. Organic, Fossiliferous Wackestone to Packstone

This microfacies is a primarily mud-supported, organic- and skeletal-rich, wackestone to packstone. Matrix is composed of black to very dark grey-brown organic material, micrite, and clay. Grains consist of sponge spicules, detrital silt, occasional pyrite, and abundant bioclasts (figure 10c). Skeletal grains include brachiopods,

ostracods, crinods, forams, and additional undifferentiated skeletal fragments. Bioclasts are primarily calcareous, and frequently replaced by coarse calcite cement.

Deposits are poorly to moderately sorted with grain size ranging from silt to medium (< 0.05 – .4 mm). Porosity is very low, and only visible in occasional horizontal micro-fractures (figure 10c). This microfacies is generally laminated and displays normal grading. Mud-supported wackestone typically increases in skeletal content towards the bottom of deposits, grading in to more grain-supported skeletal packstone characterized by widespread calcite cement and replacement of fossil grains, and occasional silicification of fossil grains. Preferential orientation of elongated grains, and occasional micritization of grains and matrix material also occurs throughout. Lower contacts are sharp, upper contacts are gradational, typically in to *microfacies 1A*, and subsequently into *microfacies 2A or 2B.*

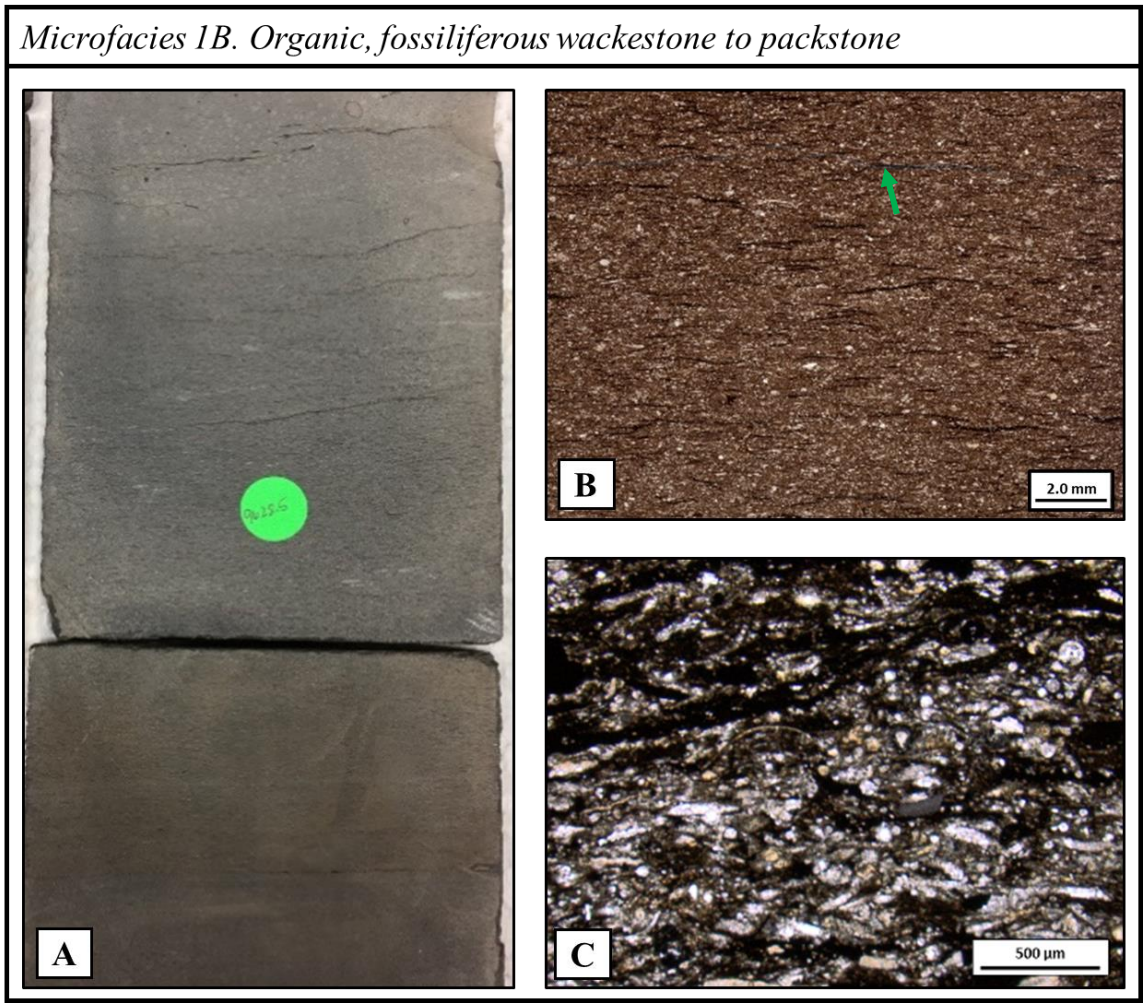

Figure 11. Macroscale and petrographic characteristics of microfacies 1B, deposits are mud-supported, organic- and skeletal-rich, wackestones to packstones. B) Note porosity (blue) in faint semi-horizontal microfacture (green arrow).

Microfacies 1C. Silty, Clay-rich Wackestone – Packstone

This microfacies is a mud-supported, laminated to bioturbated, silty, argillaceous wackestone-packstone (figure 11). Matrix is composed of micrite and clay material, patchy carbonate cement, and minor organic matter. Grains consist of detrital silt, sponge spicules, and various skeletal grains, including foraminifera, echinoderms,

brachiopods, gastropods, and additional undifferentiated skeletal fragments. Bioclasts are primarily composed of calcite, but occasionally replaced by silica. A large cephalopod was also noted, it contains preserved organic material and has undergone replacement by calcite cement.

Characteristic deposits are moderately sorted with grain sizes ranging from silt to very fine, with the exception of the noted cephalopod which is approximately 5-6 mm in diameter. Visible porosity is very low to non-existent except for occasional micro-fractures/stylolites, though these may have been induced during extraction of the core. Minor silica replacement, calcite replacement and minor calcite cementation are present. Beds are laminated to bioturbated throughout; laminations are distinguished by subtle variations in color which reflect changes in concentration of detrital silt, skeletal grains, clay material, and carbonate mud (figure 11a, c). Bioturbation is also marked by a decrease in mud and clay content, and an increase in bioclastic grains and cement. Upper contacts are difficult to discern, lower contacts are generally gradational-interbedded, becoming more mud-rich. XRD data for this microfacies indicates that quartz and calcite composition is nearly equal (figures 11, 12); quartz content is predominantly associated with silt grains as opposed to the presence of authigenic silica.

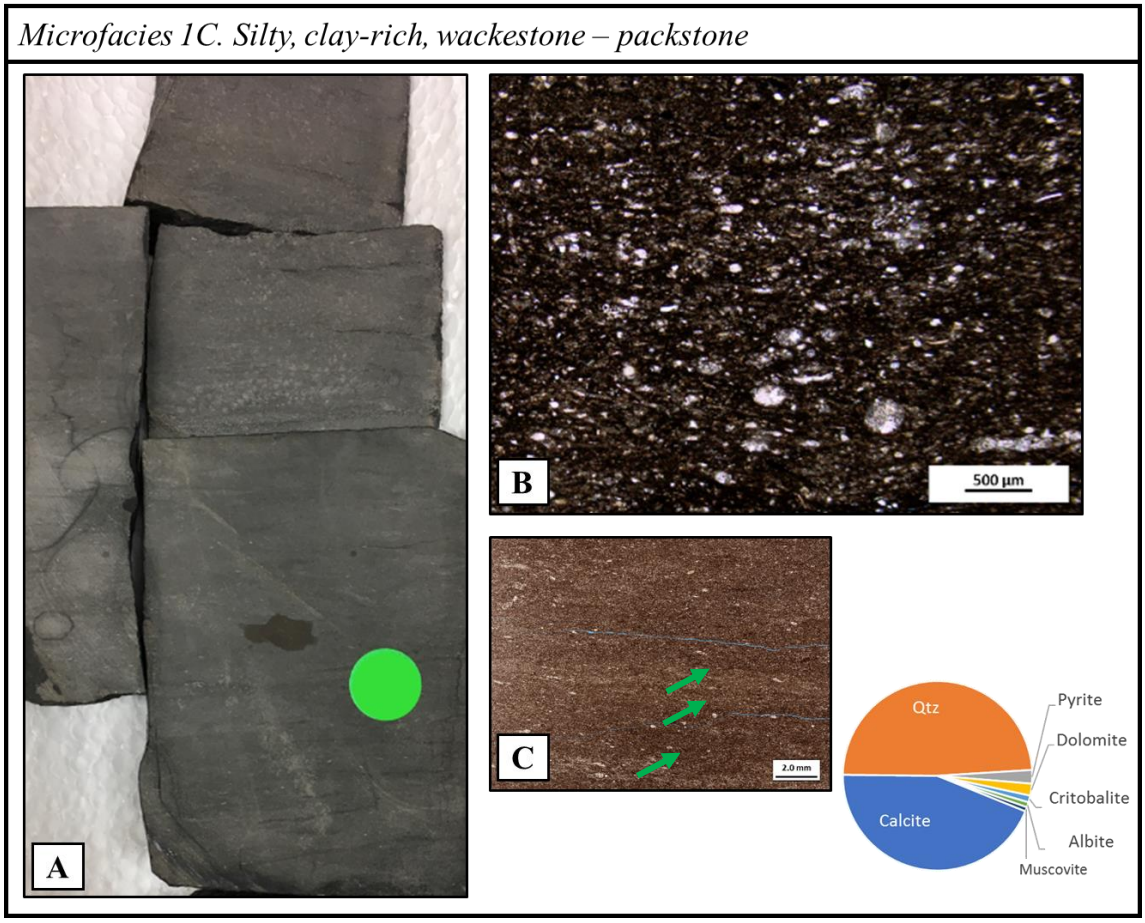

Figure 12. Macroscale and petrographic characteristics of microfacies 1C. Deposits are mud-supported, laminated to bioturbated, silty, argillaceous wackestone-packstone. Laminations are distinguished by subtle variations in color which reflect changes in concentration of detrital silt, skeletal grains, clay material, and carbonate mud (arrows).

XRD - Microfacies 1C		
Sample B - (9,706.5')		
Mineral	**Counts**	**%**
Quartz	16850	48.84
Calcite	15200	44.06
Pyrite	800	2.32
Dolomite	700	2.03
Cristobalite	400	1.16
Albite	300	0.87
Muscovite	250	0.72

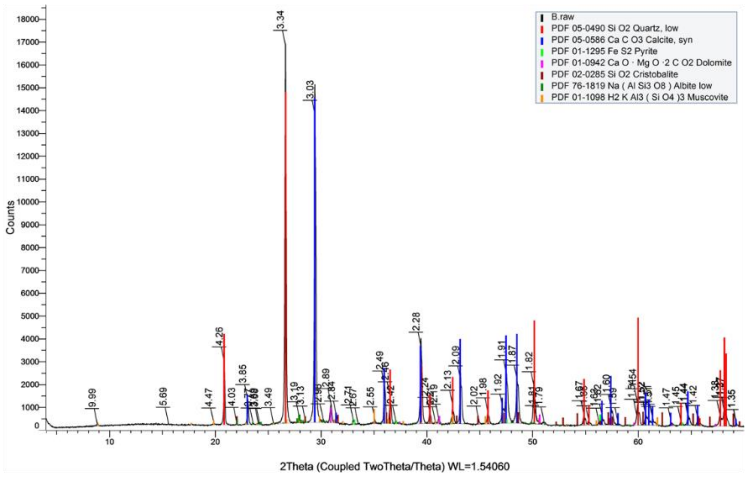

Figure 13. XRD bulk mineralogy data for microfacies 1C

Microfacies 1D. Spiculitic—Fossiliferous, Sparry Packstone

This microfacies consists of massive to vaguely laminated, mud- and grain-supported, spiculitic and/or bioclastic, sparry wackestone-packstone to packstone (figure 13). Deposits are characterized by a mixed, fine-grained micritic and sparry calcite matrix with calcite alteration and cementation, and occasional (patchy) silica cement occurring throughout. Moderately sorted, silt to very fine sized grains represent approximately fifteen to sixty percent or more of deposits, and consist of sponge spicules, skeletal fragments, and silt-sized (bioclastic) calcite grains. Bioclasts are predominantly calcareous or replaced by calcite, though minor silica replacement of grains occurs as well. No visible porosity, except for occasional sub-horizontal micro-fractures which were likely induced during core extraction; evidenced by the presence of other fractures and micro-fractures which are filled with coarse calcite and/or silica cement.

Deposits are massive to vaguely laminated, with mineralized fractures and minor preferential orientation of elongate grains. These features, in addition to the occurrence of sutured skeletal grains, stylolites, and dissolution seams indicate that this microfacies likely underwent mechanical compaction/pressure-solution, in addition to alteration and cementation by calcite cement. XRD data collected (figures 13, 14) confirms the petrographic interpretation of this microfacies as consisting predominantly of calcite grains and cement, as the data indicates that associated deposits are almost entirely composed of calcite.

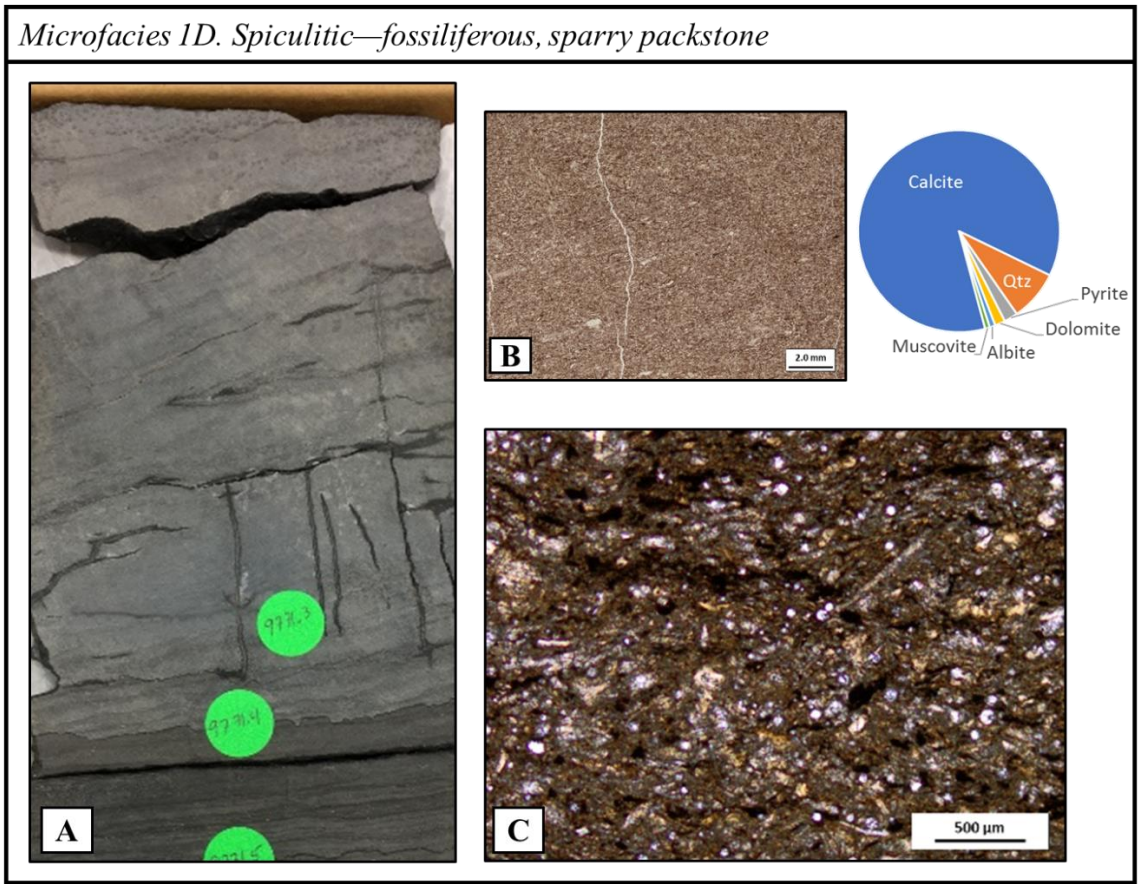

Figure 14. Macroscale and petrographic characteristics of microfacies 1D. Deposits are massive to vaguely laminated, mud- and grain-supported, spiculitic and/or bioclastic, sparry wackestone-packstones to packstones.

XRD - Microfacies 1D		
Sample C - (9,718.3')		
Mineral	**Counts**	**%**
Calcite	23450	86.37
Qtz	2200	8.10
Pyrite	600	2.21
Dolomite	450	1.66
Albite	250	0.92
Muscovite	200	0.74
Critobalite	0	0.00

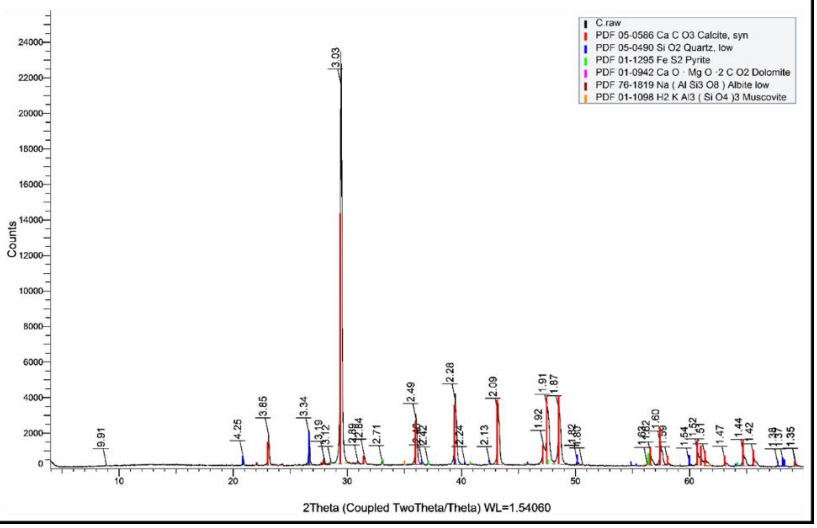

Figure 15. XRD bulk mineralogy data for microfacies 1D

Microfacies 2A. Organic, Spiculitic Mudstone—Silty Mudstone

This microfacies is a black to dark grey, highly organic spiculitic mudstone characterized by a nearly black to dark brown and brown matrix composed of organic and clay material. Grains consist of variable amounts of sponge spicules, undifferentiated microfossils, detrital silt, and occasional pyrite (figure 15B). Spicules and microfossils are predominantly to entirely siliceous, which is further supported by the non-existent to trace representation of calcite in the composition of this microfacies indicated by XRD analysis (table 5, figure 15). Siliceous microfossils may be diatoms and/or radiolarians.

This microfacies is moderately to well sorted, with mud to silt (and rarely, very fine) sized grains (< 0.005 to .05 mm; rarely ~0.1 mm). Very little to no visible porosity, though significant organic porosity likely exists. Associated deposits are generally massive to faintly laminated, with little to no bioturbation or major sedimentary

structures. Lower contacts are generally sharp to slightly gradational, and upper contacts are typically sharp-irregular, to occasionally slightly gradational and interbedded.

Table 5. XRD bulk mineralogy data for microfacies 2A.

XRD - Microfacies 2A		
(9,620.0')		
Mineral	**Counts**	**%**
Quartz	21500	94.3
Pyrite	800	3.5
Calcite	500	2.19

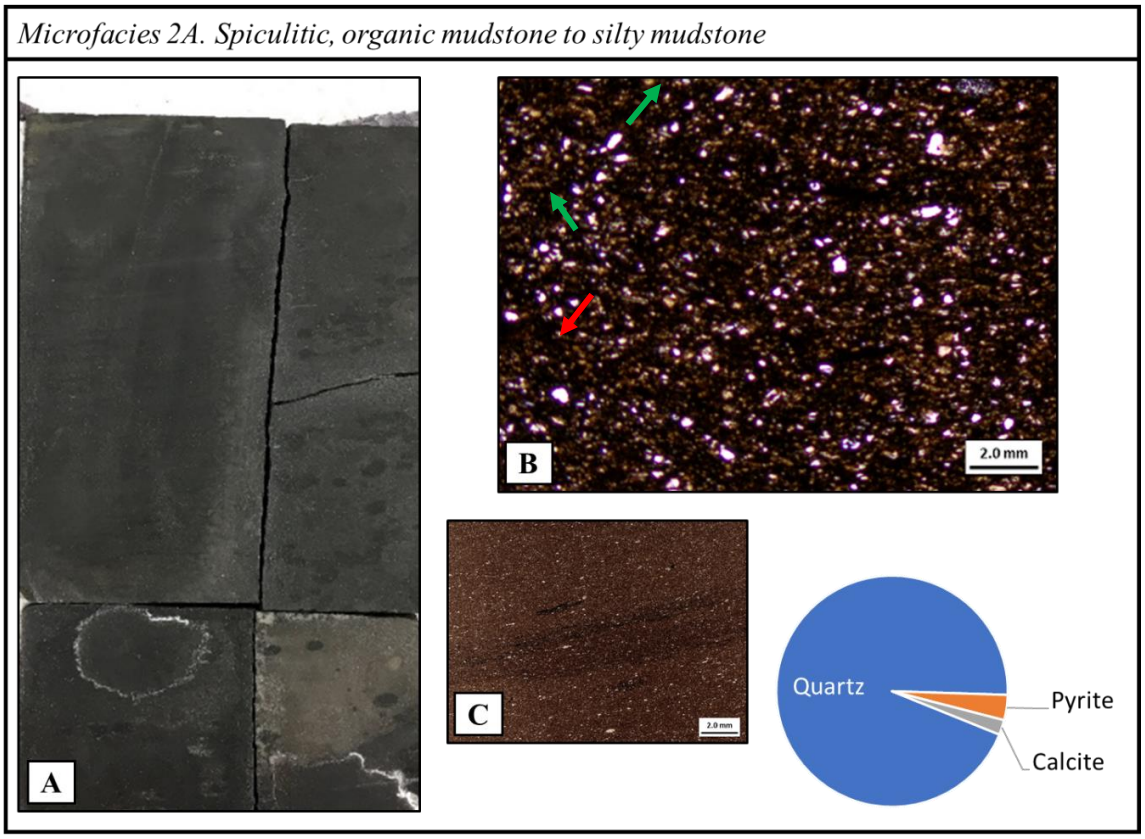

Figure 16. Macroscale and petrographic characteristics of microfacies 2A. Deposits are black to dark grey, highly organic spiculitic mudstones. Presence of pyrite (black, opaque) (red arrow) indicates the presence of organic material. Note sponge spicules (green arrows).

Microfacies 2B. Calcareous Mudstone to Silty Mudstone

This microfacies is similar to microfacies 2A in texture, fabric, and grain type, but has a matrix comprised of carbonate mud, in addition to clay content and organic material (figure 16). Grains are mud/clay to very fine (<0.02 – <0.1 mm) in size and include variable amounts of sponge spicules, detrital silt, and silt sized skeletal grains/fragments. Spicules are siliceous to calcified, indicating probable calcite replacement of biogenic opal.

This microfacies is generally well sorted and is dark gray to greyish-tan-gray, with little to no visible porosity, though organic porosity is likely present, similarly to in *microfacies 1*. Fabric is generally massive to faintly laminated, usually with gradational upper contacts, and sharp-irregular lower contacts. Macroscopic factors for differentiating this microfacies from *microfacies 1* include a lighter, slightly brownish-tan-gray tint in color, and most reliably, surface effervescent reaction to HCl related to the presence of carbonate mud.

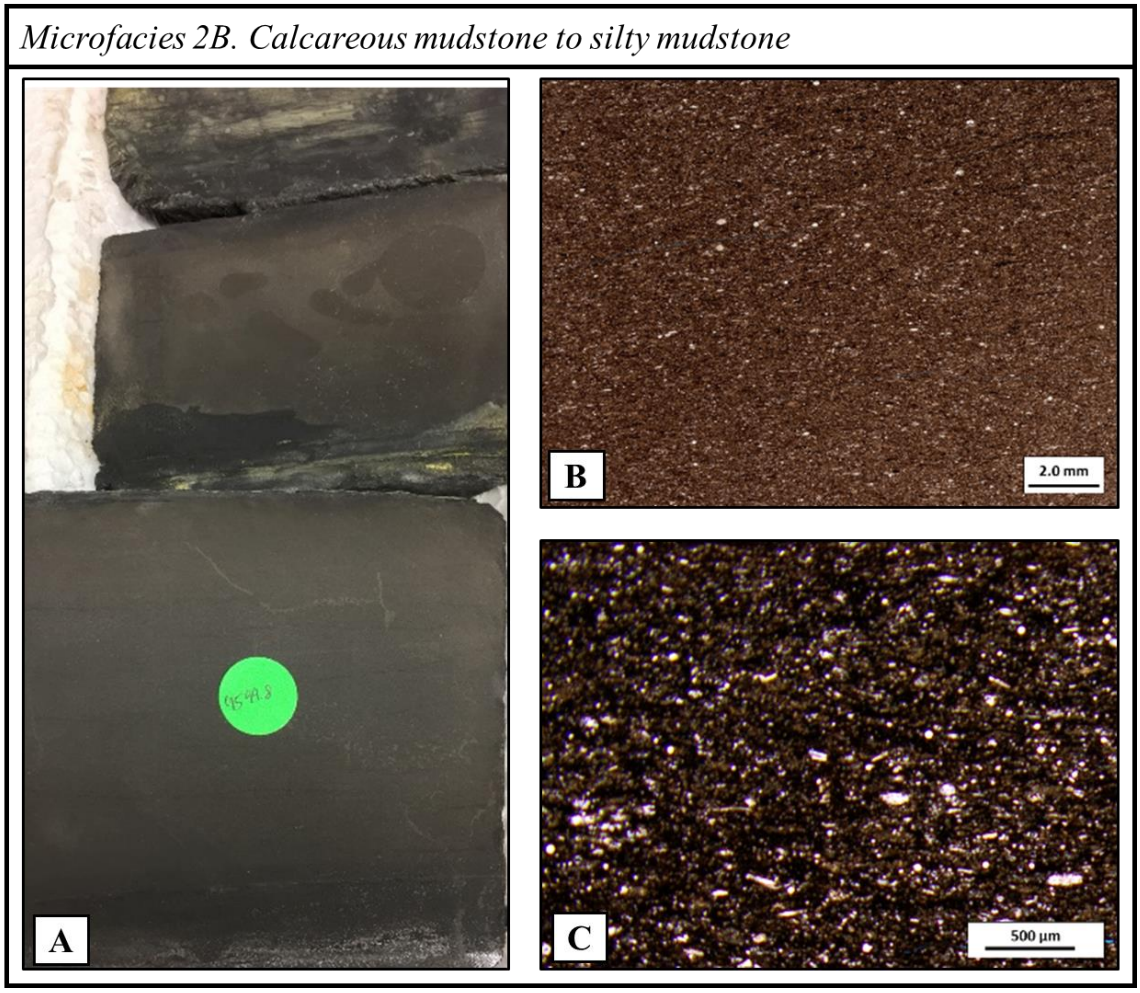

Figure 17. Macroscale and petrographic characteristics of microfacies 2B. Deposits are similar to those of MF2A but with relatively higher concentrations of carbonate mud and calcite replacement of grains.

Microfacies 2C. Bioturbated Siliceous—Silty Mudstone

This microfacies is characterized by bioturbated, siliceous to silicified, silty to calcareous mudstone (figure 17). Matrix is composed of clay, carbonate mud, and minor organic material, with occasional patches of silica cement. Grains are mud/clay to silt and occasionally very fine in size and include detrital quartz silt, sponge spicules,

undifferentiated microfossils/skeletal fragments, and silt sized calcite bioclasts. Spicules are dominantly replaced by calcite cement, but are occasionally silicified.

Characteristic deposits for this microfacies are moderately sorted, massive to faintly laminated with moderate to heavy bioturbation and burrowing throughout. Minor inter- and intra-granular (dissolution?) to intercrystalline, and microfracture porosity is visible. Sub-horizontal (~2-20°) zoophycos burrows are recognized and are somewhat characteristic for this microfacies (figure 17a, b). These, and additional burrows and bioturbation are marked by a decrease in mud and clay material, and a significant increase in bioclastic grains and cement. Burrow filling cement is primarily calcite, though silica cement is also present and occurs in patches. Lower contacts are sharp to gradational, and upper contacts are sharp to possibly scoured; confidence for identified contact types in for this microfacies is relatively low.

This microfacies is best differentiated from *microfacies 1 & 2* based the notable presence of moderate to heavy bioturbation and burrowing, and on a characteristic dark gray-brown color compared to the grey-black to dark gray colors associated with the aforementioned microfacies. Reaction to HCl is typically mild to absent throughout deposits, with the exception of burrowed and/or bioturbated areas which generally effervesce moderately. It may be worth noting that this microfacies is commonly occurs in close proximity silicified intervals.

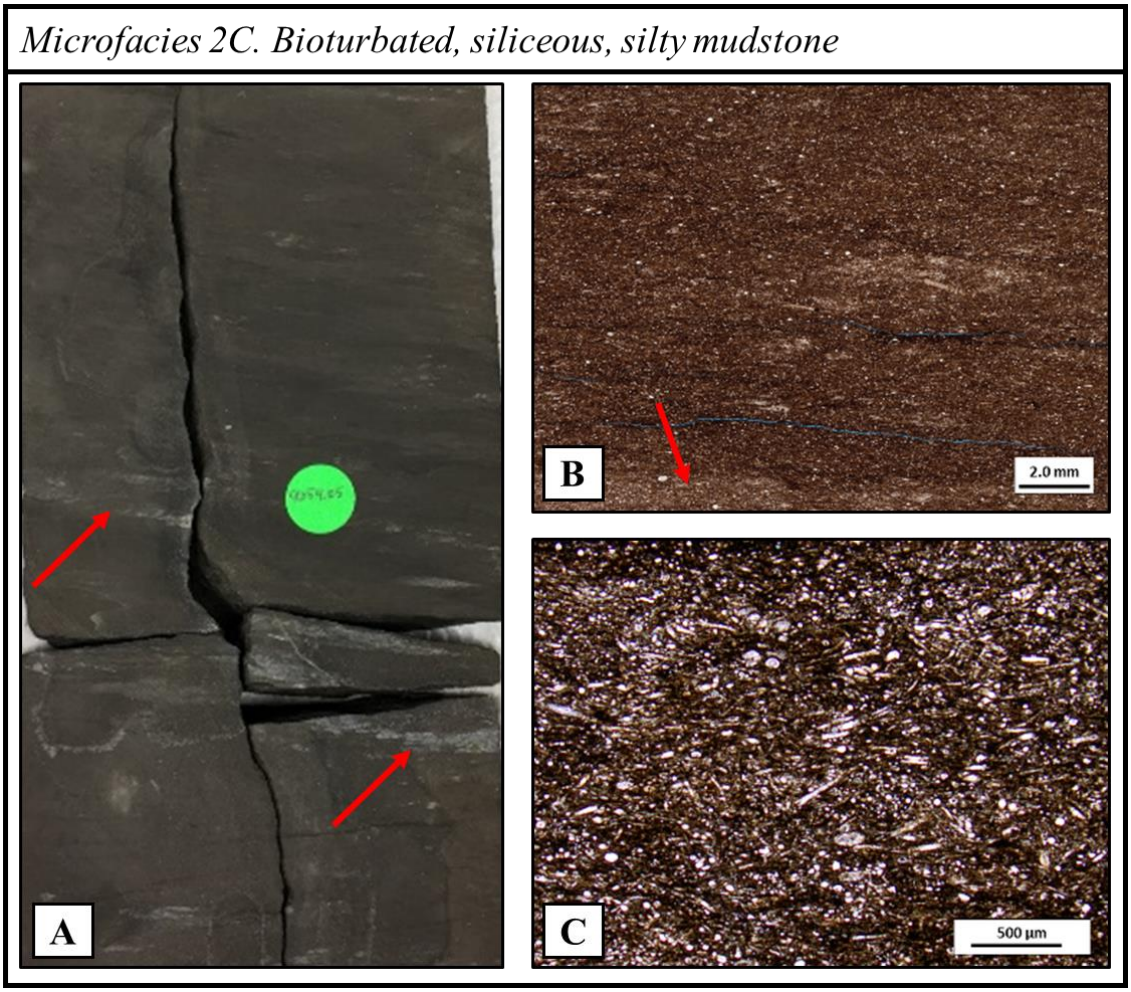

Figure 18. Macroscale and petrographic characteristics of microfacies 2C. Characteristic deposits are bioturbated, siliceous to silicified, silty to calcareous mudstones. Sub-horizontal (~2-20°) zoophycos burrows are recognized and are somewhat characteristic for this microfacies (arrows).

Microfacies 3A. Silicified to Heavily Cemented Limestone and Calcareous Chert

This microfacies consists of deposits with mixed to interlaminated lithologies drawn from calcareous chert, and heavily, variably silicified and cemented limestone endmembers. Hence, characteristic deposits can be described on the macro-scale as mixed or interlaminated, cherty-limestone to limey-chert, reflecting relative abundance between the two end-members; though both end-members also occasionally occur in

relative absence of the other. The limestone deposits incorporated by this microfacies are heavily silicified to cemented variations of mf 1B and 1D, in which all or nearly all matrix material has been removed and/or replaced by heavy silica and calcite cements.

Calcareous chert deposits incorporated by this microfacies consist of highly bioturbated, principally grain-supported, spiculitic to bioclastic calcareous chert. Matrix consists of micrite and clay material, but has primarily been replaced by silica cement (silicified), and intermittently undergone calcite alteration and cementation. Moderately sorted, silt to very fine sized grains and bioclasts are abundant and consist of sponge spicules, radiolarians, detrital silt, and additional undifferentiated skeletal fragments. Bioclasts occur both silicified and calcareous, with sponge spicules primarily replaced by coarse calcite cement. Porosity is very low, with almost imperceptible intercrystalline porosity, and an example of visible porosity along one side of a mineralized fracture.

Texture and stratification are often obscured or ‘cloudy’ as a result of heavy bioturbation and silicification, though characteristic deposits can be described as massive to vaguely and irregularly laminated, and are notably marked by the relative abundance of mineralized fractures. Concentration of cements and bioclasts appear to have a direct relationship, with the highest concentrations of each occurring in bioturbated or otherwise disturbed (often difficult to define) areas of associated deposits (figure 18); while less altered portions consist of relatively higher amounts of carbonate mud and clay. This microfacies frequently occurs as mixed or interlaminated with silicified to heavily cemented limestones (versions of *mf 1B, 1D*), and is associated with basal contacts that are slightly erosive to sharp, and gradational upper contacts. XRD data

indicates that the bulk composition of this microfacies (figure 19) is dominantly quartz (authigenic and detrital) with minor calcite.

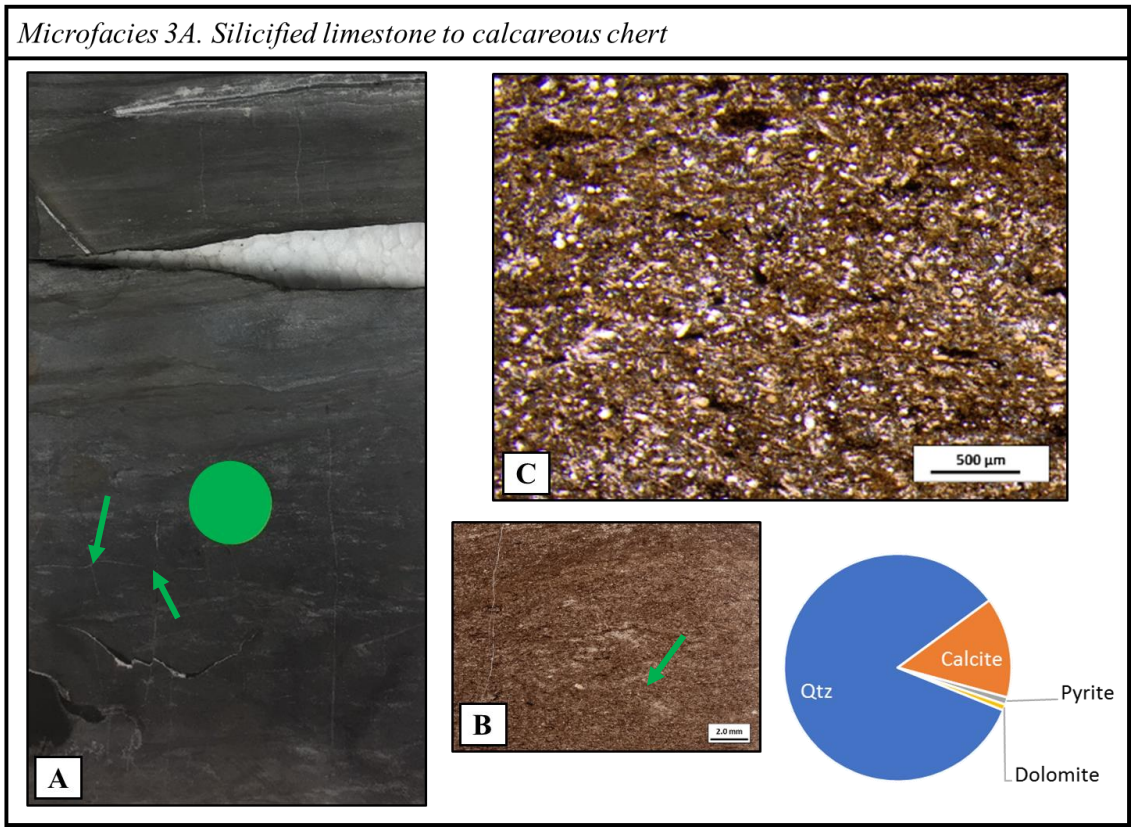

Figure 19. Macroscale and petrographic characteristics of microfacies 3A. Deposits consist of mixed to interlaminated silicified limestone and calcareous chert. Highest concentrations of cements and bioclasts appear to occur in bioturbated or otherwise disturbed areas of these deposits (arrows).

XRD – Microfacies 3A		
Sample A - (9,660.8')		
Mineral	**Counts**	**%**
Quartz	41000	85.59
Calcite	6000	12.53
Pyrite	500	1.04
Dolomite	400	0.84

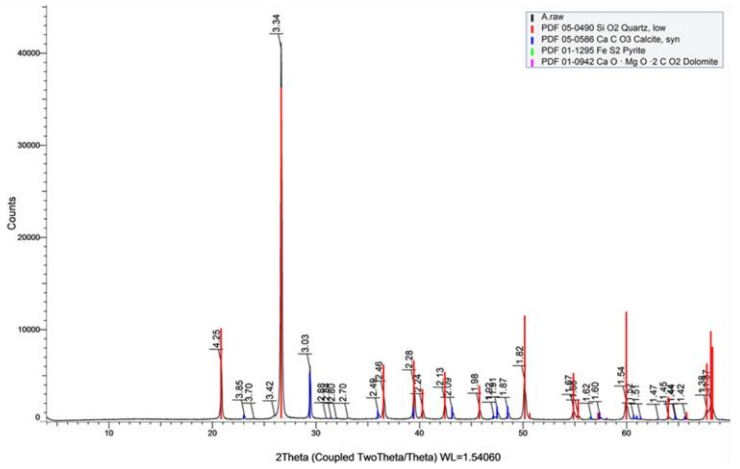

Figure 20. XRD bulk mineralogy data for microfacies 3A.

Microfacies 4A. Argillaceous Chert to Silicified, Silty Mudstone

Microfacies 4A consists of mixed lithology deposits drawn from argillaceous chert and siliceous to calcareous mudstone endmembers. Characteristic deposits can typically be described on the macroscale as mixed, silicified mudstone to muddy chert, with variability reflecting relative abundance between the two end members. The mudstone components of this microfacies are siliceous to silicified variations of microfacies 2B and 2C.

Microfacies 4A is the most difficult to constrain and define of the eleven identified microfacies, as most of the primary depositional features and fabric of characteristic deposits are altered or obscured by silicification/cementation, bioturbation, deformation, or seemingly a combination of all three, and possibly other post-depositional alterative processes. Representative deposits for this microfacies are typically variably bioturbated, clay-rich, silicified mudstones. Matrix is composed of variable amounts of clay with minor carbonate mud and organic material, and heavy to

patchy silica cement throughout. Grains consist of variable amounts of detrital silt, and semi-abundant sponge spicules and radiolarians, and are moderately to well sorted, typically ranging from silt to very fine in size. Grains are frequently silicified, but calcareous or calcified grains also occur; interestingly, sponge spicules appear dominantly replaced by calcite cement, and frequently surrounded by siliceous ooze/silicified matrix. Visible porosity is low, but relatively higher compared to other identified microfacies, and can be described as nearly undistinguishable intergranular to intercrystalline type. Texture and stratification can be described as ‘cloudy’ and are largely obscured and difficult to define with patches of highly cemented grains and matrix material throughout in muddier deposits; and conversely, patches of less cemented matrix with fewer grains relative to surrounding heavily cemented, grain rich texture throughout in more ‘cherty’ deposits. Concentration of grains and cement appear to be interrelated. Upper and basal contacts are difficult to discern, though the basal contacts in particular appear gradational. XRD data (figures 20, 21) recorded for this microfacies indicates samples are dominantly composed of quartz.

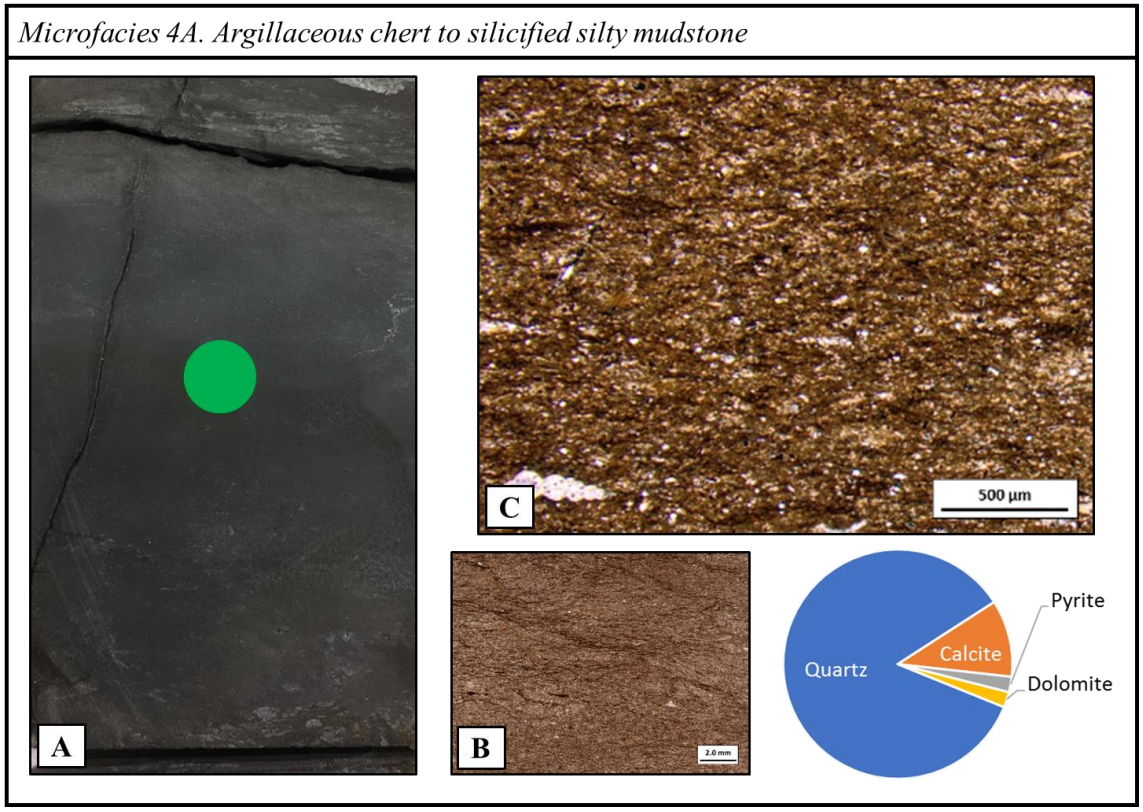

Figure 21. Macroscale and petrographic characteristics of microfacies 4A. Characteristic deposits consist of mixed lithologies drawn from clay-rich chert and siliceous to calcareous mudstone endmembers.

XRD – Microfacies 4A

Sample D - (9,781.05')

Mineral	Counts	%
Quartz	39000	84.78
Calcite	5000	10.87
Pyrite	1000	2.17
Dolomite	1000	2.17

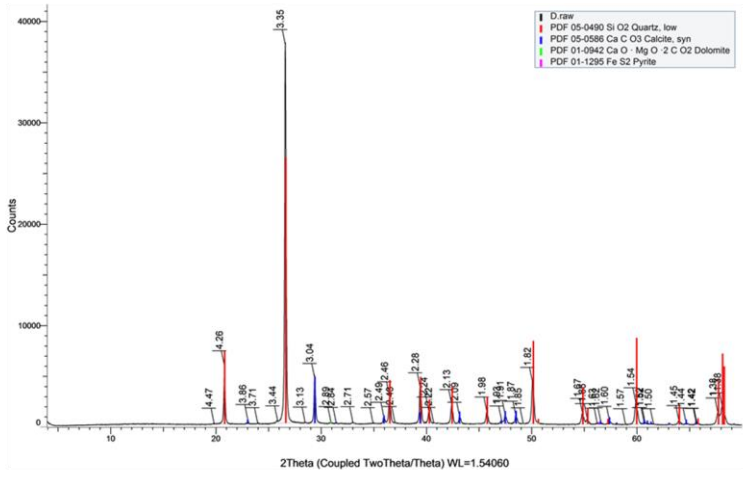

Figure 22. XRD bulk mineralogy data for microfacies 4A.

Microfacies 5A. Intraclastic Skeletal Rudstone

This microfacies is characterized by a light grey to greyish-tan, semi-translucent sparite cement matrix, with abundant skeletal grains and semi-abundant intraclasts. Skeletal grains consist of light gray, gray, and tan to off-white, very fine to granular sized bioclasts which inlcude brachiopods, bivalves, bryozoans, sponge spicules, forams, ostracods, algal fragments, crinoids, and additional undifferentiated microfossils, and skeletal fragments. Intraclasts are heavily cemented, dark gray, to gray, granular to cobble sized, sub-rounded to sub-angular wackestone-packstone and chert displaying minor plastic deformation and occasional radial pyrite replacement (figure 22).

Deposits are grain-supported, and oriented chaotically with poor sorting and a lack of internal sedimentary structures. Visible porosity is low and occurs as rare intragranular and microfracture porosity. In addition, minor normal- and inverse-grading is present. Lower contacts are sharp to erosive, upper contacts are sharp-irregular. XRD data was collected for the bioclastic sparite cement matrix for this microfacies (figures 22, 23), and confirm the composition is dominantly calcite.

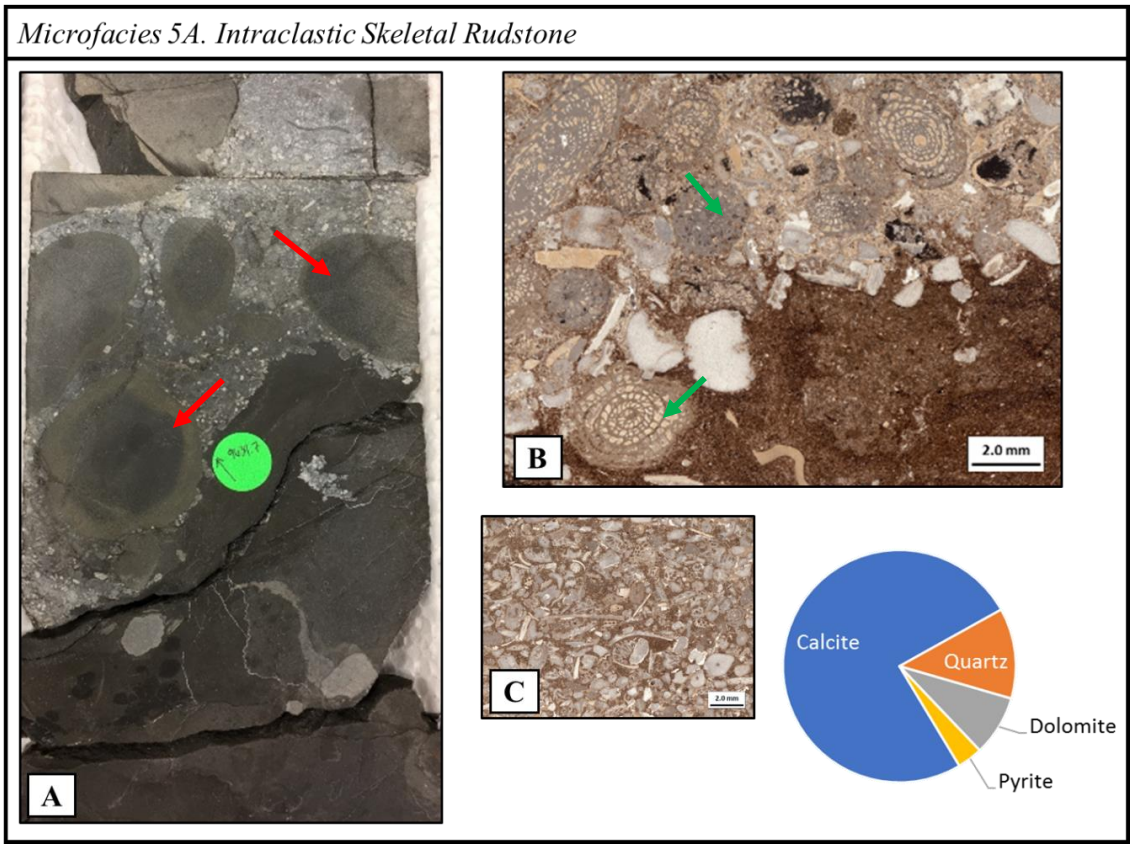

Figure 23. Macroscale and petrographic characteristics of microfacies 5A. Intraclastic skeletal rudstone debrite deposits consist of granular to cobble sized ws-ps and chert intraclasts (red arrows) and very fine to granular, well preserved skeletal grains (green arrows, C).

XRD - Microfacies 5A		
Sample E - (9,546.8')		
Mineral	**Counts**	**%**
Calcite	10800	75.52
Quartz	1800	12.59
Dolomite	1200	8.39
Pyrite	500	3.50

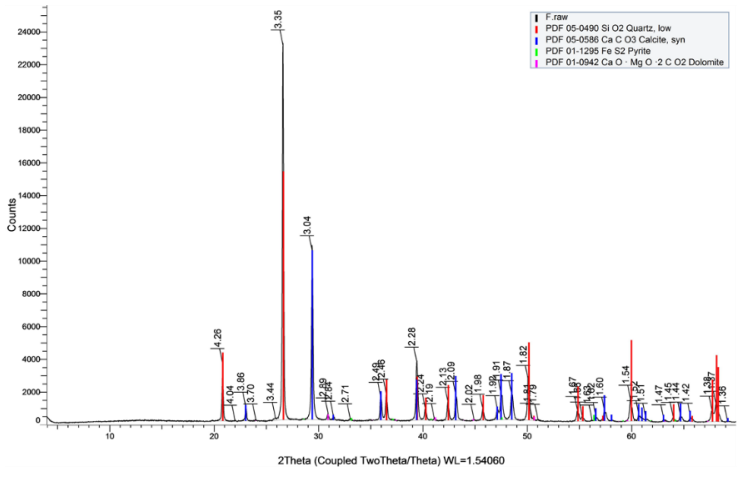

Figure 24. XRD bulk mineralogy data for microfacies 5A.

Microfacies 5B. Intraclastic Floatstone

This microfacies is a highly deformed, intraclastic floatstone. Well cemented to silicified, dark gray to gray, granular to cobble sized, sub-rounded to sub-angular, and occasionally elongate wackestone-packstone and chert clasts are predominantly supported by a dark gray, siliceous to calcareous and or organic, silty mud-matrix (*microfacies 2B, 2C with minor mf 2A*) (figure 24). Matrix can also occasionally be characterized by spiculitic mudstone-wackestone (*mf 1A*) to cemented packstone (*mf 1D*) textures; these are compositionally similar to the supported intraclasts, but are generally less grain-rich and cemented.

Deposits are oriented chaotically with poor sorting, and are heavily deformed. Soft-sediment deformation (e.g., slump structures, folded/contorted bedding, fluid escape structures) is abundant throughout. Large clasts show radial pyrite replacement and occasional plastic deformation, in like to the intraclasts of *microfacies 5A*. Visible porosity is very low to non-existent; some organic porosity may occur in mudstone matrix material unless replaced/occluded by cements. Moderate bioturbation is present and often filled or replaced by calcite cement/calcareous material. This microfacies was observed as underlying *mf5A* and is generally characterized by comparably larger intraclasts.

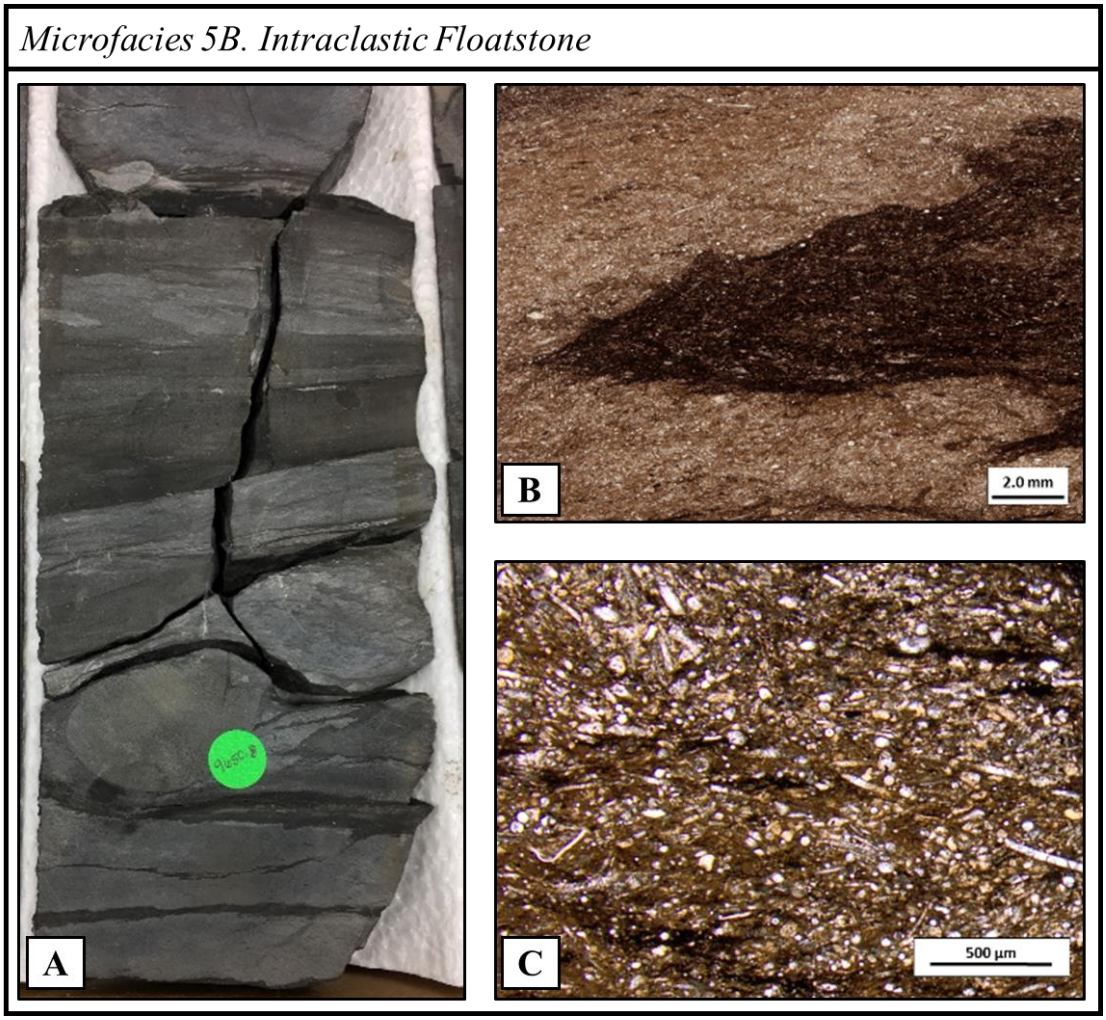

Figure 25. Macroscale and petrographic characteristics of microfacies 5B. Deposits are highly deformed, intraclastic floatstone debrites consisting of granular to cobble sized, sub-rounded to sub-angular, and occasionally elongate wackestone-packstone and chert intraclasts supported by a siliceous to calcareous and/or organic, silty mud-matrix.

4.2 Silicification Factor Analysis

Microfacies were evaluated for the presence or not, and relative degree of silicification. The primary objectives being to (1) investigate the factors which may have increased susceptibility for given deposits to become silicified, and (2) improve core-to-log correlation quality by incorporating the presence or absence, and degree of silicification to the definition and discrimination of microfacies and correlation associations in this study. Thereby also more accurately constraining associated characteristic petrophysical properties, and establishment of signature log responses.

In an effort to provide evidence for determining the factors which may have increased susceptibility for deposits to become silicified, a comparison of sedimentary characteristics and mineralogic composition was conducted between deposits characterized by: the absence of silicification, variable but minor silicification, and heavy silicification (> 50% silica replacement and/or cementation) (Table 6). The sedimentological characteristics considered for comparison of the microfacies chosen as representative of the three aforementioned ‘degrees of silicification’ included texture, matrix composition, grain types, bedding/stratification, and abundance of bioturbation/burrowing. Mineralogy was also considered based on petrographic analysis and XRD data.

Microfacies 2A was chosen and is representative of deposits characterized by the absence of silicification, *microfacies 1D* was chosen and is representative of deposits characterized by variable but minor silicification, and end member microfacies for

correlation associations 3 and 4 (*microfacies 3A and 3B*) were chosen and are representative of deposits characterized by heavy silicification.

Heavily silicified deposits were generally differentiated by an abundance of sponge spicules and moderate to abundant radiolarians, and the presence of heavy bioturbation and burrowing with highly irregular stratification. Sparse to lack of organic material, and a generally grain supported fabric were two other factors which differentiated heavily silicified deposits (*CA 3, 4*) from those with no silicification (*mf2A*); however, these are both less reliable, and non-unique as both characteristics are found in *MF1D*, where they are generally associated with heavy calcite cement, in addition to minor silicification. Although the abundance of spicules and radiolarians, accompanied by bioturbation and burrowing appear to be reliable factors associated with silicified deposits; a more detailed investigation is likely required before they and other factors can be identified as key in determining susceptibility for silicification.

Table 6. Comparison of sedmentological and mineralogic characteristics between deposits with: no silicification, minor silicification, and heavy silicification.

	No Silicification	Minor Silicification	Heavy Silicification
Representative Microfacies	2A	1D	(1) 3A (2) 4A
Texture	Mudstone	Wackestone-packstone to packstone	Silicified (1) wackestone to (2) packstone (*chert*)
Matrix	(*abundant*) Abundant organic, clay material	(*moderate to sparse*) Sparse to moderate micrite Sparse to no clay Very sparse to no organic Moderate to abundant calcite cement	(*sparse to none*) (1) Sparse micrite Sparse to no clay v. sparse to no org. material (2) Sparse to no micrite Sparse to moderate clay Sparse to no organic material
Grains	Sparse to moderate sp. spicules Sparse radiolarians Sparse to no skeletal grains Sparse to moderate detrital silt	Moderate sp. spicules Sparse radiolarians Mod. to abundant skeletal grains Moderate to abundant detrital silt	(1) **Abundant sp. spicules*** **Mod. to abund. radiolarians** Abundant skeletal grains Moderate detrital silt (2) **Abundant sp. spicules*** **Mod. to abund. radiolarians** Sparse to no skeletal grains Moderate detrital silt
Bedding & Stratification	Massive to faintly laminated	Massive to laminated Planar to slightly irreg. stratification	Cloudy to 'patchy' Highly irregular stratification
Bioturbation/Burrowing Intensity	None	Light to moderate	**Heavy**
XRD/Petrographic Mineralogy	Organic, clay, quartz XRD indicates trace to no calcite	XRD indicates range from dominantly calcite to nearly equal calcite/quartz, quartz component due to abundance of detrital quartz silt.	Dominantly Quartz with trace calcite. Quartz component is the result of silicified grains and matrix, minor detrital silt
Presence of Mineralized Fractures	None	Sparse to Moderate, occ. heavy w/ abund. calcite cement	Heavy

4.3 Wireline Log Analysis

The log suite corresponding to the cored well for this investigation included gamma-ray (GR), bulk-density (RHOB), neutron-porosity (NPHI) and density-porosity (DPHI) (adjusted to 2.71 g/cm3 matrix density), invaded zone (Ri) and uninvaded zone 'deep' (Rt) resistivity, and photoelectric (Pe) curves. Measurements from these curves, in addition to calculated measurements for neutron-density cross-plot porosity, and a density-porosity minus neutron-porosity 'neutron-density porosity crossover' value; were used to evaluate and define the range of petrophysical characteristics associated with each correlation association.

All measured and calculated log measurements were compiled and organized according to the depth intervals assigned to each correlation association. Average values for the aforementioned measurements were calculated for each correlation association (table 12) to provide an initial assessment of their characteristic petrophysical properties. Histograms were then generated to define the range and distribution of each petrophysical measurement, for each CA (figure 34) (appendix D); enabling 1) determination of the quality of each measurement as a defining petrophysical characteristic of that particular CA (e.g., a narrow range/distinct cluster of dominant values would indicate a good differentiating characteristic.), and 2) comparison of the range and characteristic values of each measurement between correlation associations. Finally, both recorded and calculated petrophysical measurements were crossplotted using *TIBCO® Spotfire®: Data Visualization & Analytics Software* to interpret the interplay between core identified correlation associations and their correlative

petrophysical properties, and to further differentiate and define the petrophysical signatures associated with each (see appendix C).

All available logging data/measurements at a given depth interval were coordinated and assigned to the correlation association present at that depth interval. Log data were recorded at every half foot throughout the cored interval, which resulted in a total of 408 data points for each recorded or calculated measurement. Correlation association 1 (CA1) made up 72 feet (21.9 m) of the cored interval with 144 assigned data points. Correlation association 2 (CA2) made up 53.5 feet (16.3 m) of the cored interval with 107 assigned data points. Correlation association 3 (CA3) represented 44 feet (13.4 m) of the cored interval with 88 assigned data points. Correlation association 4 (CA4) made up 21.5 feet (6.6 m) of the cored interval with 43 assigned data points. Lastly, correlation association 5 (CA5) was the least represented, making up 13 feet (4 m) of the cored interval with 26 assigned data points.

4.3.1 Correlation Association Petrophysical Properties

Microfacies within each correlation association display similar: major constituents; mineralogy, texture, and depositional fabric; visible pore space; and diagenetic features.

Correlation Association 1 – Petrophysical Properties and Characteristic Log Response

This correlation association consists of four microfacies: *1A) Spiculitic mudstone to sparse wackestone, 1B) Organic, fossiliferous wackestone to packstone, 1C) Silty,*

argillaceous wackestone – packstone, and *1D) Spiculitic—fossiliferous, sparry wackestone to packstone*. The range of petrophysical properties defining CA1 varied from narrow to wide with some measurements represented by a distinct cluster of prevailing values, and others being less distinct (figure 25).

Correlation association 1 is represented by the highest average bulk density (2.57 g/cm^3), highest average photoelectric factor (3.47 barns/electron), and lowest average density-porosity (0.082 v/v) amongst the five correlation associations. In addition, CA 1 is characterized by low gamma ray (32.1 gAPI), porosity (8.2 %), and neutron-porosity (0.076 v/v) values. High resistivity values (1,174.3 ohmms), and a telling average neutron- and density-porosity crossover (N-D Crossover) value of 0.006 units (table 7), which indicates the usual overlaying or near overlaying of the neutron- and density-porosity curves for intervals of this correlation association. Hence, the signature log response for correlation association 1 is characterized by low gamma-ray, high yet variable deep-resistivity, low neutron- and density-porosity response with the curves nearly overlain, high bulk-density, and a high Pe response (figure 26).

Table 7. Summary of the petrophysical/log characteristics for CA1.

Correlation association 1 – Petrophysical Properties							
Calibrated Log Curves:	**Gamma-Ray (gAPI)**	**Resistivity (Ohmm)**	**Porosity (%)**	**Porosity Crossover**	**Photoelectric Factor**	**Apparent Matrix Density**	**Bulk Density**
Average	32.1	1000.1	0.075	0.006	3.47	2.71	2.58
Range	39.4	2585.3	0.13	0.07	1.85	0.07	0.18
Min	18.7	68.6	0.02	-0.03	2.47	2.68	2.49
Max	58.0	2653.9	0.15	0.04	4.32	2.75	2.67
Std. Dev.	8.29	587.4	0.02	0.01	0.43	0.01	0.03
Dev. Coeff.	0.26	0.59	0.27	1.11	0.12	0.004	0.01
Count	144						
Net Thickness: 72 feet (21.9 m)				35.4%			

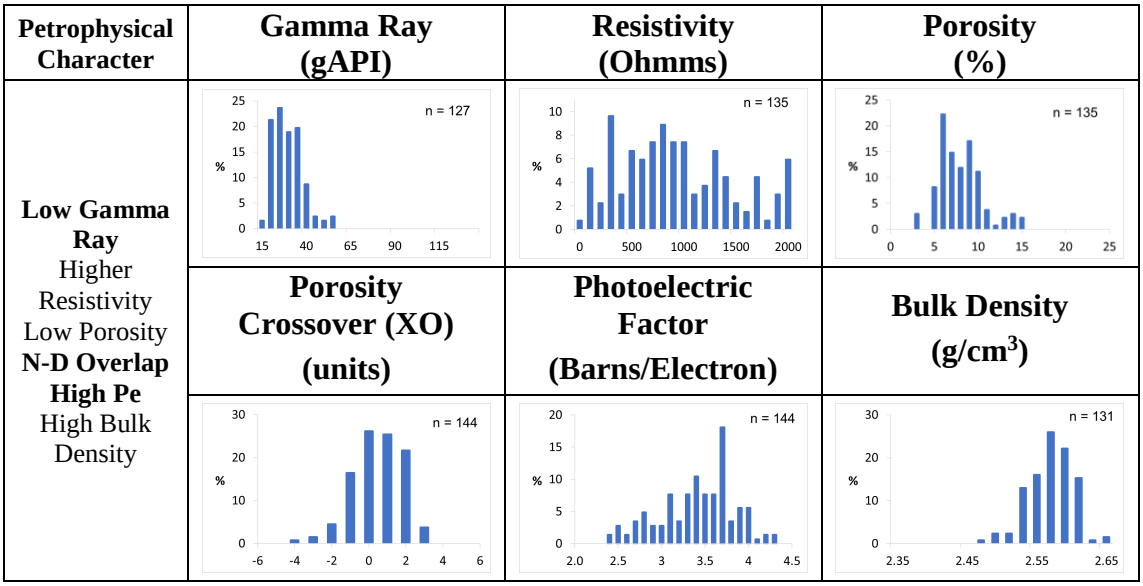

Figure 26. Range and characteristic petrophysical/log properties for correlation association 1 (CA1).

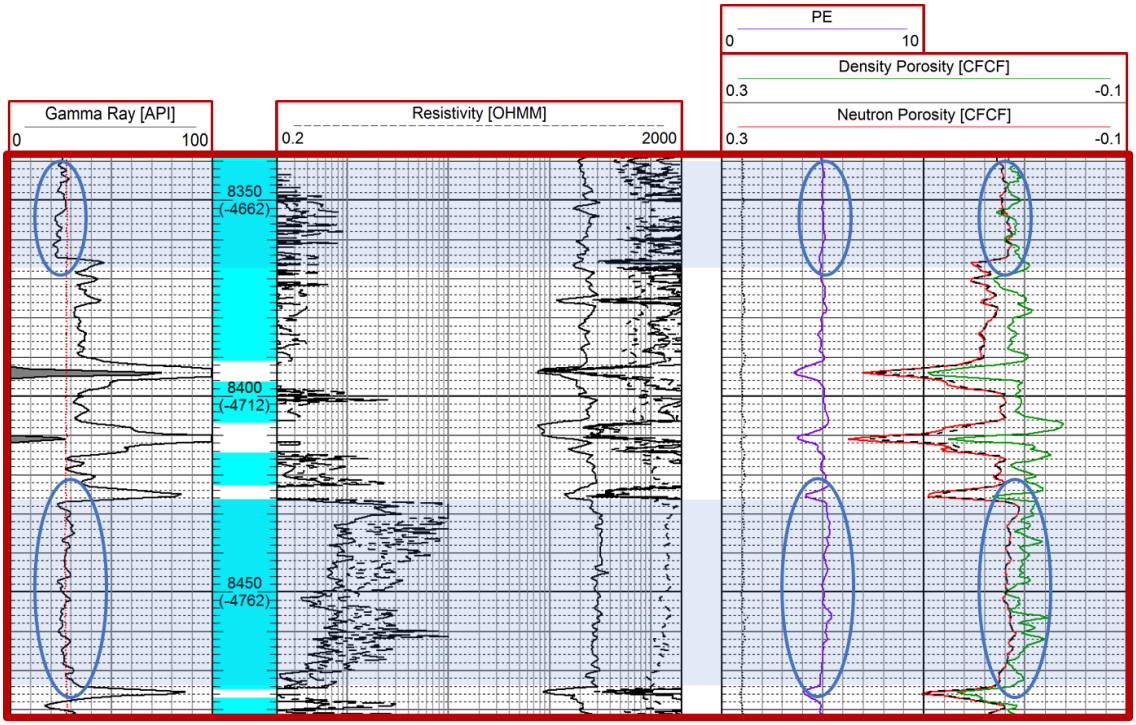

Figure 27. Low gamma-ray, high yet variable deep-resistivity, a low neutron- and density-porosity response with the curves nearly overlain, high bulk-density, and a PE response close to 5 barns/electron characterize the signature log response for correlation association 1.

Correlation Association 2 – Petrophysical Properties and Characteristic Log Response

This correlation association consists of three microfacies: *2A) Organic, spiculitic mudstone—silty mudstone, 2B) Calcareous mudstone—silty mudstone,* and *2C) Bioturbated, siliceous—silty mudstone.* Like CA 1, correlation association 2 is represented by petrophysical characteristics which include both narrowly defined measurements, and those which are less clearly defined (figure 27).

Correlation association 2 is characterized by the highest average gamma-ray (78.7 gAPI), highest average porosity (16.5%), lowest average bulk density (2.46 g/cm^3), and greatest porosity crossover separation (-0.018 counts) values among the five correlation associations. In addition, CA 2 is characterized by relatively very low

average resistivity (313.6 ohmms), and has an average photoelectric factor measurement of (2.76 barns/electron) (table 8). Hence, the signature log response for correlation association 2 is characterized by high 'hot' gamma-ray, low resistivity (generally below 500 ohmms), and high neutron- and density-porosity values, often with the two curves separated (figure 28).

Table 8. Summary of the petrophysical/log characteristics for CA2.

Correlation association 2 – Petrophysical Properties							
Calibrated Log Curves:	**Gamma -Ray (gAPI)**	**Resistivity (Ohmm)**	**Porosity (%)**	**Porosity Crossover**	**Photoelectric Factor**	**Apparent Matrix Density**	**Bulk Density**
Average	78.7	242.0	0.165	-0.018	2.74	2.75	2.46
Range	103.4	564.1	0.19	0.15	0.99	0.19	0.25
Min	28.7	47.8	0.06	-0.1	2.36	2.67	2.35
Max	132.1	611.8	0.25	0.05	3.35	2.86	2.6
Std. Dev.	29.6	138.9	0.05	0.04	0.26	0.05	0.07
Dev. Coeff.	0.38	0.57	0.30	2.26	0.09	0.018	0.03
Count	107						
Net Thickness: 53.5 feet (16.9 m)				26.3%			

Petrophysical Character	Gamma Ray (gAPI)	Resistivity (Ohmms)	Porosity (%)
High Gamma Ray Low Resistivity **High Porosity N-D Separation** Low Pe **Low Bulk Density**	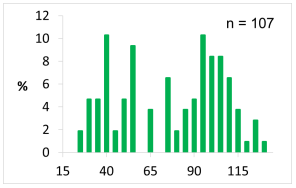	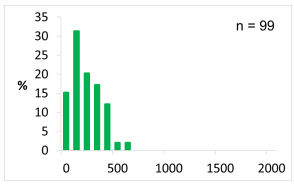	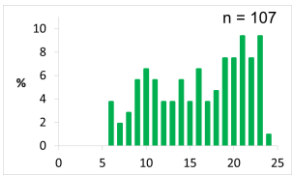
	Porosity Crossover (XO) (units)	**Photoelectric Factor (Barns/Electron)**	**Bulk Density (g/cm^3)**
	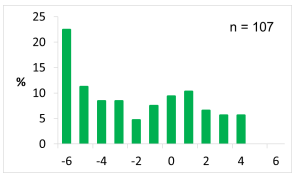	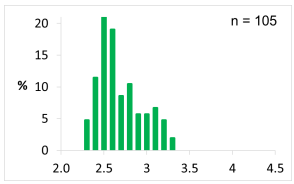	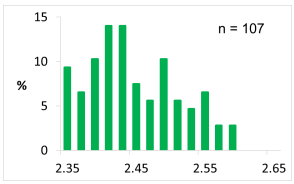

Figure 28. Range and characteristic petrophysical/log properties for correlation association 2 (CA2).

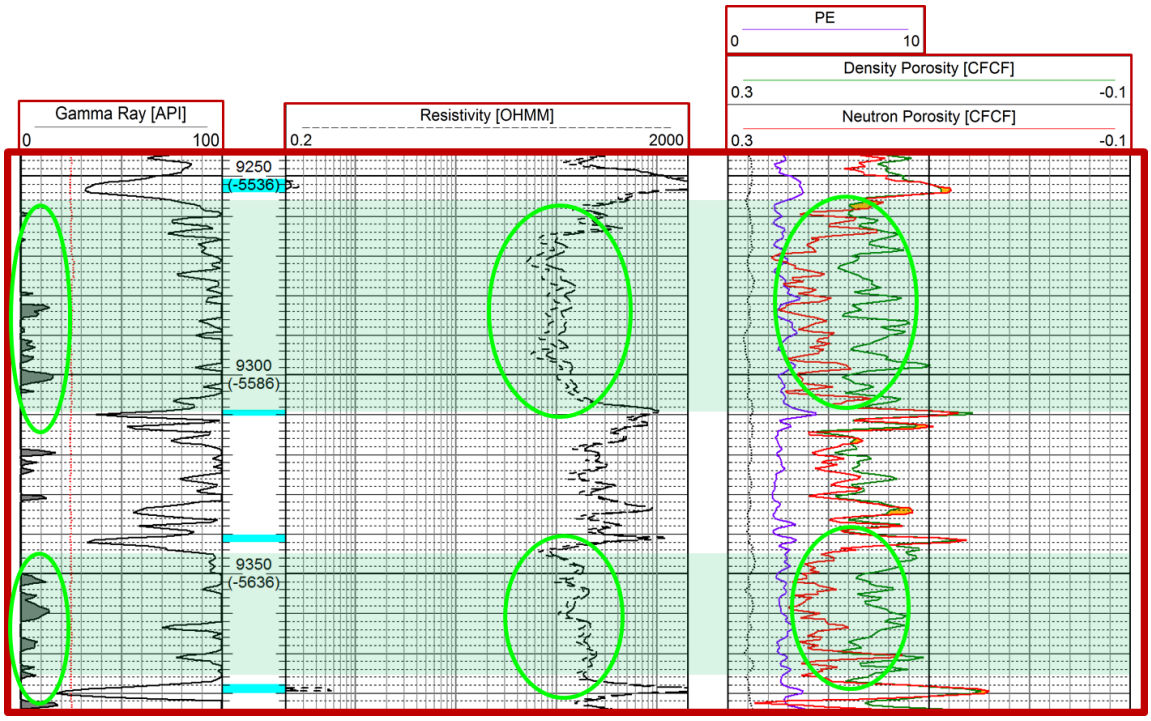

Figure 29. High 'hot' gamma-ray, low resistivity (generally below 500 ohmms), and high porosity values, often with separation between the neutron- and density-porosity values characterize the signature log response for correlation association 2 (CA2).

Correlation Association 3 – Petrophysical Properties and Characteristic Log Response

This correlation association consists of one microfacies: *3A) Silicified limestone to calcareous chert*; and is characterized by a distinct range of petrophysical properties (figure 29). Average gamma-ray (28.2 gAPI) and porosity (7.1%) values are the lowest among the five correlation associations, and average resistivity (1,385.4 ohmms) and bulk density (2.57 g/cm^3) values are the highest. The average photoelectric factor for CA 3 is 3.08 barns/electron, and the average neutron- and density-porosity crossover value is significantly, 0.025 counts (table 9), which indicates that the density-porosity curve typically overlaps the neutron-porosity curve for this correlation association.

Considering these results, the signature log response for correlation association 3 is characterized by low gamma ray, low porosity, high density and resistivity, and cross-over of the neutron- and density-porosity (ND) curves (figure 30).

Table 9. Summary of the petrophysical/log characteristics for CA3.

Correlation association 3 – Petrophysical Properties							
Calibrated Log Curves:	**Gamma-Ray (gAPI)**	**Resistivity (Ohmm)**	**Porosity (%)**	**Porosity Crossover**	**Photoelectric Factor**	**Apparent Matrix Density**	**Bulk Density**
Average	28.2	1253.3	0.071	0.025	3.08	2.69	2.57
Range	19.4	2205.4	0.07	0.047	1.48	0.04	0.1
Min	21.0	276.7	0.04	0.003	2.28	2.67	2.51
Max	40.4	2482.1	0.11	0.05	3.76	2.71	2.61
Std. Dev.	4.2	518.4	0.01	0.01	0.41	0.01	0.03
Dev. Coeff.	0.15	0.41	0.14	0.40	0.13	0.004	0.01
Count	88						
Net Thickness: 44 feet (13.4 m)				21.6%			

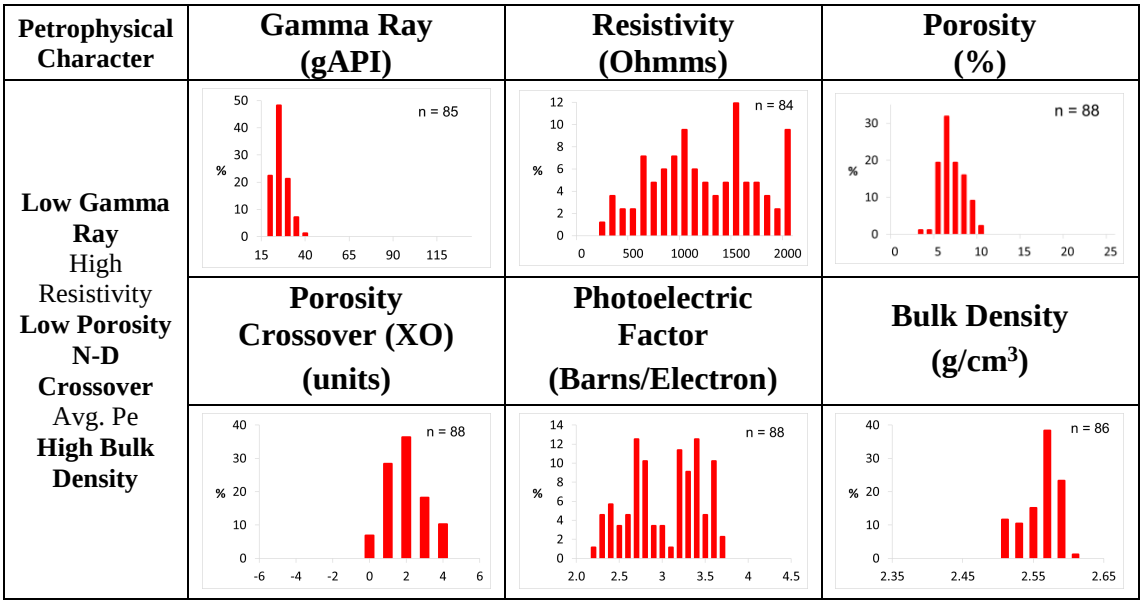

Figure 30. Range and characteristic petrophysical/log properties for correlation association 3 (CA3)

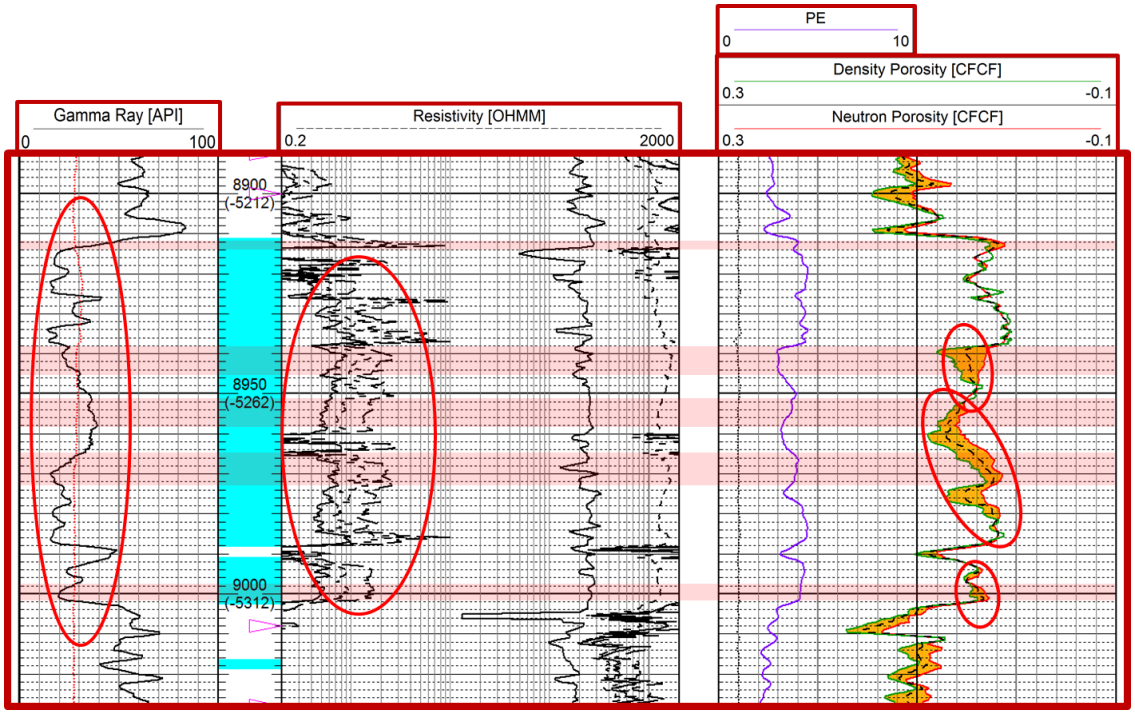

Figure 31. Low gamma ray, low porosity, high resistivity, and cross-over of the neutron- and density-porosity curves characterize the signature log response for correlation association 3. The most distinct log characteristics associated with these deposits are the combination of low gamma-ray values (generally below 40 gAPI), and low, crossed-over neutron- and density-porosity values; which enables clear differentiation of this correlation association from the other 4 characterized in this study.

Correlation Association 4 – Petrophysical Properties and Characteristic Log Response

This correlation association consists of one microfacies: *4A) Argillaceous chert to silicified, siliceous mudstone*; and is characterized by a relatively distinct range of petrophysical properties (figure 31). CA4 is indicatively defined by the highest average neutron- and density-porosity crossover (0.03 counts) values, and has the lowest average photoelectric factor (2.72 barns/electron) among the 5 correlation associations. CA 4 is characterized by relatively lower average bulk density (2.51 g/cm^3) and resistivity (633.3 ohmm) values; in addition to a relatively ambiguous average gamma ray value (37.7

gAPI), and a noteworthy (for differentiability from CA3) average porosity value of 10.5% (table 10). The signature log response for correlation association 3 is characterized by low resistivity, moderate to high porosity, and most uniquely, low PE values (typically 3 or below) and cross-over of the neutron- and density-porosity (ND) curves (figure 32).

Table 10. Summary of the petrophysical/log characteristics for CA4.

Correlation association 4 - Petrphysical Properties							
Calibrated Log Curves:	**Gamma-Ray (gAPI)**	**Resistivity (Ohmm)**	**Porosity (%)**	**Porosity Crossover**	**Photoelectric Factor**	**Apparent Matrix Density**	**Bulk Density**
Average	37.7	575.4	0.105	0.030	2.72	2.69	2.51
Range	33.7	1241.8	0.11	0.049	1.27	0.05	0.18
Min	21.6	113.9	0.05	0.001	2.29	2.67	2.44
Max	55.3	1355.7	0.16	0.05	3.56	2.72	2.62
Std. Dev.	9.4	328.0	0.03	0.01	0.36	0.01	0.05
Dev. Coeff.	0.25	0.57	0.28	0.33	0.13	0.004	0.02
Count	43						
Net Thickness: 21.5 feet (6.6 m)				10.6%			

Petrophysical Character	Gamma Ray (gAPI)	Resistivity (Ohmms)	Porosity (%)
Avg. Gamma Ray Lower Resistivity Avg. Porosity **High N-D Crossover** **Low Pe** Lower Bulk Density	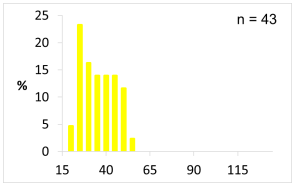	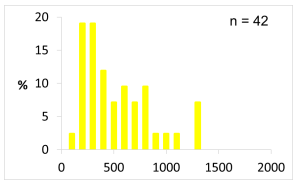	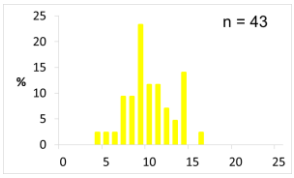
	Porosity Crossover (XO) (units)	**Photoelectric Factor (Barns/Electron)**	**Bulk Density (g/cm^3)**
	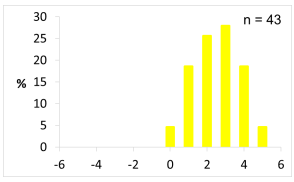	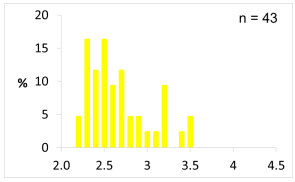	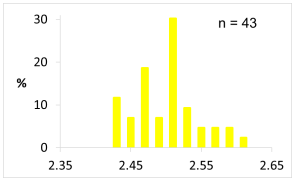

Figure 32. Range and characteristic petrophysical/log properties for correlation association 4 (CA4)

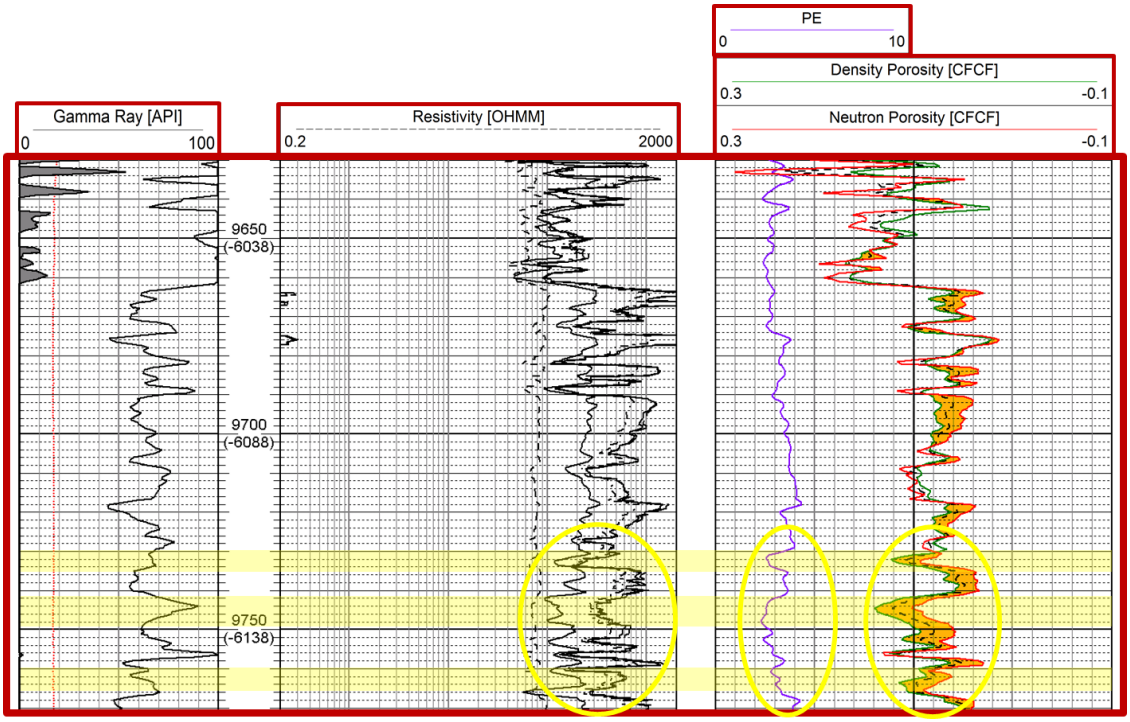

Figure 33. Low resistivity, moderate to high porosity, and most uniquely, low PE values (typically of 3 or below) and cross-over of the neutron- and density-porosity (ND) curves characterize the signature log response for correlation association 4. Comparatively low resistivity values, high porosity, and a low PE response enable differentiation of CA 4 from CA3.

Correlation Association 5 – Petrophysical Properties and Characteristic Log Response

This correlation association consists of two microfacies: *5A) Intraclastic skeletal rudstone*, and *5B) Intraclastic floatstone*. The petrophysical signature for correlation association 5 is expectedly relatively difficult to constrain due to the limited number of available data points compared to the other four correlation associations, and because of the heterogeneity of associated deposits.

The most distinct petrophysical characteristic for CA 5 is resistivity, which has the lowest average value (224.3 ohmms) among the five correlation associations. The other average petrophysical values associated with CA 5 are tellingly both less definitive, and of middling value relative to the correlative average values associated with the other 4 correlation associations. That stated, CA 5 is characterized by average bulk density (2.53 g/cm^3), gamma-ray (56.6 gAPI), and photoelectric factor (2.93 barns/electron) values, a slightly separated N-D crossover (-0.015 counts), and an average porosity value of 12.2% (table 11) (figure 33). Due to the limited number of available data points, we were not able to generate a characteristic signature log response for correlation association 5.

Table 11. Summary of the petrophysical/log characteristics for CA5.

Correlation association 5 - Petrphysical Properties							
Calibrated Log Curves:	**Gamma-Ray (gAPI)**	**Resistivity (Ohmm)**	**Porosity (%)**	**Porosity Crossover**	**Photoelectric Factor**	**Apparent Matrix Density**	**Bulk Density**
Average	56.6	200.7	0.122	-0.015	2.93	2.74	2.53
Range	70.0	277.2	0.11	0.09	0.57	0.12	0.24
Min	33.8	91.0	0.06	-0.07	2.62	2.7	2.43
Max	103.8	368.2	0.17	0.02	3.19	2.82	2.67
Std. Dev.	12.3	66.2	0.03	0.02	0.3	0.03	0.06
Dev. Coeff.	0.22	0.33	0.25	1.30	0.10	0.011	0.02
Count	26						
Net Thickness: 13 feet (4.0 m)				6.4%			

Petrophysical Character	**Gamma Ray (gAPI)**	**Resistivity (Ohmms)**	**Porosity (%)**
Avg. Gamma Ray **Low Resistivity** Avg. Porosity Low N-D Separation Avg. Pe Avg. Bulk Density	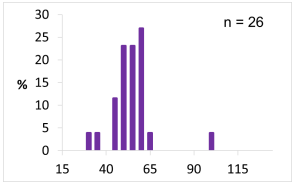	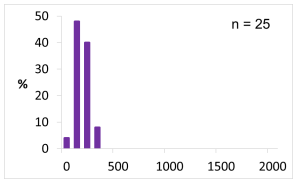	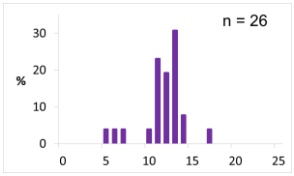
Porosity Crossover (XO) (units)	**Photoelectric Factor (Barns/Electron)**	**Bulk Density (g/cm^3)**	
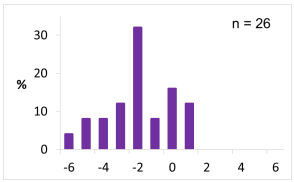	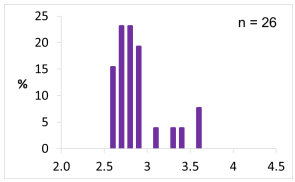	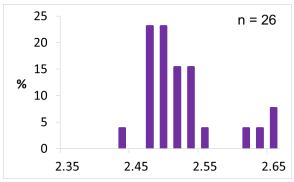	

Figure 34. Range and characteristic petrophysical/log properties for correlation association 5 (CA5)

Table 12. Average petrphysical values for all correlation associations

Correlation associations – Average Petrophysical Values							
Correlation associations	**Gamma-Ray (gAPI)**	**Resistivity (Ohmm)**	**Porosity (%)**	**Porosity Crossover**	**Photoelectric Factor**	**Apparent Matrix Density**	**Bulk Density**
CA 1	32.1	1174.3	8.2	0.006	**3.47**	2.711	**2.58**
CA 2	**78.7**	313.6	**16.5**	**-0.018**	2.76	**2.748**	**2.46**
CA 3	**28.2**	**1385.4**	**7.1**	0.025	3.08	2.691	**2.57**
CA 4	37.7	633.3	10.5	**0.030**	**2.72**	**2.688**	2.51
CA 5	56.6	**224.3**	12.2	-0.015	2.93	2.740	2.53
Standard Deviation	*21.0*	*461.4*	*3.3*	*0.020*	*0.27*	*0.025*	*0.042*
Deviation Coefficient	*0.45*	*0.62*	*0.30*	*3.61*	*0.09*	*0.01*	*0.02*

The identified characteristic petrophysical data (figure 35) and methodology outlined in this research establishes the ability to identify and predict defined correlation associations in the subsurface using commonly available logs away from core data. This predictability will increase understanding, enable new development strategies for unconventional exploration of the FBSC member, and facilitate learning from future studies utilizing new empirical data. (Figures 36, 37, 38).

Correlation association	Petrophysical Character	Gamma Ray (gAPI)	Resistivity (Ohmms)	Porosity (%)	Porosity Crossover (XO) (units)	Photoelectric Factor (Barns/Electron)	Bulk Density (g/cm^3)
CA 1	**Low Gamma Ray** Higher Resistivity Low Porosity **N-D Overlap** **High Pe** High Bulk Density	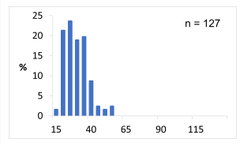	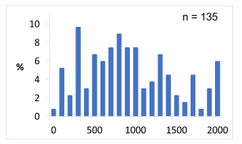	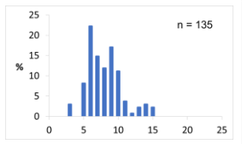	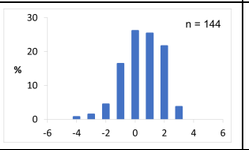	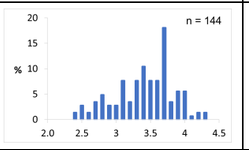	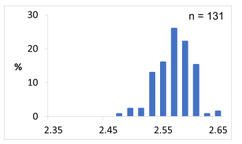
CA 2	**High Gamma Ray** Low Resistivity **High Porosity** **N-D Separation** Low Pe **Low Bulk Density**	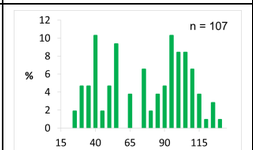	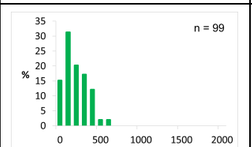	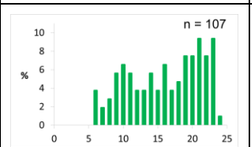	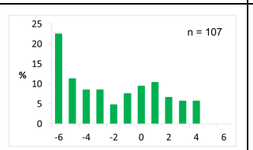	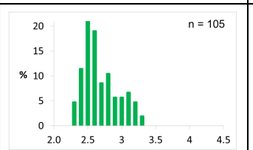	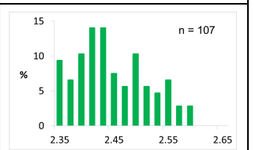
CA 3	**Low Gamma Ray** High Resistivity **Low Porosity** **N-D Crossover** Avg. Pe **High Bulk Density**	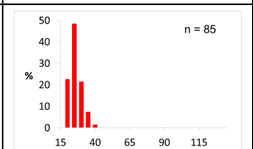	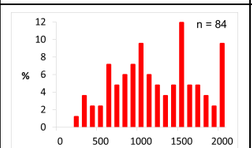	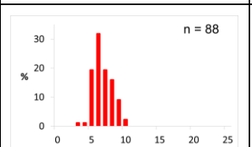	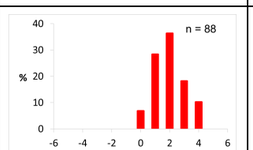	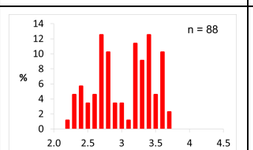	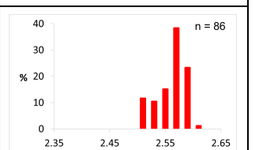
CA 4	Avg. Gamma Ray Lower Resistivity Avg. Porosity **High N-D Crossover** **Low Pe** Lower Bulk Density	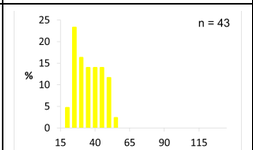	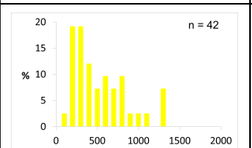	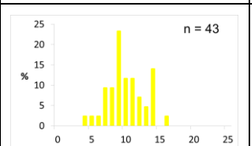	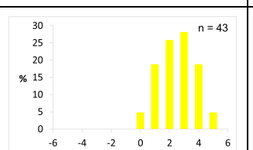	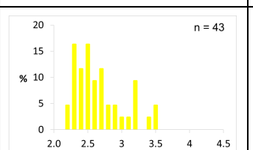	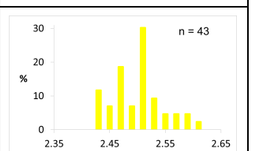
CA 5	Avg. Gamma Ray **Low Resistivity** Avg. Porosity Low N-D Separation Avg. Pe Avg. Bulk Density	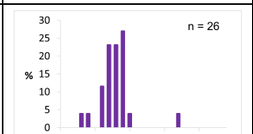	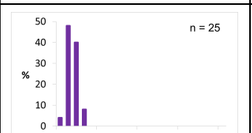	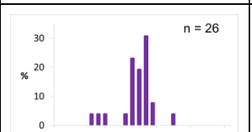	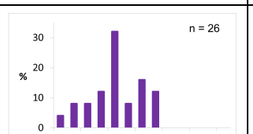	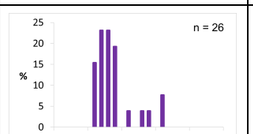	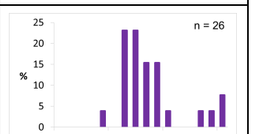
Summary		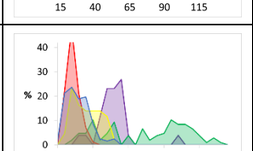	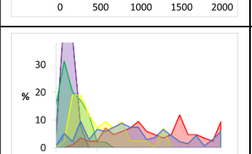	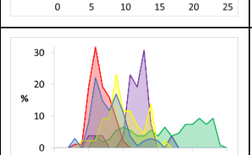	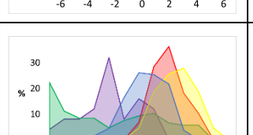	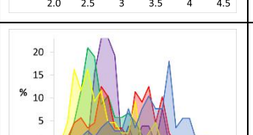	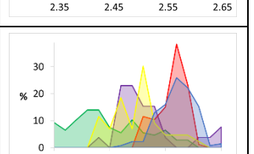
	Normalized	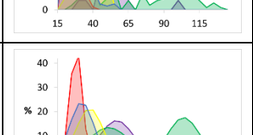	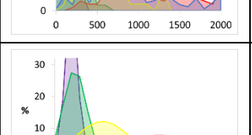	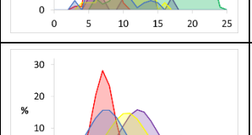			

Figure 35 Range and Distribution of all measured and calculated log prorperties for each correlation association.

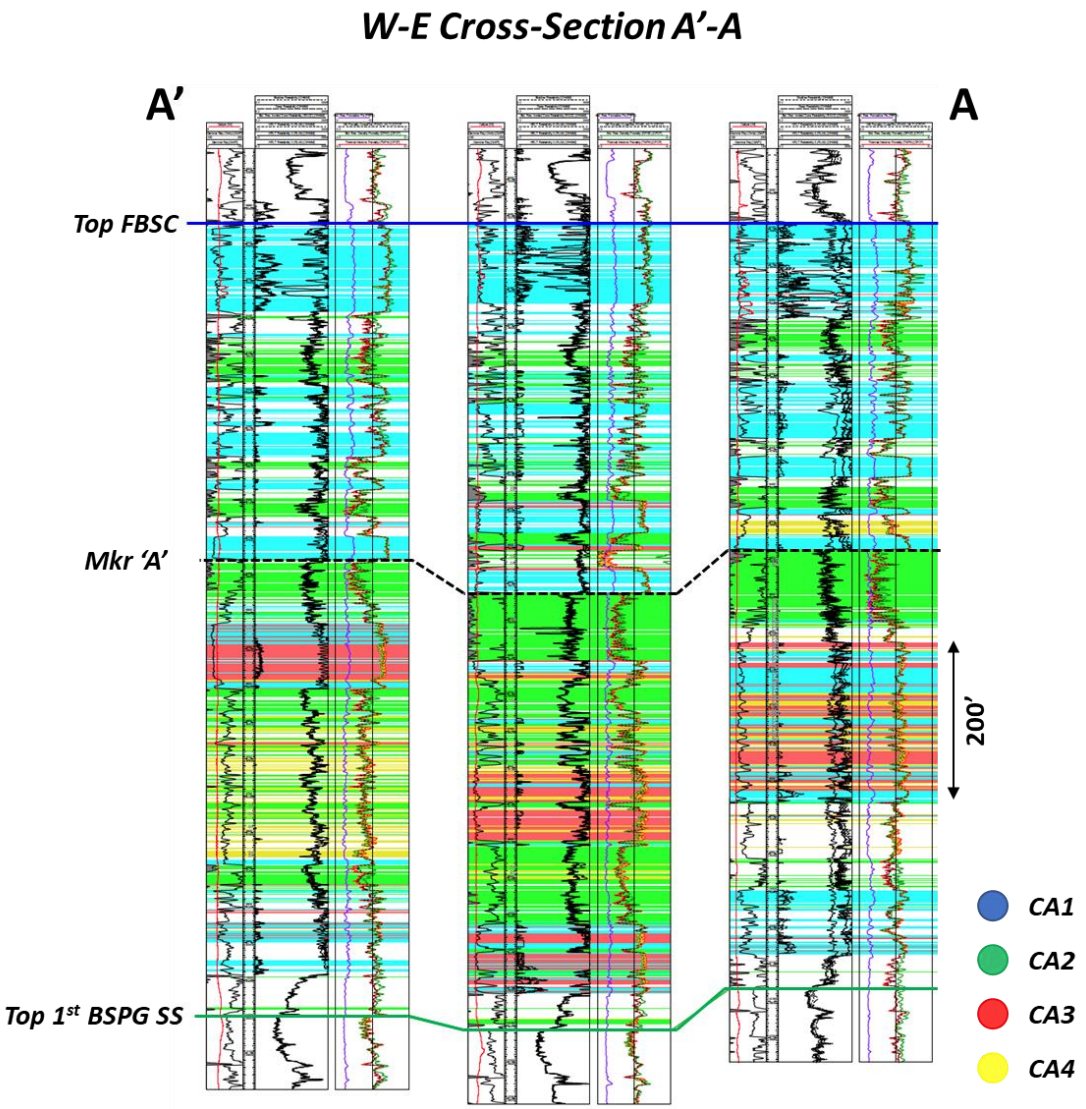

Figure 36. West to East cross-section A'-A (location noted in figure 37). This cross-section demonstrates prediction of correlation associations 1-4 in the subsurface using calibrated log responses on commonly available logs away from core data. Of note is not only the heterogeneity, but also the stratigraphically discontinuous nature of the section over a small area.

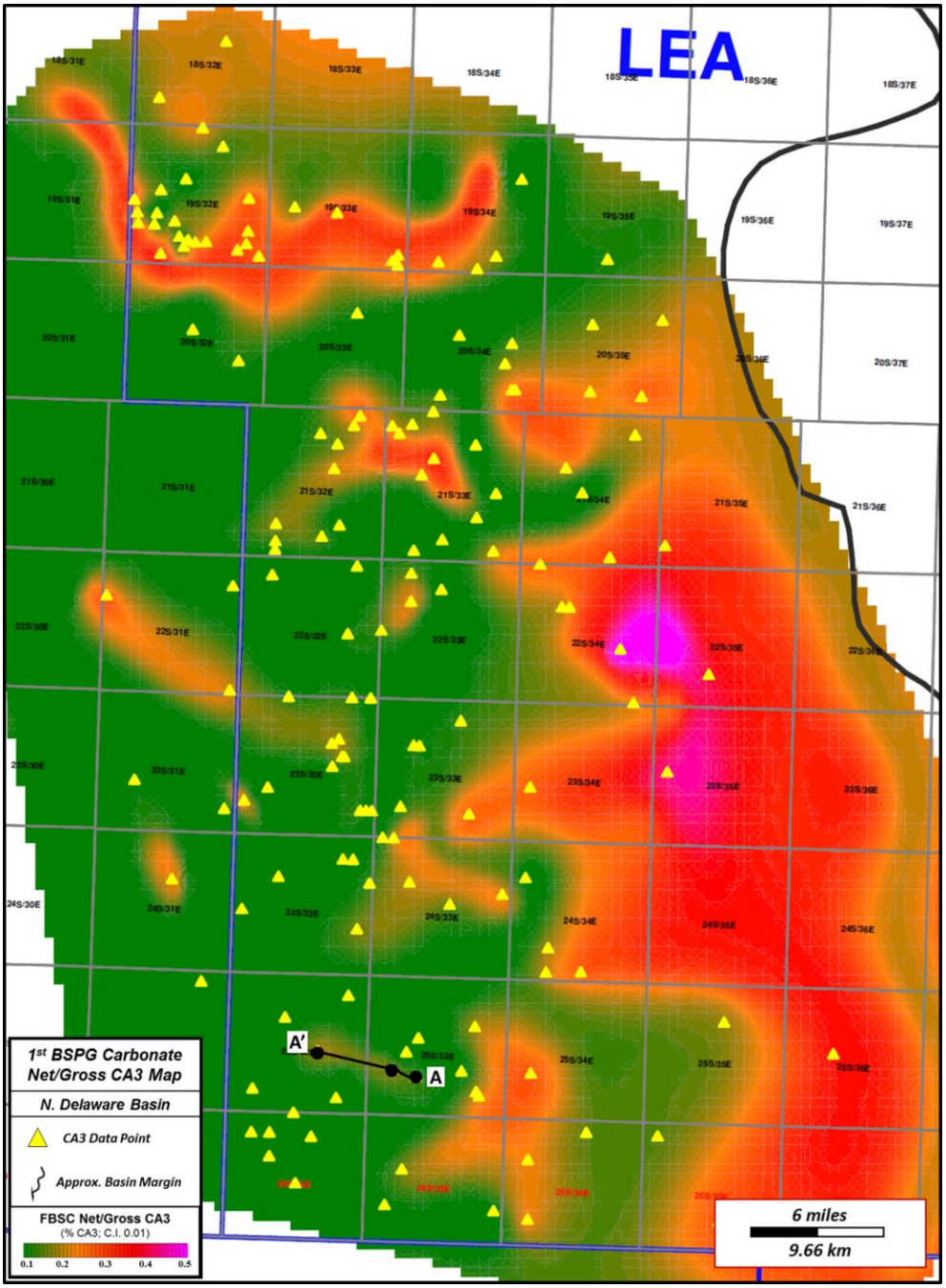

Figure 37. FBSC Member net to gross CA3 map demonstrating the percentage of CA3 deposits present within the FBSC. The ability to identify CA1 & CA3 deposits using commonly available log data not only allows for predictability in the subsurface to support avoidance of these drill-rate inhibiting, non-reservoir lithologies, but also facilitates future research and learning through empirical data, in turn enabling future development strategies for unconventional exploration of the FBSC member. The location of cross-section A-A' (figure 36) is noted.

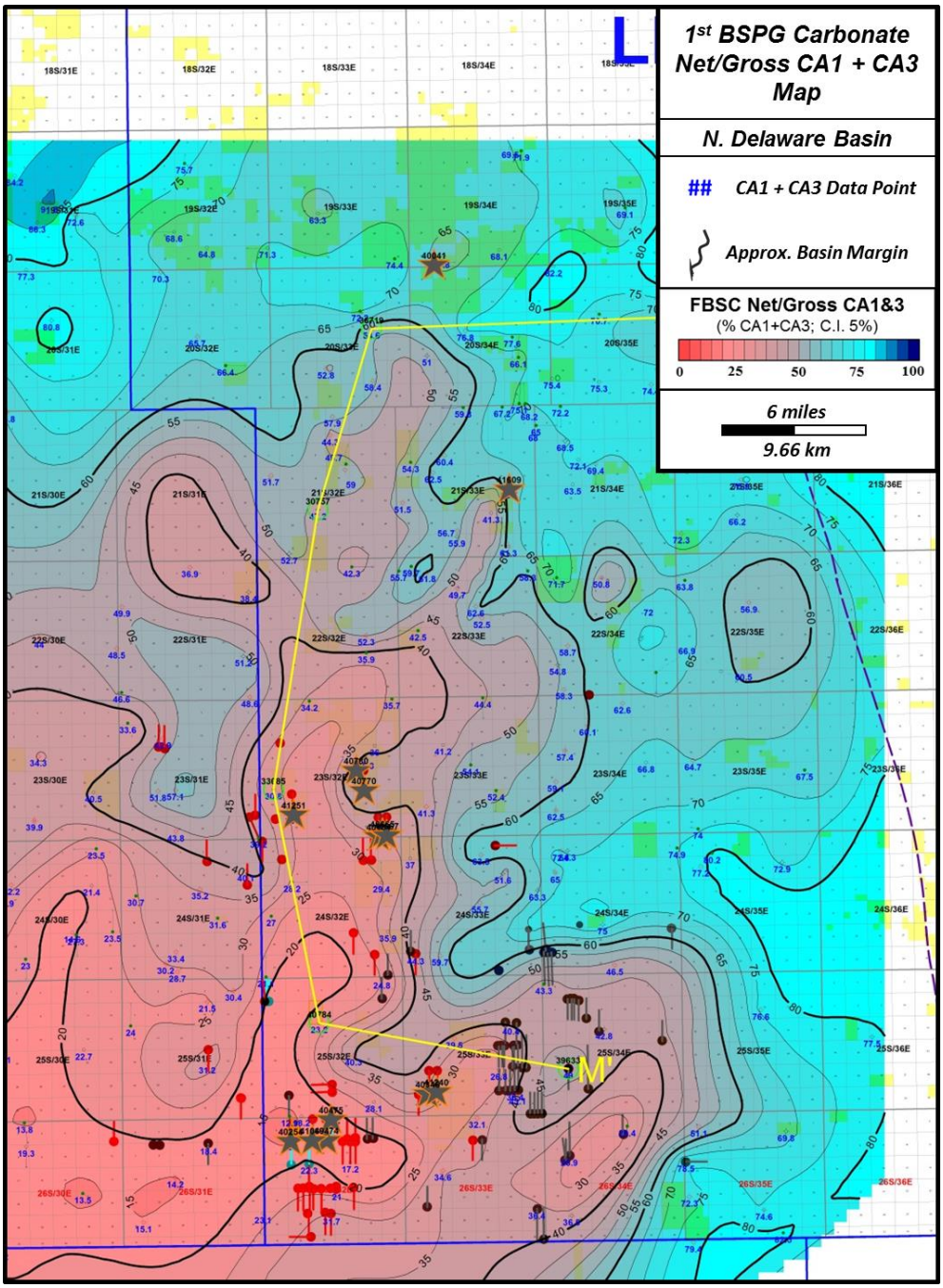

Figure 38. FBSC Member net to gross CA1 + CA3 map demonstrating the percentage of carbonate deposits present within the FBSC. The ability to identify CA1 & CA3 deposits using commonly available log data allows for predictability in the subsurface to support avoidance of these drill-rate inhibiting, non-reservoir lithologies (see figures 44, 45).

4.3.2 Core-to-Log Correlation Crossplots

Both recorded and calculated petrophysical measurements assigned to core identified correlation associations were crossplotted using TIBCO® Spotfire®: Data Visualization & Analytics Software to further differentiate and define characteristic petrophysical signatures for correlation associations, and to interpret the interplay between representative log measurements and correlative lithology.

The three cross-plots (*ρ_b (bulk density) vs. φ_N (neutron porosity*, *R_t (deep resistivity) vs. φ_N (neutron porosity)*, and *GR (gamma ray) vs. φ_N (neutron porosity)*) identified by (*Asquith)* as useful for establishing relationships between log data and carbonate lithology, were the first to be generated (figures 39, 40, 41) and evaluated.

The neutron porosity vs. bulk density plot (figure 39) is effective in further defining/differentiating log characteristics identified as representative for each correlation association; and interestingly depicts the previously interpreted lithological interrelationships between CA1 & CA3, and CA3 & CA4. As the plot portrays, CA1 (limestones) and CA3 (silicified limestone/calcareous chert) are interrelated as they both have a limestone component; similarly, overlap on the plot occurs between CA3 & CA4 as both are largely composed of authigenic silica, though with mud and clay present in CA4, compared to the aforementioned carbonate content in CA3.

Though the *neutron-porosity vs. resistivity* plot (figure 40) is not as effective in defining and differentiating log characteristics for each correlation association compared to (figure 39), however, it is useful as an indicator for the quality of the plotted measurements as well constrained, defining characteristics, or not of each correlation

association. Most notably, this plot indicates that resistivity is a well constrained measurement for CA's 2 and 5, and a poorly to moderately constrained measurement for CA's 1 and 3 (though CA3 is accurately depicted to typically represent the highest resistivity values.) Conversely, neutron-porosity is shown to be poorly constrained for CA 2, and well constrained for CA's 1, 3 and 4. The *gamma ray vs. neutron-porosity plot* (figure 40) did not clearly differentiate the 5 correlation associations, and so was not used for interpretation or discussed further.

Following analysis of these thee initial plots, *Spotfire* was used to generate additional crossplots for all combinations between: gamma-ray (GR), bulk-density (RHOB), neutron-porosity (NPHI) and density-porosity (DPHI) (2.71 g/cm3 matrix density), 'deep' resistivity (Rt), and photoelectric (Pe) curves; in addition to calculated neutron-density crossplot porosity, and crossover of the density-porosity and neutron-porosity curves (calculated as DPHI minus NPHI). The resulting plots can be found in Appendix C, and will be referenced as applicable throughout the discussion.

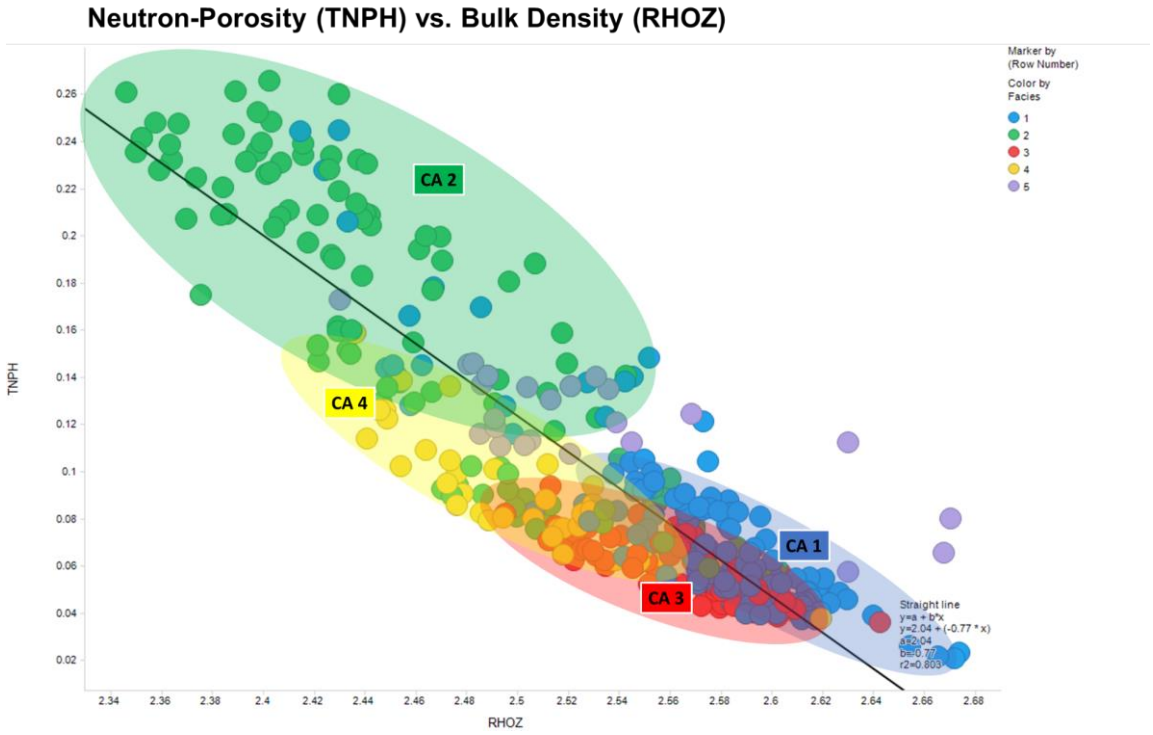

Figure 39. Neutron-porosity vs. Bulk Density cross-plot. The interrelationships between CA 1/CA 3 and CA 3/CA 4 are highlighted.

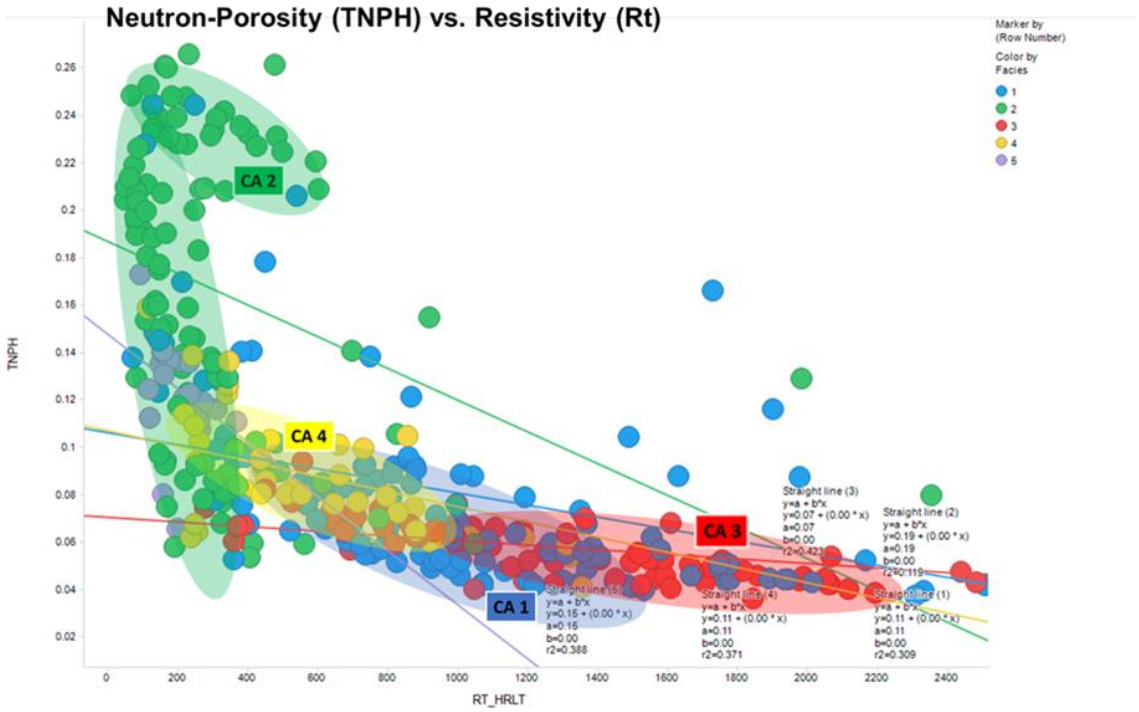

Figure 40. Neutron-Porosity (TNPH) vs. Resistivity (Rt) Crossplot.

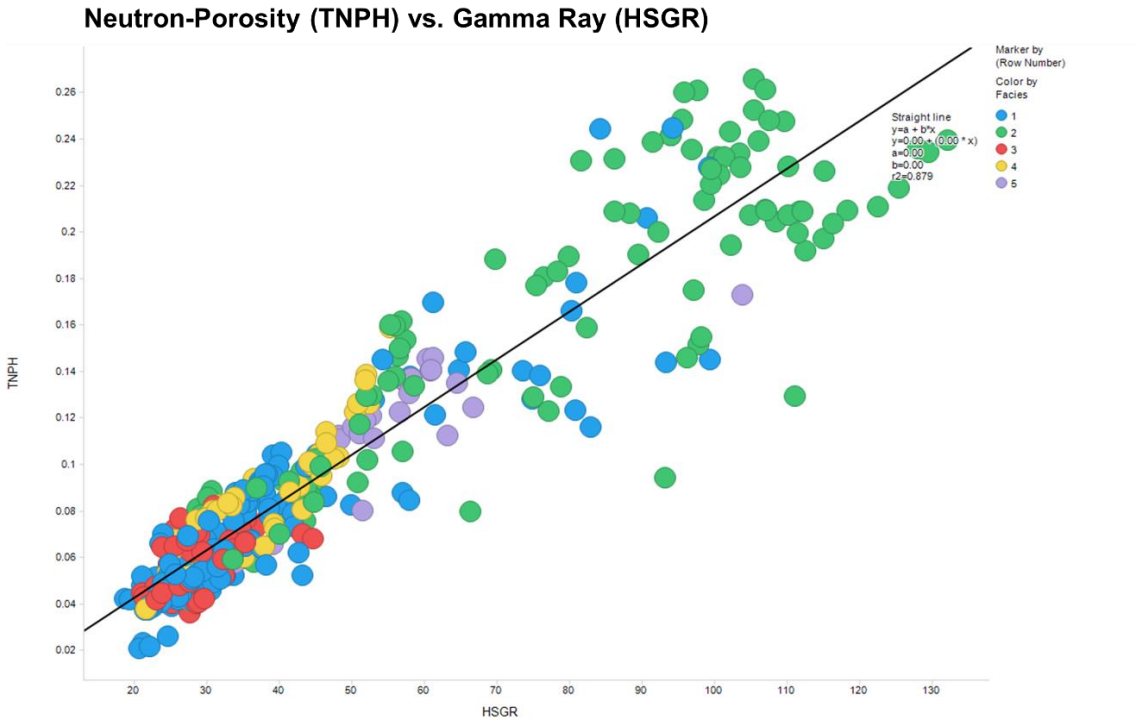

Figure 41. Neutron-Porosity (TNPH) vs. Gamma-Ray (GSGR) Crossplot

5. DISCUSSION

Detailed core description, and petrographic and XRD data analysis resulted in the identification and definition of eleven microfacies. The objectives for identifying those microfacies being to 1) better characterize, and determine the extent of the complex sedimentological and mineralogic, (in addition to depositional and diagenetic) heterogeneity of FBSC deposits, as a means to facilitate interpretation of depositional and post-depositional processes and environment, 2) evaluate associated reservoir or non-reservoir properties, and 3) enable identification and prediction of identified microfacies lithologies in the subsurface using commonly available, conventional log data.

Sedimentary facies, stratigraphy, and reservoir characteristics of the Bone Spring Fm. have been studied in Delaware Basin outcrops (e.g. Guadalupe Mountains, Glass Mountains) (Amerman et al., 2011; Boyd, 1958; Janson et al., 2007; King, 1948, 1962, 1965; Playton and Kerans; Rigby, 1958; Scholle et al., 2007), in addition to in the subsurface near basin margins (Gawloski, 1987; Mazzullo and Reid, 1987; Saller et al., 1989a, b; Wiggins and Harris, 1985). However, very few Delaware Basin outcrops contain strata correlative to deeper slope and basin deposits (Gardner, 2014; Li et al., 2015), and little to none are correlative to the FBSC member in such settings. Similarly, few subsurface Bone Spring fm. investigations have studied distal basin strata of the FBSC member, and fewer still with regard to the allochthonous carbonate deposits which frequently constitute up to 50% of the interval in deep slope and basin settings.

To facilitate the correlation of microscale facies and associated petrophysical properties (core-to-log correlation), microfacies were grouped into five 'correlation associations' on the basis of having similar: matrix and grain type and composition, mineralogy and depositional texture/fabric, visible pore space, and diagenetic features. As discussed, FBSC deposits are characterized by complex lithologic and depositional heterogeneity; diagenetic processes, particularly silicification and heavy calcite cementation, further influence, and distort the predictability of reservoir and non-reservoir facies. This study quantified that aforementioned heterogeneity through the identification of eleven representative microfacies with associated reservoir and non-reservoir characteristics, and consideration for the presence or absence, and relative abundance of silicification or calcite cementation. Accurately coordinating those microfacies into representative correlation associations enables their identification and prediction in the subsurface using commonly available convention log suites. This not only facilitates interpretation of depositional framework and associated reservoir and non-reservoir characteristics not previously achievable at the scale provided by seismic and conventional log data alone, but also sets the framework for future investigations to utilize empirical data to enhance our understanding of the physical characteristics and associated reservoir and non-reservoir implications of deep slope to basinal deposits of the FBSC member.

5.1 FBSC Environment of Deposition (EOD)

Sediments of the FBSC member of the Bone Spring Formation are interpreted to have been deposited into distal slope and basin settings of the Delaware Basin by various mass-transport, turbidite, and pelagic to hemi-pelagic processes; and post-depositionally further differentiated by both biogenic and diagenetic processes. The interpreted environment of deposition (EOD) for each microfacies, and approximate transport range for associated depositional processes (in relation to basin margin) are described below and depicted in (figure 42), a depositional model for the Northern Delaware Basin during latest Leonardian time.

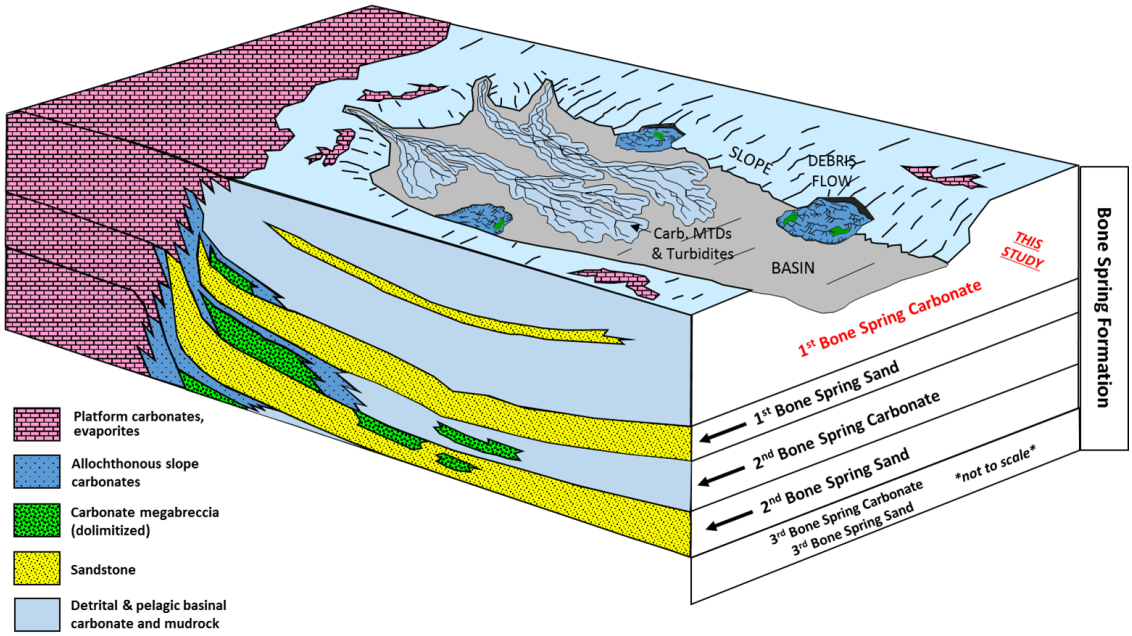

Figure 42. Depositional model for the Northern Delaware Basin during deposition of the First Bone Spring Carbonate Member (latest Leonardian time.) Modified from Hanford (1981); Montgomery (1997a); Asmus (2012).

5.1.1 Facies Interpretations

Microfacies 1A through 1D were deposited into slope and basin settings by various mass-transport, turbidite, and hemi-pelagic processes, and consist of sediments sourced from upper-slope, slope, and proximal basin settings.

Microfacies 1A is interpreted as deposited in a deep- outer-slope to basin environment, with some deposits post-depositionally reworked by bottom currents into more distal parts of the basin. Primary evidence for pelagic to hemipelagic deposition in a deep-water environment is the lack of shallow water fauna, presence (but not abundance) of sponge spicules and radiolarians, and predominantly fine grained massive to faintly laminated fabric associated with characteristic deposits. The abundance of carbonate mud can indicate deposition during transgressive to highstand periods of sea level when shallow water carbonate production was high (Tucker and Wright, 1990; Asmus, 2012), and occasional angular to slightly wavy laminations may be indicative of reworking by bottom currents and/or transportation deeper into the basin. Additional evidence for deep-water, low-energy deposition of mf1A is provided by both the volume and siliceous composition of sponge spicules, as preservation of the original opaline, siliceous mineralogy of spicules is best in low energy basinal carbonates because silica dissolution is slow relative to rapid micrite cementation in such settings (Flügel, 2004). The presence, but lesser amount of sponge spicules relative to microfacies 1B, 1C & 1D supports this, as the abundance of sponge spicules is commonly inversely related to distance from shelf (Flügel, 2004).

Microfacies 1B sediments are interpreted to have been originally deposited in a slope setting, and subsequently redeposited into deep- slope to basinal settings by turbidity currents. Original deposition in shallower settings followed by resedimentation in a deep slope to basin setting is supported by the significant presence of shallow water fauna, and the typical occurrence of normal grading and sharp basal contacts associated with these deposits, which are key characteristics for recognition of resedimented carbonates/carbonate turbidites (Flügel, 2004; Hart, 2014). Typical underlying of black organic mudstones (mf 2A) and grading into overlying pelagic carbonates (MF 1A) and/or organic mudstones (MF 2A, B) also supports the aforementioned interpretations.

Microfacies 1C is interpreted as likely deposited in slope or outer slope settings during a high-order highstand to early lowstand period of sea level fluctuation. This is evidenced by the presence but not abundance of shallow water fauna (echinoderms, gastropods, spicules, etc.) and both bioturbation and planar laminations which can indicate less interrupted outer slope deposition by settling and benthic organism activity. The increased presence of detrital quartz silt and terrigenous clay, supports the theory for a short late highstand to early lowstand period marked by increased fine grained siliciclastic input to basin. Bone Spring Fm. (and Delaware Basin as a whole) lowstands are characterized by increased to dominant siliciclastic deposition onto slope and into basin settings, while transgressions and highstand sequence tracts are dominantly marked by pelagic and carbonate deposition (Silver and Todd, 1969; Wiggins and Harris, 1985; Gawloski, 1987; Saller et al., 1989b; Montgomery, 1997b; Hart et al., 2000; Nester et al., 2014; Li et al., 2015).

Microfacies 1D sediments are interpreted as sourced from a higher energy, shallow, possibly marginal slope setting (similar to MF1B), and to have been transported to a deep slope to basin setting. The primary differentiator relative to MF 1B deposits is a decrease in clay content and organic material, and increase in carbonate cement; which is interpreted to be the result of original deposition in a higher energy, less anoxic, less organic rich, marginal setting. These interpretations are further supported by the increased abundance of sponge spicules; considering the aforementioned inverse relationship between sponge spicule quantity and distance from the shelf discussed by (Flügel, 2004). Further, deposition in a higher energy environment can lead to reduced mud content, in turn resulting in more original porosity/permeability, exposure to saturated pore fluids, and increased dissolution and cementation; potentially explaining the abundance of calcite cement, calcite replacement in sponge spicules, and paucity of matrix material characteristic of these deposits. Sharp basal contacts, in addition to allochthonous fauna support the interpretation for re-sedimentation after original deposition in a shallower environment. Increased cementation appears to be indicated at the macroscale by the presence of mineralized fractures.

Microfacies 2A, 2B, and 2C were deposited into deep-water, distal slope to basin settings by pelagic to hemi-pelagic settling.

Microfacies 2A is interpreted to have been deposited in a deep-water slope to basin setting by pelagic settling on to the ocean floor, likely during anoxic conditions. The interpretation of deposition by pelagic settling in an open, deep slope to basin environment is supported by the massive to faintly planar laminations, lack of shallow

water fauna, moderate to sparse presence of sponge spicules and radiolarians, and siliceous composition of sponge spicules associated with these deposits. Sponge spicules are often indicative deeper open marine deposits, and their original siliceous composition is generally best preserved in low energy environments where water turbulence is low and silica dissolution is relatively slow (Flügel, 2004). The interpretation for deposition in a deep, anoxic environment is further supported by the abundance of organic material, lack of bioturbation and burrowing by marine organisms, and black color of associated deposits. Anoxic, reducing conditions are also supported by the semi-frequent occurrence of pyrite, which is a product of bacterial reduction of organic matter (Tucker and Wright, 1990; Asmus, 2012).

Microfacies 2B is similar to microfacies 2A in texture, fabric, and grain type, but includes undifferentiated silt-sized calcareous skeletal grains/fragments, minor carbonate mud, and occasional very vague inclined stratification. Associated deposits were likely originally deposited by pelagic to hemipelagic settling in a distal slope setting, possibly being reworked by bottom currents, which resulted in deposition deeper into the basin. The presence of carbonate mud and silt sized carbonate grains is evidence for the interpretation of original deposition closer to the shelf (relative to *mf2A*); occasional presence of vaguely sharp basal contacts, lesser amounts of organic material (also relative to *mf2A*), and common grading into overlying *mf2A* support the possibility for reworking by bottom currents and eventual deposition deeper in the basin.

Microfacies 2C is interpreted to have been deposited in a deep-water slope to basin setting by pelagic to hemipelagic suspension settling, possibly during periods of

increased oxidation relative to the anoxic depositional environment associated with *mf2A*. Massive fabric with mud to silt sized grains, lack of shallow water fauna, moderate but variable presence of organic material and sponge spicules support the interpretation for deposition by pelagic settling in an open, deep slope to basin setting. Microfacies 2C is also interpreted as probably deposited during periods of increased oxidation based on the abundance of burrowing and bioturbation associated with these deposits; and specifically, based on the characteristic presence of centimeter scale sub-horizontal zoophycos burrows (figure 17), left by deposit feeding 'worm-like' organisms which lived in deep-sea oozes and are characteristic trace fossils for pelagic facies (Tucker and Wright, 1990). Both bioturbation and burrowing are marked by a decrease in matrix material, an increase in grains, and abundant silica cement encasing calcified grains. Bioturbation and burrowing frequently results in the removal of organic material, and can act as conduits for fluid flow (Flügel, 2004). It is possible that bioturbation increased diagenetic fluid flow throughout the burrowed portions of these deposits, resulting in the dissolution and replacement of siliceous spicules and radiolarians by calcite, and subsequent silicification of remaining pore space. It was noted that this microfacies frequently occurs in close proximity to silicified intervals (*CA 3, CA 4*), we can postulate that bioturbation and burrowing lead to increased dissolution of siliceous organisms, which in turn sourced silicification of more originally porous detrital carbonate deposits.

Microfacies 3A sediments are interpreted as sourced from a shallower, relatively high energy slope environment, from which they were transported to deeper slope and

basin settings. This is evidenced by the abundance of shallow water fauna, markedly sponge spicules and radiolarians, and sharp, slightly erosive basal contacts characterizing CA 3 deposits. The abundance of sponge spicules, in addition to characteristic sedimentary structures supports classifying mf3A sediments as turbidite deposits in distal basin settings (Kiessling, 1996).

Silicification is prevalent throughout MF3A deposits and is thought to be sourced biogenically. The widespread occurrence of sponge spicules and radiolarians in this facies, many of which have been replaced by calcite, supports this idea. The interpreted higher energy source environment and depositional processes associated with MF3A sediments likely would have winnowed matrix material and resulted in a 'grainier', more porous and permeable deposit compared to other more mud and clay rich facies. This could have increased exposure to permeating diagenetic fluids and catalyzed silicification processes. Bioturbation would have resulted in additional exposure to subsurface pore waters, increasing dissolution of radiolarians and sponge spicules, and further catalyzing diagenetic reactions.

Microfacies 5A and 5B sediments are likely sourced from upper slope settings, and were deposited via debris flow and other mass-transport processes into distal slope and proximal basin settings. Highly deformed, chaotically oriented, poorly sorted, granular- to cobble-sized clasts, in addition to lack of internal sedimentary structures and sharp-erosive basal contacts are indicative characteristics for debrites. Abundant shallow water fauna are evidence for an upper slope source setting; and cobble-sized intraclasts

provide evidence for deposition in a more proximal setting relative to other identified microfacies.

5.2 Interpretation and Differentiation of CA Log Characteristics

Low gamma-ray values (generally below 50 gAPI), a low magnitude overlapping neutron- and density-porosity curve response, and the highest Pe response relative to surrounding deposits are the most distinct characteristics associated with correlation association 1 (CA1), and enable clear differentiation from *CA's 2,4,* and *5*. Log characteristics for CA1 & CA3 can appear similar, however CA 1 can be distinguished by a higher Pe response, and the characteristic overlaying of the neutron- and density-porosity curves. These distinguishing characteristics are interpreted to be a result of the high calcite content associated with CA1 deposits as the Pe curve indicates deposits are more calcite rich as the measured value approaches 5, and overlapping of the neutron- and density-porosity curves when calibrated to a 2.71 matrix density also indicates limestone lithology (Asquith and Krygowski, 2004).

The most distinct log characteristics associated with correlation association 3 deposits are the combination of low gamma-ray values (generally below 40 gAPI), low, crossed-over neutron- and density-porosity values, and very high resistivity; the combination of which enables clear differentiation of this correlation association from the other four characterized in this study.

Prior to this study, considerable uncertainty existed for the driving factor behind crossover of the neutron-porosity and density-porosity curves (N-D curves) in the carbonate facies of the FBSC member. When referenced to limestone units, N-D curve crossover (density-porosity > neutron porosity) can be indicative of a sandstone, or more silica rich lithology; but, could also be a result of the 'gas-crossover' effect (Asquith and Krygowski, 2004). Considering the low gas to oil ratio for hydrocarbon production in this interval of the Northern Delaware Basin, and the non-reservoir quality associated with this facies, gas-effect can largely be discounted as a primary driver behind the crossover, particularly in carbonate deposits. However, even if gas-effect is counted as negligible, and N-D crossover was assumed to be related to presence of silica, no evidence has been provided for differentiating detrital silt content from the presence of authigenic silica (silicification) as the primary driver for N-D crossover in limestones.

This study was able to establish that silicified limestone intervals (*CA3*) can be identified by crossover of the N-D curves, when accompanied by low porosity and gamma ray values, and high magnitude resistivity; and can be differentiated from silt-rich limestones (e.g., *mf 1C, CA1*) by relatively lower porosity, higher resistivity, and higher magnitude N-D crossover (figure 43). It should be emphasized that the characteristic log response for CA3 identified in this study is valuable as it not only facilitates future research and learning through empirical data, but also enables avoidance of this drill-rate inhibiting, non-reservoir lithology while targeting unconventional reservoirs in the FBSC member.

The correlation quality associated with the CA1 and CA3 log responses is fairly high, and while these correlation associations can confidently be differentiated from the other three characterized in this study, the range of values recorded for some measurements reflects the variability between the lithologies represented by CA1 & 3 (e.g., silt-rich limestone, silicified limestone-calcareous chert, chert). Thus there may be room for further discrimination within these correlation associations to improve correlation quality of associated petrophysical properties and signature log responses.

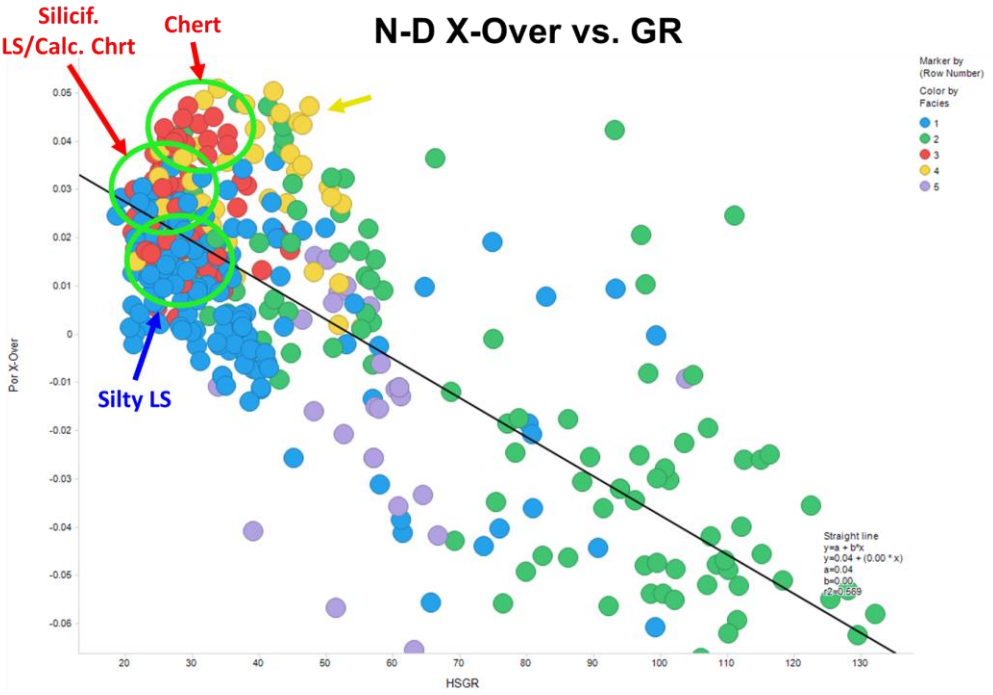

Figure 43. Porosity crossover vs. gamma ray log response cross-plot. Of note are identified variability between lithogies represented by correlation associations 1 and 3; particularly the differentiation between silt-rich limestone and silicified limestone-calcareous chert.

5.3 CA Exploration and Reservoir Implications

5.3.1 CA1 & CA3 Exploration and Reservoir Implications

CA1 (particularly microfacies 1D) and CA3 deposits are interpreted to have very poor reservoir quality as a result of low associated permeability and porosity, and sparse to no organic content. Low organic content is commonly associated with resedimented carbonates because they are sourced from low-TOC shelf sediments (Hart, 2014). The lower permeability and porosity in these deposits compared to interbedded source rocks is likely the result of diagenesis (silicification/cementation) and transportation, both of which can reduce and occlude porosity and permeability, destroying reservoir quality. In addition to poor associated reservoir quality, these deposits can be drilling inhibitors; a hazardous characteristic which often has a significantly negative impact on exploration economics.

CA3 deposits are essentially variants of CA1 deposits, with high degrees of cementation and/or silicification; and so, are not only interpreted to have the lowest reservoir quality of all the identified CA's, but also to represent the greatest inhibitors to drilling and completion when targeting unconventional reservoir intervals in the FBSC member. These interpretations are supported by petrophysical and empirical data which were able to be collected as a result of the distinctive log responses characterized for each correlation association identified in this study. Correlation of the characteristic log response for CA3 deposits against rate of penetration (ROP) logs provides a clear example of the inhibiting effect these deposits have when drilling within the FBSC

interval (Figures 44, 45). With poor associated reservoir quality, and little to no organic content, these deposits not only represent non-reservoir intervals and drilling inhibitors (as discussed), but with increasing content can also further negatively affect unconventional reservoirs targeted in the FBSC member, as they add to the gross thickness of these unconventional reservoir intervals without contributing to hydrocarbon generation or storage (Hart, 2014).

The understudied nature of CA1 and CA3 deposits in the FBSC member prior to this study has resulted in miscalculation of risk, inefficient exploitation of reservoir rock, and decreased drilling and completion efficiency during previous exploration and development of hydrocarbon bearing source rocks within the interval. New understanding, and the ability to identify CA1 and CA3 deposits using commonly available log data will allow for predictability in the subsurface and enable new development strategies for unconventional exploration of the FBSC member (Figures 36, 37, 38).

5.3.2 CA2 Exploration and Reservoir Implications

Unlike detrital carbonate deposits in the FBSC, the mud rock facies represented by correlation association 2 (CA2) have been investigated in detail (Nester et al., 2014; Schwartz et al., 2014; Stolz, 2014). CA2 deposits are considered the source rock and reservoir facies for unconventional exploration within the FBSC, and are informally referred to as the Avalon or Leonard ‘shales’ depending on their stratigraphic location within the interval. It’s important to reiterate that drilling rates in CA2 deposits are far

more efficient compared to those associated with CA's 1&3 (Figures 42, 43), which further highlights the importance of avoiding those non reservoir facies when drilling within the FBSC member in a deep slope and basin setting.

It is conceivable and worth noting that the siliceous, intermittently lightly silicified microfacies 2C deposit intervals could represent especially good unconventional reservoira, as brittleness may be increased compared to the more clay rich microfacies, which would increase stimulated fracture efficiency; though that interpretation is beyond the scope of this study.

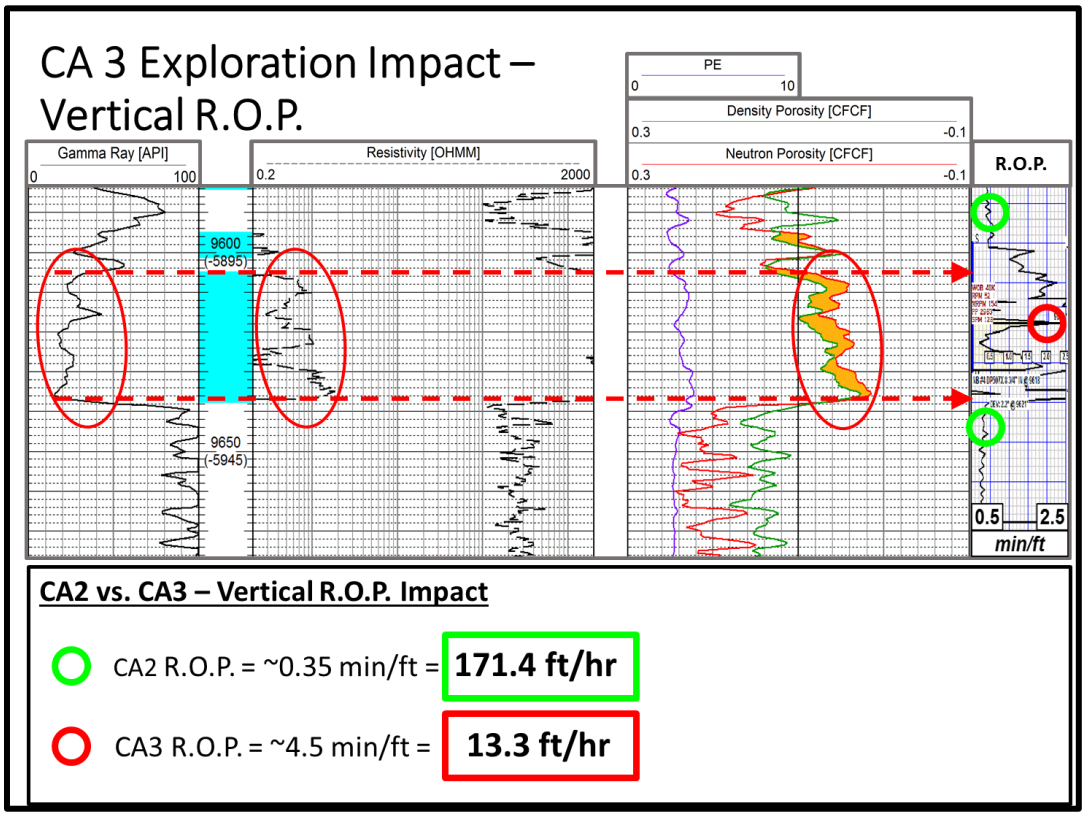

Figure 44. Correlation of the characteristic log responses for CA2 and CA3 deposits against vertical rate of penetration (ROP) clearly demonstrates the negative impact detrital carbonates have when drilling within the FBSC interval.

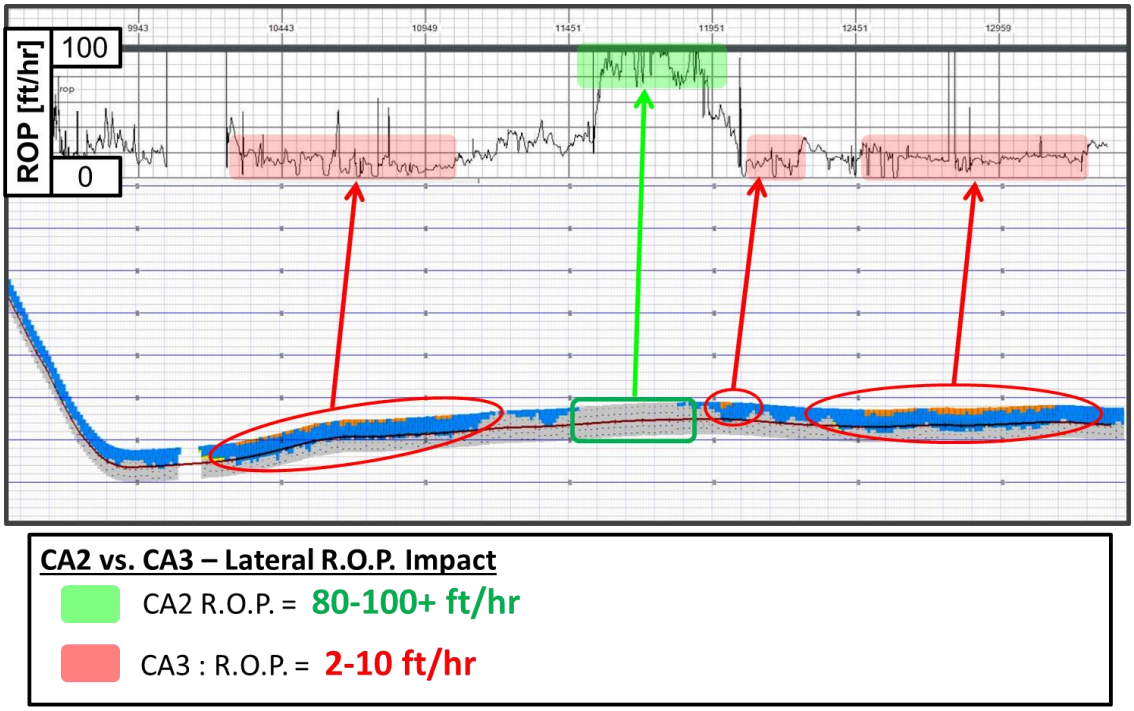

Figure 45. Lateral rate of penetration (ROP) impact of CA1 & CA3 deposits relative to CA2 deposits. Horizontal drilling rates in CA2 are far more efficient than those associated with CA's 1&3, which further highlights the importance of avoiding non-reservoir facies when drilling within the FBSC member.

5.4 Silicification Susceptibility

The presence and relative abundance of silicification in characteristic deposits was determined through petrographic and XRD analysis, and further confirmed by log measurements. An abundance of siliceous skeletal grains (namely sponge spicules and radiolarians), and the presence of heavy bioturbation were consistent sedimentological features associated with identified silicified deposits. It is interpreted that higher levels in depositional or syndepositional porosity and permeability, especially when increased by the presence of extensive bioturbation and burrowing, in congruence with an abundance

of siliceous bioclasts were significant factors which increased the susceptibility for silicification to occur. Support for these interpretations includes the postulation that silicification in limestones is commonly biogenically sourced from the tests of siliceous organisms (Hesse, 1989; Scholle and Ulmer-Scholle, 2003; Butts and Briggs, 2011; Butts, 2014), and that burrows and other bioturbation can act as significant conduits for diagenetic fluid flow (Flügel, 2004). Further, it makes sense that allochthonous, more grain-rich, matrix poor deposits would have higher initial porosity than surrounding clay and/or mud-rich deposits, and hence would be exposed to higher levels of saturated pore fluids. That said, characterizing the detailed diagenetic framework for silica and carbonate diagenetic reaction sequences was beyond the scope of this project, and additional data and a more detailed investigation will be required before the susceptibility of deposits for silicification can be fully defined.

The incorporation of the presence and relative abundance of silicification to the definition and discrimination of microfacies and correlation associations served as a useful methodology for improving correlation quality between core identified facies and petrophysical properties; and for the establishment of characteristic log signatures. This study was able to determine that heavy silicification of limestones can be identified using commonly available log data (see interpretation and differentiation of CA log characteristics section); and further, can be differentiated from silt-rich limestones which generate a similar log response. This newly established technique enhances recognition of identified deposits in the subsurface, not only enabling identification of complex, variable reservoir and non-reservoir lithologies using commonly available data sets

(where core data is not available), but improving our understanding of their implications and physical characteristics through empirical data.

6. CONCLUSIONS & FUTURE WORK

Heterogeneity of the FBSC in a deep, slope and basin setting was constrained through the identification and definition of 7 macrofacies and 11 representative microfacies. These deposits consisted of organic to calcareous and/or siliceous mudstones and silty mudstones; spiculitic and variably: fossiliferous, clay-rich, silty, and silicified wackestones, wackestone-packstones, and packstones; calcareous to argillaceous chert, and rarely intraclastic floatstones, to skeletal rudstones.

Coordination of the identified microfacies into 5 ‘correlation associations’ facilitated the establishment of characteristic petrophysical properties and signature log responses, which in turn enables the identification and prediction of defined facies and their associated reservoir or non-reservoir properties in the subsurface using commonly available, limited data sets away from core data. The ability established here to more accurately identify and predict FBSC deposits in the subsurface will continue to improve our previous understanding of associated diagenetic processes, physical properties, and related implications by means of empirical data. Significantly, this research narrows relevant subsurface uncertainty ranges to enable exploration and development strategies for unconventional drilling and completion within the FBSC based not only on reservoir quality, but also on drilling favorability (i.e. hazard avoidance); thus increasing the potential for identifying prospective areas previously overlooked.

It was determined that while CA2 represents the reservoir facies within the FBSC member, CA’s 1 and 3 represent non-reservoir facies which not only consist of the

deposits with the poorest reservoir qualities, but also (particularly in CA3) those which can inhibit drilling and (likely) completion within the studied interval. Importantly, this new understanding, and the ability to identify and predict CA1 & 3 deposits in the subsurface will improve exploitation efficiency and economics for exploration of unconventional reservoirs within the FBSC member.

Heavy silicification and/or cementation was identified as a primary driver behind reservoir quality degradation. Although the use of diagenetic features as a variable for coordinating and defining facies is non-standard methodology, the incorporation of silicification as an element for the definition and differentiation of microfacies and correlation associations was useful for improving core-to-log correlation quality between core identified facies and petrophysical properties in this study. Most significantly, this practice resulted in determination of the driving factor behind crossover of the N-D curves seen in some carbonate facies of the FBSC member, establishing that silicified limestone intervals (CA3) can be identified by crossover of the N-D curves, when accompanied by low porosity and gamma ray values, and high resistivity; and can be differentiated from silt-rich limestones and clay-rich chert which have similar log responses.

In regards to the investigation of controlling factors for silicification susceptibility of a given FBSC deposit, it was concluded that the abundant presence of originally siliceous sponge spicules and radiolarians, in addition to heavy bioturbation, and the ability for diagenetic pore fluids to permeate a deposit are factors which increase susceptibility for silicification. However, additional data and a more detailed

investigation is required before susceptibility and diagenetic history can be more wholly constrained. This research provides the framework for such studies which can further our understanding of those diagenetic processes and associated physical properties.

REFERENCES

Amerman, R., 2007, Deepwater mass-transport deposits: Structure, stratigraphy, and implications for basin evolution: Dissertation thesis, Colorado School of Mines, Golden, Colorado, 239 p.

Amerman, R., E. P. Nelson, M. H. Gardner, and B. Trudgill, 2011, Submarine Mass-Transport Deposits of the Permian Cutoff Formation, West Texas, U.S.A.: Internal Architecture and Controls on Overlying Reservoir Sand Deposition, *in* R. C. Shipp, P. Weimer, and H. W. Posamentier, eds., Mass-Transport Deposits in Deepwater Settings: SEPM Special Publication 96: SEPM Special Publications: Tulsa, Oklahoma, Society for Sedimentary Geology, p. 235-267.

Asmus, J. J., 2012, Characterizing the Internal Architecture of Upper Bone Spring Limestone Turbidites and Mass-Transport Deposits (MTDs) Utilizing High-Resolution Image Log Technology, Western Michigan University, Kalamazoo, Michigan, 471 p.

Asmus, J. J., and G. M. Grammer, 2013, Characterization of Deepwater Carbonate Turbidites and Mass-Transport Deposits Utilizing High-Resolution Electrical Borehole Image Logs: Upper Leonardian (Lower Permian) Upper Bone Spring Limestone, Delaware Basin, Southeast New Mexico and West Texas: Gulf Coast Association of Geological Societies Transactions, v. 63, p. 27-65.

Asquith, G. B., 1979, Subsurface carbonate depositional models: a concise review: Tulsa, Oklahoma, PennWell Books, 121 p.

Asquith, G. B., and D. Krygowski, 2004, Basic Well Log Analysis: AAPG Methods in Exploration Series, v. 16: Tulsa, Oklahoma, American Association of Petroleum Geologists, 244 p.

Bebout, D. G., and R. G. Loucks, 1984, Handbook 5: Handbook for Logging Carbonate Rocks: Austin, TX, Bureau of Economic Geology, The University of Texas at Austin, 43 p.

Boyd, D. W., 1958, Permian Sedimentary Facies, Central Guadalupe Mountains, New Mexico, Bulletin, Socorro, New Mexico, New Mexico Institute of Mining & Technology, p. 100.

Butts, S. H., 2004, Silica diagenesis in the Lower Devonian Helderberg Group of New York: Geological Society of America Abstracts with Programs, v. 36(5), p. 383-384.

Butts, S. H., 2007, Silicified Carboniferous (Chesterian) Brachiopoda of the Arco Hills Formation, Idaho: Journal of Paleontology, v. 81, p. 48-63.

Butts, S. H., 2014, Silicification: The Paleontological Society Papers, v. 20, p. 15-34.

Butts, S. H., and D. E. G. Briggs, 2011, Silicification through time, *in* P. A. Allison, and D. J. Bottjer, eds., Taphonomy: Process and Bias Through Time: Topics in Geobiology, Springer Netherlands, p. 411-434.

Daley, R. L., 1987, Patterns and controls of skeletal silicification in a Mississippian fauna, northwestern Wyoming: Unpublished Masters thesis, University of Wyoming, 140 p.

Doveton, J. H., 1994, Compositional Analysis of Lithologies from Wireline Logs, AAPG Special Publications, CA 2: Geologic Log Analysis Using Computer Methods: AAPG Special Publications: Computer Applications, AAPG, p. 47-64.

Dunham, R. J., 1962, Classification of Carbonate Rocks According to Depositional Textures, *in* W. E. Ham, ed., Memoir 1: Classification of Carbonate Rocks--A Symposium: Tulsa, Oklahoma, American Association of Petroleum Geologists, p. 108-121.

Erwin, D. H., and D. L. Kidder, 2000, Depositional controls on selective silicification of Permian fossils, southwestern United States, *in* B. R. Wardlaw, R. E. Grant, and D. M. Rohr, eds., Guadalupian Symposium. Smithsonian Contributions to Earth Science, v. 32: Washington, D. C., Smithsonian Institution Press, p. 407-415.

Fitchen, W., M. A. Starcher, R. T. Buffler, and G. L. Wilde, 1995, Sequence Stratigraphic Framework of Lower Permian Carbonate Platform Margins, Sierra Diablo, West Texas, *in* R. A. Garber, and R. F. Lindsay, eds., Wolfcampian-Leonardian Shelf Margin Facies of the Sierra Diablo: Seismic Models for Subsurface Exploration, West Texas Geological Society Publication No. 95-97, p. 23-66.

Flügel, E., 2004, Microfacies of Carbonate Rocks: Analysis, Interpretation, and Application: New York, Springer-Verlag Berlin Heidelberg, 976 p.

Gardner, M. H., 2014, Back to Basics: The ABCs of Correlation of Basin-Restricted Middle Perian Carbonates of the Delaware Basin: Unraveling the Avalon, Bone Canyon and Cutoff Stratigraphy, Midland Center.

Gawloski, T. F., 1987, Nature, Distribution, and Petroleum Potential of Bone Spring Detrital Sediments Along the Northwest Shelf of the Delaware Basin, *in* D. Cromwell, and L. Mazzullo, eds., The Leonardian Facies in W. Texas and S.E. New Mexico and Guidebook to the Glass Mountains, West Texas: Permian Basin

Section-SEPM Publication 87-27: Midland, TX, Permian Basin Section: Society of Economic Paleontologists and Mineralogists, p. 85-105.

Hart, B., 2014, The Calcites of Shale Plays: Why Moving Beyond Quantitative Mineralogy Will Improve Project Economics, Unconventional Resources Technology Conference.

Hart, B., R. Pearson, R. Smith, and D. Leiphart, 2000, The Bone Spring Formation, Delaware Basin: progress and future directions, *in* S. R. Tomlinson, ed., Southwest Section AAPG GEO 2000: Into The Future, Midland, TX, West Texas Geological Society, p. 98-115.

Hastings, H. R., 2016, Characterization and implications of carbonate mass transport deposits within the Upper Leonardian First Bone Spring Carbonate Interval: Delaware Basin, Southeast New Mexico, GSA Annual Meeting, Denver, Co.

Hesse, R., 1989, Silica Diagenesis: Origin of Inorganic and Replacement Cherts: Earth-Science Reviews, v. 26, p. 253-284.

Hill, C. A., 1996, Geology of the Delaware Basin Guadalupe, Apache, and Glass Mountains New Mexico and West Texas: Permian Basin Section - SEPM Publication 96-39: Albuquerque, New Mexico, Permian Basin Section - Society for Sedimentary Geology, 480 p.

Hills, J. M., 1984, Sedimentation, Tectonism, and Hydrocarbon Generation in Delaware Basin, West Texas and Southeastern New Mexico: AAPG Bulletin, v. 68, p. 250-267.

Hinman, N. W., 1998, Sequences of silica phase transitions: effects of Na, Mg, K, Al, and Fe ions: Marine Geology, v. 147, p. 13-24.

Janson, X., C. Kerans, J. A. Bellian, and W. Fitchen, 2007, Three-dimensional geological and synthetic seismic model of Early Permian redeposited basinal carbonate deposits, Victorio Canyon, west Texas: AAPG Bulletin, v. 91, p. 1405-1436.

Kastner, M., J. B. Keene, and J. M. Gieskes, 1977, Diagenesis of siliceous oozes—I. Chemical controls on the rate of opal-A to opal-CT transformation—an experimental study: Geochimica et Cosmochimica Acta, v. 41, p. 1041-1059.

Kiessling, W., 1996, Facies characterization of mid-mesozoic deep-water sediments by quantitative analysis of siliceous microfaunas: Facies, v. 35, p. 237.

King, P. B., 1948, Geology of the southern Guadalupe Mountains, Texas: U.S. Geol. Surv., Prof. Paper 215, Geological Survey (U.S.) Professional paper ; 215; Professional paper (Geological Survey (U.S.)) ; no. 215., p. 183.

King, P. B., 1962, Leonard and Wolfcamp Series of Sierra Diablo, Texas, *in* W. E. Hall, and A. Thomson, eds., Leonardian Facies of the Sierra Diablo Region, West Texas: Permian Basin Section-SEPM Publication 62-7, Permian Basin Section - Society of Economic Paleontologists and Mineralogists, p. 42 - 65.

King, P. B., 1965, Geology of the Sierra Diablo Region, Texas: U.S. Geological Survey Professional Paper 480, *in* U. S. D. o. t. Interior, ed., Washington, United States Government Printing Office, p. 185.

Knoll, A. H., 1985, Exceptional Preservation of Photosynthetic Organisms in Silicified Carbonates and Silicified Peats: Philosophical Transactions of the Royal Society of London. B, Biological Sciences, v. 311, p. 111-122.

Kostic, B., and T. Aigner, 2004, Sedimentary and poroperm anatomy of shoal-water carbonates (Muschelkalk, South-German Basin): an outcrop-analogue study of inter-well spacing scale: Facies, v. 50, p. 113-131.

Lancelot, Y., 1973, Chert and silica diagenesis in sediments from the central Pacific: Initial Reports of the Deep Sea Drilling Project, v. 17, p. 377-405.

Laschet, C., 1984, On the Origin of Cherts: Facies, v. 10, p. 257-290.

Laya, J. C., and M. E. Tucker, 2012, Facies analysis and depositional environments of Permian carbonates of the Venezuelan Andes: Palaeogeographic implications for Northern Gondwana: Palaeogeography, Palaeoclimatology, Palaeoecology, v. 331-332, p. 1-26.

Li, S., X. Yu, S. Li, and K. Giles, 2015, Role of sea-level change in deep water deposition along a carbonate shelf margin, Early and Middle Permian, Delaware Basin: implications for reservoir characterization Geologica Carpathica, v. 66, p. 99-116.

Mazzullo, L. J., and A. M. Reid, 1987, Stratigraphy of the Bone Spring Formation (Leonardian) and Depositional Setting in the Scharb Field, Lea County, New Mexico, *in* D. Cromwell, and L. Mazzullo, eds., The Leonardian Facies in W. Texas and S.E. New Mexico and Guidebook to the Glass Mountains, West Texas: Permian Basin Section-SEPM Publication 87-27: Tulsa, Oklahoma, Permian Basin Section: Society of Economic Paleontologists and Mineralogists, p. 107-111.

Montgomery, S. L., 1997a, Permian Bone Spring Formation: Sandstone Play in the Delaware Basin Part I-Slope: AAPG bulletin, v. 81, p. 1239-1258.

Montgomery, S. L., 1997b, Permian Bone Spring Formation: Sandstone Play in the Delaware Basin, Part II--Basin: AAPG bulletin, v. 81, p. 1423-1434.

Moscardelli, L., 2007, Mass Transport Processes and Deposits in Offshore Trinidad and Venezuela, and their role in Continental Margin Development: Dissertation thesis, The University of Texas at Austin, 172 p.

Moscardelli, L., L. Wood, and P. Mann, 2006, Mass-Transport Complexes and Associated Processes in the Offshore Area of Trinidad and Venezuela: AAPG Bulletin, v. 90, p. 1059-1088.

Nester, P., K. Schwartz, J. Bishop, and M. Garcia-Barriuso, 2014, The Avalon Shale: Tying Geologic Variability to Productivity in a Burgeoning Shale Play in the Delaware Basin of Southeast New Mexico, SPE/AAPG/SEG Unconventional Resources Technology Conference, Society of Petroleum Engineers, p. 9.

Newell, N. D., J. K. Rigby, A. G. Fischer, A. J. Whiteman, J. E. Hickox, and J. S. Bradley, 1953, The Permian Reef Complex of the Guadalupe Mountains Region, Texas and New Mexico; A Study in Paleoecology: San Francisco, W. H. Freeman, 287 p.

Pickett, G. R., 1977, Recognition of environments and carbonate rock type identification, Formation Evaluation Manual Unit II, section Exploration Wells: Tulsa, Oklahoma, Oil and Gas Consultants International, Inc., p. 4-25.

Piper, D. J. W., C. Pirmez, P. L. Manley, D. Long, R. D. Flood, W. R. Normark, and W. Showers, 1997, Mass-transport Deposits of the Amazon Fan, *in* R. D. Flood, D. J. W. Piper, A. Klaus, and L. C. Peterson, eds., Proceedings of the Ocean Drilling Program, Scientific Results, v. 155: College Station, TX, Ocean Drilling Program, p. 109-146.

Playton, T., and C. Kerans, 2006, Early Leonardian to Late Wolfcampian, Deep-Water Carbonate Systems in the Permian Basin: Evidence from West Texas Outcrops: Jackson School of Geosciences, Austin, Texas, Bureau of Economic Geology, University of Texas at Austin.

Prélat, A., D. M. Hodgson, M. Hall, C. A.-L. Jackson, C. Baunack, and B. Tveiten, 2015, Constraining sub-seismic deep-water stratal elements with electrofacies analysis; A case study from the Upper Cretaceous of the Maloy Slope, offshore Norway: Marine and Petroleum Geology, v. 59, p. 268-285.

Rigby, J. K., 1958, Mass Movements in Permian Rocks of Trans-Pecos Texas: Journal of Sedimentary Petrology, v. 28, p. 298-315.

Saller, A. H., J. W. Barton, and R. E. Barton, 1989a, Mescalero Escarpe Field, Oil From Carbonate Slope Detritus, Southeastern New Mexico, *in* J. E. Flis, R. C. Price, and J. F. Sarg, eds., Search for the Subtle Trap, Hydrocarbon Exploration in Mature Basins, West Texas Geological Society Publication No. 89-85, WTGS, p. 59-74.

Saller, A. H., J. W. Barton, and R. E. Barton, 1989b, Slope Sedimentation Associated with a Vertical Building Shelf, Bone Spring Formation, Mescalero Escarpe Field, Southeastern New Mexico, *in* P. D. Crevello, J. L. Wilson, J. F. Sarg, and J. F. Read, eds., Controls on Carbonate Platform and Basin Development, SEPM Special Publication No. 44: Tulsa, Oklahoma, Society of Economic Paleontologists and Mineralogists, p. 275-288.

Scholle, P., R. Goldstein, and D. Ulmer-Scholle, 2007, Classic upper Paleozoic reefs and bioherms of west Texas and New Mexico: New Mexico Institute of Mining and Technology, Socorro, NM.

Scholle, P. A., and D. S. Ulmer-Scholle, 2003, A Color Guide to the Petrography of Carbonate Rocks: Grains, Textures, Porosity, Diagenesis, AAPG Memoir 77: Tulsa, Oklahoma, American Association of Petroleum Geologists, 459 p.

Schwartz, K., G. Muscio, P. Nester, I. Easow, and M. Javalagi, 2014, Petrophysical and Geochemical Evaluation of an Avalon Shale Horizontal Well in the Delaware Basin: SPE/AAPG/SEG Unconventional Resources Technology Conference, p. 1-6.

Serra, O., and H. T. Abbott, 1982, The Contribution of Logging Data to Sedimentology and Stratigraphy: Society of Petroleum Engineers Journal, v. 22, p. 117-131.

Shanmugam, G., R. B. Bloch, S. M. Mitchell, G. W. J. Beamish, R. J. Hodgkinson, J. E. Damuth, T. Straume, S. E. Syvertsen, and K. E. Shields, 1995, Basin-Floor Fans in the North Sea: Sequence Stratigraphic Models vs. Sedimentary Facies: AAPG Bulletin, v. 79, p. 477-511.

Shipp, R. C., J. A. Nott, and J. A. Newlin, 2004, Physical Characteristics of Mass Transport Complexes on Deepwater Jetted Conductors and Suction Anchor Piles, Offshore Technology Conference, Houston, Tx, Offshore Technology Conference, p. 11.

Silver, B. A., and R. G. Todd, 1969, Permian Cyclic Strata, Northern Midland and Delaware Basins, West Texas and Southeastern New Mexico: AAPG Bulletin, v. 53, p. 2223-2251.

Stolz, D. J., 2014, Reservoir Character of the Avalon Shale (Bone Spring Formation) of the Delaware Basin, West Texas and Southeast New Mexico: Effect of Carbonate-rich Sediment Gravity Flows, University of Kansas, 155 p.

Swanson, R. G., 1981, Methods in Exploration Series 1: Sample Examination Manual: Methods in Exploration Series: Tulsa, Oklahoma, American Association of Petroleum Geologists, 117 p.

Tucker, M. E., and V. P. Wright, 1990, Carbonate Sedimentology, Blackwell Science Ltd., 482 p.

Watney, W. L., 1979, Gammaray - neutron cross-plots as an aid in sedimentological analysis (p. 81-100), *in* D. Gill, and D. F. Merriam, eds., Geomathematical and Petrophysical Stuides in Sedimentology: New York, Pergamon Press, p. 266.

Watney, W. L., 1980, Cyclic sedimentation of the Lansing-Kansas City groups in northwestern Kansas and southwestern Nebraska: Kansas Geological Survey Bulletin, v. 220: Lawrence, Kansas, The University of Kansas, 72 p.

Weimer, P., R. M. Slatt, R. Bouroullec, R. Fillon, H. Pettingill, M. Pranter, and G. Tari, 2006, Overview of Deepwater-Reservoir Elements, Introduction to the Petroleum Geology of Deepwater Settings: AAPG Studies in Geology, No. 57; Datapages Discovery Series, No. 8, American Association of Petroleum Geologists, p. 149-170.

Wiggins, W. D., and P. M. Harris, 1985, Burial Diagenetic Sequence in Deep-Water Allochthonous Dolomites, Permian Bone Spring Formation, Southeast New Mexico, *in* P. D. Crevello, and P. M. Harris, eds., Deep-Water Carbonates - A Core Workshop, SEPM Core Workshop No. 6, Society of Economic Paleontologists and Mineralogists, p. 140-173.

APPENDIX A

CORE DESCRIPTION AND LOGS

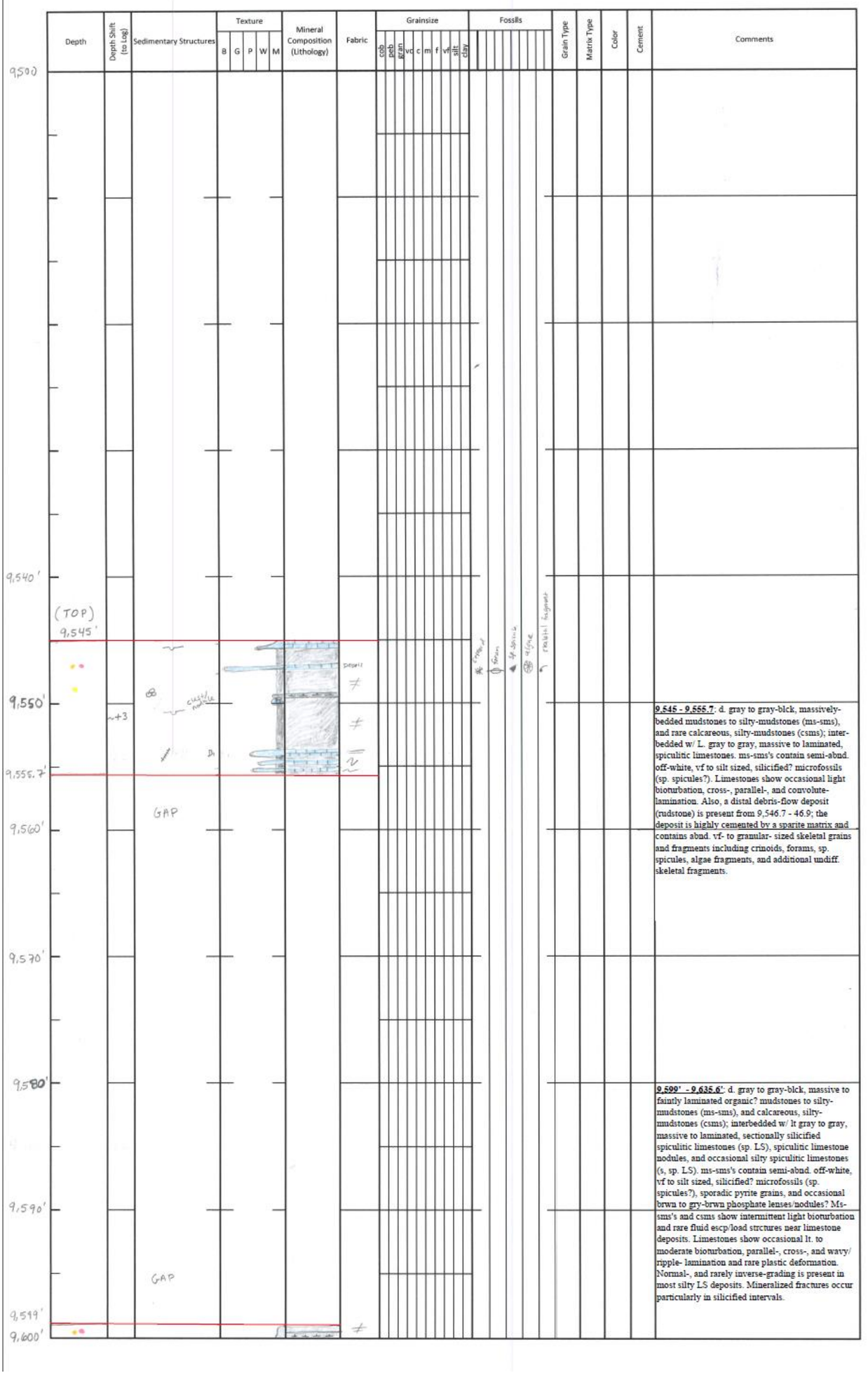
Depth
Depth Shift (to Log)
Sedimentary Structures
Texture
B G P W M
Mineral Composition (Lithology)
Fabric
Grainsize
cob peb gran vc c m f vf silt clay
Fossils
Grain Type
Matrix Type
Color
Cement
Comments
9,500'
9,540'
(TOP)
9,545'
9,550'
9,555.7'
9,560'
9,570'
9,580'
9,590'
9,599'
9,600'
+3
GAP
GAP
9,545 - 9,555.7': d. gray to gray-blck, massively-bedded mudstones to silty-mudstones (ms-sms), and rare calcareous, silty-mudstones (csms); inter-bedded w/ L. gray to gray, massive to laminated, spiculitic limestones. ms-sms's contain semi-abnd. off-white, vf to silt sized, silicified? microfossils (sp. spicules?). Limestones show occasional light bioturbation, cross-, parallel-, and convolute-lamination. Also, a distal debris-flow deposit (rudstone) is present from 9,546.7 - 46.9; the deposit is highly cemented by a sparite matrix and contains abnd. vf- to granular- sized skeletal grains and fragments including crinoids, forams, sp. spicules, algae fragments, and additional undiff. skeletal fragments.
9,599' - 9,635.6': d. gray to gray-blck, massive to faintly laminated organic? mudstones to silty-mudstones (ms-sms), and calcareous, silty-mudstones (csms); interbedded w/ lt gray to gray, massive to laminated, sectionally silicified spiculitic limestones (sp. LS), spiculitic limestone nodules, and occasional silty spiculitic limestones (s, sp. LS). ms-sms's contain semi-abnd. off-white, vf to silt sized, silicified? microfossils (sp. spicules?), sporadic pyrite grains, and occasional brwn to gry-brwn phosphate lenses/nodules? Ms-sms's and csms show intermittent light bioturbation and rare fluid escp/load strctures near limestone deposits. Limestones show occasional lt. to moderate bioturbation, parallel-, cross-, and wavy/ripple- lamination and rare plastic deformation. Normal-, and rarely inverse-grading is present in most silty LS deposits. Mineralized fractures occur particularly in silicified intervals.

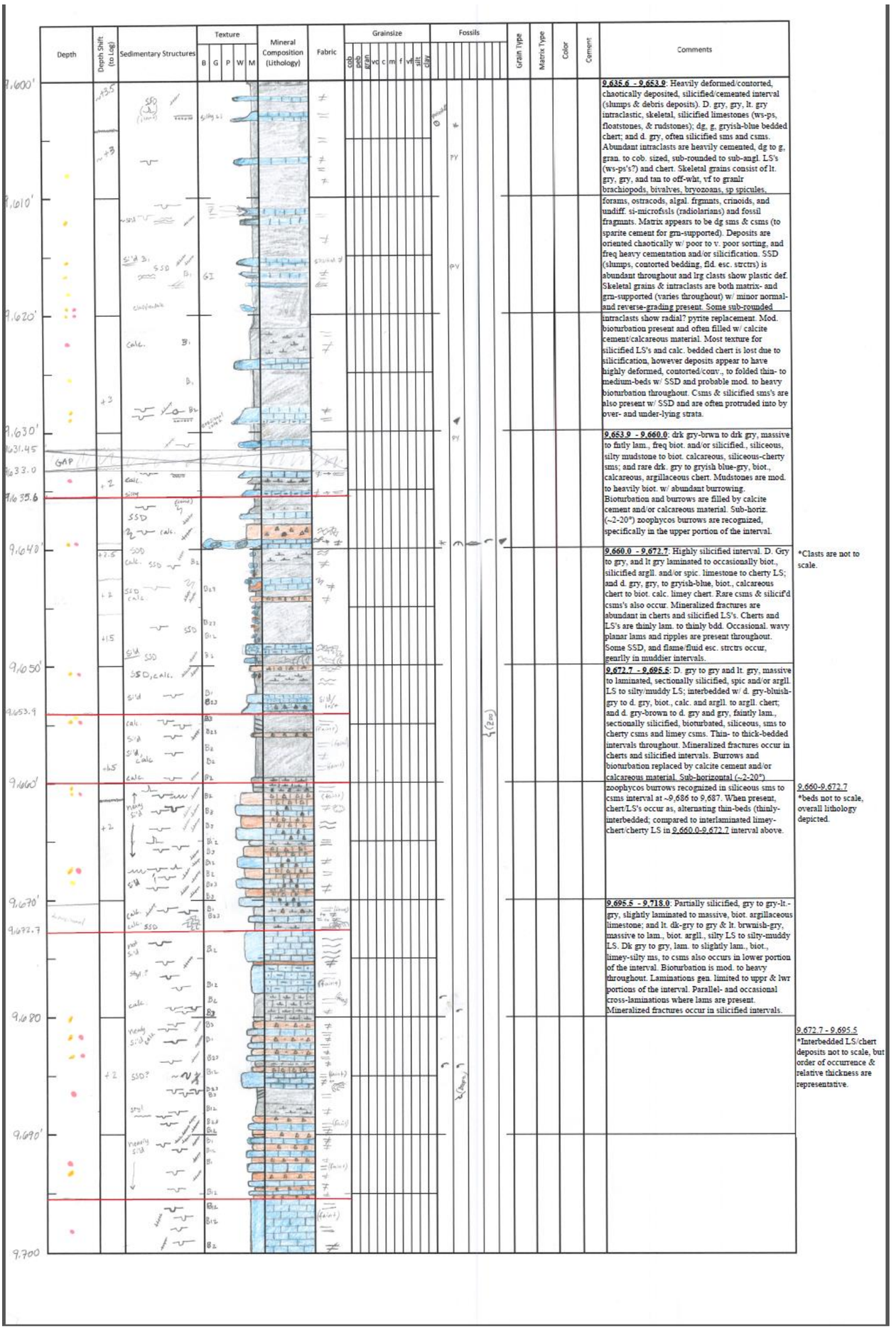
Depth
Depth Shift (to Log)
Sedimentary Structures
Texture
B G P W M
Mineral Composition (Lithology)
Fabric
Grainsize
cob peb gran vc c m f vf silt clay
Fossils
Grain Type
Matrix Type
Color
Cement
Comments
9,600'
9,610'
9,620'
9,630'
9,631.45
GAP
9,633.0
9,635.6
9,640'
9,650'
9,653.9
9,660'
9,670'
9,672.7
9,680
9,690'
9,700
SSD
calc.
GAP
9,635.6 - 9,653.9: Heavily deformed/contorted, chaotically deposited, silicified/cemented interval (slumps & debris deposits). D. gry, gry, lt. gry intraclastic, skeletal, silicified limestones (ws-ps, floatstones, & rudstones); dg, g, gryish-blue bedded chert; and d. gry, often silicified sms and csms. Abundant intraclasts are heavily cemented, dg to g, gran. to cob. sized, sub-rounded to sub-angl. LS's (ws-ps's?) and chert. Skeletal grains consist of lt. gry, gry, and tan to off-wht, vf to grainr brachiopods, bivalves, bryozoans, sp spicules,
forams, ostracods, algal. frgmnts, crinoids, and undiff. si-microfssls (radiolarians) and fossil fragmnts. Matrix appears to be dg sms & csms (to sparite cement for grn-supported). Deposits are oriented chaotically w/ poor to v. poor sorting, and freq heavy cementation and/or silicification. SSD (slumps, contorted bedding, fld. esc. strctrs) is abundant throughout and lrg clasts show plastic def. Skeletal grains & intraclasts are both matrix- and grn-supported (varies throughout) w/ minor normal- and reverse-grading present. Some sub-rounded
intraclasts show radial? pyrite replacement. Mod. bioturbation present and often filled w/ calcite cement/calcareous material. Most texture for silicified LS's and calc. bedded chert is lost due to silicification, however deposits appear to have highly deformed, contorted/conv., to folded thin- to medium-beds w/ SSD and probable mod. to heavy bioturbation throughout. Csms & silicified sms's are also present w/ SSD and are often protruded into by over- and under-lying strata.
9,653.9 - 9,660.0: drk gry-brwn to drk gry, massive to fntly lam., freq biot. and/or silicified., siliceous, silty mudstone to biot. calcareous, siliceous-cherty sms; and rare drk. gry to gryish blue-gry, biot., calcareous, argillaceous chert. Mudstones are mod. to heavily biot. w/ abundant burrowing. Bioturbation and burrows are filled by calcite cement and/or calcareous material. Sub-horiz. (~2-20°) zoophycos burrows are recognized, specifically in the upper portion of the interval.
9,660.0 - 9,672.7: Highly silicified interval. D. Gry to gry, and lt gry laminated to occasionally biot., silicified argll. and/or spic. limestone to cherty LS; and d. gry, gry, to gryish-blue, biot., calcareous chert to biot. calc. limey chert. Rare csms & silicif'd csms's also occur. Mineralized fractures are abundant in cherts and silicified LS's. Cherts and LS's are thinly lam. to thinly bdd. Occasional. wavy planar lams and ripples are present throughout. Some SSD, and flame/fluid esc. strctrs occur, genrlly in muddier intervals.
*Clasts are not to scale.
9,672.7 - 9,695.5: D. gry to gry and lt. gry, massive to laminated, sectionally silicified, spic and/or argll. LS to silty/muddy LS; interbedded w/ d. gry-bluish-gry to d. gry, biot., calc. and argll. to argll. chert; and d. gry-brown to d. gry and gry, faintly lam., sectionally silicified, bioturbated, siliceous, sms to cherty csms and limey csms. Thin- to thick-bedded intervals throughout. Mineralized fractures occur in cherts and silicified intervals. Burrows and bioturbation replaced by calcite cement and/or calcareous material. Sub-horizontal (~2-20°)
zoophycos burrows recognized in siliceous sms to csms interval at ~9,686 to 9,687. When present, chert/LS's occur as, alternating thin-beds (thinly-interbedded; compared to interlaminated limey-chert/cherty LS in 9,660.0-9,672.7 interval above.
9,660-9,672.7
*beds not to scale, overall lithology depicted.
9,695.5 - 9,718.0: Partially silicified, gry to gry-lt.-gry, slightly laminated to massive, biot. argillaceous limestone; and lt. dk-gry to gry & lt. brwnish-gry, massive to lam., biot. argll., silty LS to silty-muddy LS. Dk gry to gry, lam. to slightly lam., biot., limey-silty ms, to csms also occurs in lower portion of the interval. Bioturbation is mod. to heavy throughout. Laminations gen. limited to uppr & lwr portions of the interval. Parallel- and occasional cross-laminations where lams are present. Mineralized fractures occur in silicified intervals.
9,672.7 - 9,695.5
*Interbedded LS/chert deposits not to scale, but order of occurrence & relative thickness are representative.

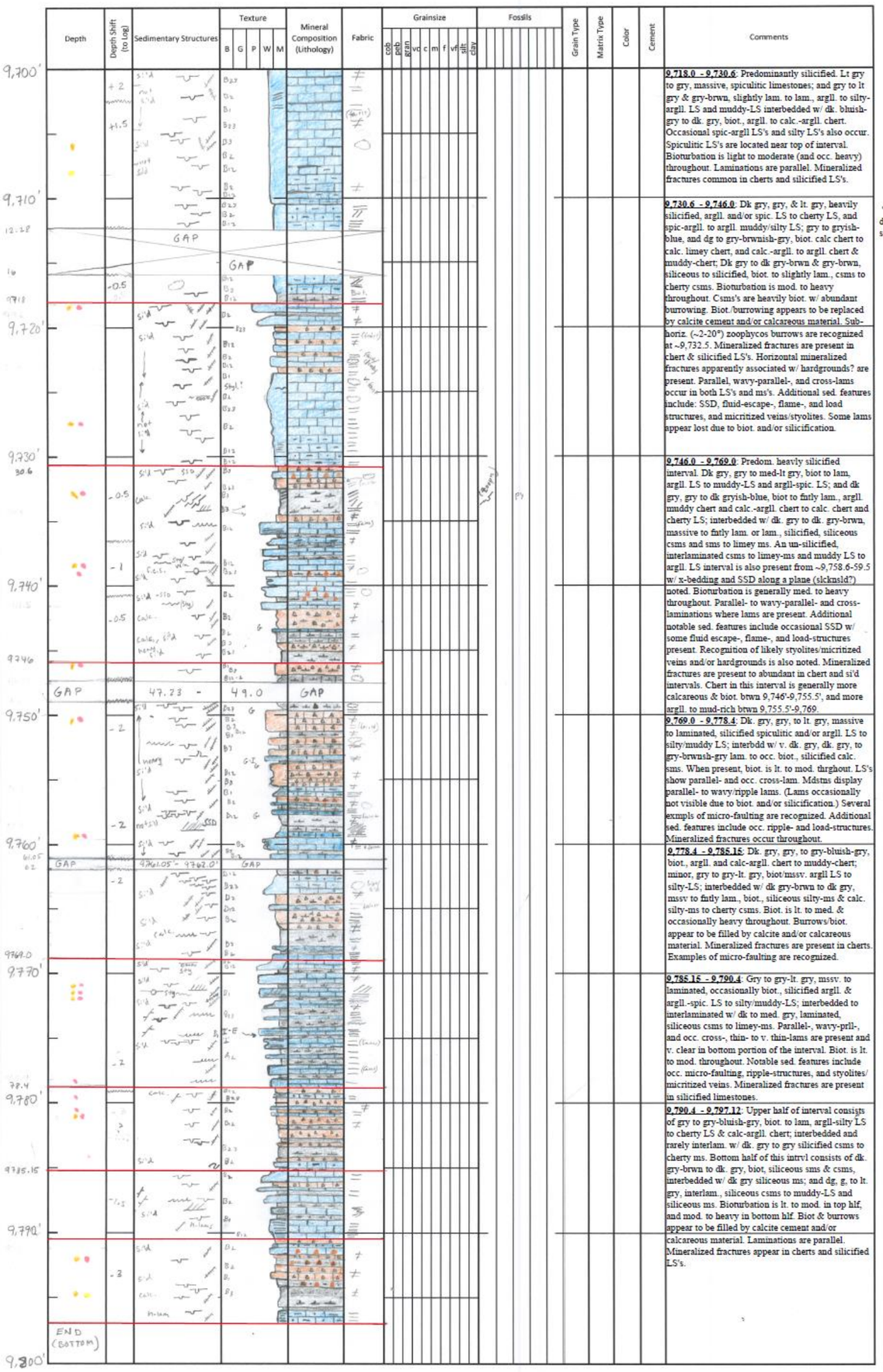

9,718.0 - 9,730.6: Predominantly silicified. Lt gry to gry, massive, spiculitic limestones; and gry to lt gry & gry-brwn, slightly lam. to lam., argll. to silty-argll. LS and muddy-LS interbedded w/ dk. bluish-gry to dk. gry, biot., argll. to calc.-argll. chert. Occasional spic-argll LS's and silty LS's also occur. Spiculitic LS's are located near top of interval. Bioturbation is light to moderate (and occ. heavy) throughout. Laminations are parallel. Mineralized fractures common in cherts and silicified LS's.

9,730.6 - 9,746.0: Dk gry, gry, & lt. gry, heavily silicified, argll. and/or spic. LS to cherty LS, and spic-argll. to argll. muddy/silty LS; gry to gryish-blue, and dg to gry-brwnish-gry, biot. calc chert to calc. limey chert, and calc.-argll. to argll. chert & muddy-chert; Dk gry to dk gry-brwn & gry-brwn, siliceous to silicified, biot. to slightly lam., csms to cherty csms. Bioturbation is mod. to heavy throughout. Csms's are heavily biot. w/ abundant burrowing. Biot./burrowing appears to be replaced by calcite cement and/or calcareous material. Sub-

*Bedding is more distinct in un-silicified intervals

horiz. (~2-20°) zoophycos burrows are recognized at ~9,732.5. Mineralized fractures are present in chert & silicified LS's. Horizontal mineralized fractures apparently associated w/ hardgrounds? are present. Parallel, wavy-parallel-, and cross-lams occur in both LS's and ms's. Additional sed. features include: SSD, fluid-escape-, flame-, and load structures, and micritized veins/stylolites. Some lams appear lost due to biot. and/or silicification.

9,746.0 - 9,769.0: Predom. heavly silicified interval. Dk gry, gry to med-lt gry, biot to lam, argll. LS to muddy-LS and argll-spic. LS; and dk gry, gry to dk gryish-blue, biot to fntly lam., argll. muddy chert and calc.-argll. chert to calc. chert and cherty LS; interbedded w/ dk. gry to dk. gry-brwn, massive to fntly lam. or lam., silicified, siliceous csms and sms to limey ms. An un-silicified, interlaminated csms to limey-ms and muddy LS to argll. LS interval is also present from ~9,758.6-59.5 w/ x-bedding and SSD along a plane (slicknsld?) noted. Bioturbation is generally med. to heavy throughout. Parallel- to wavy-parallel- and cross-laminations where lams are present. Additional notable sed. features include occasional SSD w/ some fluid escape-, flame-, and load-structures present. Recognition of likely stylolites/micritized veins and/or hardgrounds is also noted. Mineralized fractures are present to abundant in chert and si'd intervals. Chert in this interval is generally more calcareous & biot. brwn 9,746'-9,755.5', and more argll. to mud-rich brwn 9,755.5'-9,769.

9,769.0 - 9,778.4: Dk. gry, gry, to lt. gry, massive to laminated, silicified spiculitic and/or argll. LS to silty/muddy LS; interbdd w/ v. dk. gry, dk. gry, to gry-brwnsh-gry lam. to occ. biot., silicified calc. sms. When present, biot. is lt. to mod. thrghout. LS's show parallel- and occ. cross-lam. Mdstns display parallel- to wavy/ripple lams. (Lams occasionally not visible due to biot. and/or silicification.) Several exmpls of micro-faulting are recognized. Additional sed. features include occ. ripple- and load-structures. Mineralized fractures occur throughout.

9,778.4 - 9,785.15: Dk. gry, gry, to gry-bluish-gry, biot., argll. and calc-argll. chert to muddy-chert; minor, gry to gry-lt. gry, biot/mssv. argll LS to silty-LS; interbedded w/ dk gry-brwn to dk gry, mssv to fntly lam., biot., siliceous silty-ms & calc. silty-ms to cherty csms. Biot. is lt. to med. & occasionally heavy throughout. Burrows/biot. appear to be filled by calcite and/or calcareous material. Mineralized fractures are present in cherts. Examples of micro-faulting are recognized.

9,785.15 - 9,790.4: Gry to gry-lt. gry, mssv. to laminated, occasionally biot., silicified argll. & argll.-spic. LS to silty/muddy-LS; interbedded to interlaminated w/ dk to med. gry, laminated, siliceous csms to limey-ms. Parallel-, wavy-prll-, and occ. cross-, thin- to v. thin-lams are present and v. clear in bottom portion of the interval. Biot. is lt. to mod. throughout. Notable sed. features include occ. micro-faulting, ripple-structures, and styolites/micritized veins. Mineralized fractures are present in silicified limestones.

9,790.4 - 9,797.12: Upper half of interval consists of gry to gry-bluish-gry, biot. to lam, argll-silty LS to cherty LS & calc-argll. chert; interbedded and rarely interlam. w/ dk. gry to gry silicified csms to cherty ms. Bottom half of this intrvl consists of dk. gry-brwn to dk. gry, biot, siliceous sms & csms, interbedded w/ dk gry siliceous ms; and dg, g, to lt. gry, interlam., siliceous csms to muddy-LS and siliceous ms. Bioturbation is lt. to mod. in top hlf, and mod. to heavy in bottom hlf. Biot & burrows appear to be filled by calcite cement and/or calcareous material. Laminations are parallel. Mineralized fractures appear in cherts and silicified LS's.

Detailed core description was split into fourteen core depth intervals, based on significant changes in lithology and/or depositional texture, or gaps represented by intervals where core was not recovered.

Detailed Core Description – Core A	
Core Depth Interval	**Macro-Scale Interval Descriptions**
9,545.0 – 9,555.7	Black to gray-black, and dark gray massively-bedded (organic?) mudstone to silty-mudstone (ms-sms), and infrequent calcareous, silty-mudstone (csms); inter-bedded with light gray to gray, massive to vaguely laminated limestone (wackestone-packstone). Mudstone to silty-mudstone deposits contain semi-abundant, off-white, very fine to silt sized microfossils (possibly sponge spicules). Limestones show occasional light bioturbation, faint cross-, parallel-, and convolute-lamination. Also, a highly cemented skeletal rudstone with abundant very fine to granular sized bioclasts is present from ~9,546.7 – 9546.95 (possibly representing a distal debris flow deposit). Skeletal grains include: crinoids, forams, sponges and sponge spicules, algae fragments, brachiopods, and additional undifferentiated skeletal fragments.
9,545.0 – 9,555.7	Black to gray-black, and dark gray, massive to faintly laminated (organic?) mudstone to silty-mudstone (ms-sms), and occasional calcareous, silty-mudstone (csms); interbedded with light gray to gray, massive to vaguely laminated, sectionally cemented or silicified limestone (ws-ps), limestone nodules (ps), and occasional silty limestone (ws-ps). Mudstone to silty-mudstone deposits contain semi-abundant, off-white, very fine to silt sized microfossils (possibly sponge spicules), sporadic pyrite, and occasional brown to gray-brown (~muddy) lenses (phosphate?) Intermittent, light bioturbation and rare fluid escape/load structures occur in mudstone to silty mudstones near limestone deposits. Limestones show occasional light to moderate bioturbation, faint parallel-, cross-, and wavy/ripple-lamination, and rare plastic deformation. Normal grading is present in silty LS deposits. Intervals with apparent silicification/cementation are marked by the presence of mineralized fractures.
9,635.6 – 9,653.9	Heavily deformed/contorted, chaotically deposited, silicified/cemented interval (slump & debris deposits). Dark gray, gray, and light gray intraclastic, skeletal, silicified/cemented limestone (ws-ps, floatstone, & rudstone); dark gray to gray, and grayish-blue bedded chert; and dark gray, calcareous silty mudstone.

	Abundant intraclasts are heavily cemented, dark gray to gray, granule to cobble sized, sub-rounded to sub-angular limestone (ws-ps) and chert. Light gray, gray, and tan to off-white, very fine to granular sized bioclasts include brachiopods, bivalves, bryozoans, sponge spicules, forams, ostracods, algal. fragments, crinoids, and additional undifferentiated microfossils and fossil fragments. Matrix appears to be dark gray silty mudstone to calcareous silty mudstone for mud-supported portion, and biosparite for the grain-supported portion. Deposits are oriented chaotically w/ poor to v. poor sorting, and frequent heavy cementation and/or silicification. SSD (slumps, contorted bedding, fld. esc. structures) is abundant throughout and several large clasts show plastic deformation. Skeletal grains & intraclasts are both matrix- and grain-supported (varies throughout) with minor normal- and reverse-grading present. Some sub-rounded intraclasts show radial pyrite? replacement. Moderate bioturbation is present and often filled w/ calcite cement/calcareous material. Most texture for silicified limestone to calcareous bedded chert is lost or cloudy due to silicification, however these deposits appear to have highly deformed, contorted/convoluted, to folded thin- to medium-beds w/ SSD and probable mod. to heavy bioturbation throughout. silty- and calcareous, silty- mudstones also present with SSD and are often protruded into by over- and under-lying strata.
9,653.9 – 9,660.0	Dark gry-brwn to drk gry, massive to fntly lam., freq biot. and/or silicified/cemented, (siliceous?), silty mudstone to calcareous sms; and rare drk. gry to gryish blue-gry, biot., calcareous, muddy chert. Mudstones are mod. to heavily biot. w/ abundant burrowing. Bioturbation and burrows filled by calcite cement and/or calcareous material. Sub-horiz. (~2-20°) zoophycos burrows are recognized, specifically in the upper portion of the interval.
9,660.0 – 9,672.7	Highly silicified and/or cemented interval. Dark Gray to gray, and light gray, laminated to occasionally bioturbated, silicified and/or cemented limestone to cherty LS; and d. gry, gry, to gryish-blue, biot., calcareous chert to biot. calc. limey chert. Rare csms to (siliceous?) csms's also occur. Mineralized fractures are abundant in cherts and silicified and/or cemented LS's. Cherts and LS's are thinly interlaminated to thinly interbedded. Occasional. wavy planar lams and ripples are present throughout. Some SSD, and flame/fluid esc. structures occur, genrlly in muddier intervals.
9,672.7 – 9695.5	Dark gray to gray and light gray, massive to laminated, sectionally silicified and/or cemented limestone (ws-ps) to silty/muddy LS (ws);

	interbedded w/ d. gry-bluish-gry to d. gry, biot., calcareous-muddy to muddy chert; and d. gry-brown to d. gry and gry, faintly lam., sectionally silicified or cemented, bioturbated, (siliceous?) sms to cherty csms and limey csms. Thin- to thick-bedded intervals throughout. Mineralized fractures indicate the presence of probable silicification and/or cementation. Burrows and bioturbation replaced by calcite cement and/or calcareous material. Sub-horizontal (~2-20°) zoophycos burrows recognized in siliceous? sms to csms interval at ~9,686 to 9,687. When present, chert/limestones occur as alternating thin-beds (thinly-interbedded); compared to interlaminated limey-chert to cherty limestone in the 9,660.0-9,672.7 interval above.
9,695.5 – 9,718.0	Partially silicified and/or cemented, gray to gray-light-gray, slightly laminated to massive, bioturbated limestone; and light dk-gray to gray & light brownish-gray, massive to lam., bioturbated silty to silty-muddy LS. Dk gry to gry, lam. to slightly lam., biot., limey-silty ms, to csms also occurs in lower portion of the interval. Bioturbation is mod. to heavy throughout. Laminations gen. limited to uppr & lwr portions of the interval. Parallel- and occasional cross-laminations where lams are present. Probable silicification and/or cementation evidenced by occurrence of mineralized fractures.
9,718.0 – 9,730.6	Predominantly silicified and/or cemented. Lt gry to gry massive limestone, and gry to lt gry & gry-brwn, laminated to slightly laminated muddy to silty-muddy LS interbedded w/ dk. bluish-gry to dk. gry, biot., muddy. to calc.-muddy chert. Occasional massive silty LS's also occur. Massive, highly cemented, and/or silicified LS occurs near top of interval. Bioturbation is light to moderate (and occ. heavy) throughout. Laminations are parallel. Probable silicification and/or cementation evidenced by occurrence and relative abundance of mineralized fractures.
9,730.6 – 9,746.0	Dark gray, gray, & light gray, cemented and/or silicified, vaguely laminated to bioturbated limestone (ws-ps) to muddy/silty laminated and bioturbated limestone (ws); interlaminated with gray to grayish-blue, and dark gray to gray-brown-gray, generally heavily bioturbated calcareous and/or muddy chert. Interbedded with dark gray to dark gray-brown & gray-brown, (siliceous?), bioturbated to laminated, burowed silty to calcareous silty mudstone. Bioturbation is moderate to heavy throughout. Bioturbation/burrowing in silty to calcareous silty mudstones appears to be replaced by calcite cement and/or calcareous material, sub-horizontal (~2-20°) zoophycos burrows are recognized at ~9,732.5. Apparent heavy silicification and/or

	cementation is indicated by the presence of mineralized fractures. Horizontal mineralized fractures possibly associated with pressure dissolution/compaction are present in limestones. Parallel, wavy-parallel-, and cross-laminations (often irregular) occur in both limestone and mudstone intervals. Additional sedimentary features include: soft-sediment deformation, fluid-escape-, flame-, and load structures, and micritized veins/styolites. Some laminations are nearly indiscernible due to bioturbation, and cementation and/or silicification.
9,746.0 – 9,769.0	Predominantly heavily silicified and/or cemented interval. Dark gray, gray to med-light gray, bioturbated to laminated limestone (ws-ps) to muddy-limestone (ws), and dark gray, gray to dark grayish-blue, bioturbated to 'cloudy', muddy to calcareous chert; interbedded with dark gray to dark gray-brown, massive to faintly laminated or laminated, (siliceous?) silty to calcareous silty mudstone. An unsilicified/uncemented, interlaminated calcareous to limey mudstone and muddy limestone (ws) interval is also present from ~9,758.6-59.5 with angular cross-bedding and soft-sediment deformation along a plane (slickenslide?) noted. Bioturbation is generally medium to heavy throughout. Parallel- to wavy-parallel- and cross-laminations where lams are present. Additional notable sedimentary features include occasional soft-sediment deformation with some fluid escape-, flame-, and load-structures present. Recognition of likely styolites/micritized veins and/or hardgrounds is also noted. Mineralized fractures are present in intervals with apparent silicification and/or cementation. This interval is generally more calcareous & bioturbated between 9,746'-9,755.5', and more mud-rich and massive between 9,755.5'-9,769.
9,769.0 – 9,778.4	Dk. gry, gry, to lt. gry, massive to laminated, silicified and/or cemented LS to silty/muddy LS; interbdd w/ v. dk. gry, dk. gry, to gry-brwnsh-gry lam. to occ. biot., siliceous calc. sms. When present, biot. is lt. to mod. thrghout. LS's show parallel- and occ. cross-lam. Mdstns display parallel- to wavy/ripple lams. (Lams are often vague or non-existent in sections due to biot. and/or silicification.) Several exmpls of micro-faulting are recognized. Additional sed. features include occ. ripple- and load-structures. Mineralized fractures occur throughout.
9,778.4 – 9,785.15	Dark gray, gray, to gray-bluish-gray, and dark gray-brown, bioturbated, muddy to calcareous-muddy chert; minor, gray to gray-light-gray, bioturbated/massive limestone to silty-limestone;

	interbedded w/ dark brown-gray to dark gray, mssv to fntly lam., biot., (siliceous?) silty-ms & calc. silty-ms. Bioturbation is generally light to med., (but occasionally heavy) throughout. Burrows/bioturbation appear to be filled by calcite and/or calcareous material. Mineralized fractures are present in cemented and/or silicified intervals. Examples of micro-faulting are recognized.
9,785.15 – 9,790.4	Gry to gry-lt. gry, mssv. to laminated, occasionally biot., silicified and/or cemented LS to silty/muddy-LS; interbedded to interlaminated w/ dk to med. gry, laminated, (siliceous?) csms to limey-ms. Parallel-, wavy-parallel-, and occ. cross-, thin- to v. thin-laminations are present and v. clear in bottom portion of the interval (likely indicating non- or reduced-presence of silica or carbonate cement. Biot. is lt. to mod. throughout. Notable sed. features include occ. micro-faulting, ripple-structures, and styolites/micritized veins. Intervals with apparent silicification/cementation are marked by the presence of mineralized fractures.
9,790.4 – 9,797.12	Upper half of interval consists of gry to gry-bluish-gry, biot. to lam, silty LS (ws-ps) to silicified and/or heavily cemented LS & calc-muddy chert; interbedded and rarely interlam. w/ dk. gry to gry (siliceous?) csms to cherty ms. Bottom half of this intrvl consists of dk. gry-brwn to dk. gry, biot, (siliceous?) sms & csms, interbedded w/ dk gry ms; and dg, g, to lt. gry, interlam csms and muddy-LS. Bioturbation is lt. to mod. in top hlf, and mod. to heavy in bottom hlf. Biot & burrows appear to be filled by calcite cement and/or calcareous material. Laminations are parallel. Intervals with apparent silicification/cementation are marked by the presence of mineralized fractures.

‘Well A’

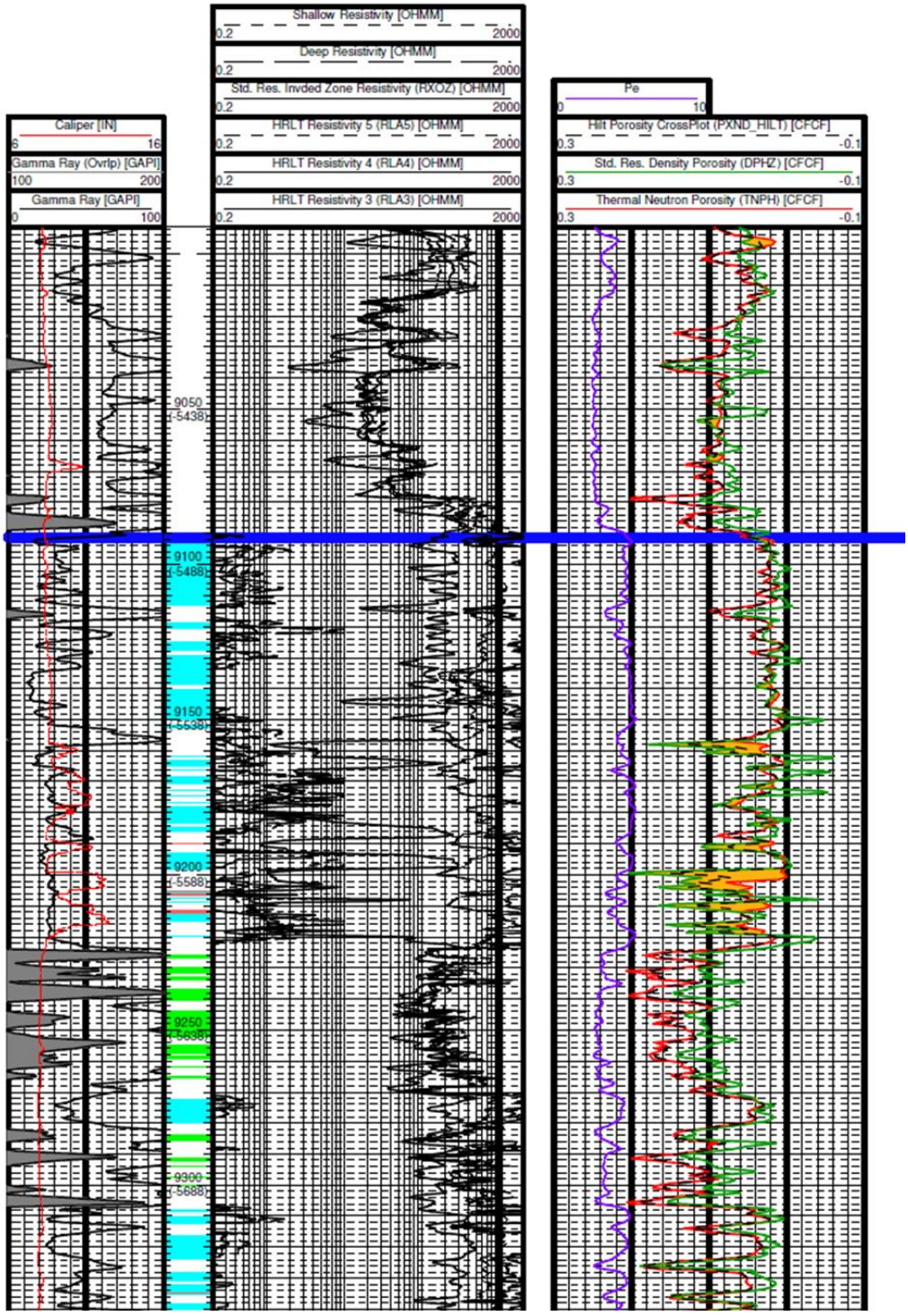
Shallow Resistivity [OHMM]
0.2
2000
Deep Resistivity [OHMM]
0.2
2000
Std. Res. Invded Zone Resistivity (RXOZ) [OHMM]
0.2
2000
HRLT Resistivity 5 (RLA5) [OHMM]
0.2
2000
HRLT Resistivity 4 (RLA4) [OHMM]
0.2
2000
HRLT Resistivity 3 (RLA3) [OHMM]
0.2
2000
Caliper [IN]
6
16
Gamma Ray (Ovrlp) [GAPI]
100
200
Gamma Ray [GAPI]
0
100
Pe
0
10
Hilt Porosity CrossPlot (PXND_HILT) [CFCF]
0.3
-0.1
Std. Res. Density Porosity (DPHZ) [CFCF]
0.3
-0.1
Thermal Neutron Porosity (TNPH) [CFCF]
0.3
-0.1
9050
(-5438)
9100
(-5488)
9150
(-5538)
9200
(-5588)
9250
(-5638)
9300
(-5688)

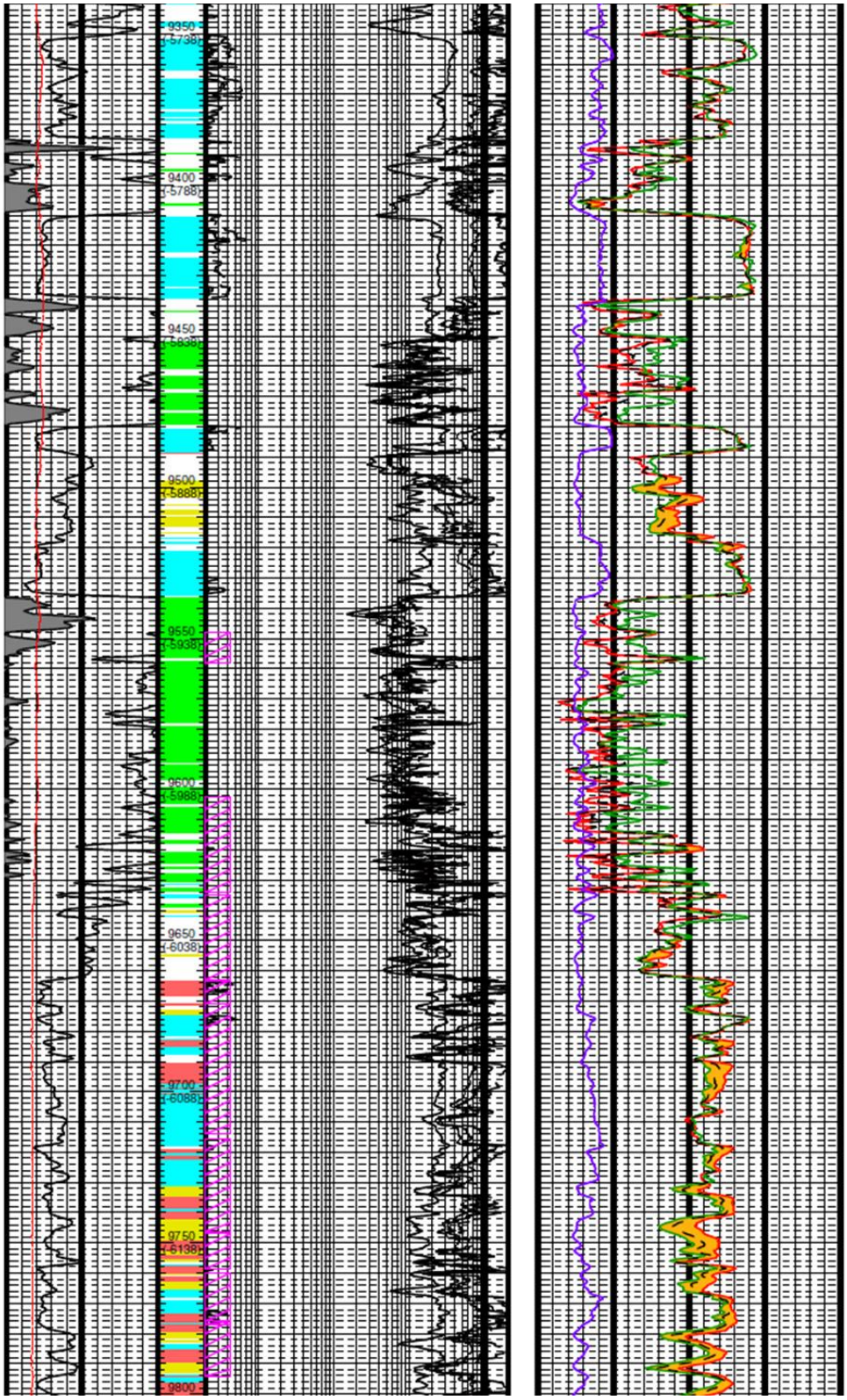
9350
(-5738)
9400
(-5788)
9450
(-5838)
9500
(-5888)
9550
(-5938)
9600
(-5988)
9650
(-6038)
9700
(-6088)
9750
(-6138)
9800

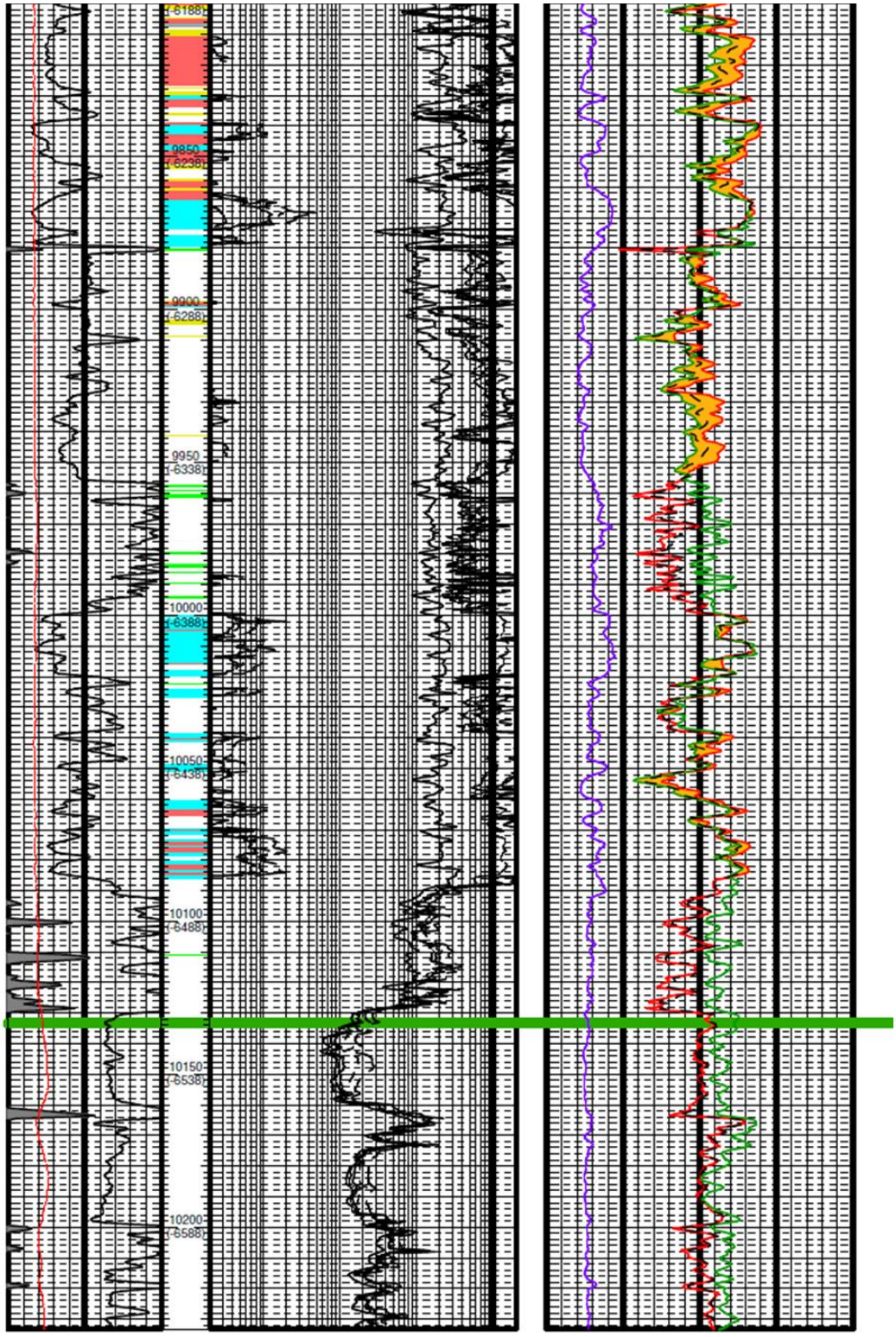
9850
9900
9950
10000
10050
10100
10150
10200

APPENDIX B

THIN-SECTIONS

9,546.8

9,599.8

9,612.4

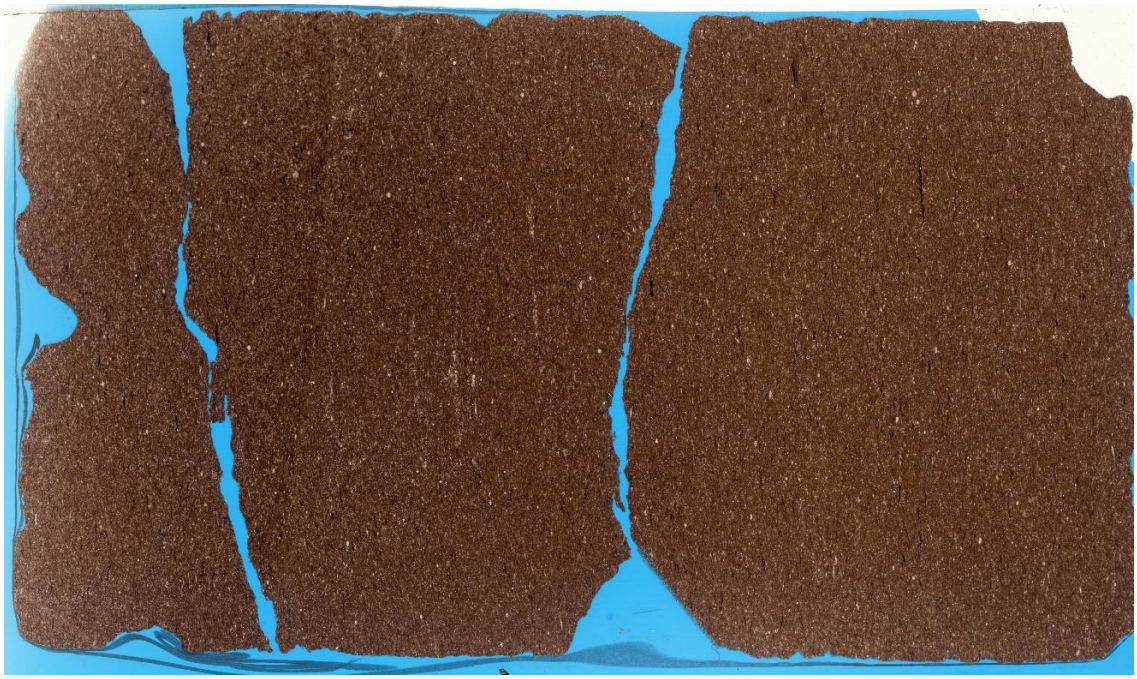

9,615.8

9,616.9

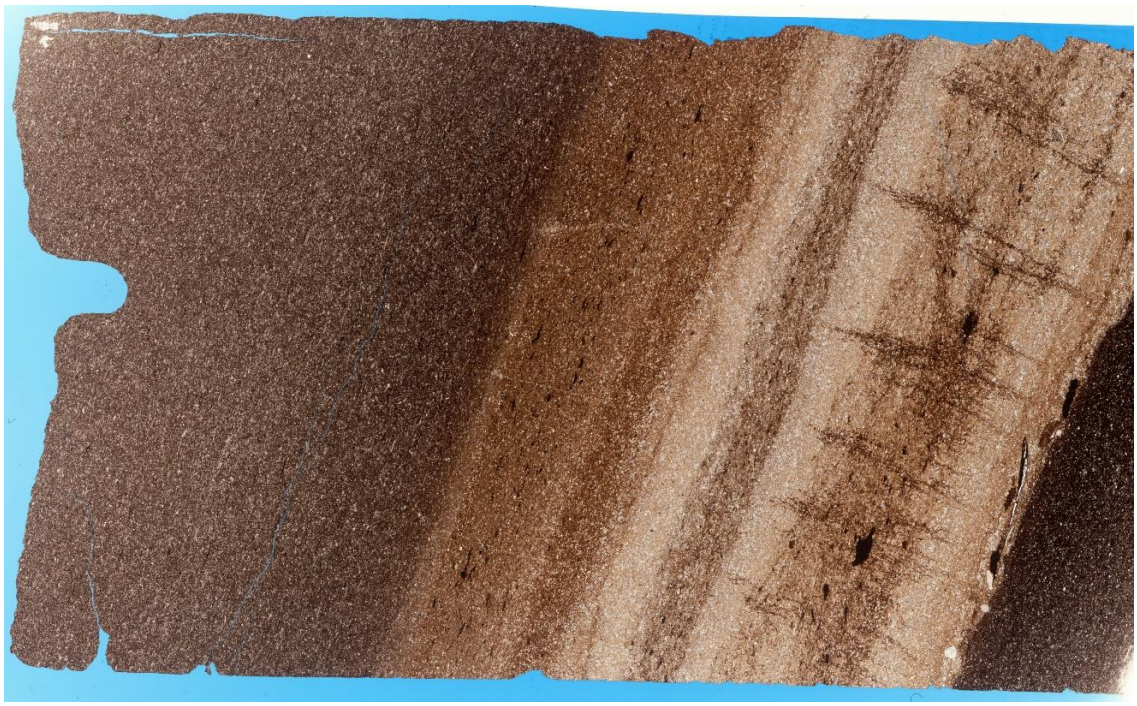

9,619.7

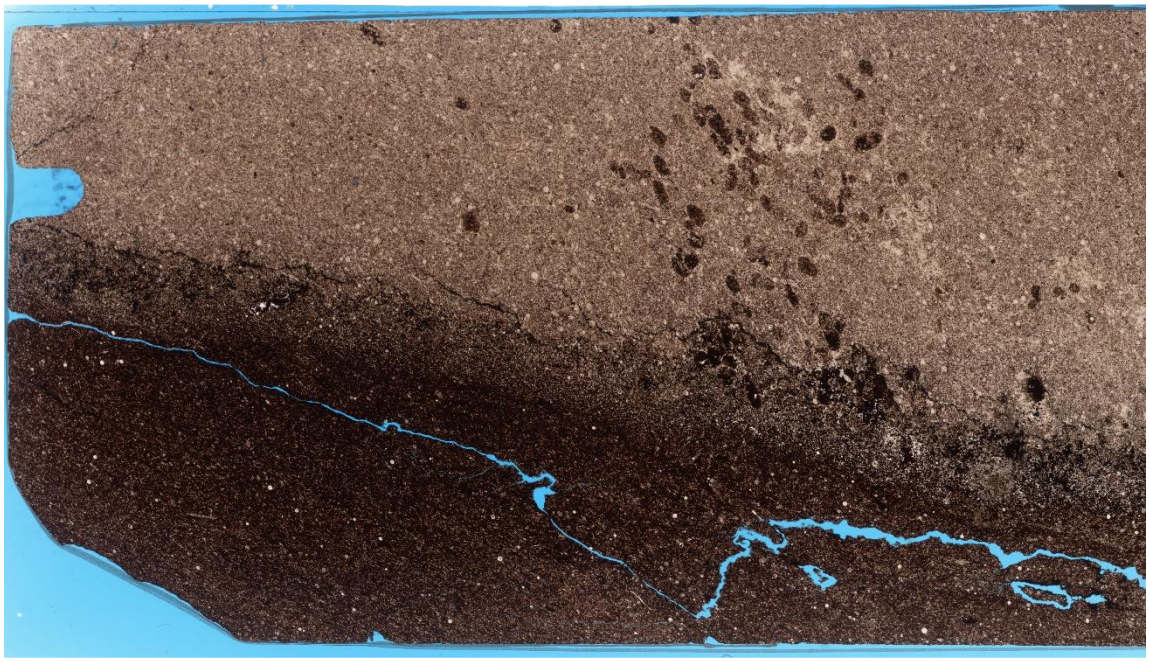

9,620.0

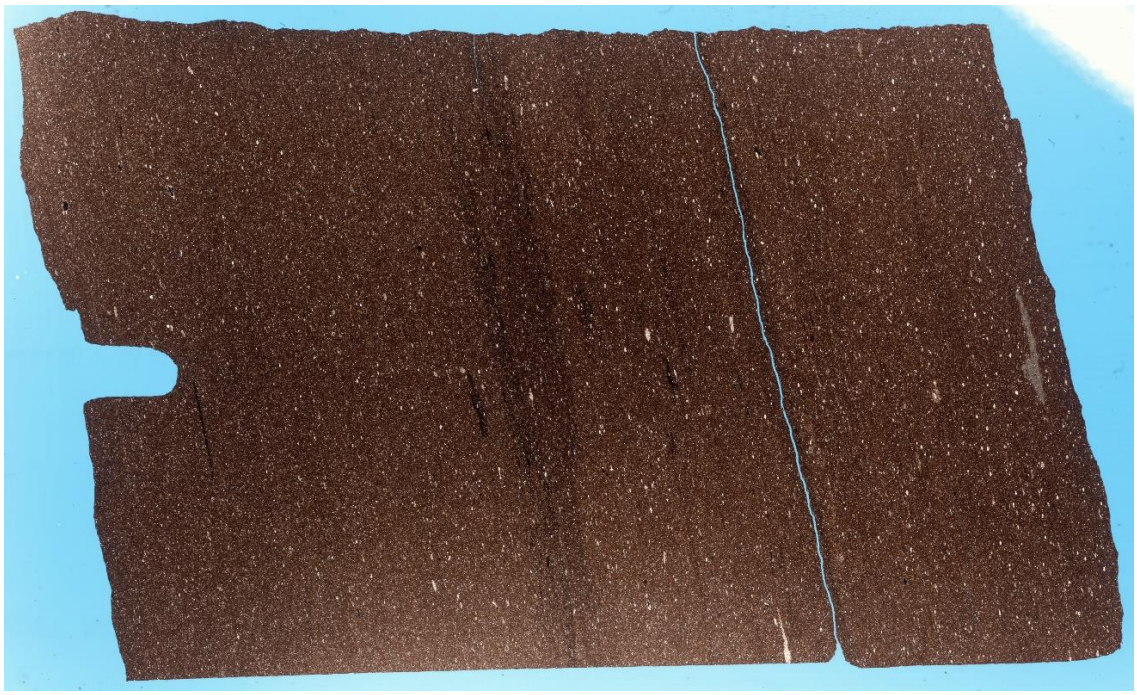

9,628.5

9,628.95

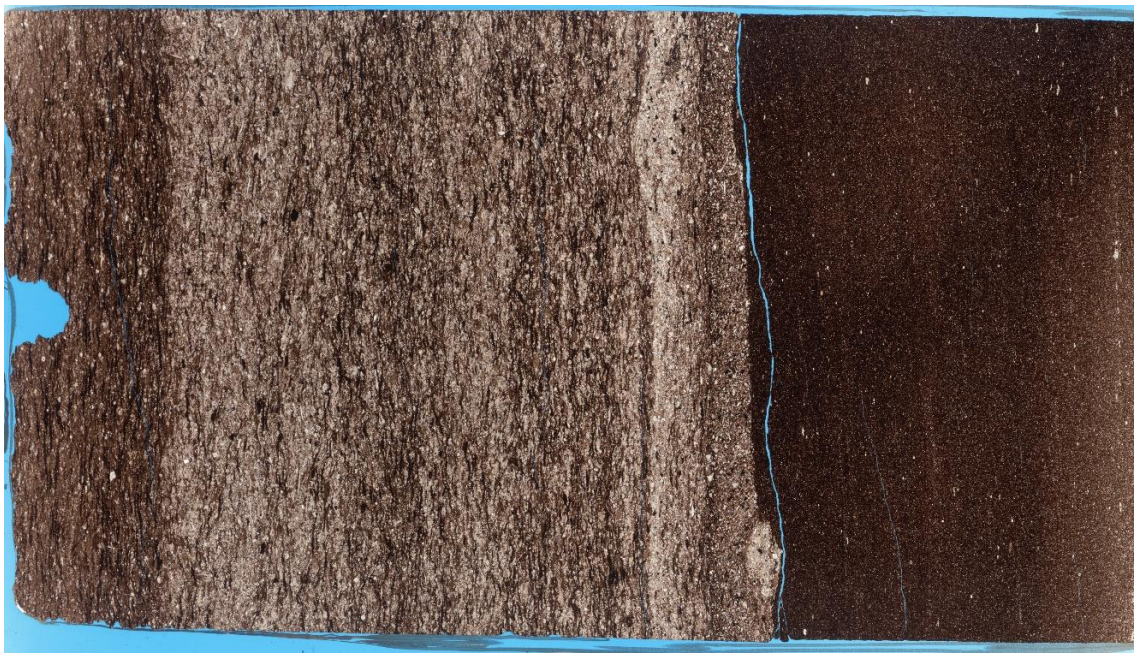

9,639.7

9,650.8

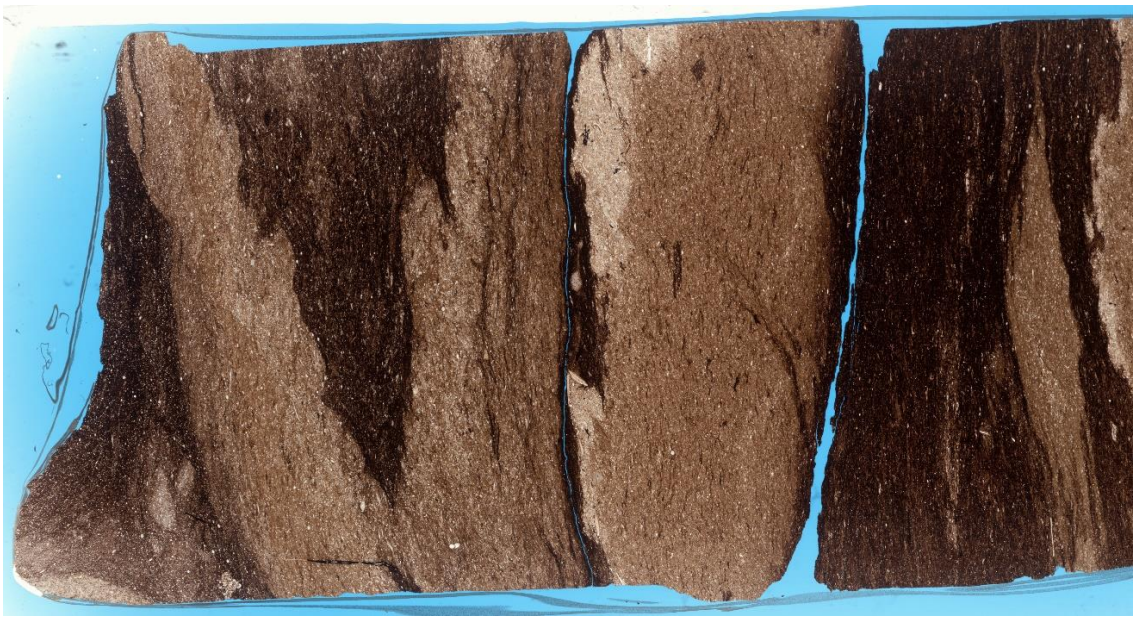

9,654.65

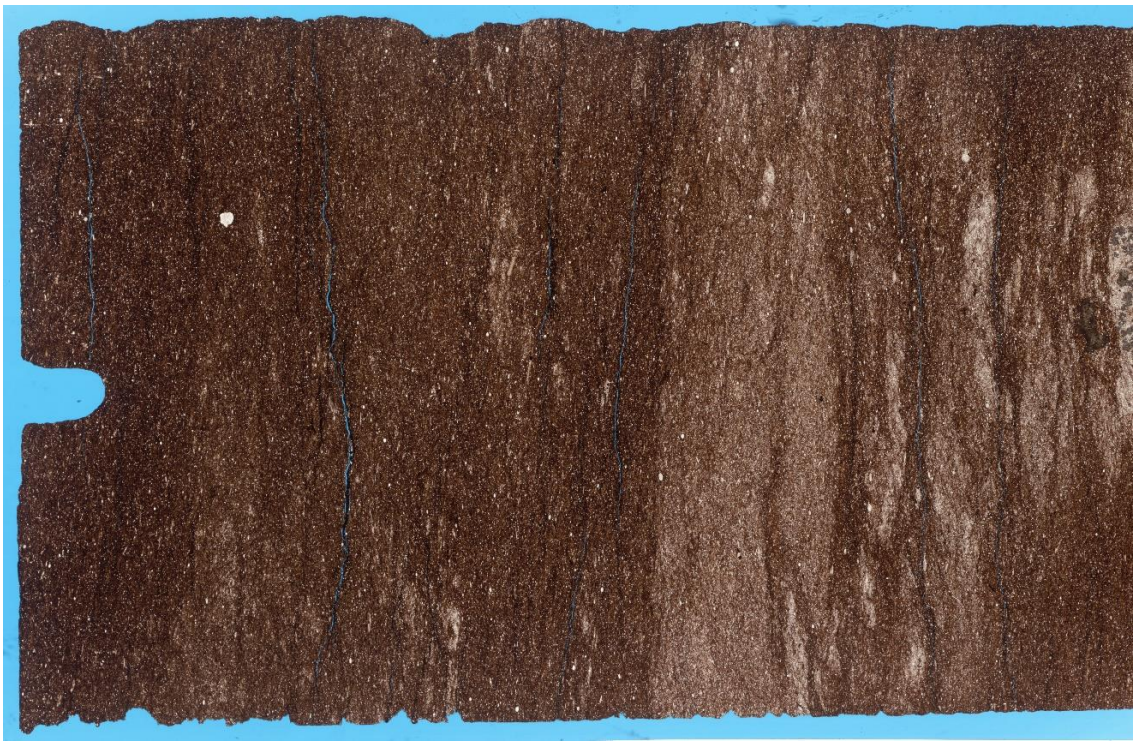

9,660.6

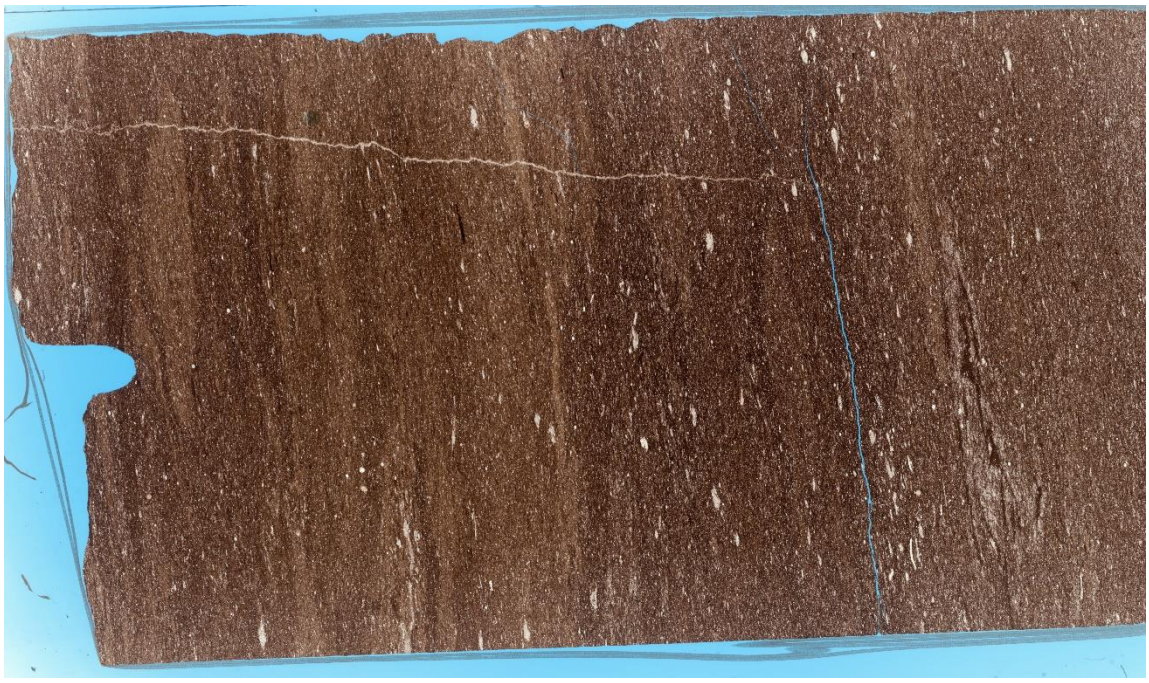

9,660.8

9,667.6

9,674.3

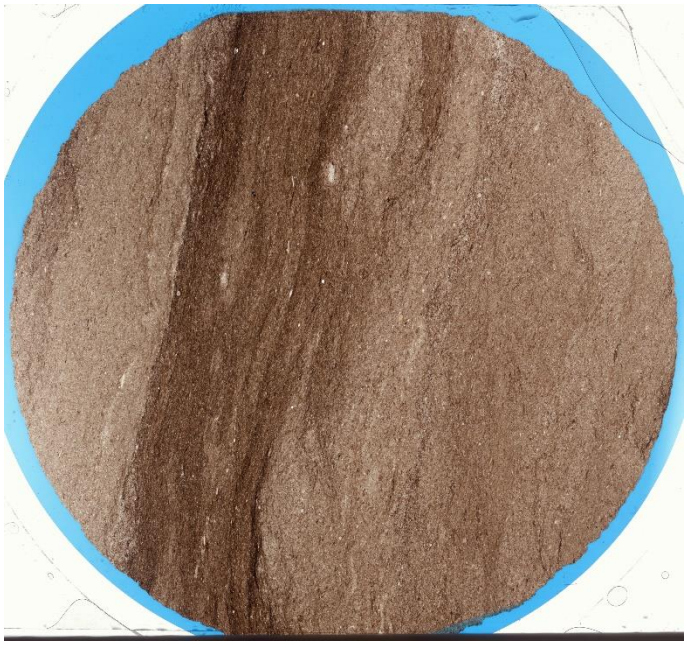

9,680.2

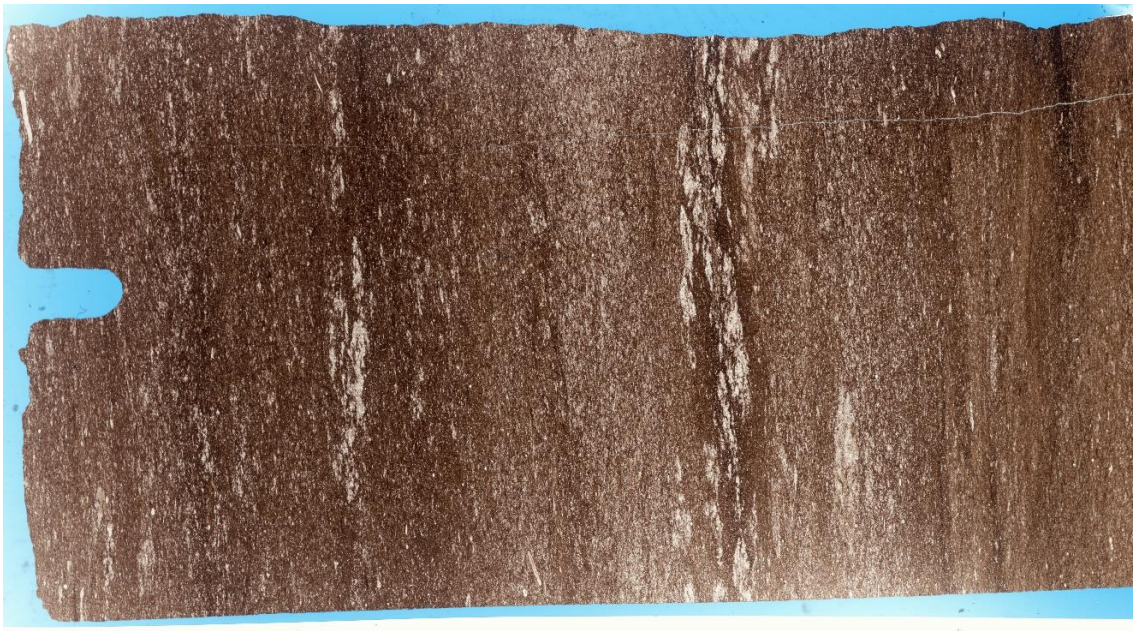

9,682.2

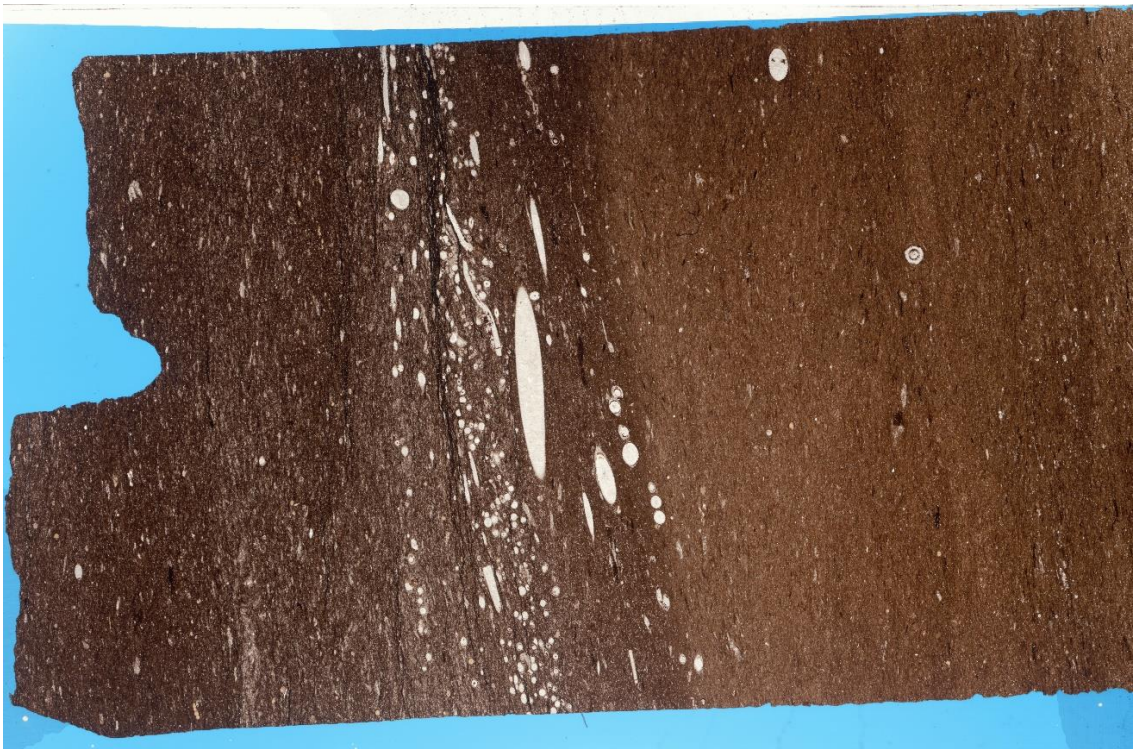

9,683.3

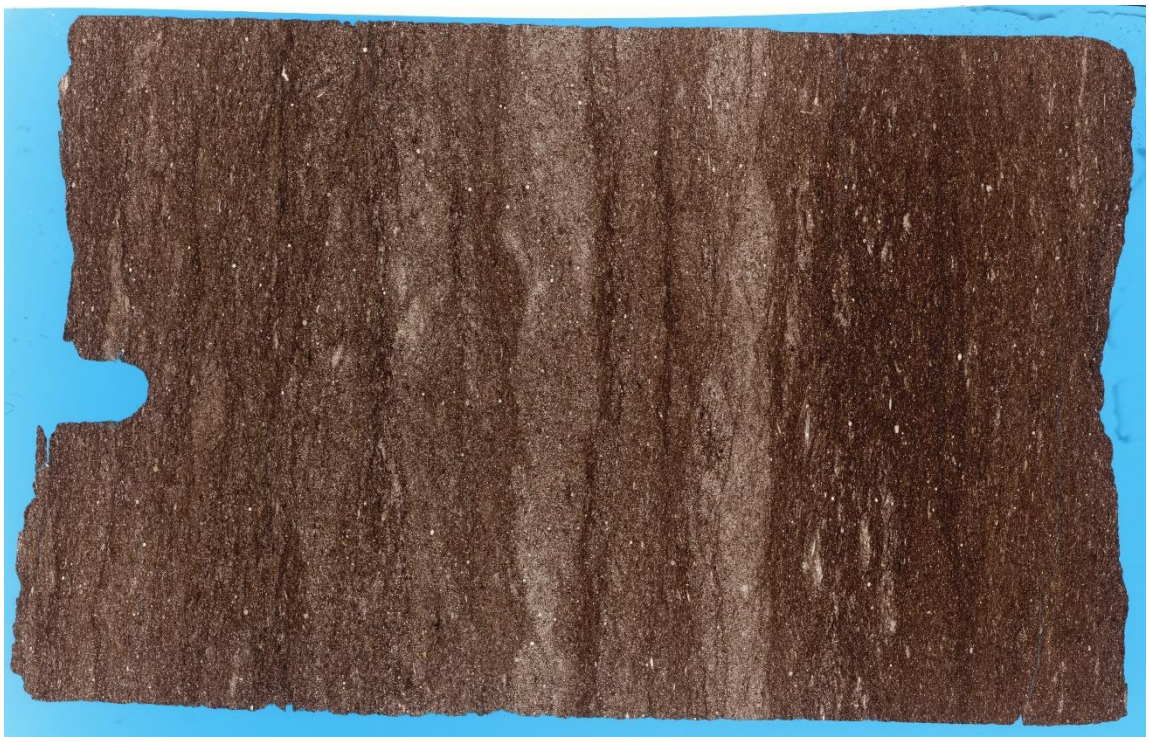

9,693.5

9,706.5

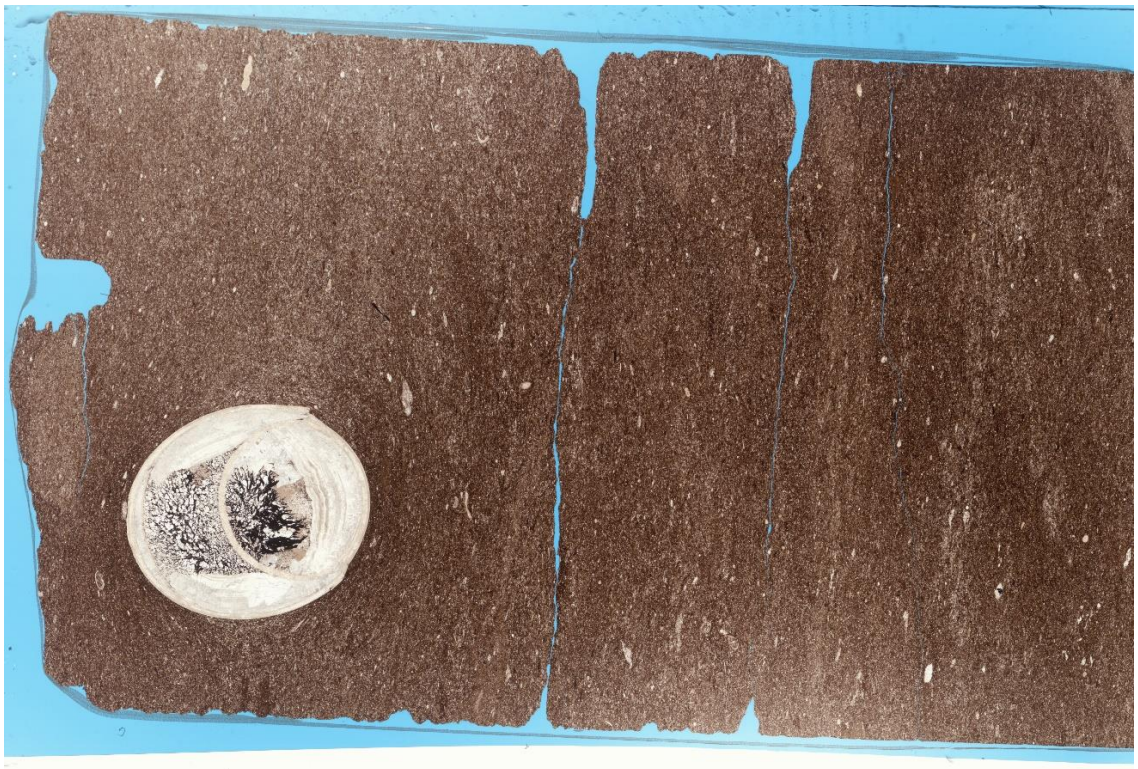

9,718.3

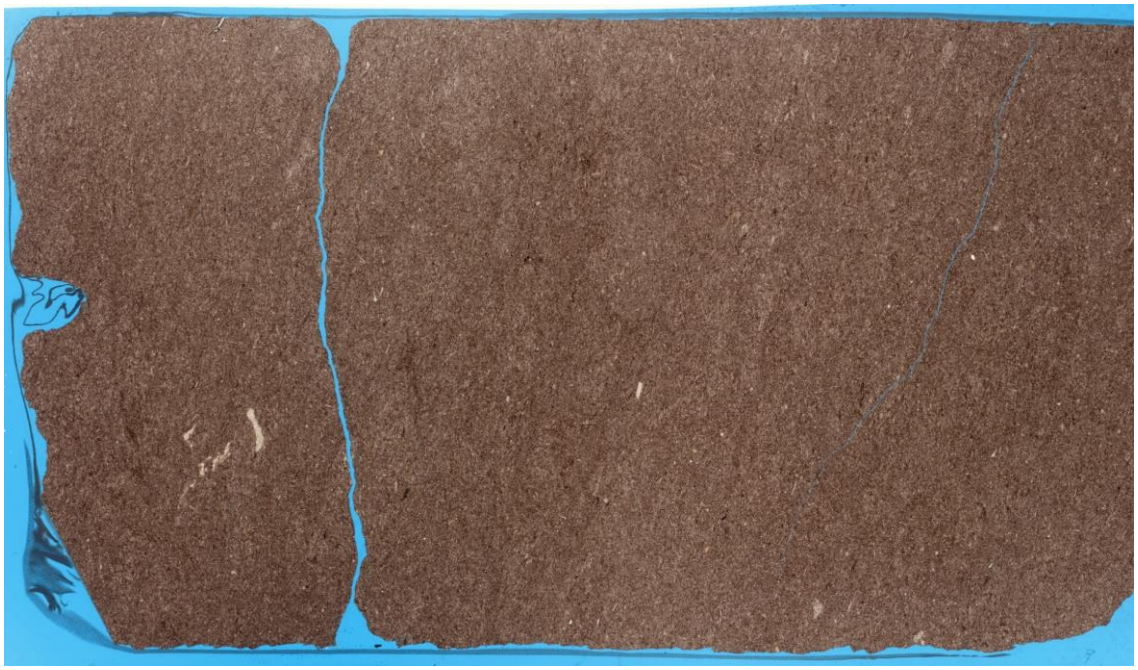

9,727.3

9,732.3

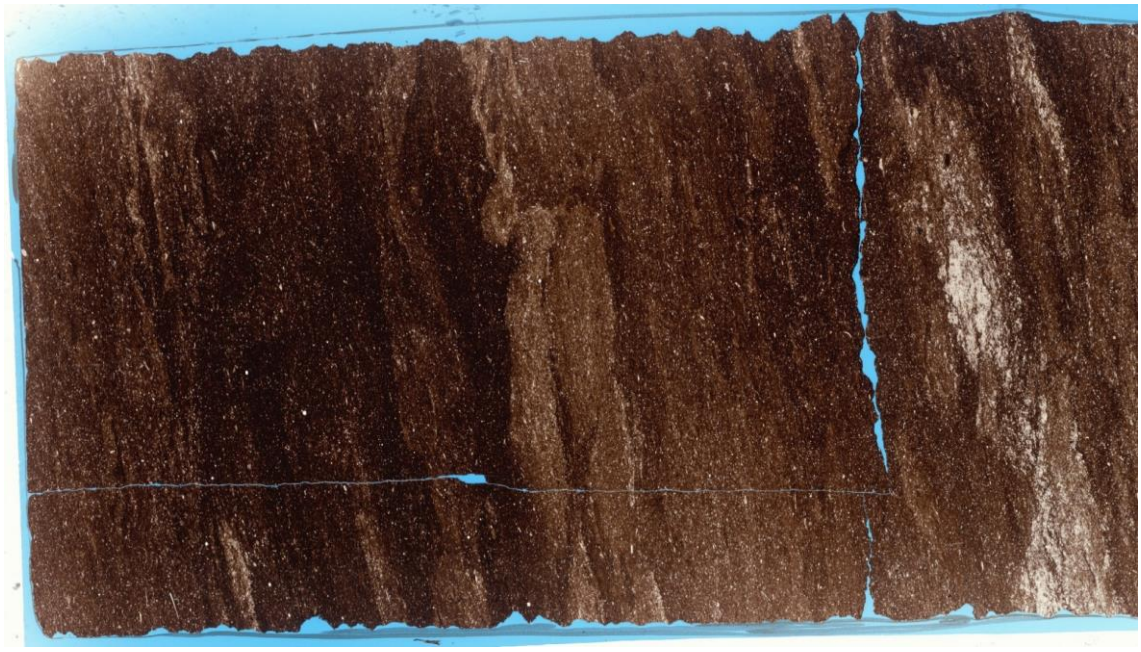

9,738.1

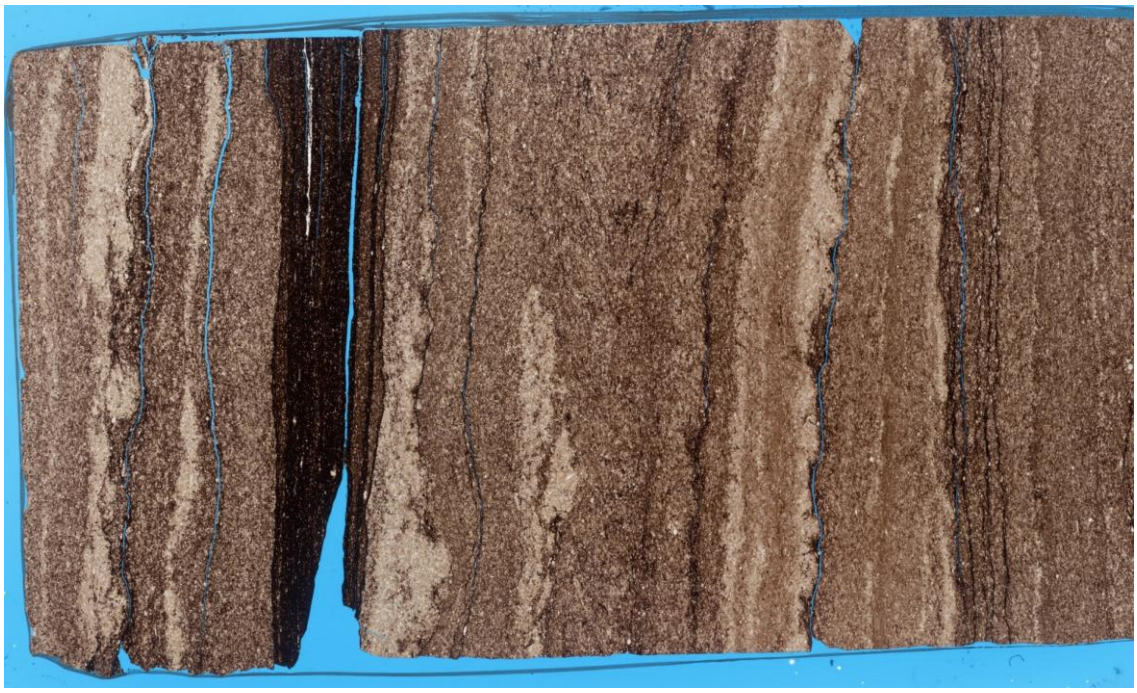

9,746.2

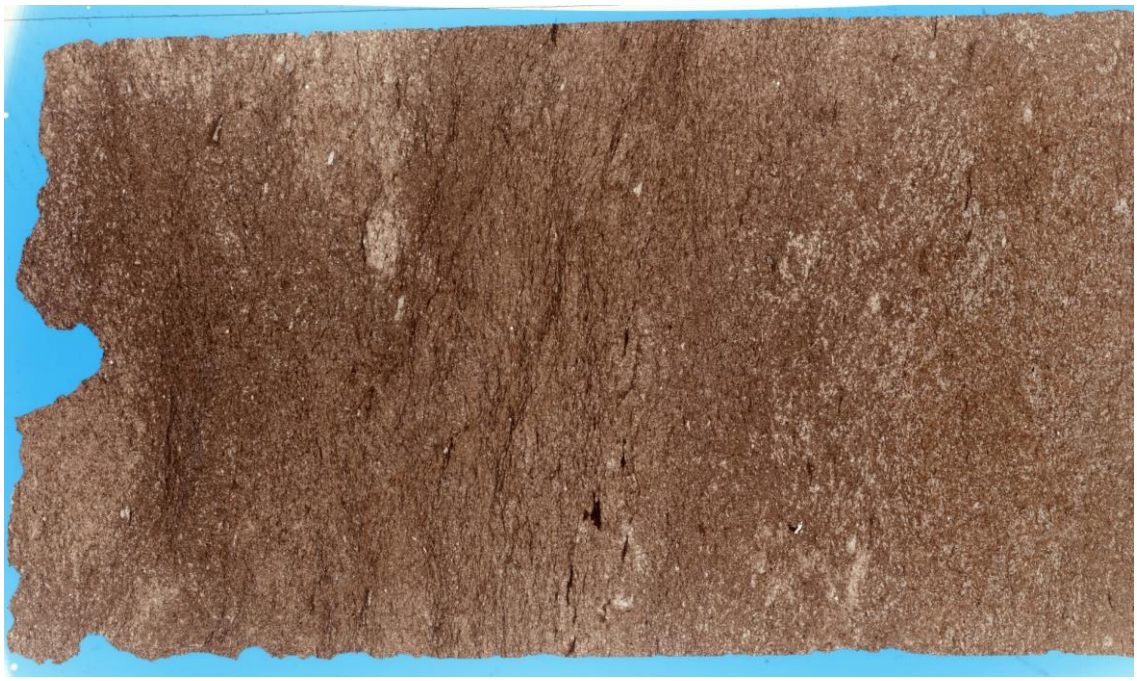

9,750.35

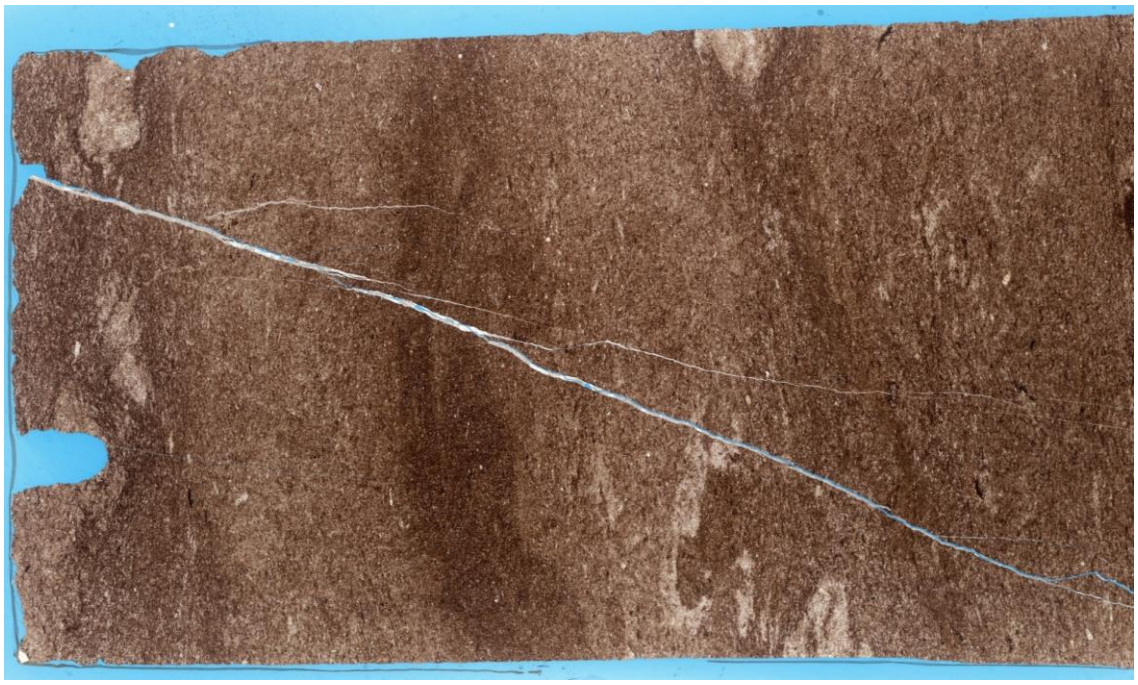

9,759.3

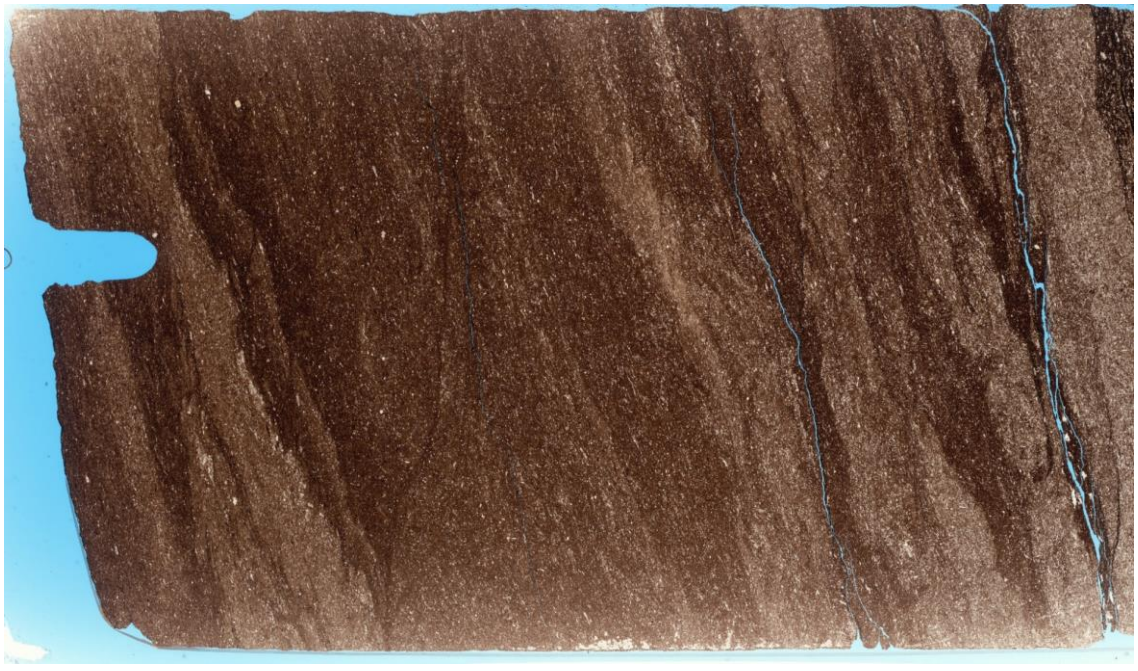

9,771.3

9,771.4

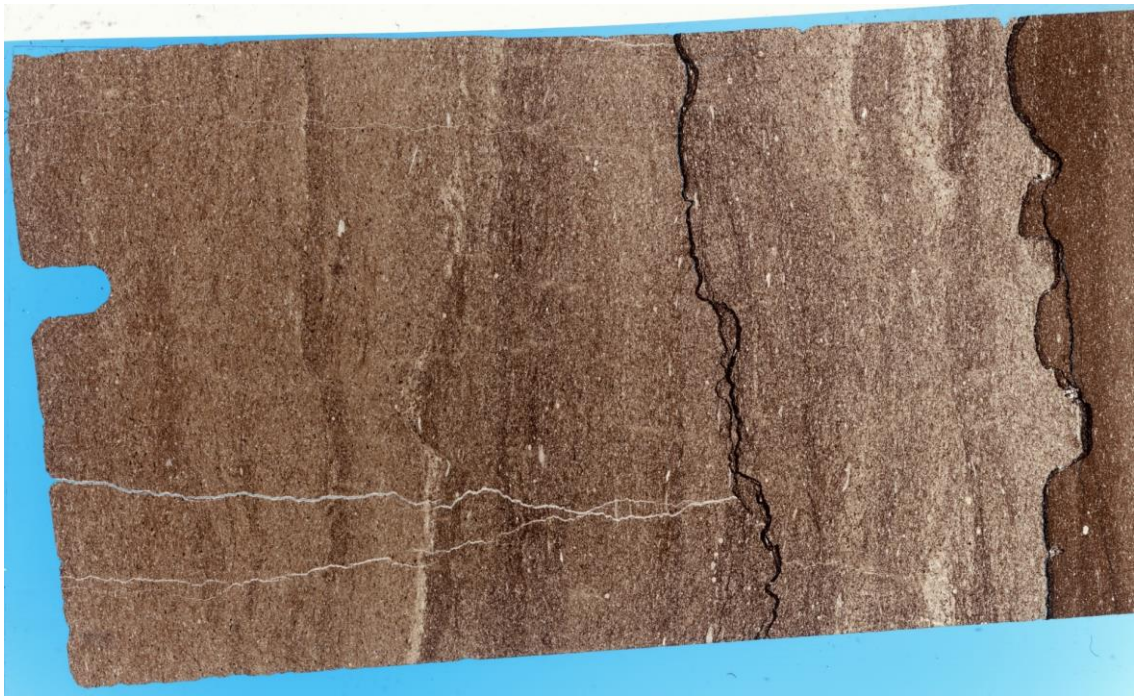

9,771.5

9,781.05

9,792.5

9,794.75

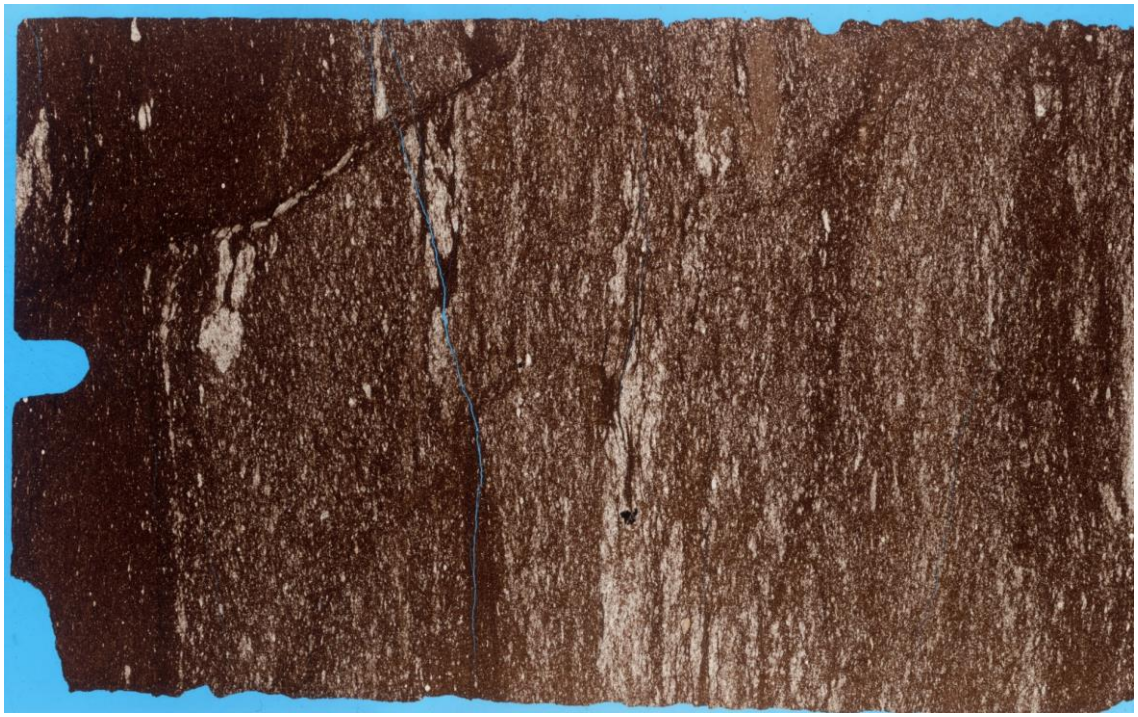

APPENDIX C

CORE-TO-LOG CORRELATION CROSSPLOTS

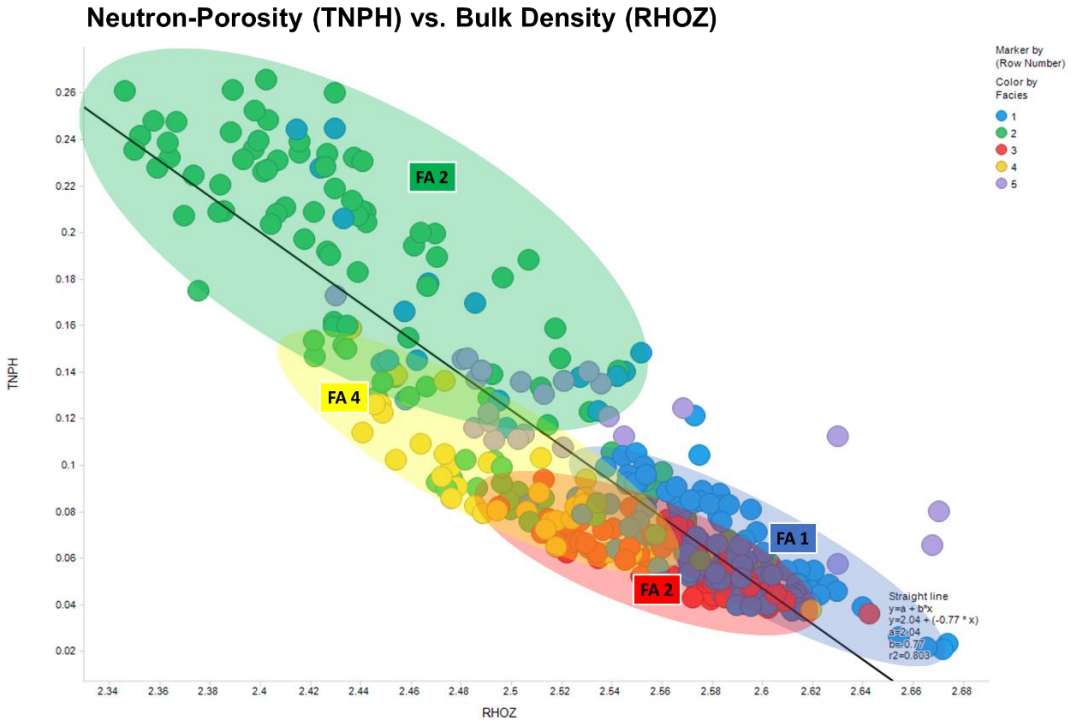
Neutron-Porosity (TNPH) vs. Bulk Density (RHOZ)
Marker by (Row Number)
Color by Facies
1
2
3
4
5
FA 2
FA 4
FA 1
FA 2
Straight line
y=a + b*x
y=2.04 + (-0.77 * x)
a=2.04
b=-0.77
r2=0.803
TNPH
RHOZ
0.26
0.24
0.22
0.2
0.18
0.16
0.14
0.12
0.1
0.08
0.06
0.04
0.02
2.34
2.36
2.38
2.4
2.42
2.44
2.46
2.48
2.5
2.52
2.54
2.56
2.58
2.6
2.62
2.64
2.66
2.68

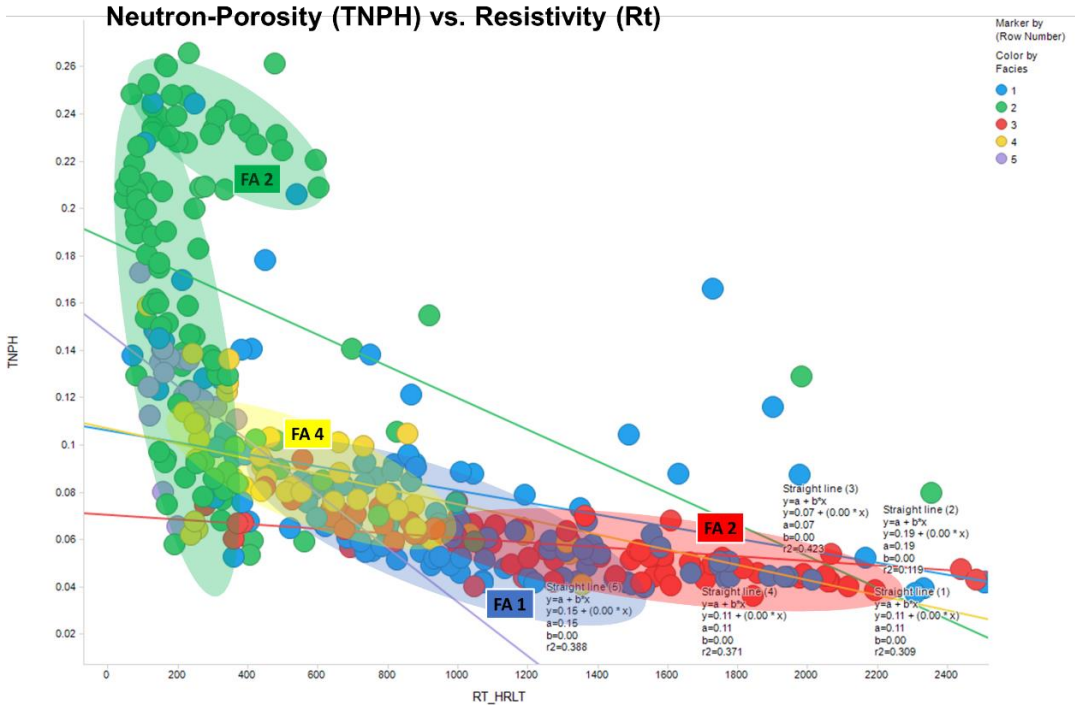
Neutron-Porosity (TNPH) vs. Resistivity (Rt)
Marker by (Row Number)
Color by Facies
1
2
3
4
5
FA 2
FA 4
FA 1
FA 2
Straight line (5)
y=a + b*x
y=0.15 + (0.00 * x)
a=0.15
b=0.00
r2=0.388
Straight line (4)
y=a + b*x
y=0.11 + (0.00 * x)
a=0.11
b=0.00
r2=0.371
Straight line (3)
y=a + b*x
y=0.07 + (0.00 * x)
a=0.07
b=0.00
r2=0.423
Straight line (2)
y=a + b*x
y=0.19 + (0.00 * x)
a=0.19
b=0.00
r2=0.119
Straight line (1)
y=a + b*x
y=0.11 + (0.00 * x)
a=0.11
b=0.00
r2=0.309
TNPH
RT_HRLT
0.26
0.24
0.22
0.2
0.18
0.16
0.14
0.12
0.1
0.08
0.06
0.04
0.02
0
200
400
600
800
1000
1200
1400
1600
1800
2000
2200
2400

Neutron-Porosity (TNPH) vs. Gamma Ray (HSGR)

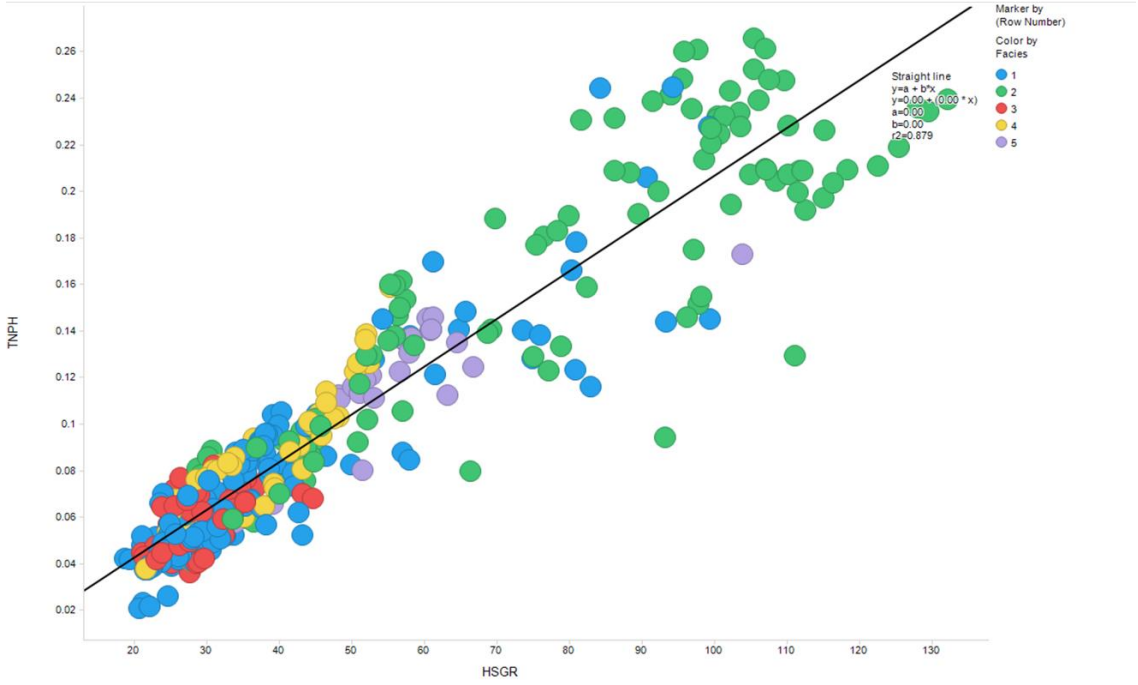

Bulk Density (RHOZ) vs. Photoelectric factor (PEFZ)

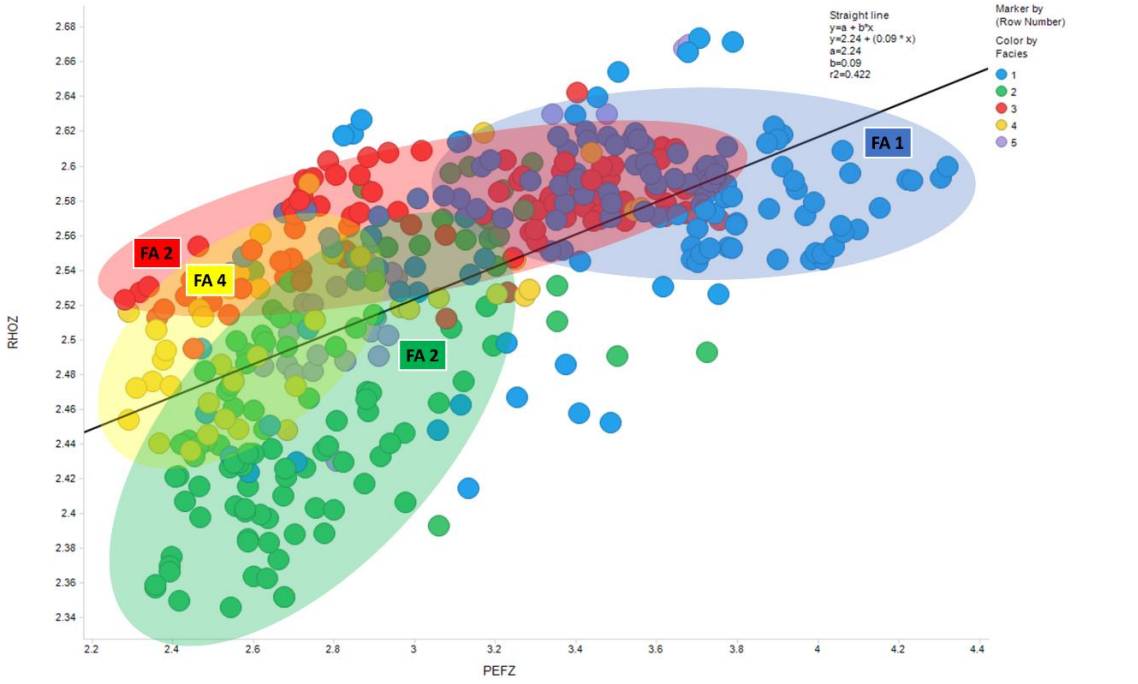

Porosity (PXND) vs. Photoelectric factor (PEFZ)

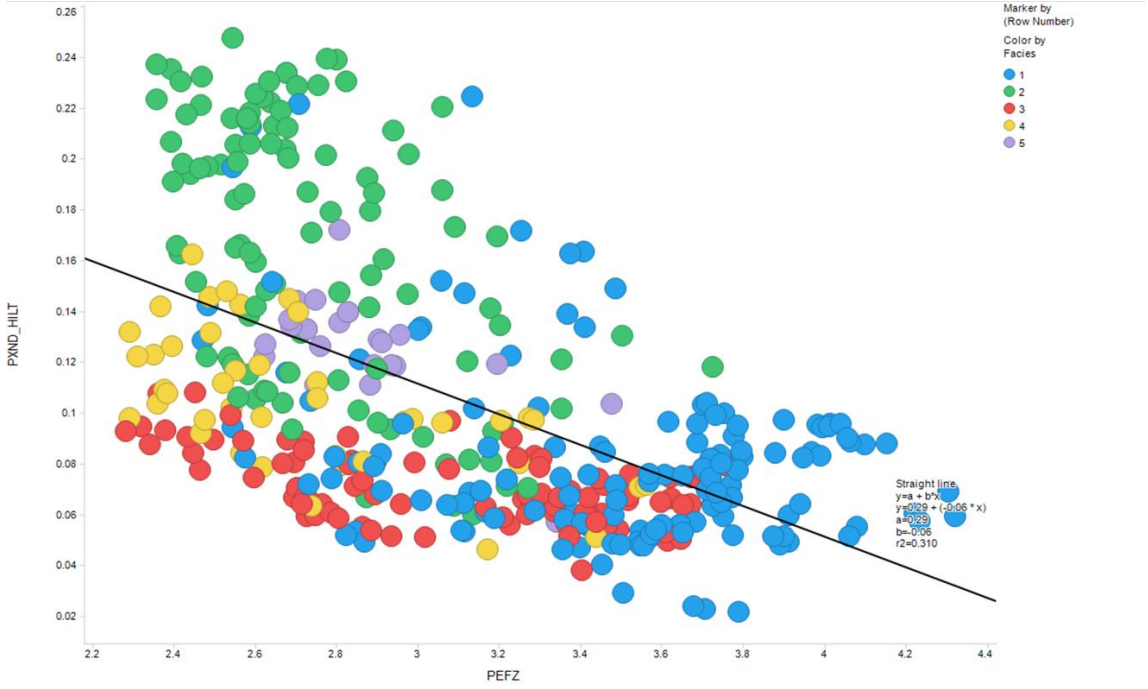

Photoelectric factor (PEFZ) vs. Gamma Ray (HSGR)

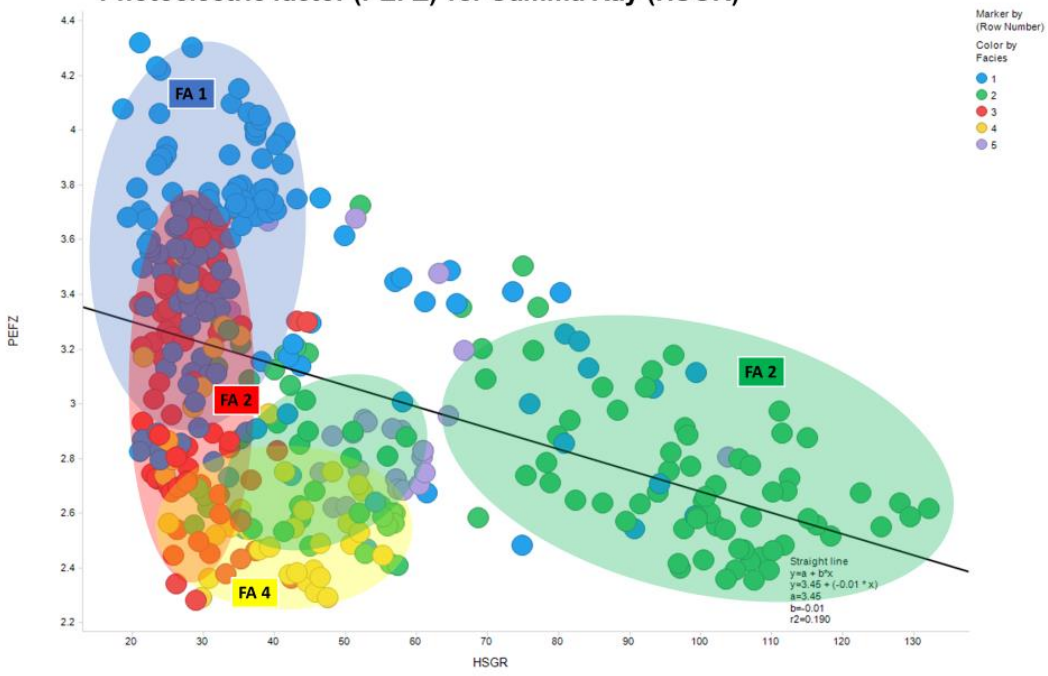

Bulk Density (RHOZ) vs. Gamma Ray (HSGR)

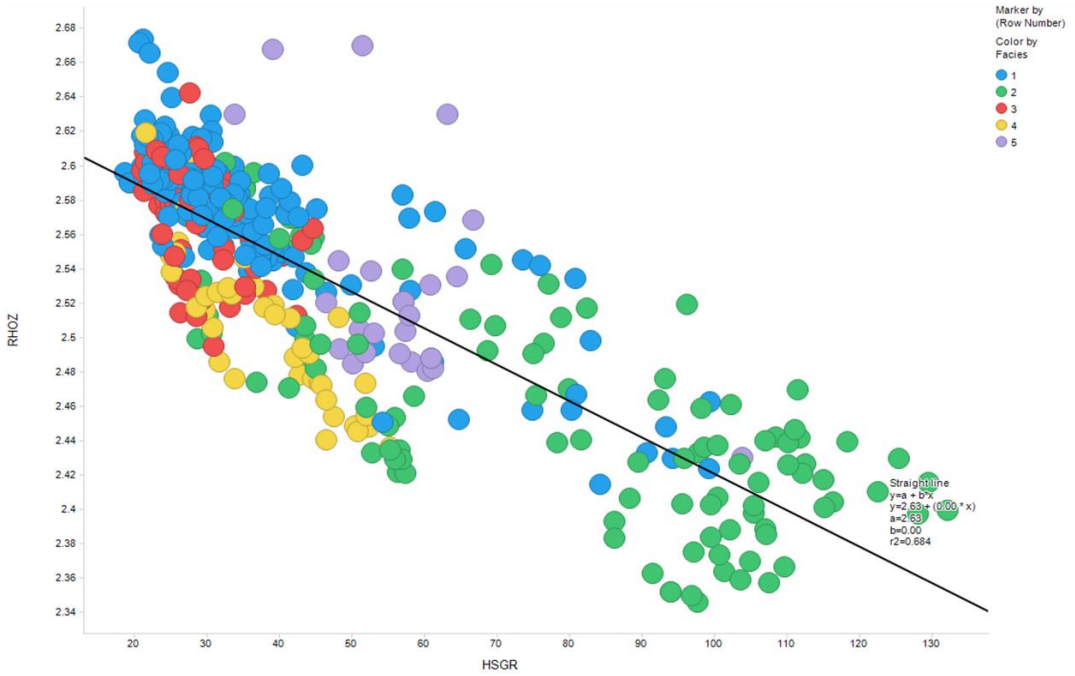

Neutron-Porosity (TNPH) vs. Density-Porosity (DPHZ)

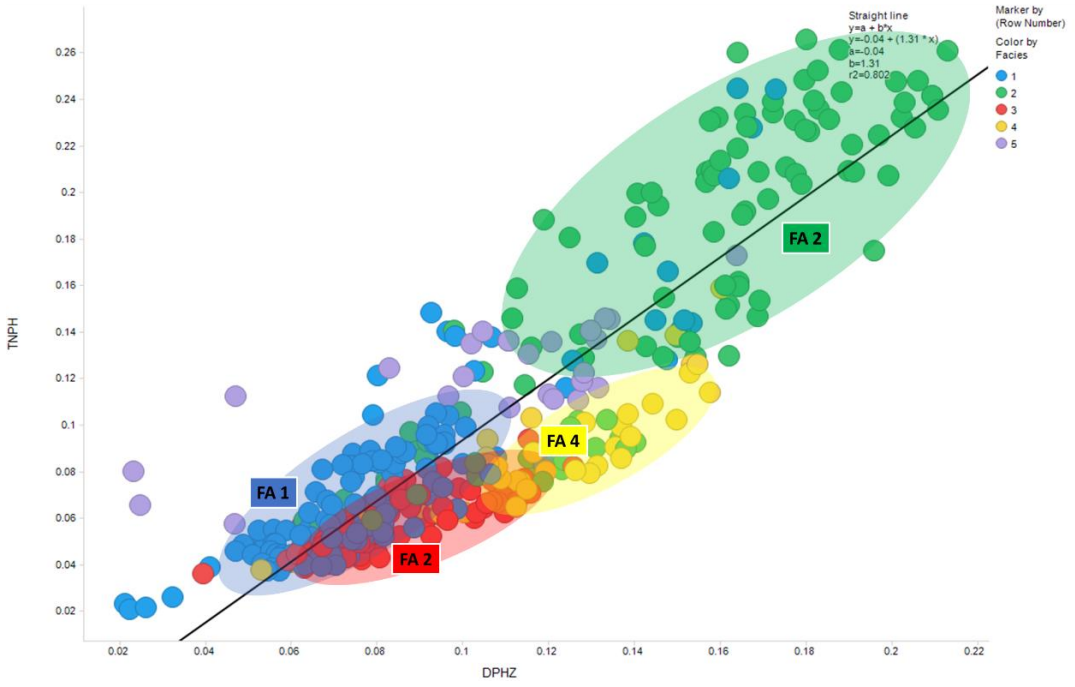

Neutron-Porosity (TNPH) vs. Photoelectric factor (PEFZ)

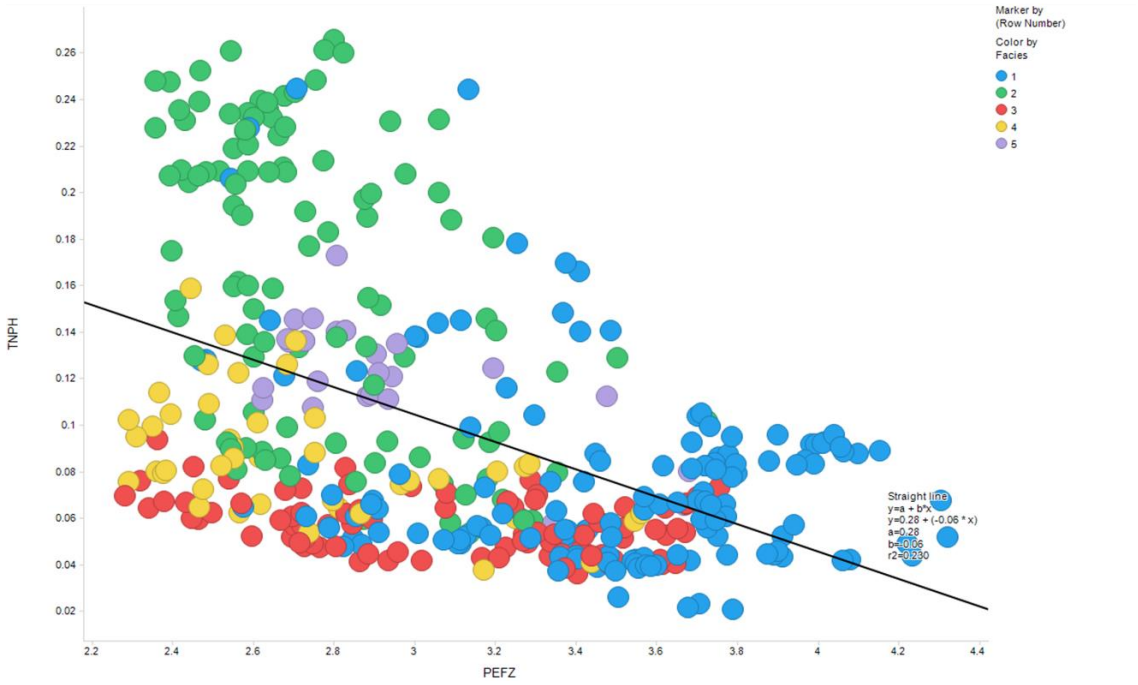

Resistivity (Rt) vs. Porosity Crossover

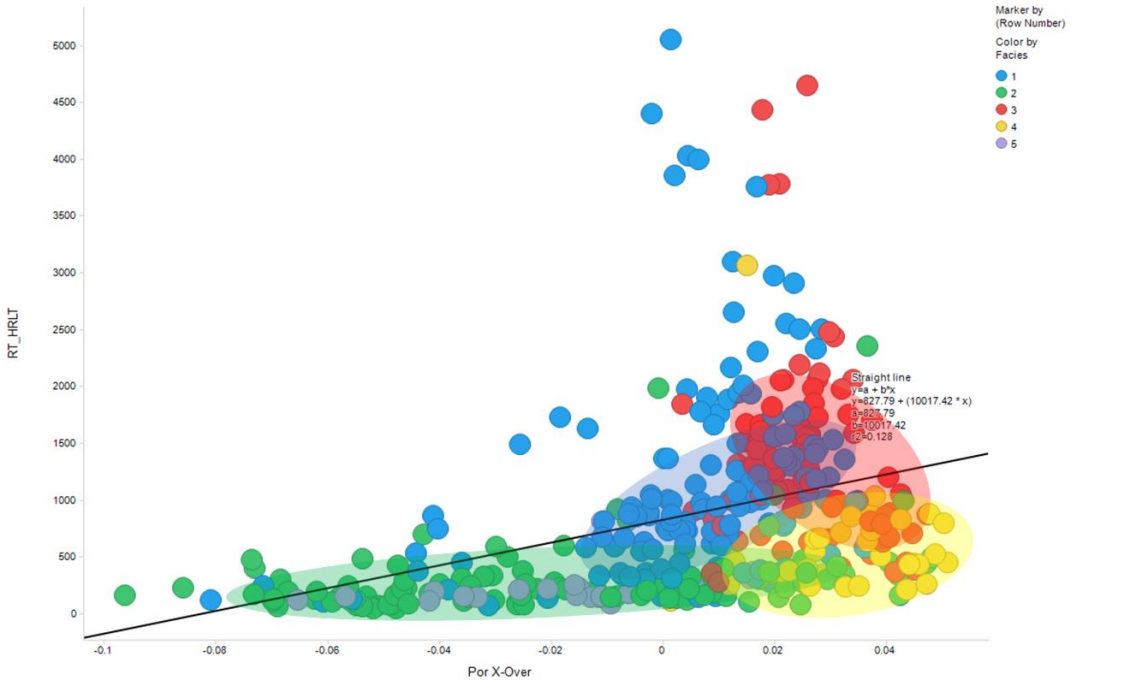

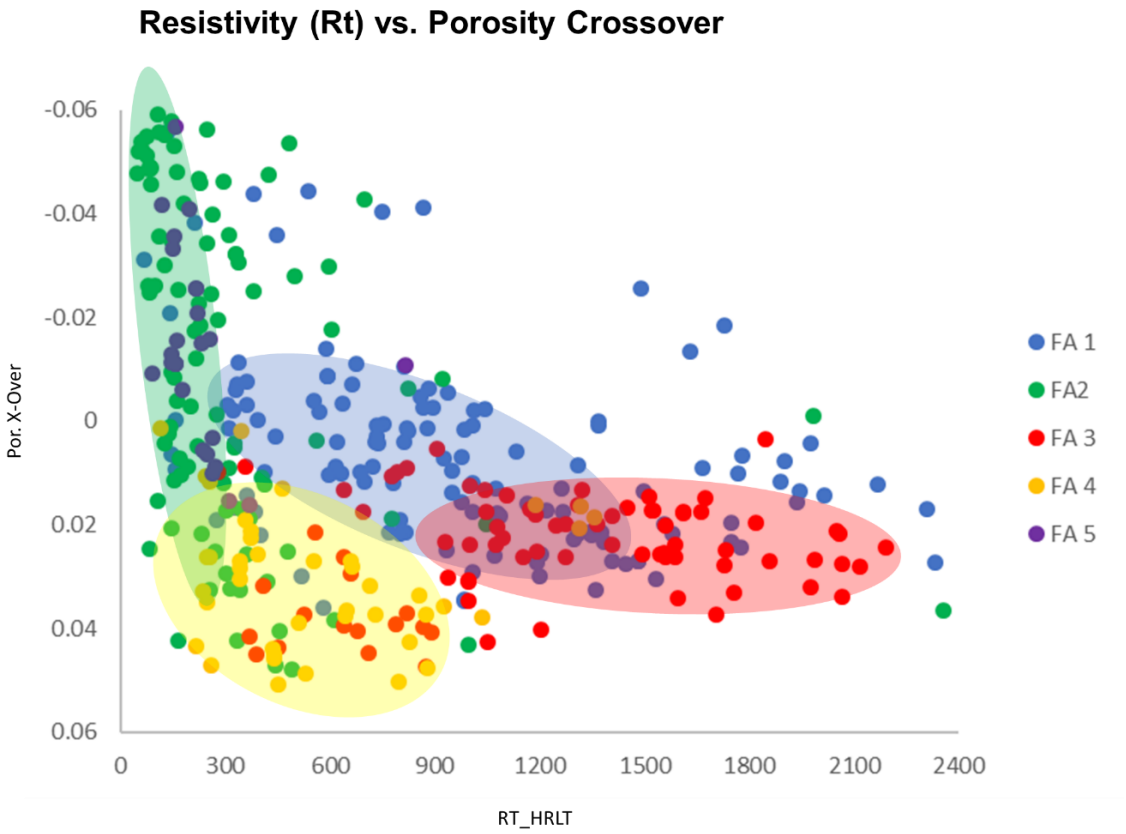
Resistivity (Rt) vs. Porosity Crossover
Por. X-Over
-0.06
-0.04
-0.02
0
0.02
0.04
0.06
0
300
600
900
1200
1500
1800
2100
2400
RT_HRLT
FA 1
FA2
FA 3
FA 4
FA 5

APPENDIX D

CA WIRELINE LOG HISTOGRAMS AND STATISTICS

Range and Distribution of Porosity Values

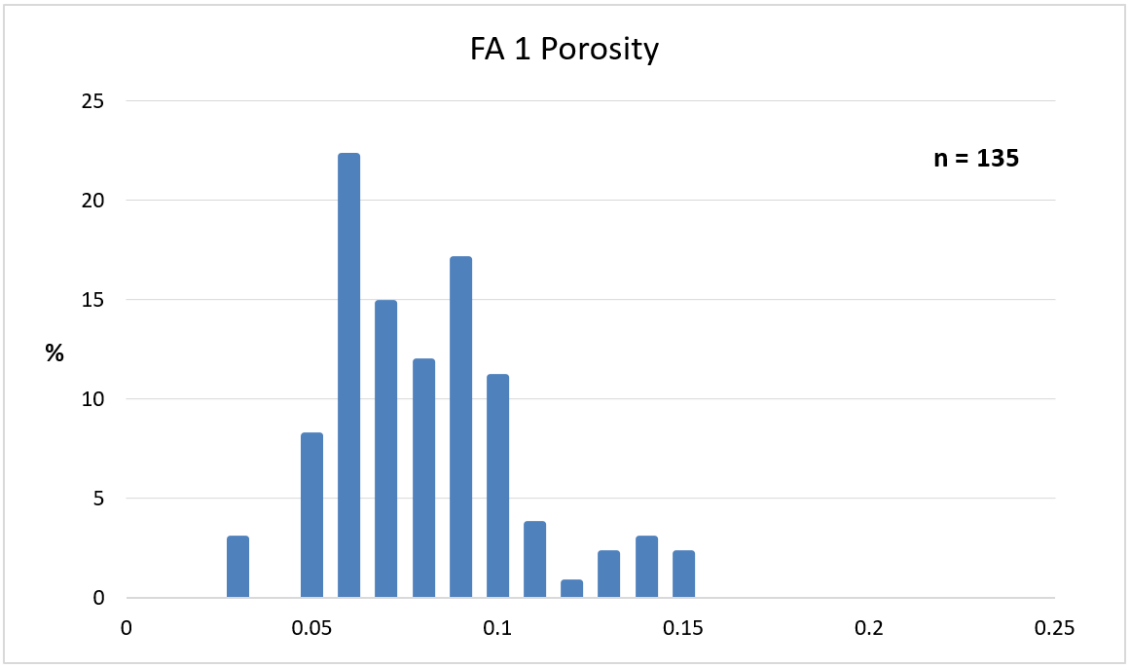

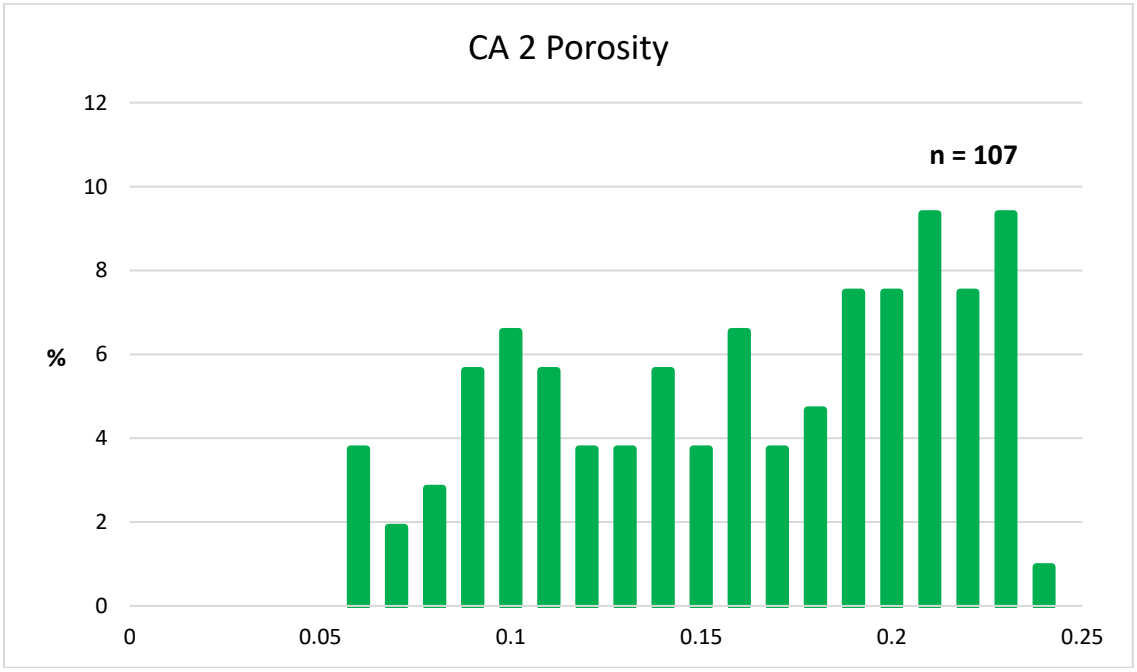

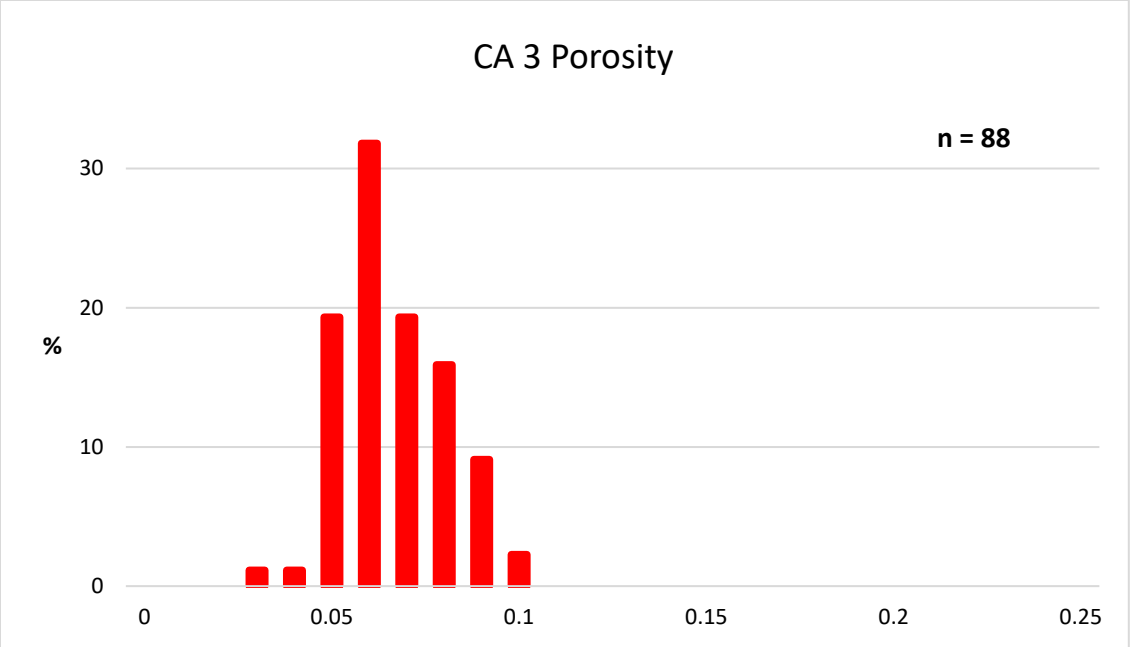
CA 3 Porosity
n = 88
30
20
%
10
0
0
0.05
0.1
0.15
0.2
0.25

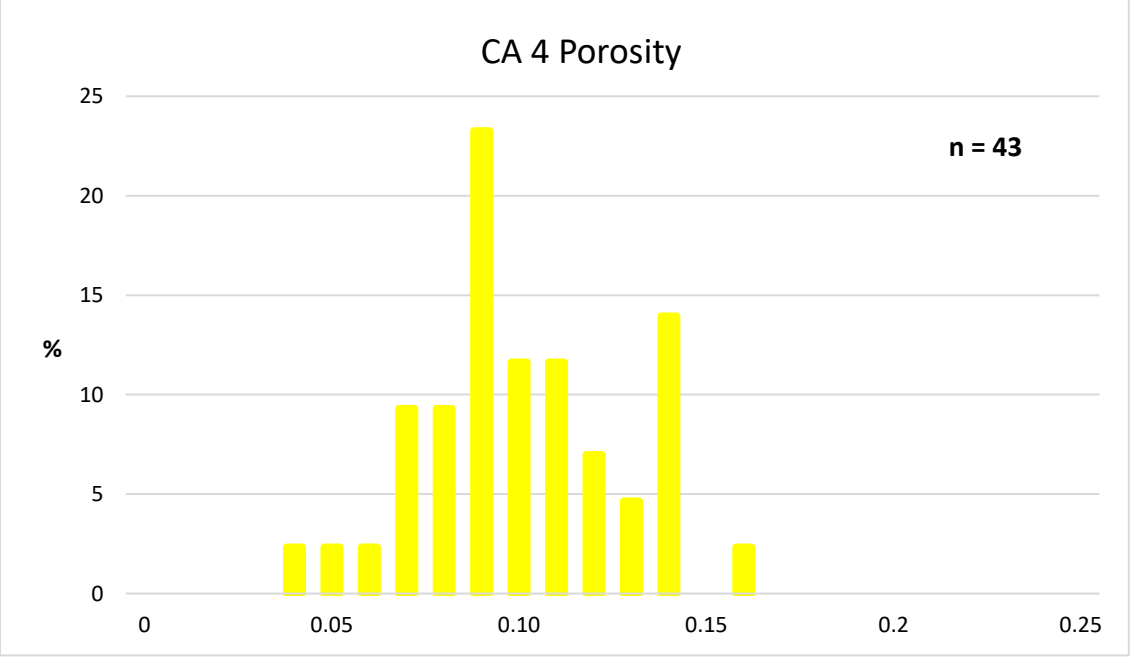
CA 4 Porosity
n = 43
25
20
15
%
10
5
0
0
0.05
0.10
0.15
0.2
0.25

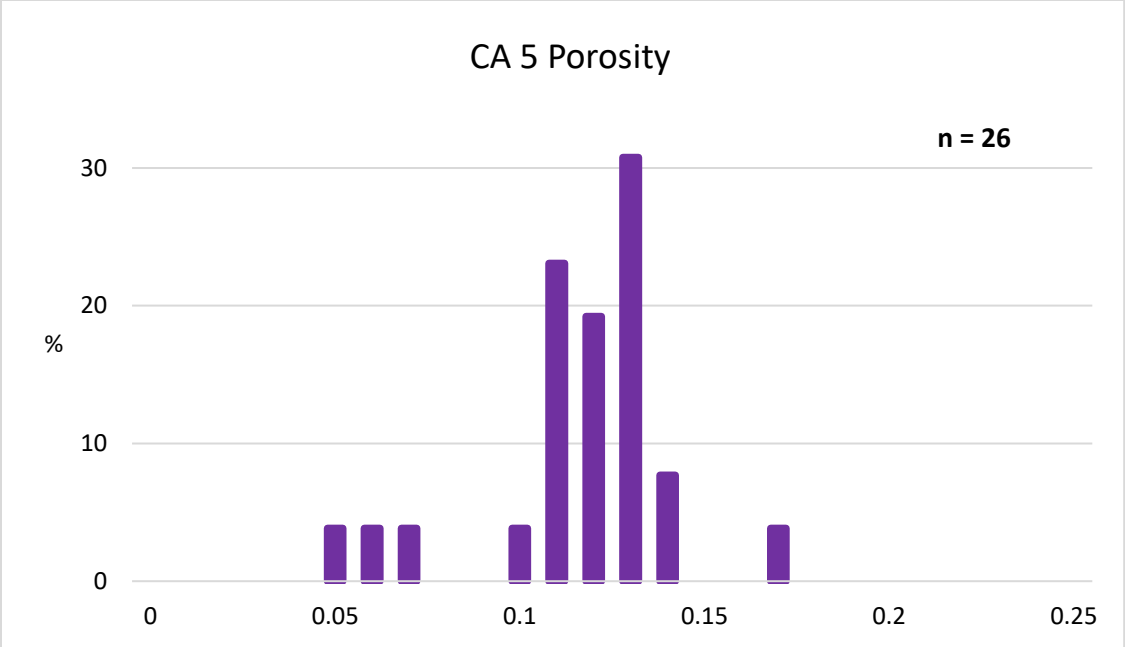
CA 5 Porosity
n = 26
30
20
%
10
0
0
0.05
0.1
0.15
0.2
0.25

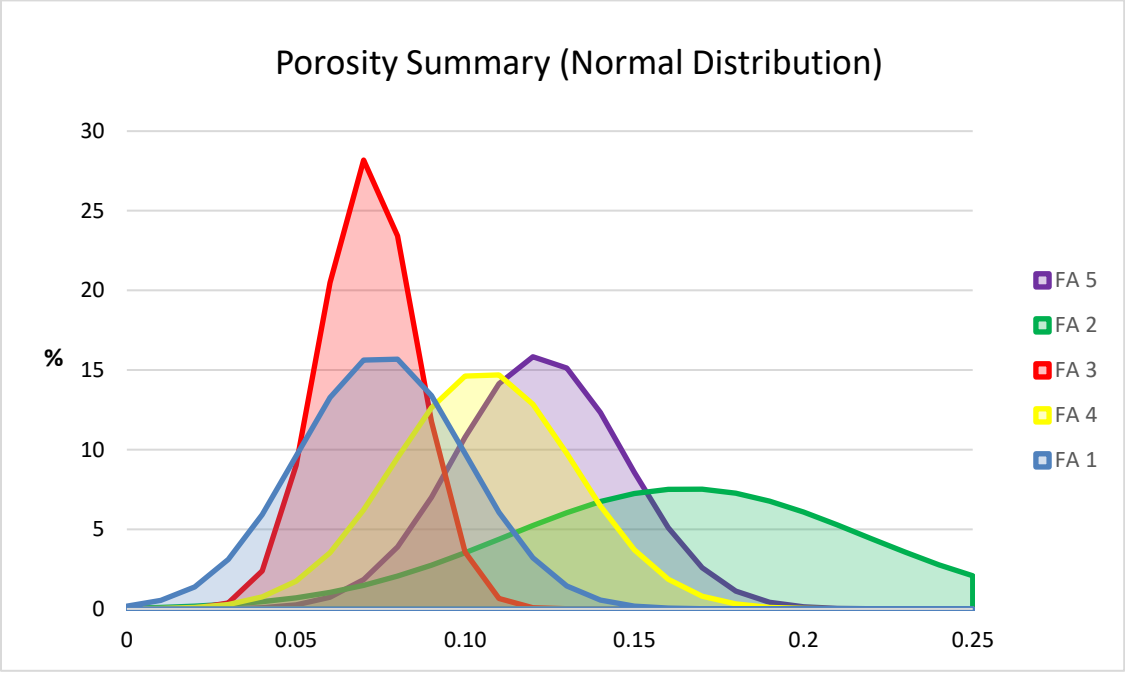
Porosity Summary (Normal Distribution)
30
25
20
%
15
10
5
0
0
0.05
0.10
0.15
0.2
0.25
FA 5
FA 2
FA 3
FA 4
FA 1

Range and Distribution of Gamma Ray Values

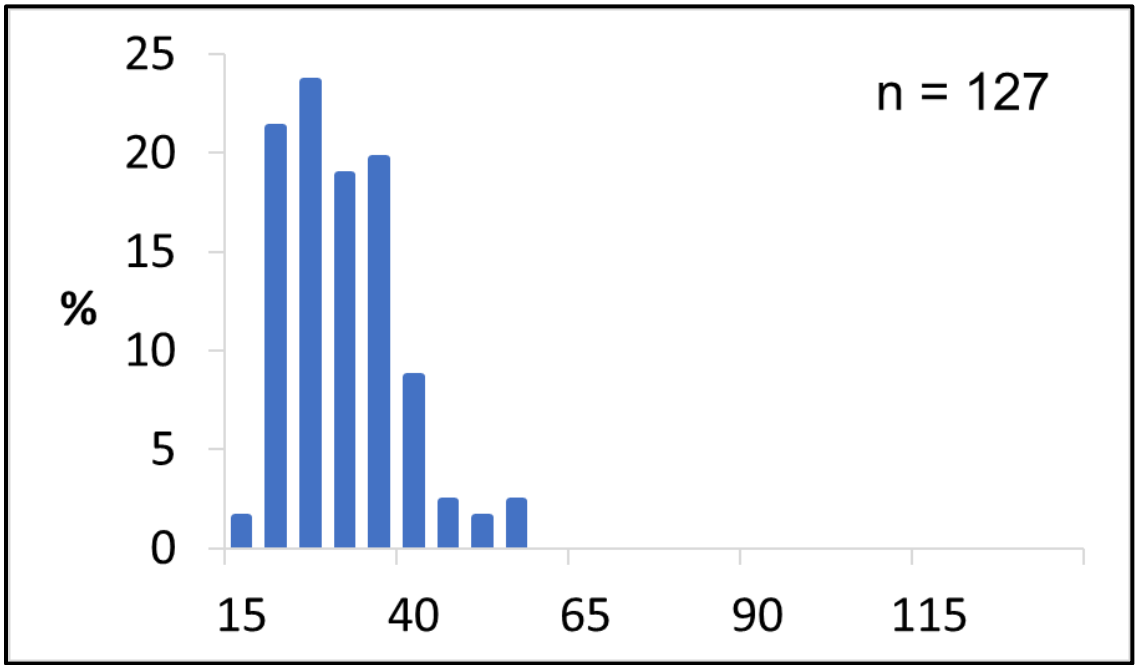

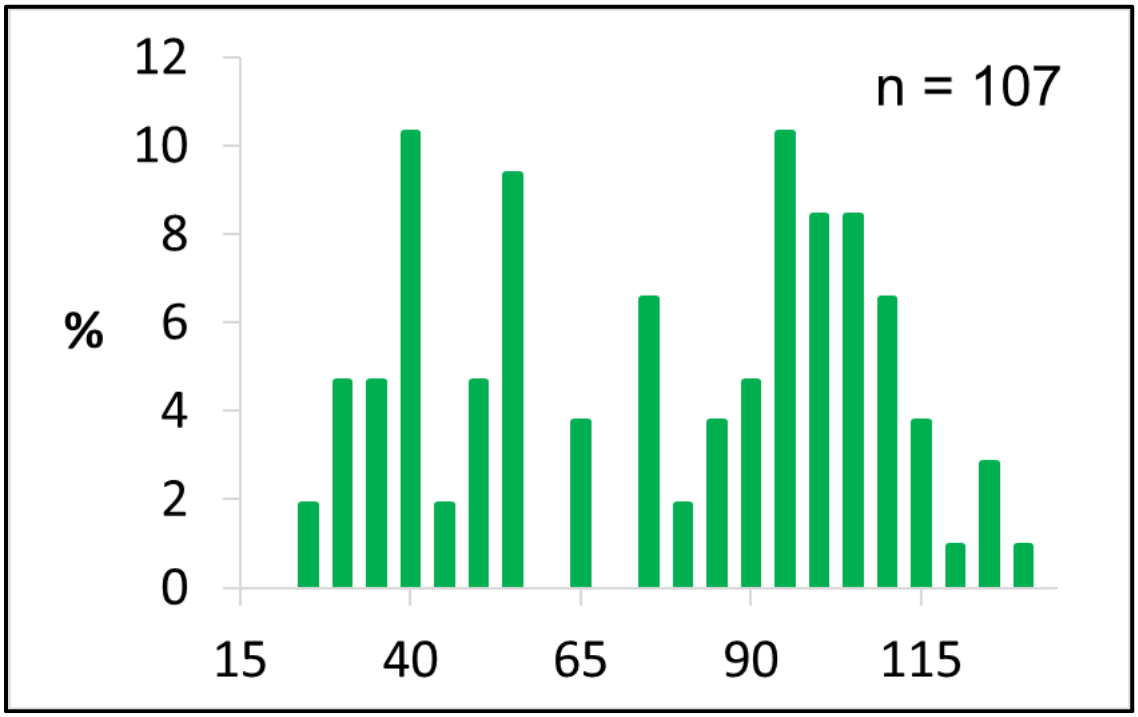

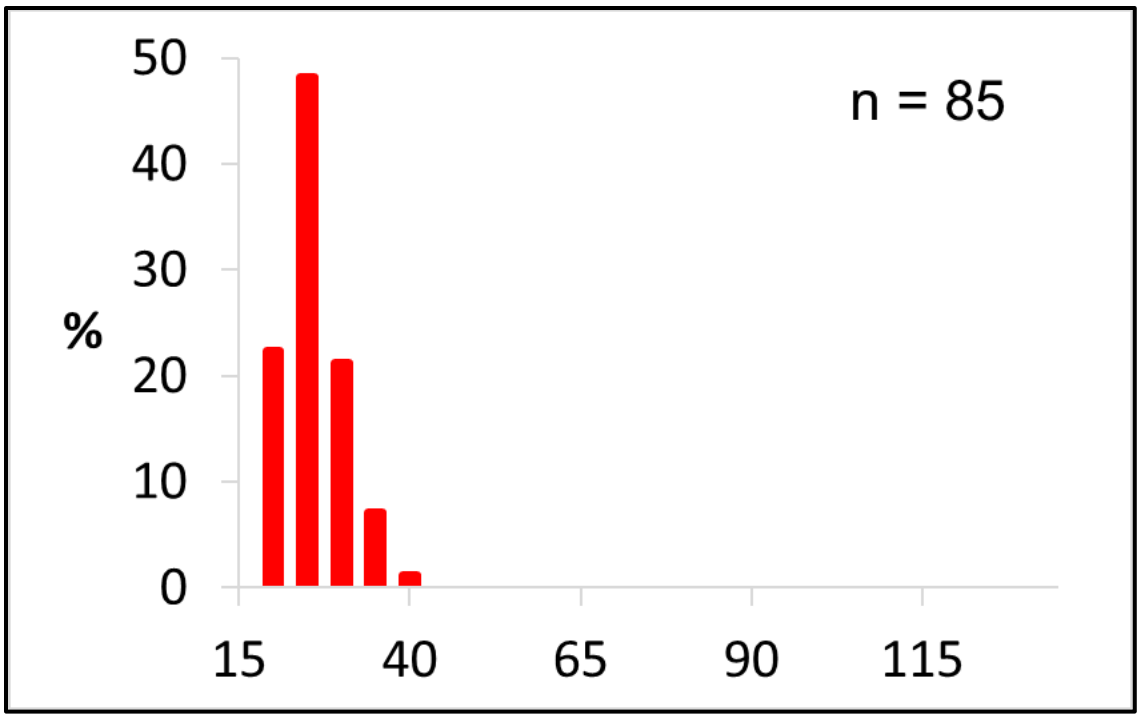
50
40
30
%
20
10
0
n = 85
15
40
65
90
115

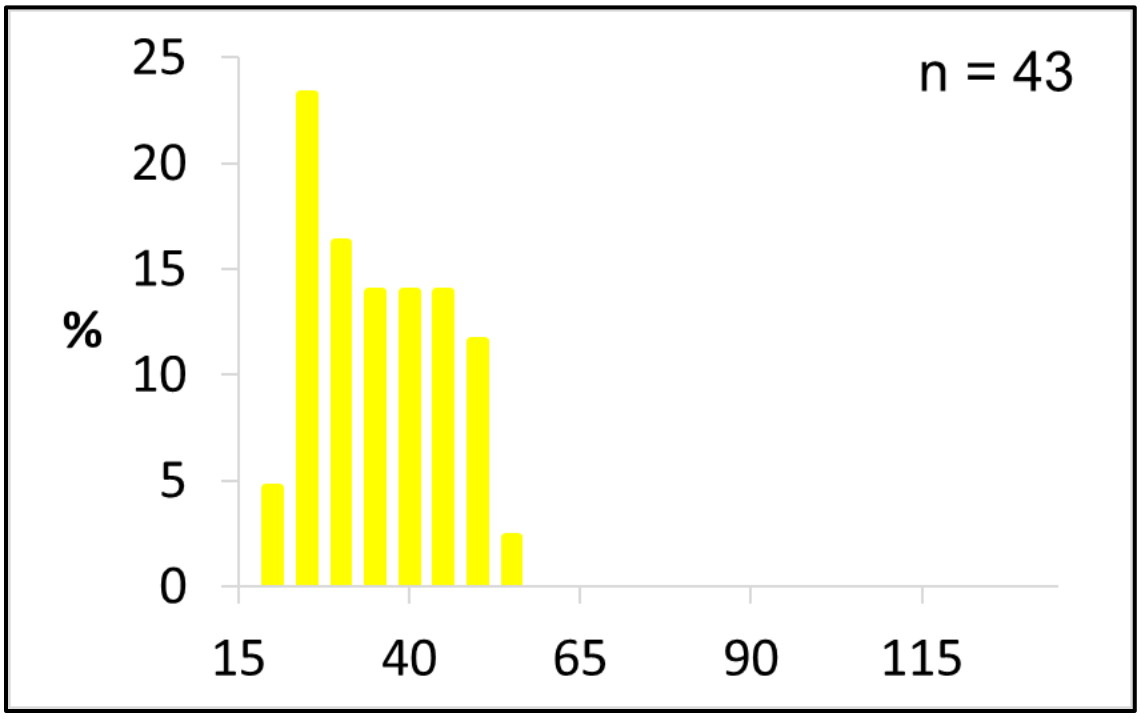
25
20
15
%
10
5
0
n = 43
15
40
65
90
115

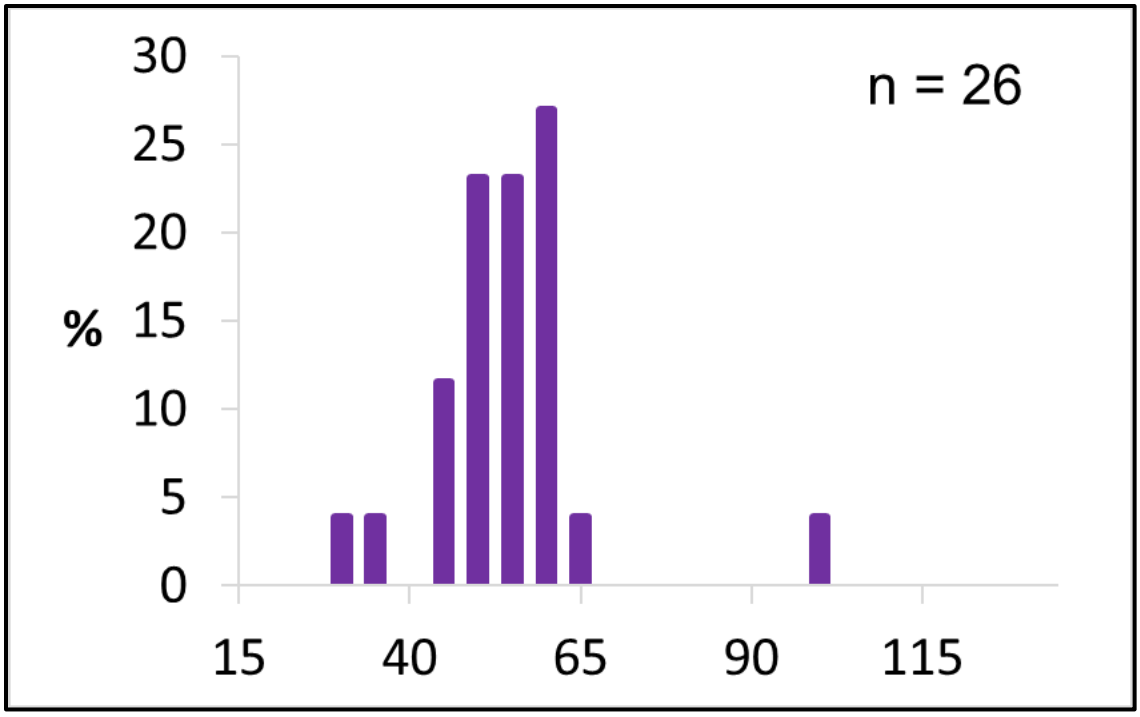
n = 26
%
30
25
20
15
10
5
0
15
40
65
90
115

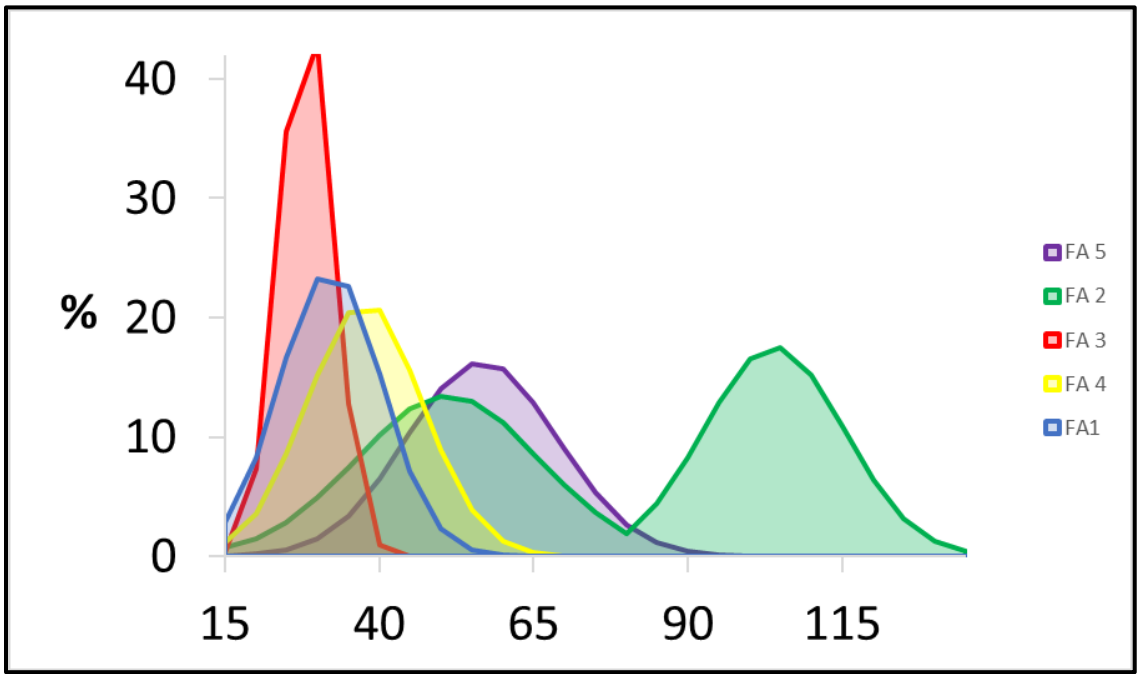
%
40
30
20
10
0
15
40
65
90
115
FA 5
FA 2
FA 3
FA 4
FA1

Range and Distribution of Resistivity Values

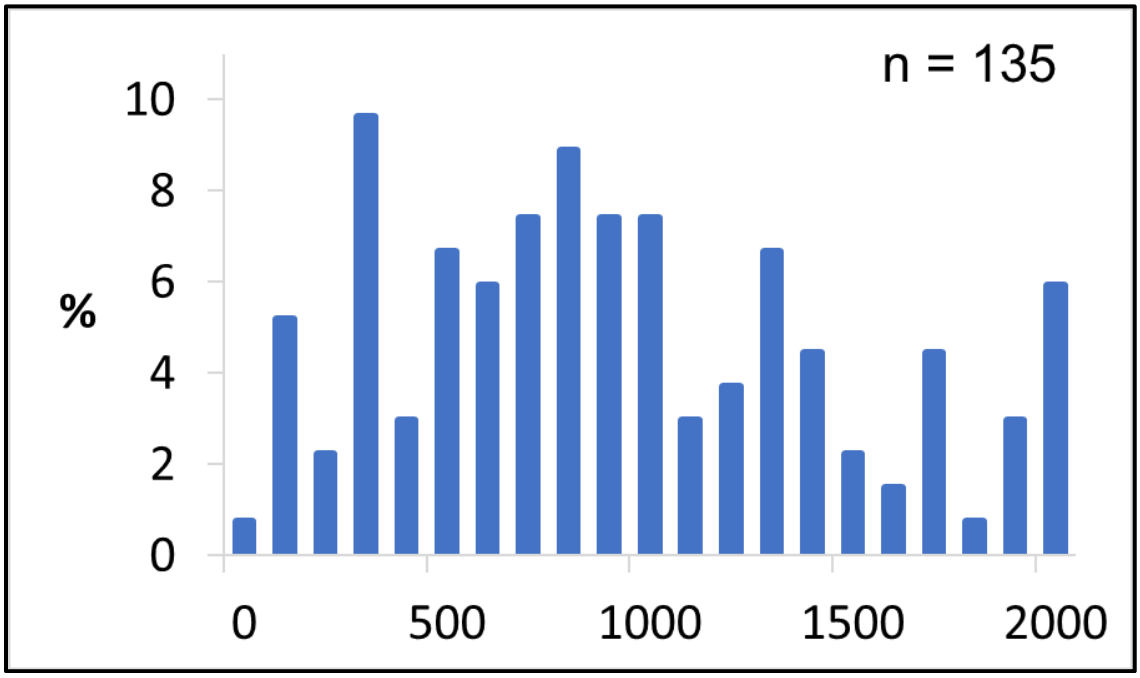

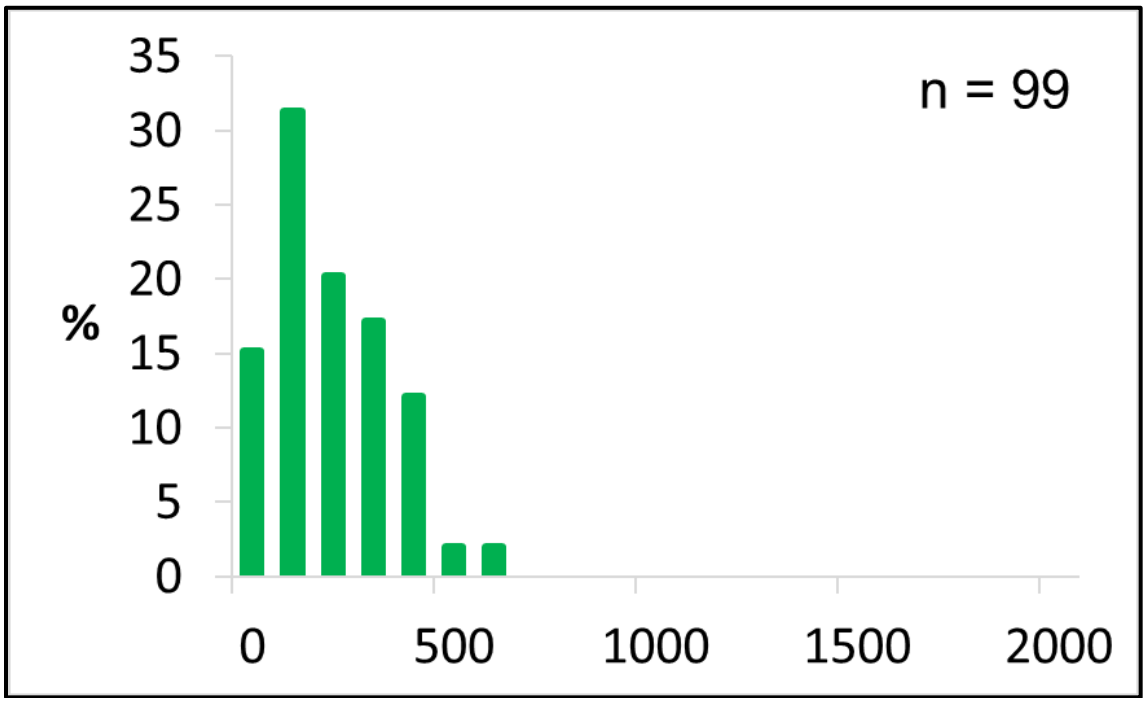

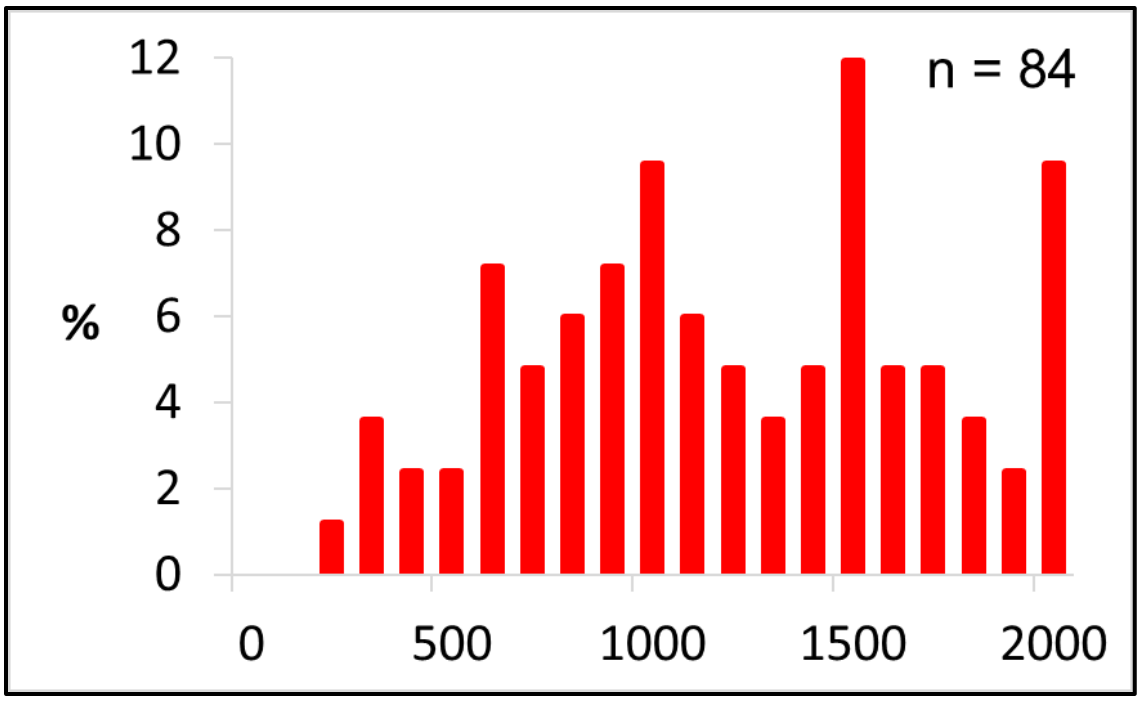
n = 84
%
12
10
8
6
4
2
0
0
500
1000
1500
2000

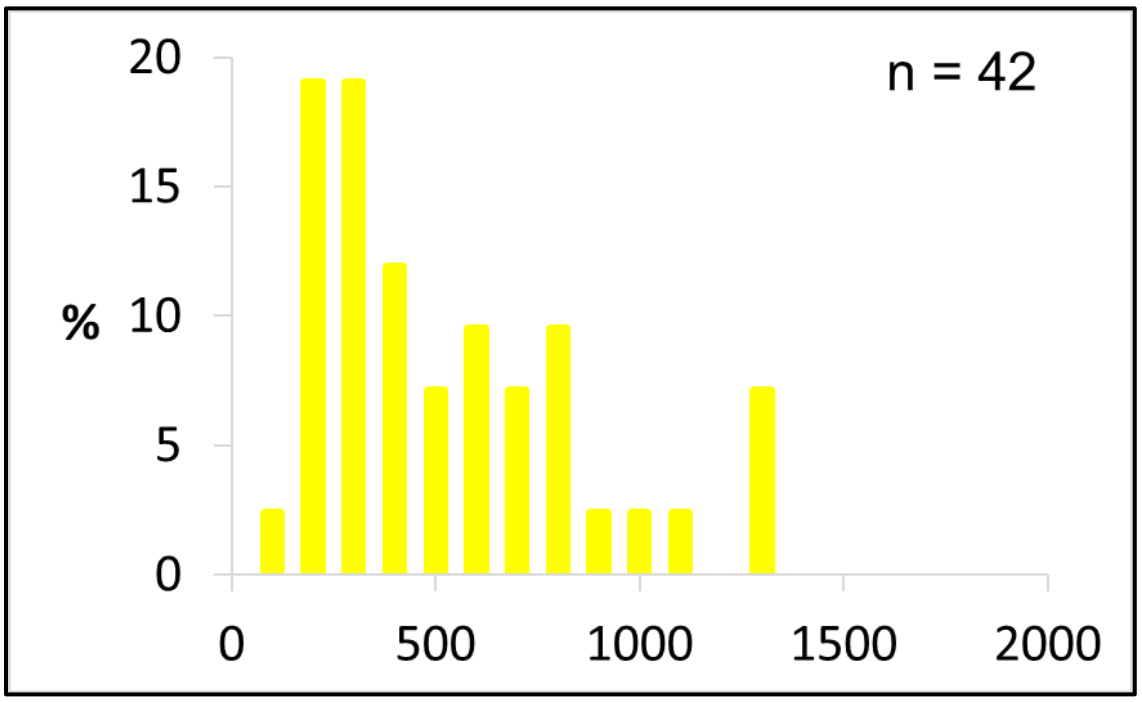
n = 42
%
20
15
10
5
0
0
500
1000
1500
2000

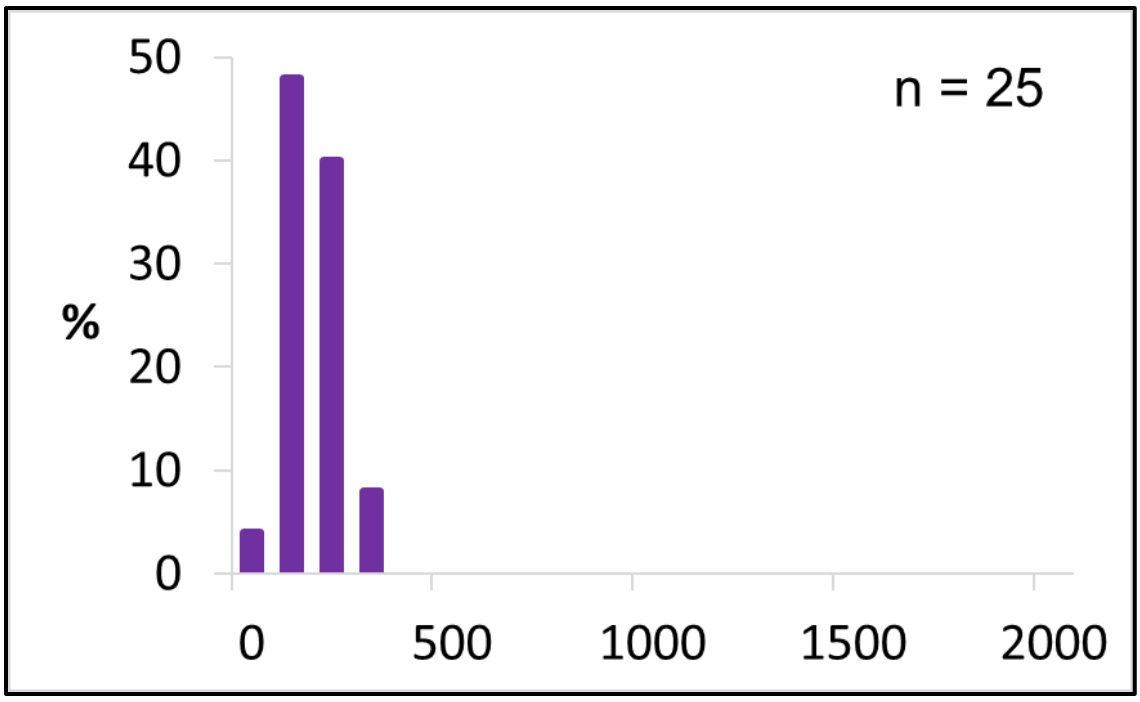
50
40
30
%
20
10
0
n = 25
0
500
1000
1500
2000

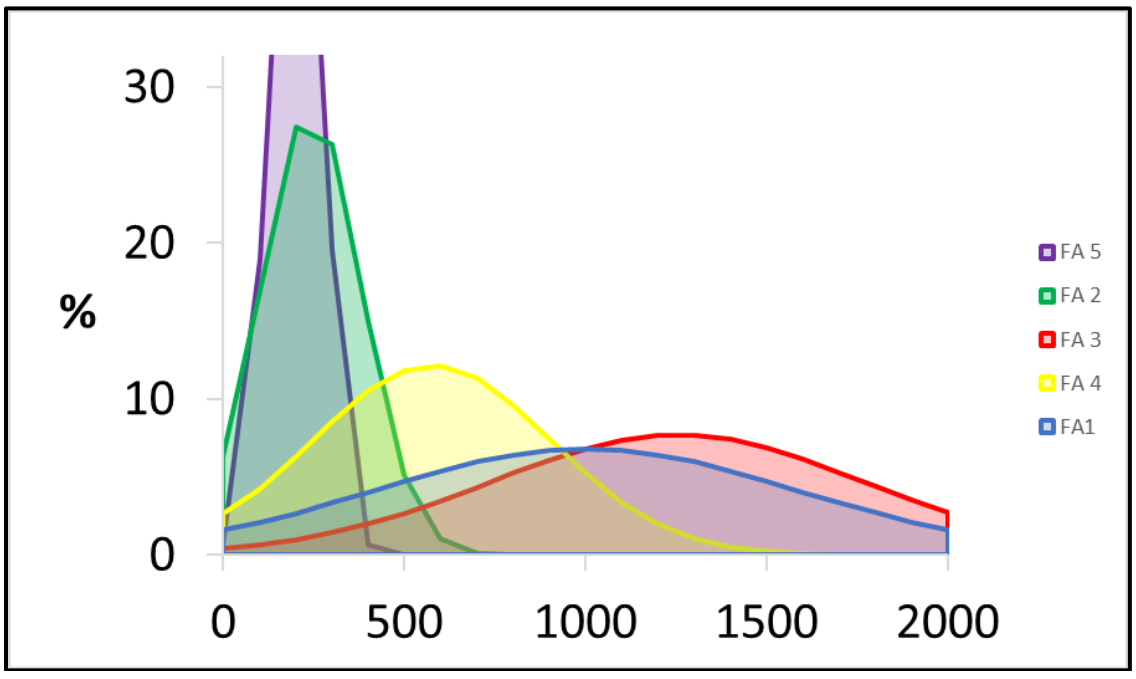
30
20
%
10
0
0
500
1000
1500
2000
FA 5
FA 2
FA 3
FA 4
FA1

Range and Distribution of Neutron-Porosity/Density-Porosity Crossover

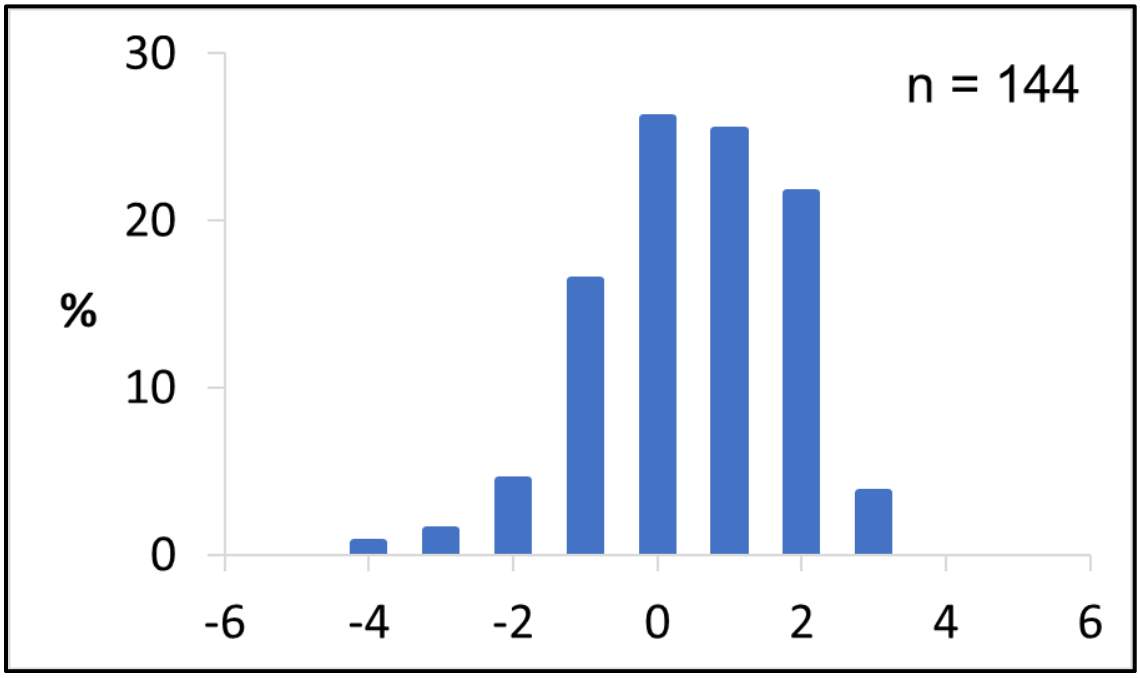

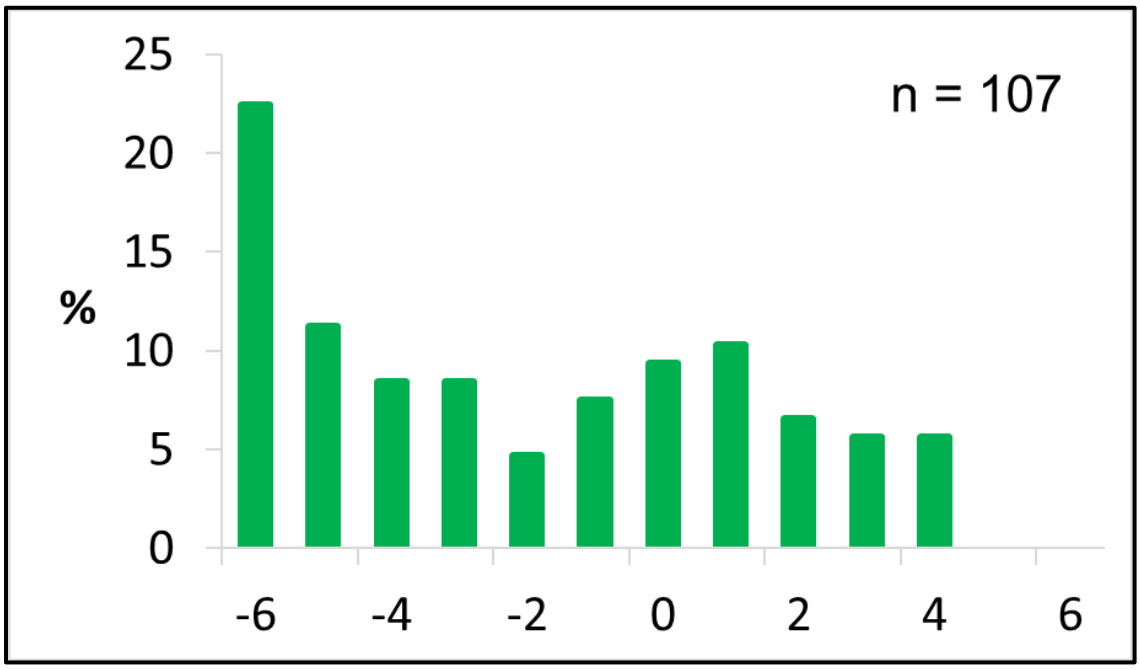

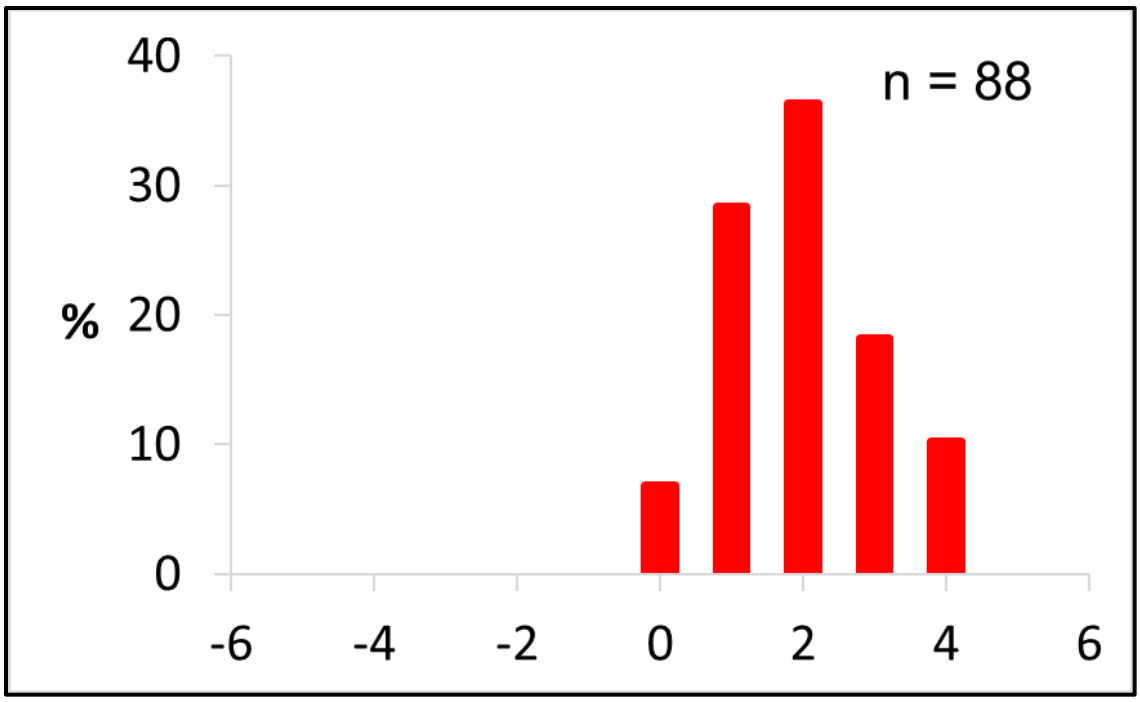
n = 88
%
40
30
20
10
0
-6
-4
-2
0
2
4
6

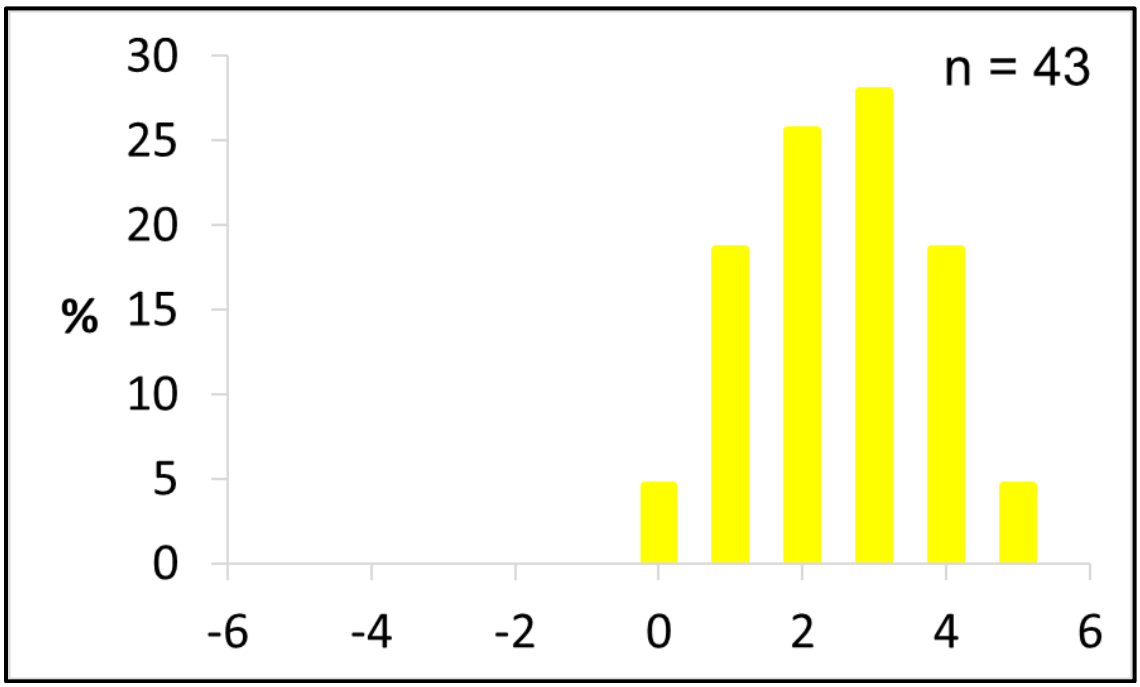
n = 43
%
30
25
20
15
10
5
0
-6
-4
-2
0
2
4
6

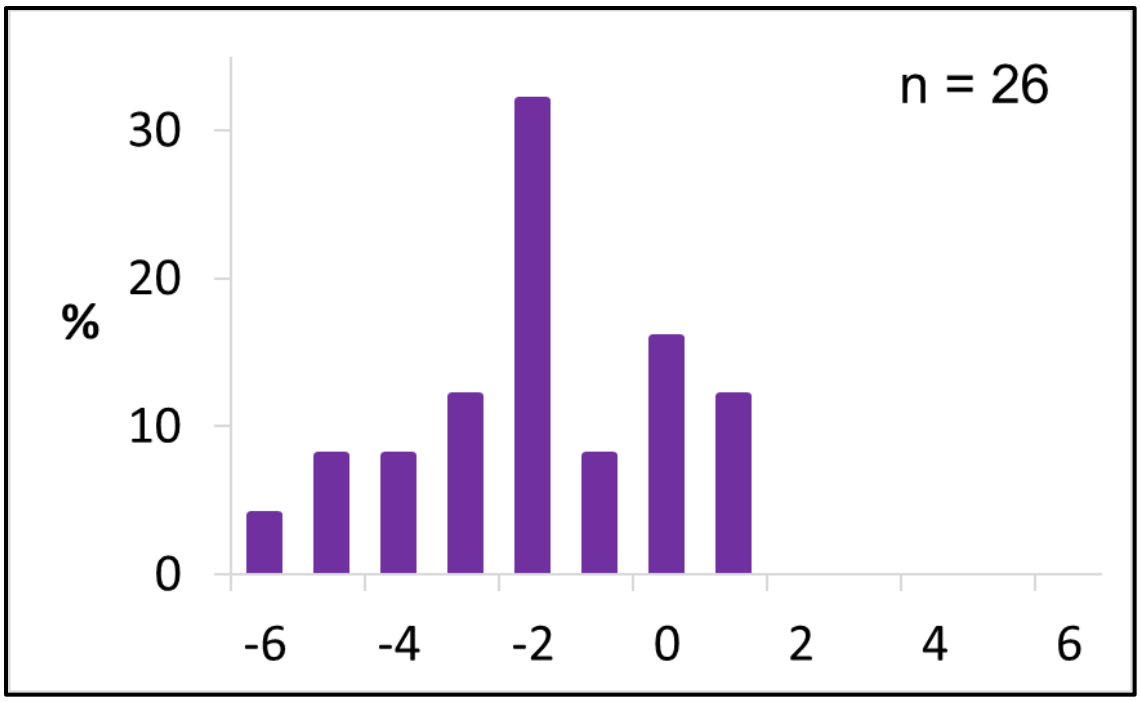
n = 26
%
30
20
10
0
-6
-4
-2
0
2
4
6

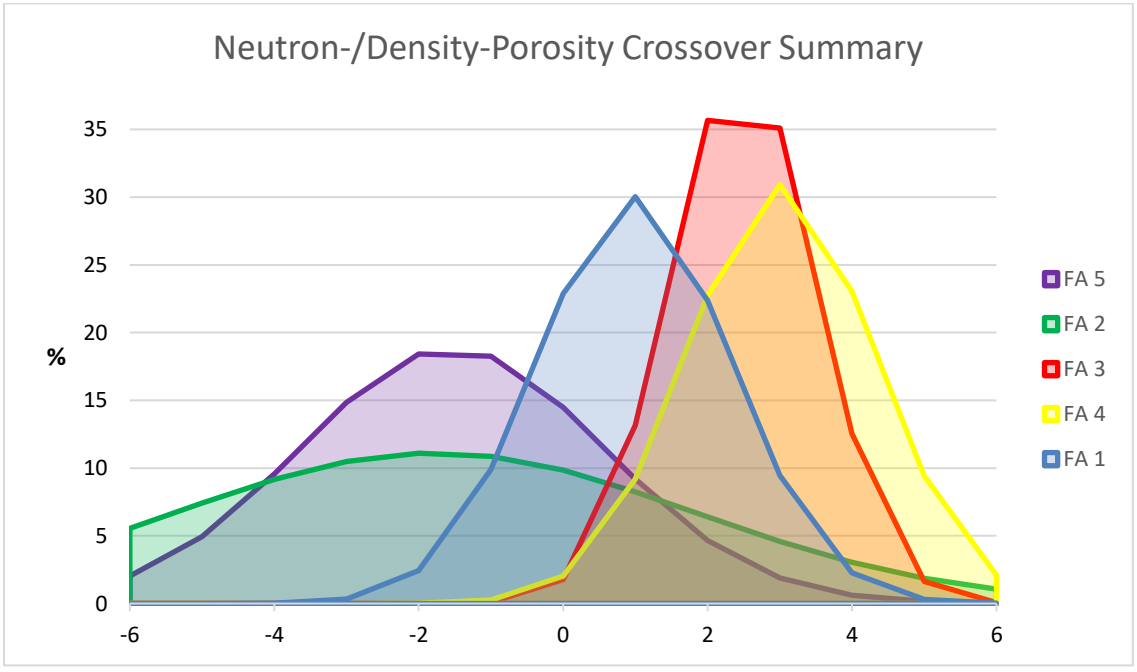
Neutron-/Density-Porosity Crossover Summary
%
35
30
25
20
15
10
5
0
-6
-4
-2
0
2
4
6
FA 5
FA 2
FA 3
FA 4
FA 1

Range and Distribution of Photoelectric Factor Values

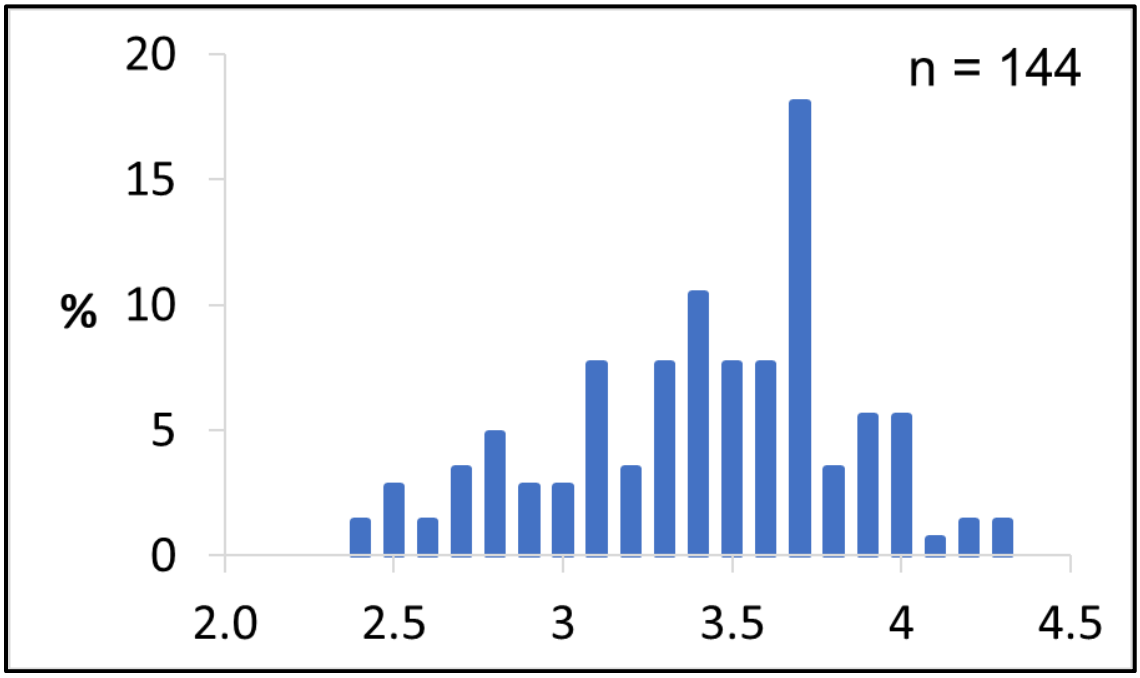

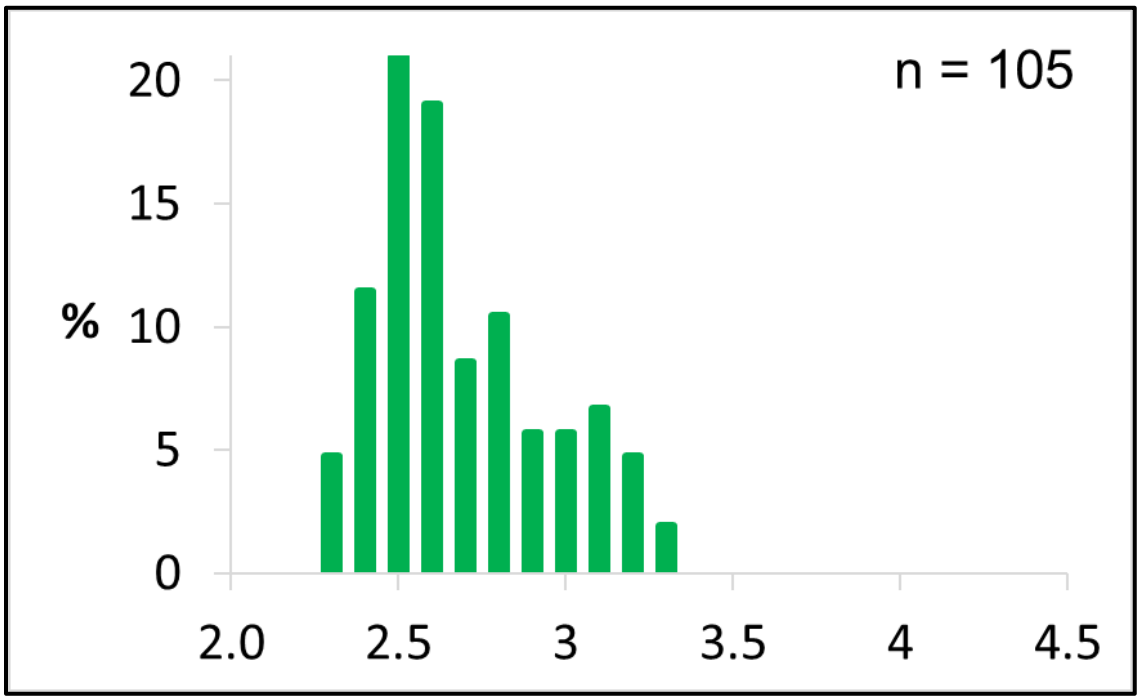

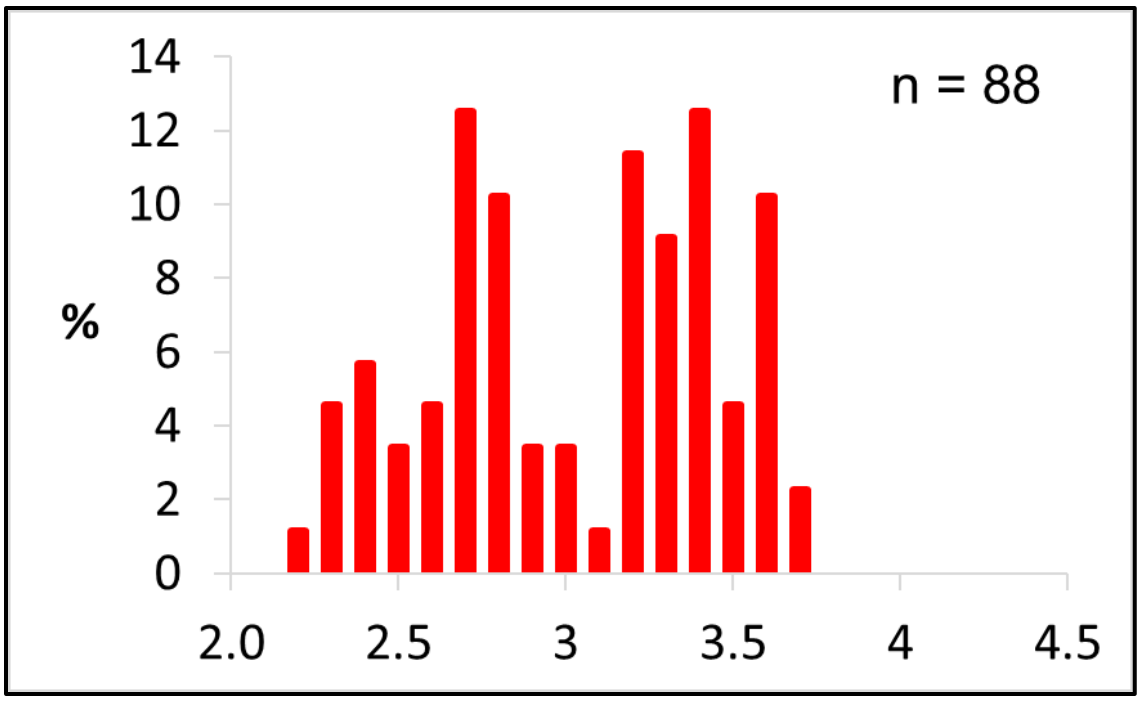
n = 88
%
14
12
10
8
6
4
2
0
2.0
2.5
3
3.5
4
4.5

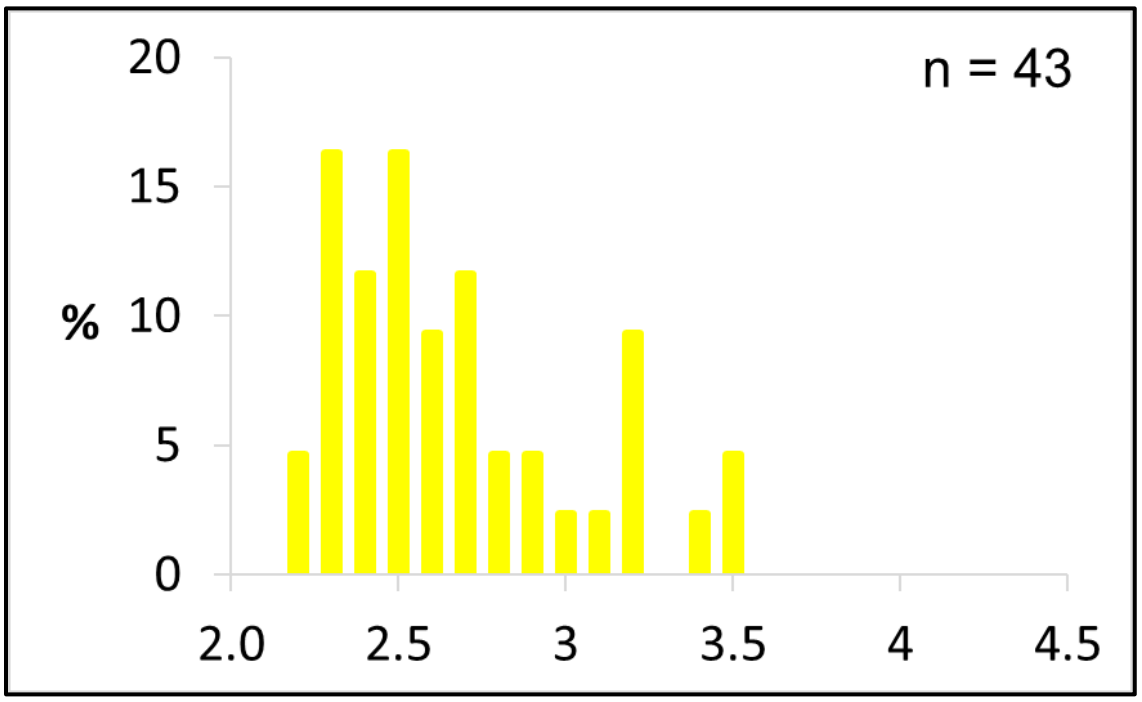
n = 43
%
20
15
10
5
0
2.0
2.5
3
3.5
4
4.5

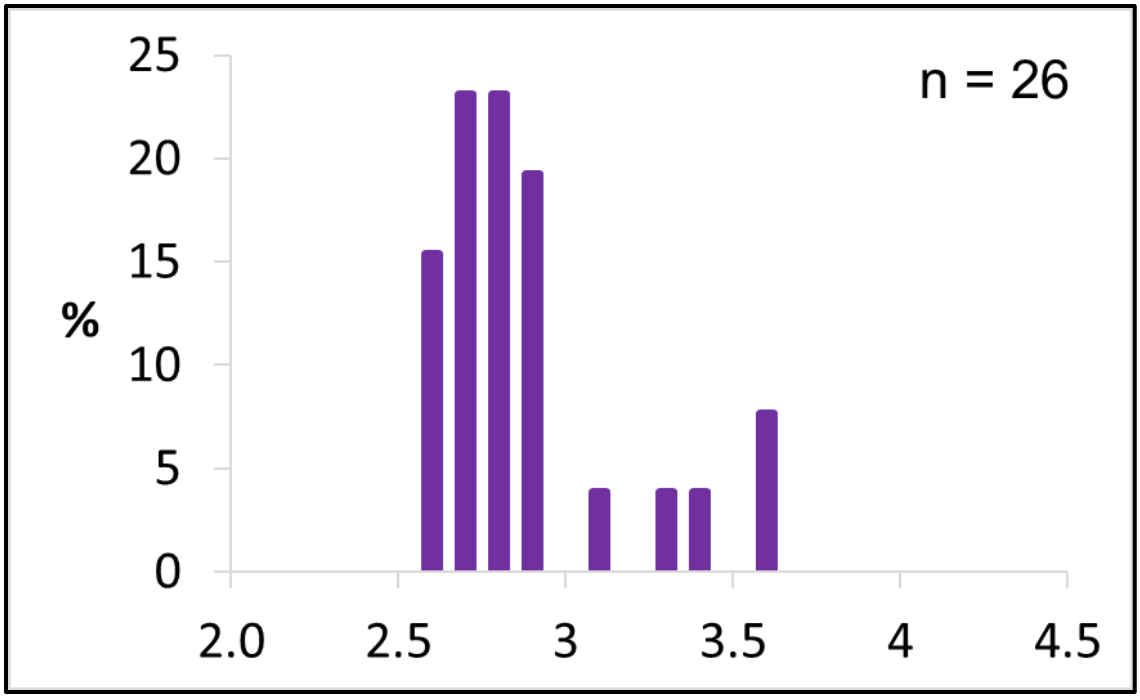
n = 26
%
25
20
15
10
5
0
2.0
2.5
3
3.5
4
4.5

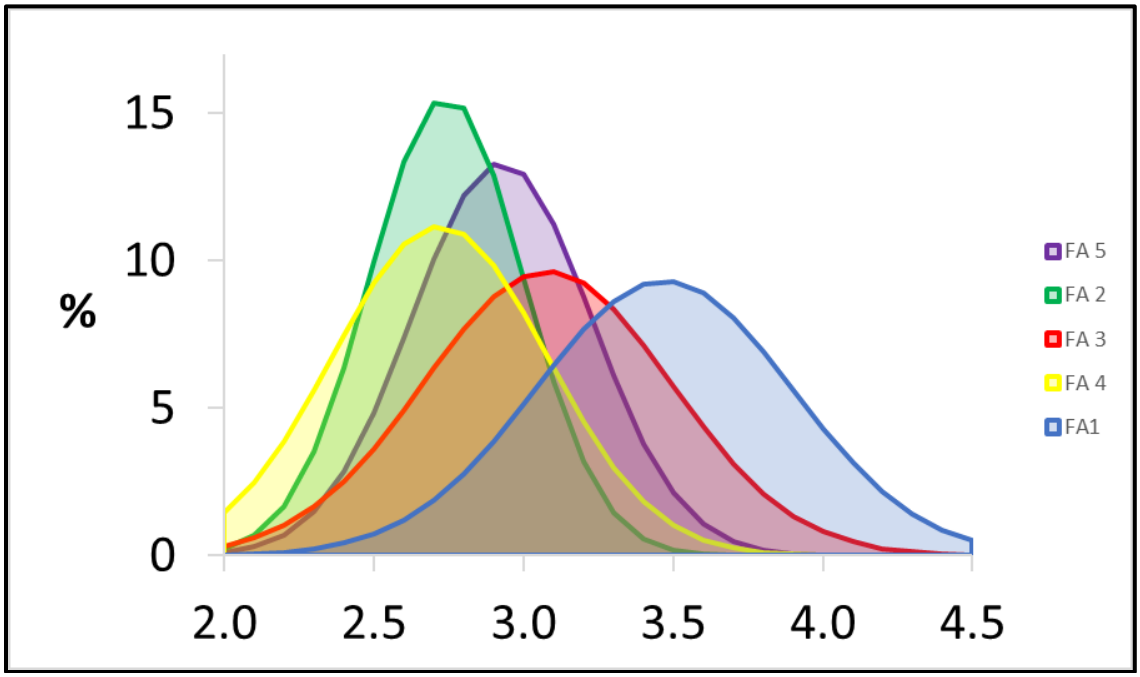
%
15
10
5
0
2.0
2.5
3.0
3.5
4.0
4.5
FA 5
FA 2
FA 3
FA 4
FA1

Range and Distribution of Bulk Density Values

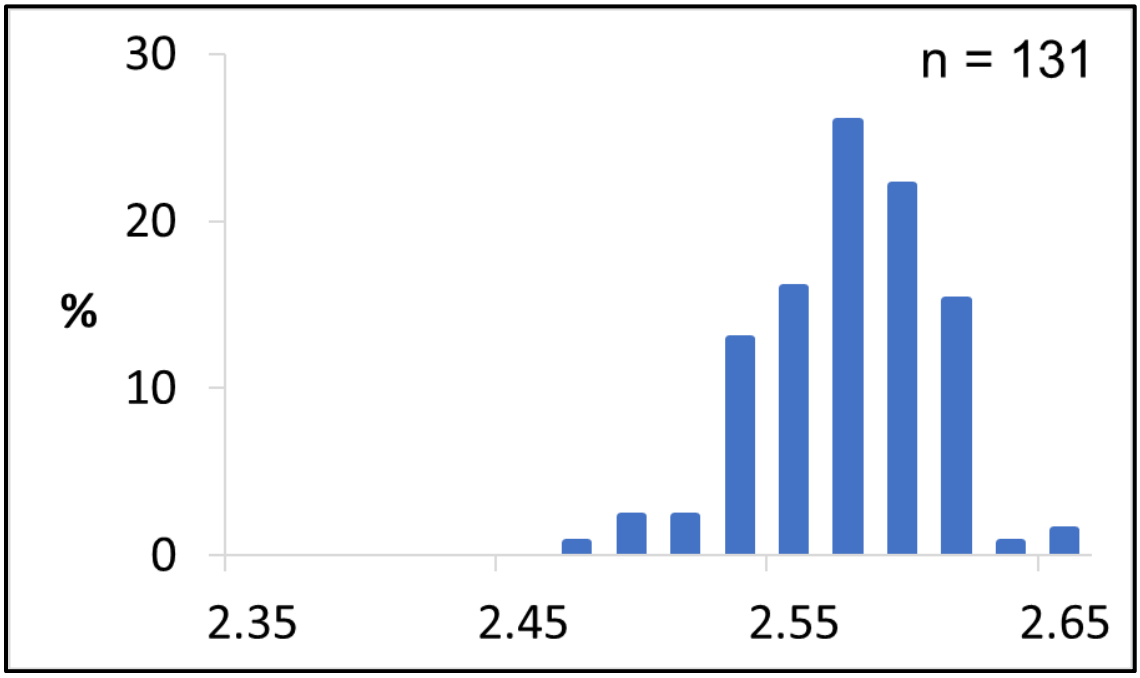

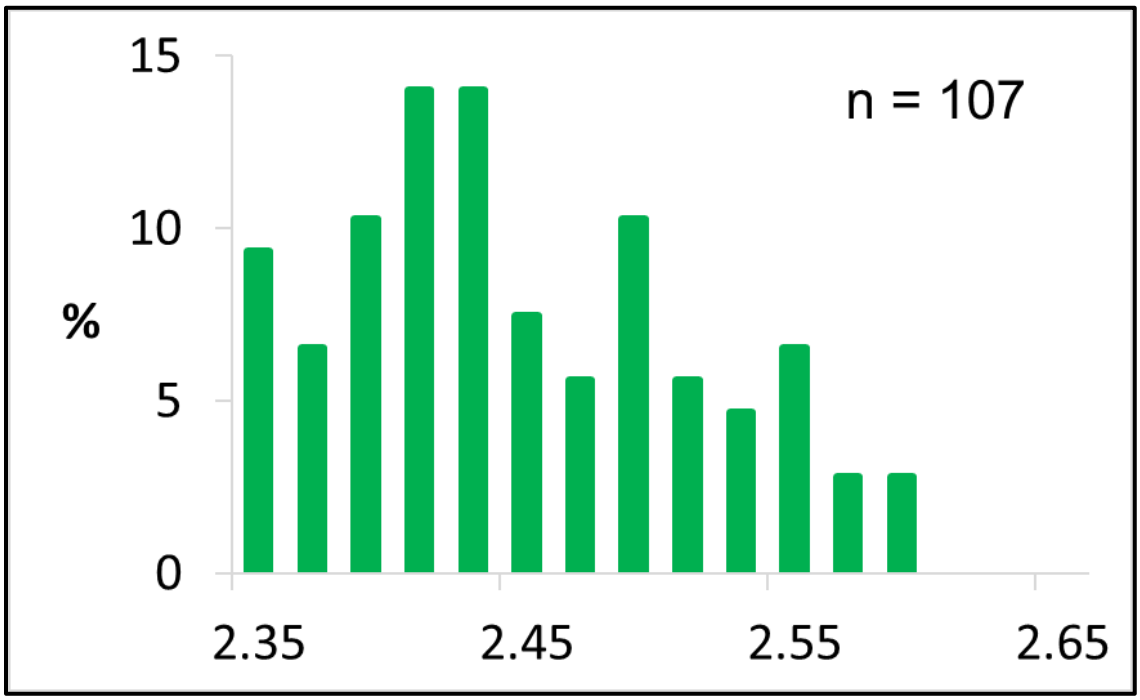

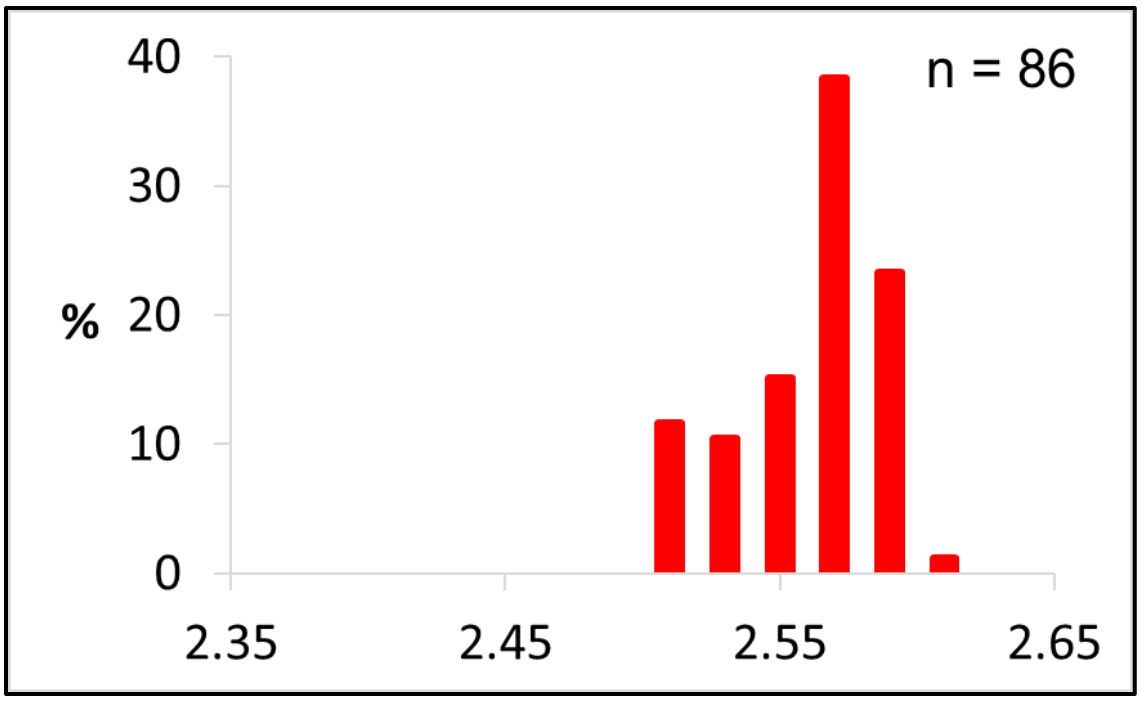
40
30
%
20
10
0
n = 86
2.35
2.45
2.55
2.65

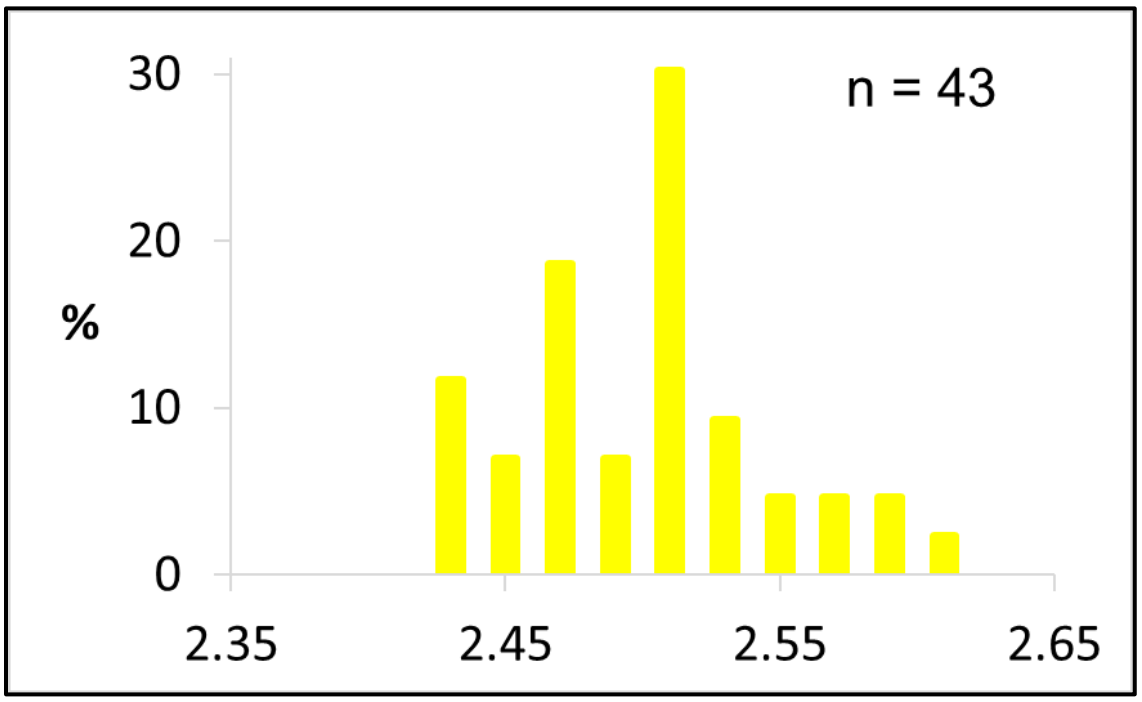
30
20
%
10
0
n = 43
2.35
2.45
2.55
2.65

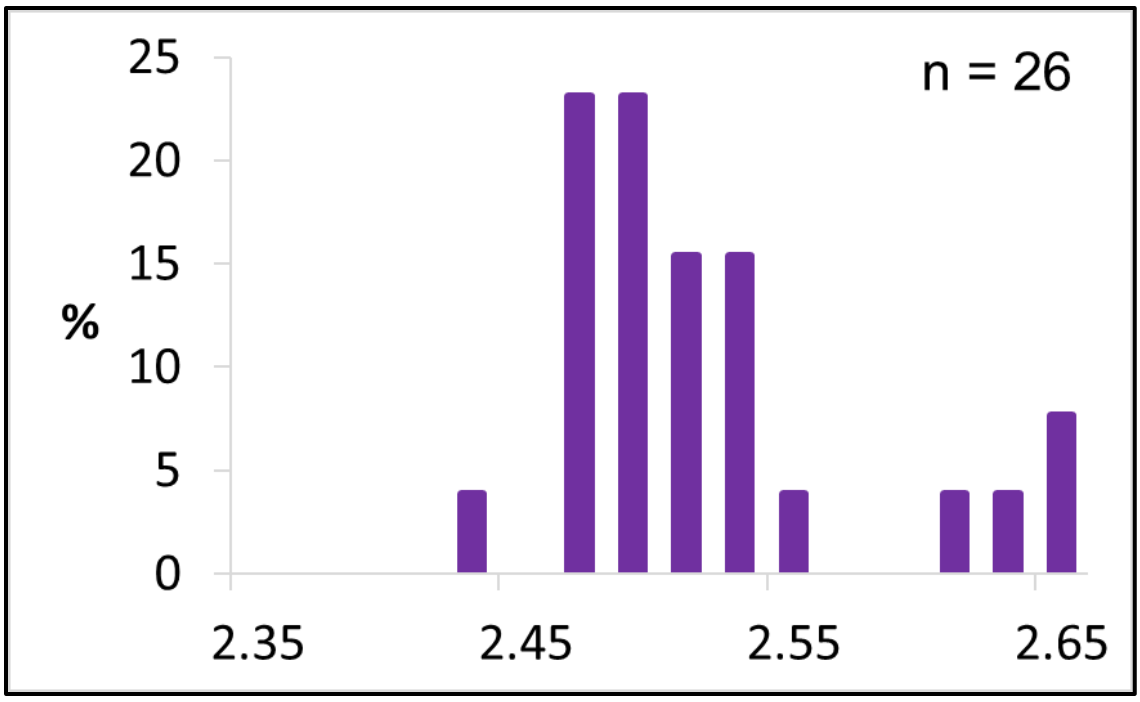
n = 26
%
25
20
15
10
5
0
2.35
2.45
2.55
2.65

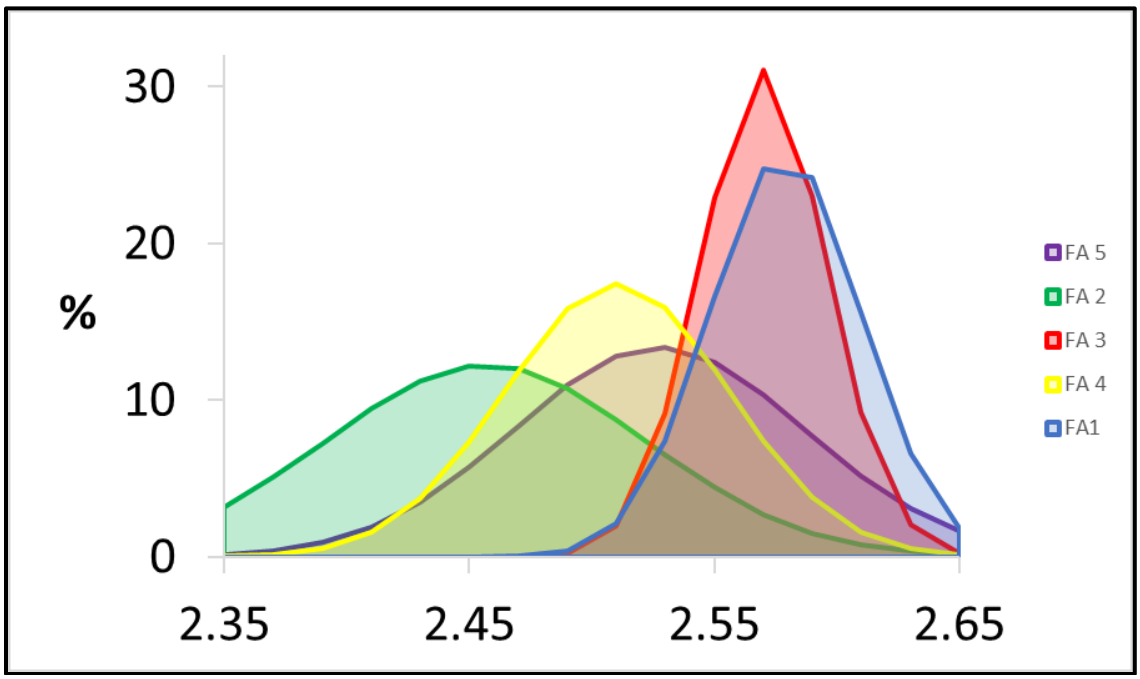
%
30
20
10
0
2.35
2.45
2.55
2.65
FA 5
FA 2
FA 3
FA 4
FA1

Range and Distribution of Apparent Matrix Density Values

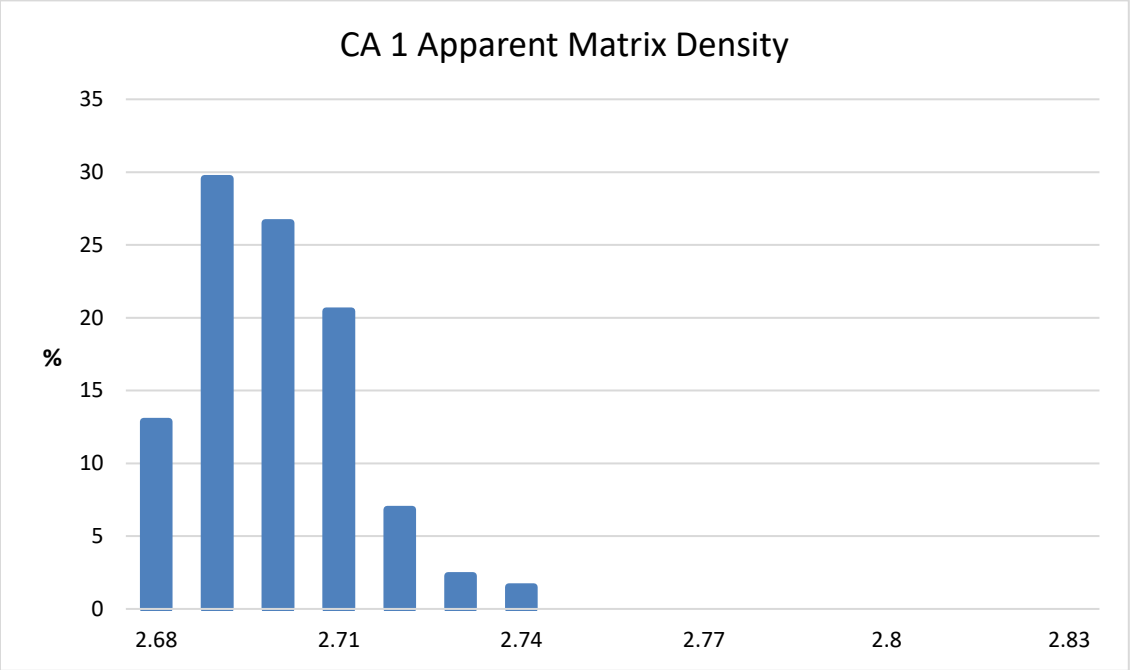

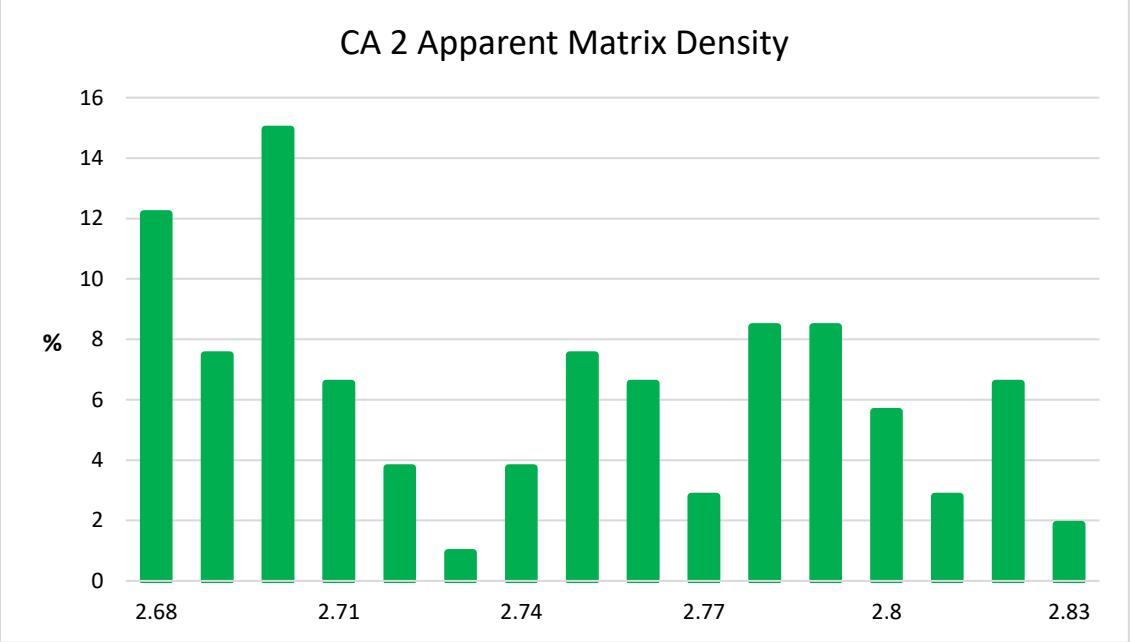

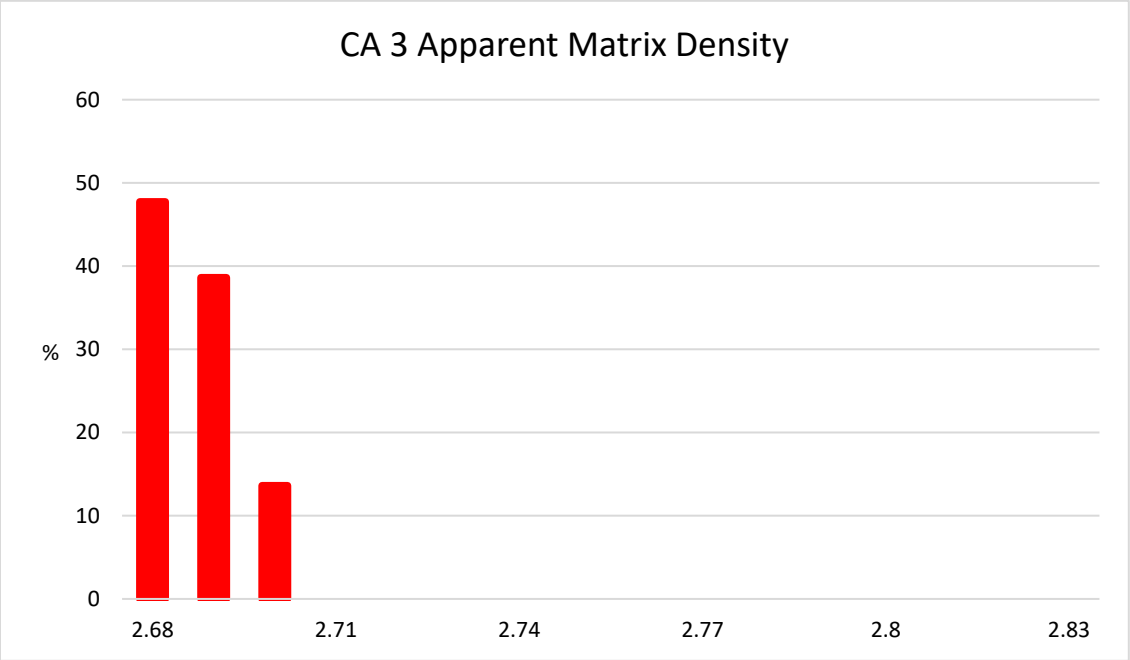
CA 3 Apparent Matrix Density
60
50
40
%
30
20
10
0
2.68
2.71
2.74
2.77
2.8
2.83

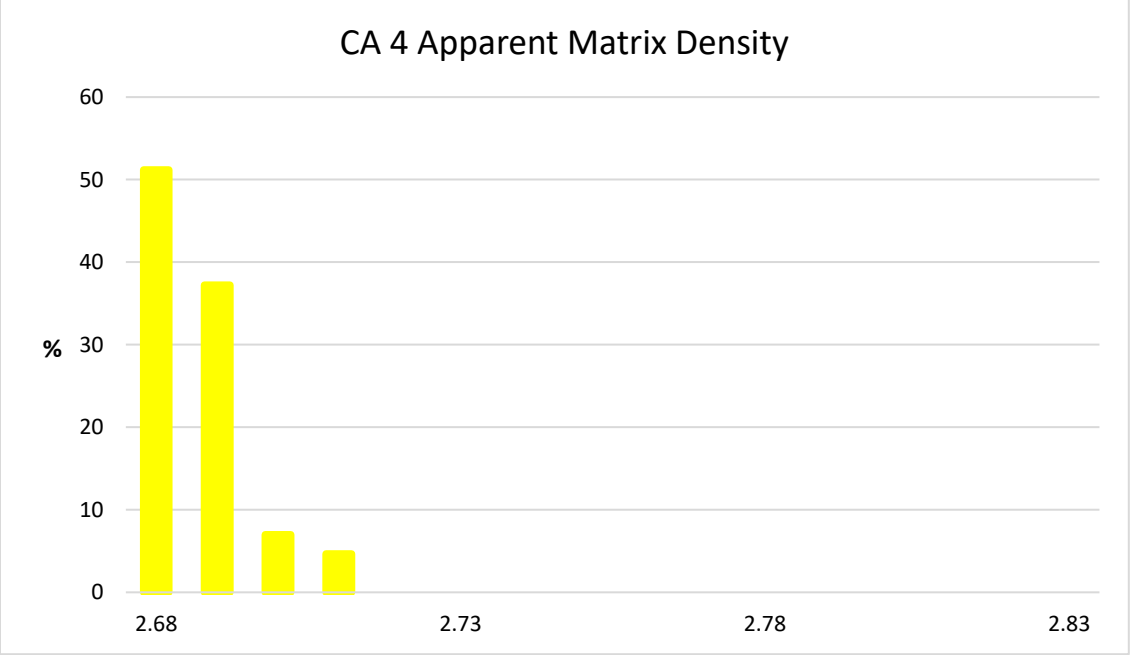
CA 4 Apparent Matrix Density
60
50
40
%
30
20
10
0
2.68
2.73
2.78
2.83

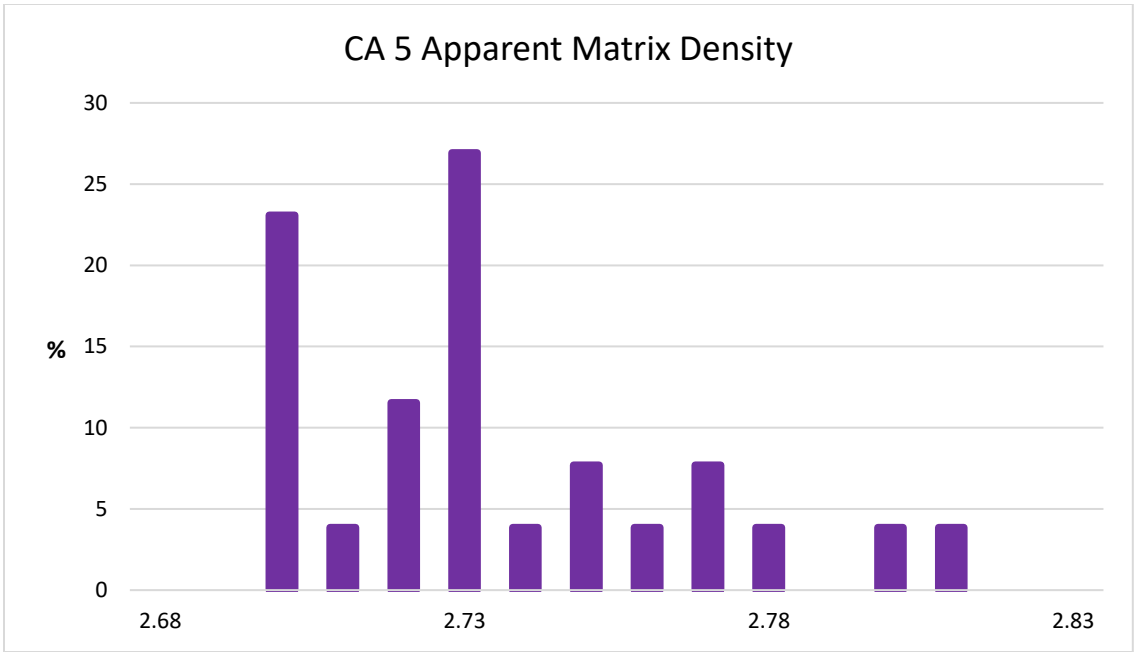
CA 5 Apparent Matrix Density
30
25
20
%
15
10
5
0
2.68
2.73
2.78
2.83

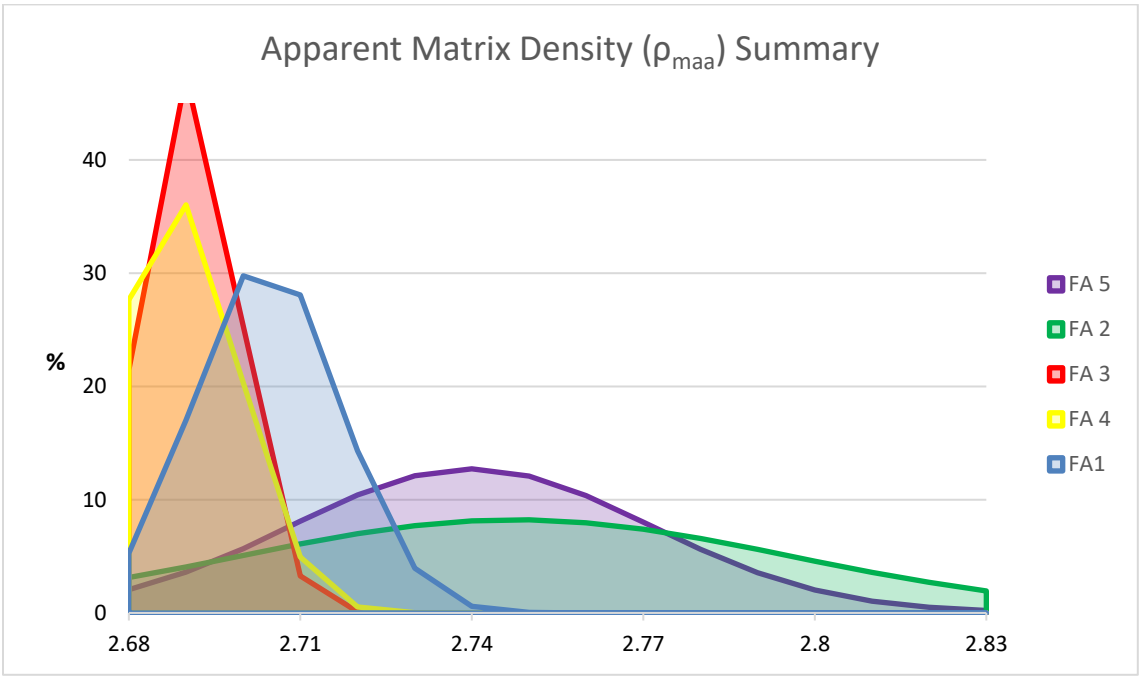
Apparent Matrix Density (ρmaa) Summary
40
30
%
20
10
0
2.68
2.71
2.74
2.77
2.8
2.83
FA 5
FA 2
FA 3
FA 4
FA1

APPENDIX E

XRD SEMI-QUANTITATIVE ANALYSIS AND RAW DATA

(A) 9,660.8

XRD – Microfacies 3A		
Sample A - (9,660.8')		
Mineral	**Counts**	**%**
Quartz	41000	85.59
Calcite	6000	12.53
Pyrite	500	1.04
Dolomite	400	0.84

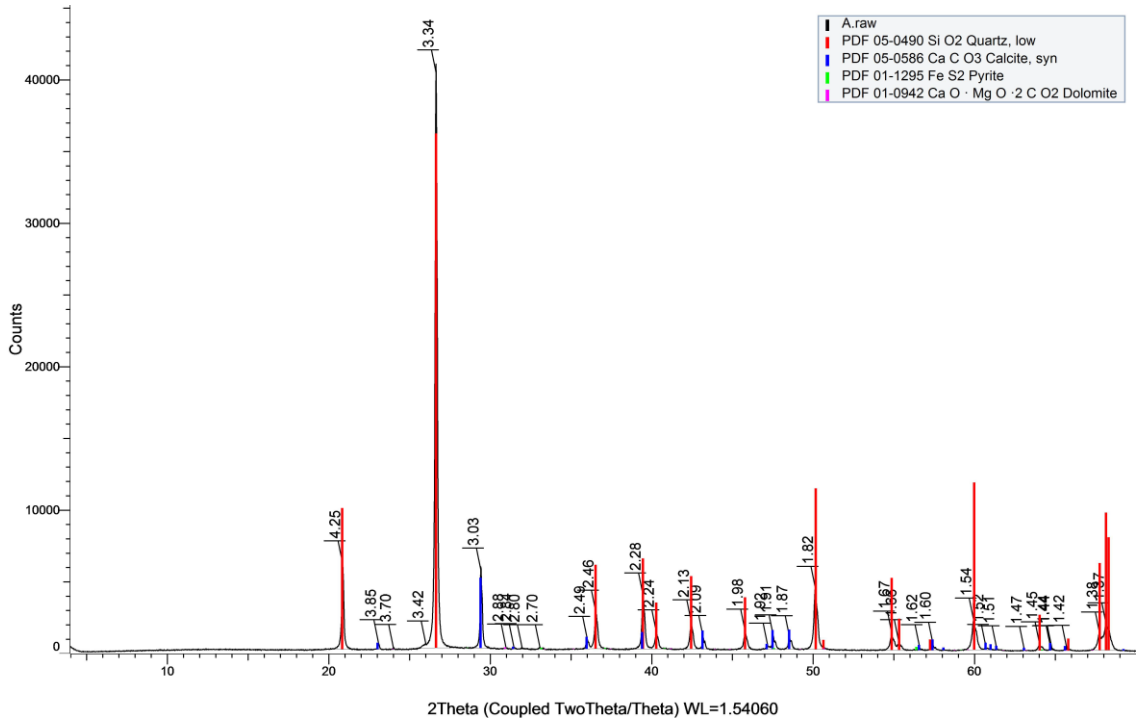

(B) 9,706.5

XRD - Microfacies 1C		
Sample B - (9,706.5')		
Mineral	**Counts**	**%**
Quartz	16850	48.84
Calcite	15200	44.06
Pyrite	800	2.32
Dolomite	700	2.03
Cristobalite	400	1.16
Albite	300	0.87
Muscovite	250	0.72

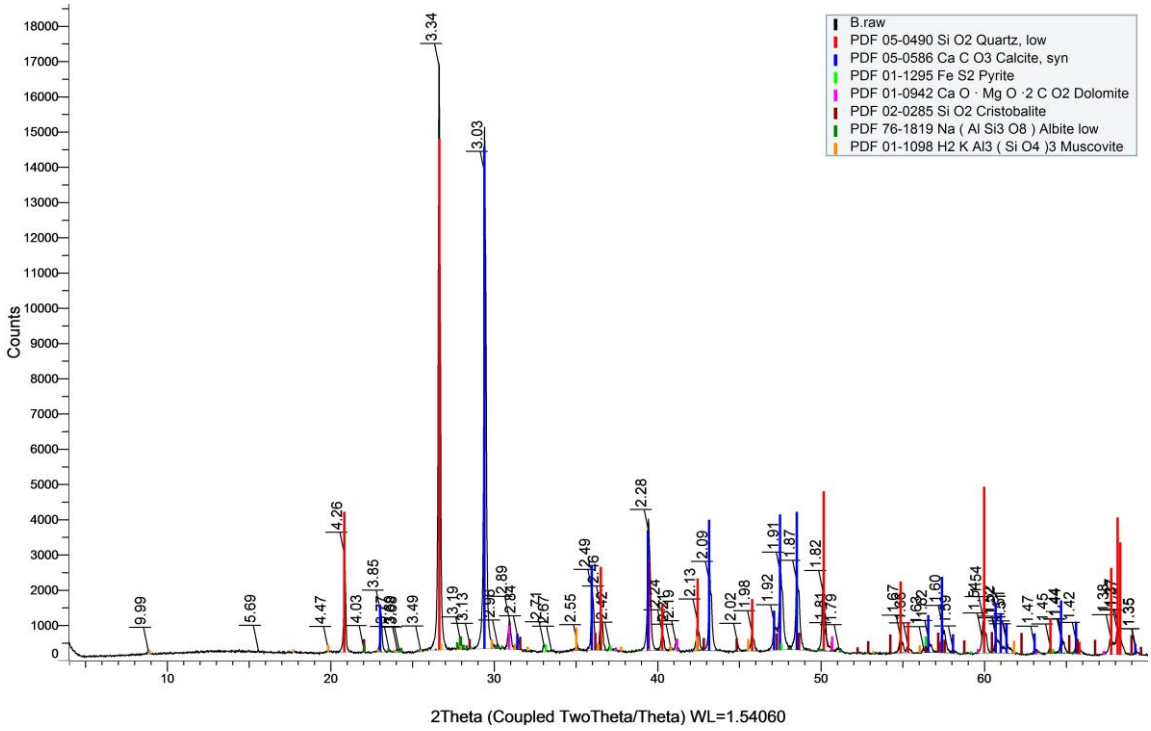

(C) 9,718.5

XRD - Microfacies 1D		
Sample C - (9,718.3')		
Mineral	**Counts**	**%**
Calcite	23450	86.37
Qtz	2200	8.10
Pyrite	600	2.21
Dolomite	450	1.66
Albite	250	0.92
Muscovite	200	0.74
Critobalite	0	0.00

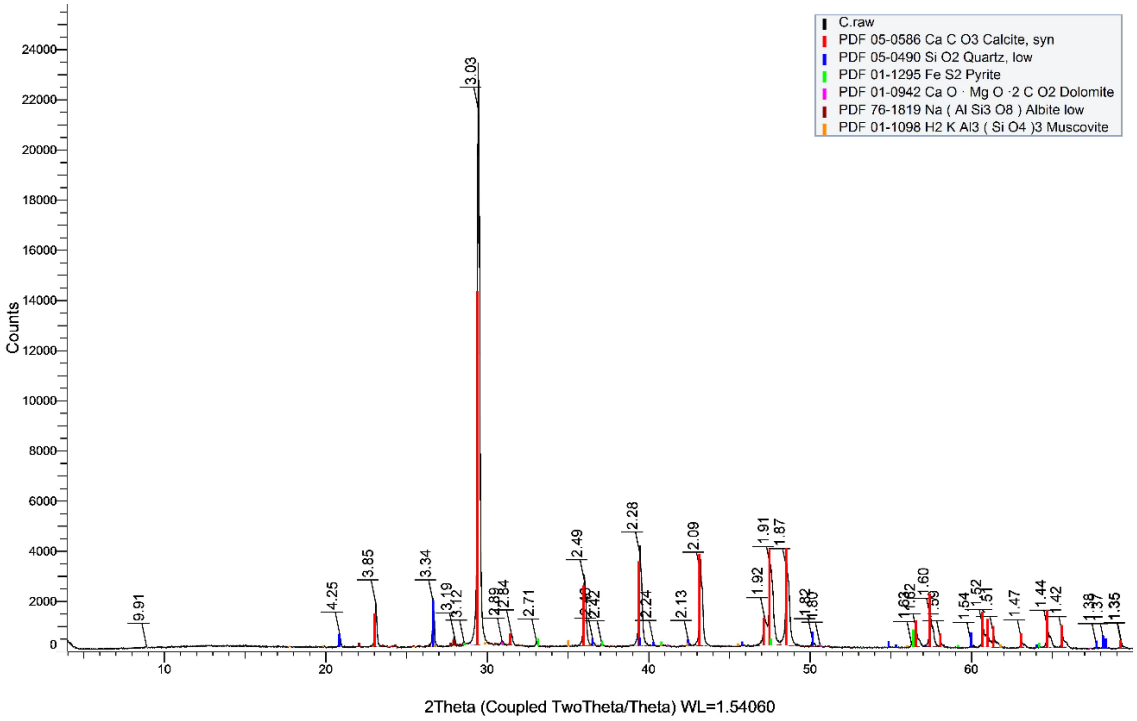

(D) 9,781.05’

XRD – Microfacies 4A		
Sample D - (9,781.05')		
Mineral	**Counts**	**%**
Quartz	39000	84.78
Calcite	5000	10.87
Pyrite	1000	2.17
Dolomite	1000	2.17

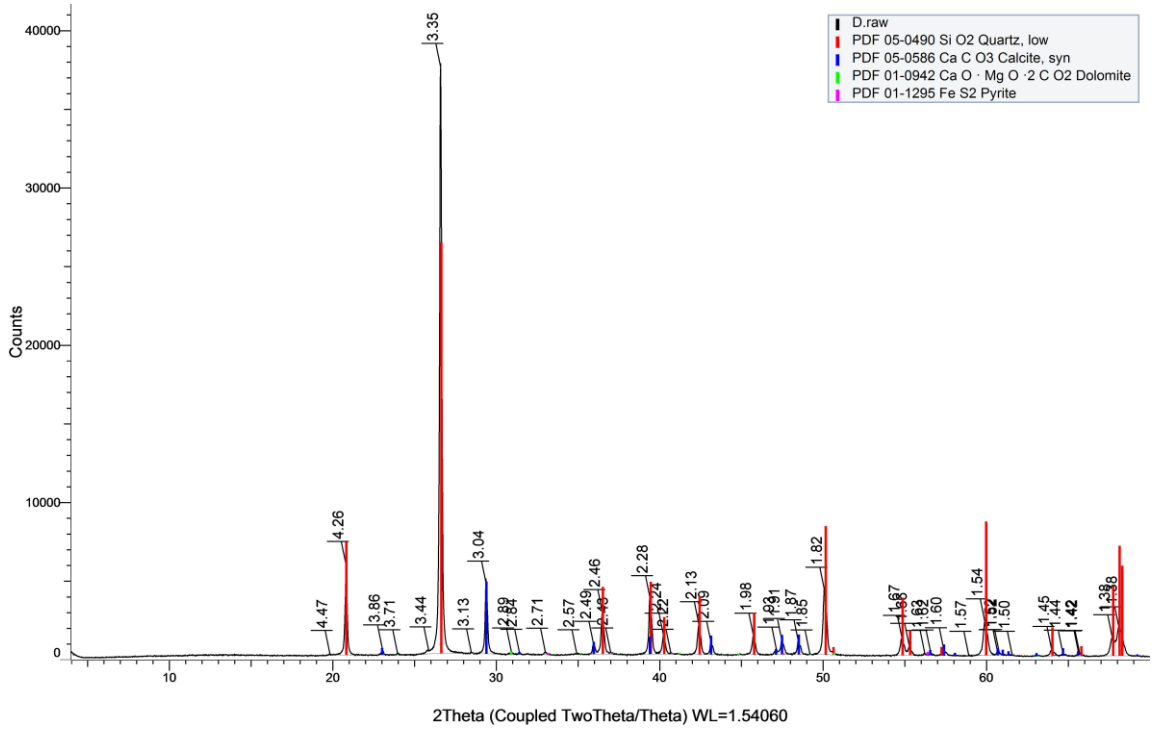

(E) 9,546.8’

XRD - Microfacies 5A		
Sample E - (9,546.8')		
Mineral	**Counts**	**%**
Calcite	10800	75.52
Quartz	1800	12.59
Dolomite	1200	8.39
Pyrite	500	3.50

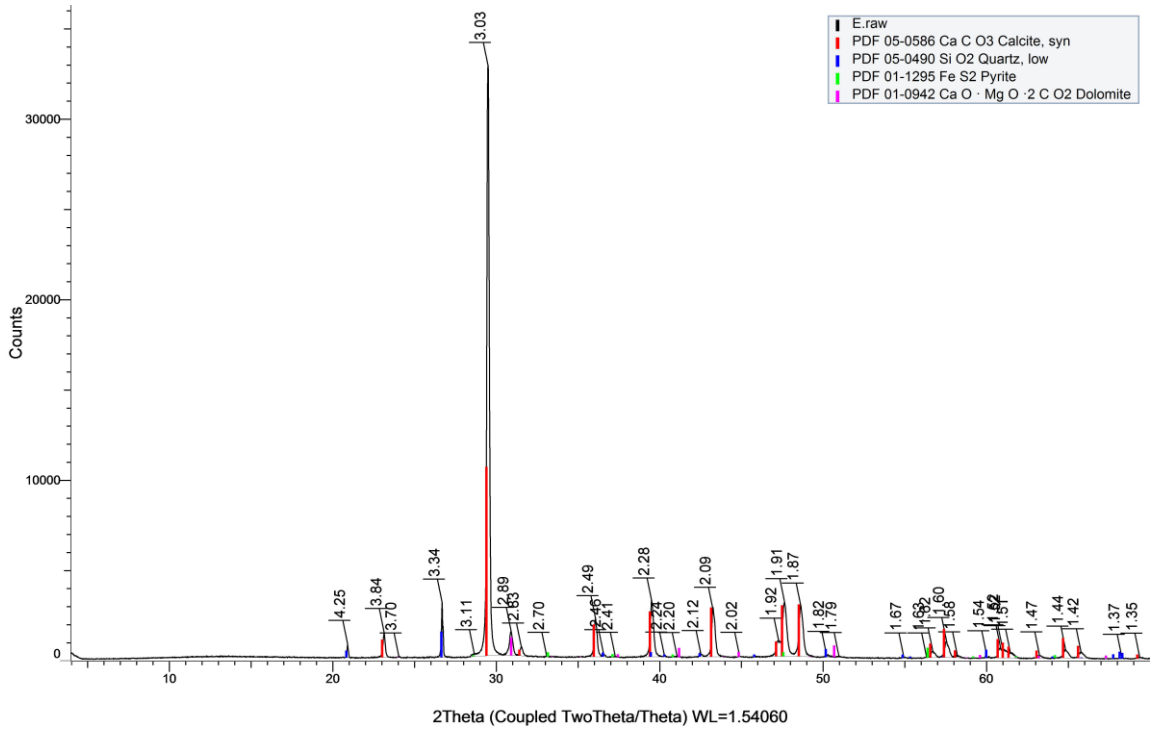

(F) 9,674.35’

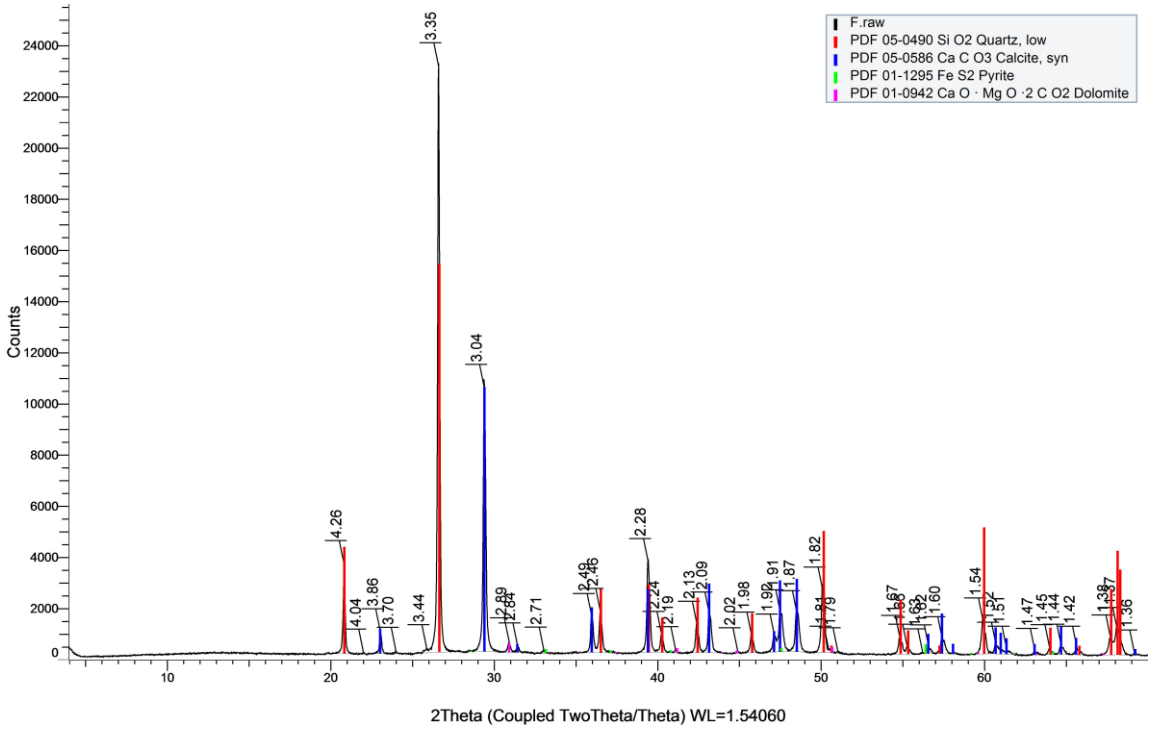
F.raw
PDF 05-0490 Si O2 Quartz, low
PDF 05-0586 Ca C O3 Calcite, syn
PDF 01-1295 Fe S2 Pyrite
PDF 01-0942 Ca O · Mg O ·2 C O2 Dolomite
Counts
2Theta (Coupled TwoTheta/Theta) WL=1.54060
3.35
3.04
4.26
2.28
4.04
3.86
3.70
3.44
2.71
1.82
1.54